

THE UNIVERSITY OF HULL

THE TOOL:WORKPIECE INTERACTION WHEN MACHINING WELDED  
HARDFACING USING PCBN TOOLS

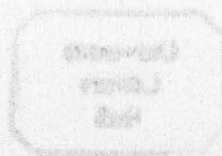
being a Thesis submitted for the Degree of  
DOCTOR OF PHILOSOPHY

in the University of Hull

by

XUEJUN REN, BSc MSc

May 2000



## ACKNOWLEDGEMENT

I would like to express my gratitude to my supervisor, Dr. R D James for his continuous support and guidance during the production of this thesis. My sincere thanks also go to Dr. E J Brookes, for many insights, discussion and advice.

I also would like to express my thanks to Prof. C A Brookes and Dr. M.J. Fagan for their advice and encouragement during this project.

Thanks to Mr G Robinson, Mr B Swain and Mr D. Wright, whose technical experience has helped me in many ways.

I would like to acknowledge De Smet Rosedowns Ltd., Seco Tools (U.K.) Ltd., De Beers Ltd. and Engineering Diamond Ltd. for providing the workpiece and tool materials; My gratitude also goes to some technical personnel from these companies, for their co-operation and many valuable discussion in this work, with special thanks to Mr S P Eccersley and Mr P Harrison at DSR.

Great thanks to my parents, brothers and sisters for their support and encouragement.

My greatest thanks go to my wife, Li Wang, for her unending love and support.

## ABSTRACT

The work presented in this thesis is concerned with turning chromium carbide based hardfacings using PCBN tools. The chip formation and tool wear process was studied by quick-stop and machining tests. Cutting temperature was investigated by means of a remote thermocouple and the chip-tool interface temperature was simulated by an ANSYS Finite Element Analysis model. Cutting performance of PCBN tools from different suppliers was compared in field cutting tests. Hardness, microstructure and the adhesion between the workpiece and cutting tool material were assessed.

In the turning process, saw-tooth chips were formed, with a short chip:tool contact length. Quick-stop tests revealed that the machining process involved fracture of large carbides ahead of the cutting edge in the primary zone. Temperature measurements showed that the cutting temperature for the hardfacing material was lower than that with titanium alloy but much higher than that with machining mild steel. The cutting temperature predicted at the tool chip interface was in the range of 600-700°C when cutting hardfacing.

The tool wear process was found to involve three main progressive stages — from small scale edge chipping to large scale flaking and fracture. Four types of wear were identified: flank wear, microchipping, flaking of the rake face and delamination of the flank face. Abrasion appears to be the principal flank wear mechanism and it showed a minimum value for different speeds but increased with feedrate. The main mechanism for microchipping involved failure through the CBN particle boundaries. Flaking of the rake face occurred in the later stages and transgranular fracture was the main mechanism.

In field tests, PCBN material from various sources achieved different cutting performance, which reflected the structural differences in the PCBN materials. A dense structure with strong particle binding is essential for satisfactory performance of PCBN in this application.

# CONTENTS

## ABSTRACT

## ACKNOWLEDGEMENT

## CONTENTS

### CHAPTER 1 INTRODUCTION

1.1 Introduction	1
1.2 Materials for hardfacing	3
1.3 Application of hardfacing alloys in industry	6
1.4 Machining of iron-based hardfacing materials: a challenge to hardfacing techniques	7
1.5 Objectives of the project	8

### CHAPTER 2 LITERATURE REVIEW

2.1 Metal cutting processes	9
2.1.1 Chip formation processes	9
2.1.2 Chip types	13
2.1.3 The chip : tool interface	14
2.2 Surface quality	16
2.2.1 Surface roughness	16
2.2.2 Surface integrity	17
2.3 Forces in metal cutting and stress on the tool	19
2.4 Thermal effects in metal cutting	21
2.4.1 Heat generation in metal cutting process	21
2.4.2 Temperature measurement	22
2.5 Cutting tool materials	25
2.5.0 Development of cutting tool materials	25
2.5.1 High speed steel (HSS) and related materials	27
2.5.2 Sintered tungsten carbide	27
2.5.3 Cermets	27
2.5.4 Ceramics	28

2.5.5 Polycrystalline cubic boron nitride	30
2.5.6 Polycrystalline diamond (PCD)	30
2.6 Cutting tool wear	34
2.6.1 Tool wear forms	34
2.6.2 Tool wear mechanisms	36
2.7 Manufacturing process of PCBN materials	40
2.7.1 Formation and properties of cubic boron nitride	40
2.7.2 Manufacturing process of PCBN tools	41
2.8 Structure and properties of PCBN materials	42
2.9 Application of PCBN tools	44
2.9.1 Machining of hardened steels	44
2.9.2 Machining of cast irons	46
2.9.3 Machining of cobalt- and nickel-based super alloys	48
2.9.4 Machining of hardfacing materials	48
2.9.5 Machining other difficult-to-machine workpiece materials	49
2.10 Cutting forces and temperatures of PCBN tools	51
2.10.1 Cutting forces	51
2.10.2 Cutting temperatures	52
2.11 Failure mode of PCBN tools	54
2.12 Wear mechanisms of PCBN tools	56
2.12.1 Wear mechanisms of PCBN tools in machining steels	56
2.12.2 Wear mechanisms of PCBN tools in machining cast iron, super-alloy and titanium alloy	59
2.12.3 Wear mechanisms of PCBN tools in machining hardfacing materials	60

## **CHAPTER 3 EXPERIMENTAL WORK**

3.1 Introduction	62
3.2 Experimental equipment and set-up	63
3.2.1 Machining equipment	63
3.2.2 Quick stop device	63
3.2.3 Quasi-static adhesion experiments	64
3.2.4 Temperature measurement	65

3.2.5 Testing and analytical instruments	65
3.3 Workpiece material	66
3.4 Tool materials and tool geometry	68

## **CHAPTER 4 MICROSTRUCTURE AND FUNCTIONAL CHARACTERICS OF PCBN TOOL MATERIALS**

4.1 Microstructure and hardness of the tool materials	70
4.2 Adhesion test results	74

## **CHAPTER 5 QUICK STOP TEST RESULTS**

5.1 Introduction	76
5.2 Deformation of the hardfacing material in the cutting process	77
5.3 Chip morphology	78
5.4 Hardness profile and subsurface structure of the transient surface	80

## **CHAPTER 6 CUTTING TESTS RESULTS**

6.0 Introduction	82
6.1 Laboratory cutting tests	82
6.1.1 Introduction	82
6.1.2 Machining of Hardfacing A (fine structure)	83
6.1.2.1 Chip-tool contact in the cutting process	83
6.1.2.2 Tool wear processes	84
6.1.2.3 Tool wear modes	86
6.1.3 Machining of hardfacing B (coarse carbides)	88
6.2 Industrial cutting test results	90
6.2.1 Introduction	90
6.2.2 Cutting performance of PCBN materials	91
6.2.3 Tool failure mode and wear processes	92

## **CHAPTER 7 TEMPERATURE MEASUREMENTS AND NUMERICAL SIMULATION RESULTS**

7.0 Introduction	96
7.1 The measured tool:shim interface temperature	96
7.2 FE Simulation results	98
7.2.1 The FEA model	98
7.2.2 Boundary conditions and Materials properties	99
7.2.3 Simulated temperature distributions and tool:chip temperatures	100

## **CHAPTER 8 DISCUSSION**

8.1 Chip formation process of the hardfacing materials	103
8.2 Deformation of the carbide and their interaction with the tool	104
8.3 Cutting forces and cutting temperatures	106
8.3.1 Cutting forces and stress on the tool	106
8.3.2 Cutting temperatures and its effect on the cutting process	107
8.4 Tool failure process	108
8.5 Wear mechanism of the PCBN materials	109
8.5.1 Mechanism of the flank wear	109
8.5.2 Mechanism of the chipping process	110
8.5.3 Mechanism of the fracture of the PCBN material	112
8.6 Requirement of the tools materials	112
8.7 Effect of the microstructure of PCBN tools on their performance	114

## **CHAPTER 9 CONCLUSIONS AND RECOMMENDATION FOR FUTURE WORKS**

9.1 Conclusions	116
9.2 Recommendation for future works	117

<b>REFERENCES</b>	<b>118- 127</b>
-------------------	-----------------

# CHAPTER 1 INTRODUCTION

## 1.1 INTRODUCTION

In 1966 a government enquiry chaired by Professor Jost estimated that each year British industry lost in excess of £500M through worn engineering components and their subsequent effects. His estimation has highlighted the problem of wear and, after that, efforts have been made to identify the problem and looking for means to solve the problem. According to a later estimation in 1980's by Peate and Gregory (1980), a potential saving around £1500M could be anticipated if the problem of wear can be solved or controlled effectively. To date, due to the increasing demand for protection of the environment, better use of resources and more fierce competition, techniques to deal with this problem are of growing importance. Hard surfacing techniques have great potential to help to reduce the enormous losses that industry incurs each year through wear.

Basically, a hardfacing process is the application of a hard, wear resistant material to a surface by welding, spraying, or allied processes to decrease deterioration of the surface under different service conditions. The coating can be in the form of a single layer or multiple layers. The coating or cladding of a substrate can help to reduce wear or loss of material by abrasion, impact, erosion, galling or cavitation and by combinations of these factors and high temperatures. In addition, resistance to corrosion can be obtained by depositing alloys which do not come under the heading of hardfacing alloys, e.g. the many types of stainless steel. Hardfacing alloys vary in hardness from 250 to over 1800HV compared with about 150HV for normal constructional steels, and this fact alone makes most of the hardfacing materials more wear-resistant. Due to the difference in their microstructures, for the same level of bulk hardness, a hardfacing alloy will have a much longer life than a conventional materials like mild steel. In a manufacturing process using hardfacing, a low cost substrate material can be used, thus reducing the cost of the whole component. Normally, a material with optimum wear resistance for the working surface would probably be too brittle to withstand the effects of impact loading. Consequently, the

design has to be a compromise between wear resistance and the required bulk toughness. Components made by hardfacing can have optimum bulk and surface properties by properly choosing the substrate, the coating materials and the application techniques.

The hardfacing industry has matured substantially since its inception in the early 1920s. Numerous welding techniques have been developed and field proven. Among the list of the welding techniques currently employed in hardfacing industry (Table 1.1), the most widely used are arc welding, oxyfuel gas and thermal spraying.

**Table 1.1** Comparison of hardfacing processes (Department of Trade and Industry, 1985).

Method	Form of filler	Approx. deposit thickness (mm)	Usual mode of application	deposition* rate (kg/h)
Oxy-acetylene, with welding rods	Bare wire, rod or tub	0.5	Manual	1/2 to 3
Oxy-acetylene with powders	Powder	0.08	Manual	1/2 to 7
Tungsten-insert gas (TIG)	Bare rod, wire or tube	1	Manual	1/2 to 2
Plasma transferred arc	Powder	0.25	Fully automatic	1/2 to 7
Shielded metal arc	Flux coated wire, rod or tube, flux cored wire	2	Manual Semi-automatic	1 to 3 2 to 10
Open arc	Tubular wire, which may be flux-cored	2	Semi-automatic	2 to 10
Metal insert gas (MIG)	Bare wire or tube	2	Semi-automatic	2 to 10
Submerged arc	Bare wire, tube or strip	2	Fully automatic	2 to 70
Electroslag	Bare rod or tube	20	Fully automatic	50 to 350

\* Overall or effective rate, taking into account any necessary breaks in the deposition process (such as changing electrodes). The gross deposition rate in arc hardfacing is dependent on the welding current.

## 1.2 MATERIALS FOR HARDFACING

### 1.2.1 WEAR CONDITIONS

The choice of an alloy system depends to a great degree on the nature of the wear process encountered. The possible wear conditions are outlined below (Menon, 1995):

- 1) *Low-Stress Abrasion*. In this type of wear (also known as sliding abrasion), the abrading particles essentially remove layers of the substrate as they slide on the surface. The stresses are low enough to prevent the abradant from crushing.
- 2) *High-Stress Abrasion*. In this condition, the abradant particles are crushed in the operation. This condition can be accompanied by impact.
- 3) *Impact*. In this mode of wear, sudden and severe application of high loads results in fracture and spalling.
- 4) *Adhesive Wear*. In this condition, contacting metal surfaces undergo localised bonding resulting in material transfer and loss.
- 5) *Erosion*. In this condition, surface damage is caused by high-velocity liquids and gases that may contain solid particles. The damage is accelerated by heat and corrosion. This problem is particularly evident in utility boiler operation.
- 6) *Cavitation Erosion*. This form of erosion results from the collapse of vapour bubbles during the transport of water and other liquids. This leads to roughening and pitting on the surface. This type of wear is seen most often in hydroturbine machinery such as runners and pump impellers. Cavitation erosion is also observed on the propeller blades of water transport vehicles.

## 1.2.2 CLASSIFICATION OF HARDFACING ALLOYS

Hardfacing alloys can be generally classified by dividing them into four Groups (Table 1.2):

**Table 1.2** Classification of hardfacing alloys (Menon, 1995).

HARDFACING			
Group I	Group II	Group III	Group IV
Iron-based, containing less than 20% alloy additions	Iron-based, containing more than 20% alloy additions	Non-ferrous (Cobalt- or nickel-based alloys)	Tungsten carbide based
250-650HV	600-700HV	300-720HV	900-1800HV

**Table 1.3** Typical Iron-based hardfacing alloys (Menon, 1995).

Nominal Composition	Typical Hardness (HRC)	Microstructure, Carbide
0.2-1.5Mn-0.7Cr	28	Ferrite-Bainite
0.3C-5Cr-1W	50	Martensite-Retained Austensite
1.0C-14Mn-4Cr-3.5Ni	As-welded: 20; Work hardened: 35	Austenite
3C-25Cr	47	Austenite/Chromium Carbide
5C-25Cr	47	Austenite/Chromium Carbide
2C-7Cr-6Ti	53	Martensite/Titanium Carbide
6C-28Cr	59	Austenite/Chromium Carbide
6C-19Cr-5Mo-5Cb-2W-2V	60	Austensite/Chromium Carbide/Complex Cb, W, V Carbides

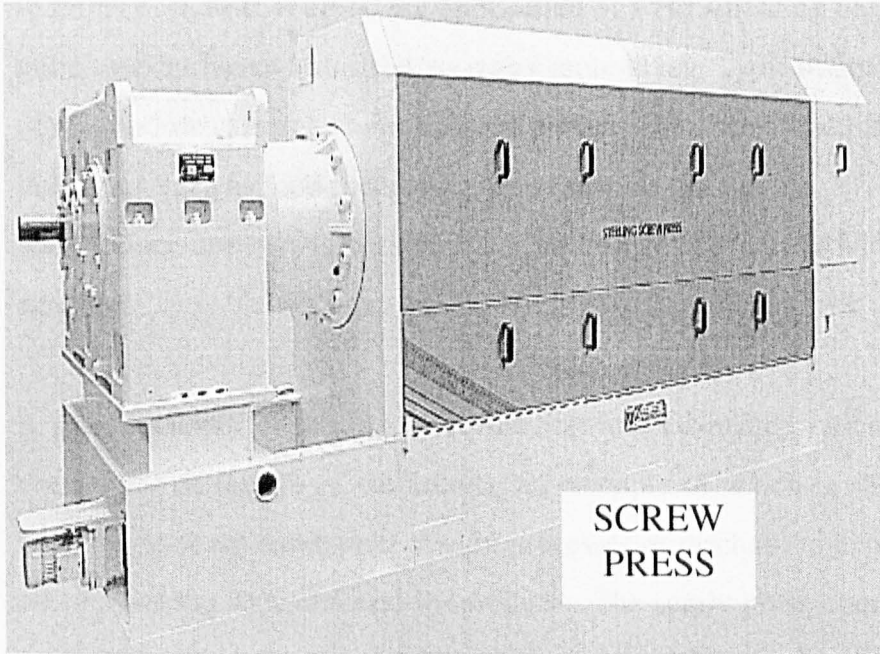
Iron-based alloys are the most popular group of alloys for hardfacing primarily because of their relatively low cost and ease of application. The separation of the iron-based hardfacings into two groups is mainly due to economical considerations. Examples of typical iron-based alloys are shown in Table 1.3. The low-alloy materials are used for applications where worn areas on components are built up to near original dimensions before they are clad with the surfacing material. The martensitic alloys are used primarily for wear applications that involve metal to metal wear as well as sliding and impact loading. With adequate pre- and post-weld precautions, these alloys can be applied crack-free. The austenitic manganese steels are used in conditions where impact is the primary mode of wear. The abrasion resistance of iron-based alloys, which is typically needed in many applications, is increased by the incorporation of various types of carbides, in varying volume fractions, into their microstructure. The most popular of these carbides is chromium carbide. Chromium carbide is a relatively large microconstituent and has a significant area exposed to contact with the abradant. This structure provides excellent wear resistance in low stress abrasion. In high-stress conditions, alloys with the addition of other carbides (referred usually to as secondary carbides) have to be used in order to obtain satisfactory wear resistance.

Some companies have set up their own classification and standards in order to use hardfacing techniques more effectively. For example, a Hardfacing Working Party within British Steel Corporation (BSC) has set up a four-part series of standards under general heading 'Applied Surfaces for Wear protection' (Gregory, 1980). The consumable classification involves: group and type of hardfacing, composition, deposited hardness, characteristics applicable to deposit and typical applications. The document is intended to facilitate the control of subcontracted work and work undertaken within BSC's own workshops. It provides and describes procedures for the manufacture of new components specially designed for hardfacing, giving advice on the most economic combination of substrate and surface coating materials.

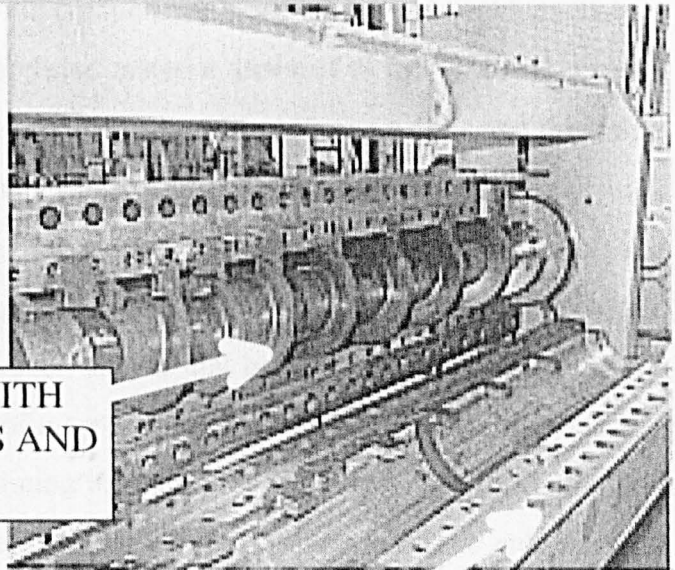
### 1.3 APPLICATION OF HARDFACING ALLOYS IN INDUSTRY

In general, hardfacing has been being used in industry in two ways. Initially, hardfacing techniques were used to restore some worn or damaged components, which would otherwise be scrapped. In many instances, no attempt was made to improve the service performance of the component, but simply restore it to the original dimensions with a compatible surfacing material. This may be a deliberate policy on the engineer's part to overcome some short-term difficulty, or an expedient because of inability to obtain a new replacement within a satisfactory period. Reclamation of components is still the greatest use of weld surfacing at present. With the development of welding techniques and welding materials, it is now possible to reclaim a component quickly and economically, producing a component that is superior to the original.

The other application of hardfacing is to manufacture duplex components, which have much better service performance and are more cost effective. This change of concept has brought about big developments in hardfacing technology and has widened its application to a large extent. Today, hardfacing has become an important consideration at the design stage for many engineering projects. Design is essentially a process to satisfy a variety of interconnected requirements, which include maintainability, quality, and above all reliability and fitness for purpose. In general, wear resistance increases at the expense of toughness and this means, for example, that a component which must withstand shock loading and high wear at the working surface cannot usually be made from an ideal monolithic material. A material with optimum wear resistance for the working surface would probably be too brittle to withstand the shock load. Consequently, the designer must compromise on wear resistance to achieve the required bulk toughness. Weld surfacing can be used to exploit the potential of both the bulk mechanical properties and the wear resistance properties of the working surface. Therefore, to make the most effective use of weld surfacing it is necessary to think in total life cycle terms and begin at the beginning with design.



SCREW  
PRESS



WORM ASSEMBLY WITH  
HARDFACED WORMS AND  
DISTANCE PIECES

LINING  
BARS

Figure 1.1 Application of hardfacing in a screwpress (Courtesy of DE SMET ROSEDOWNS Ltd., UK)

In terms of industrial areas, the application of weld surfacing has extended from the initial use by heavy industries to many more areas. Typical areas now include the mining industry, iron and steel plants, power plants, chemical plants and some light industries, such as food processing, paper manufacturing, etc. Today, many welding maintenance companies specialise in hardfacing and can provide a wide range of services.

A good example of the use of hardfacing in food-related industry is in the screw presses for extraction of edible oils, an example of which is shown in Figure 1.1. Screw presses are commonly used in processes of mechanical extraction of vegetable oil or breaking down animal by-products. The screw press operates under extreme conditions where abrasion on the vital components is a predominant problem. This is mainly caused by the passage of abrasive material attached to the oil seeds. Over a period of weeks or months the main components, which are the worms and the lining bars, lose their performance through abrasion. Breakdown of production and high frequency routine maintenance can be very expensive for the press users. Thus, long service life presents a big challenge to screwpress manufacturers wishing to retain and increase their markets. It has been shown that hardfacing techniques can very effectively extend the service life of a screwpress thus minimise the downtime and maintenance. The worms and the lining bars are first machined from mild steel and then coated with a hardfacing material. All the working surfaces are subsequently machined by milling or grinding to produce the necessary dimensional accuracy and surface finish.

#### **1.4 MACHINING OF IRON-BASED HARDFACING — A CHALLENGE TO HARDFACING TECHNIQUES**

The wear performance of a hardfacing material basically depends upon both hardness and carbide content. The structure of hardfacing materials, by their nature, makes machining very difficult. Apart from the problems incurred from the microstructure, the nature of welding process itself makes machining more difficult, because of surface irregularities, structural inhomogeneity, welding defects, etc.. The three

most common machining processes used are grinding, milling and turning. Most of the iron-based hardfacing materials can be machined by grinding but, the grinding process usually means a very low material removal rate making the processes very time-consuming and expensive. Turning and milling were mainly restricted to low alloy or low hardness facing materials before new, harder and tougher tool materials appeared, such as reinforced ceramic and polycrystalline cubic boron nitride. Although, some developments have been made with these new tool materials, the machining of hardfacing materials is still a problem for industry.

Based on industrial investigations, problems with machining hardfacing alloys, especially some high-hardness hardfacing- alloys (HRC55-65) can be summarised as following:

- limited tool materials and tool geometry available
- low material removal rate
- short tool life and low reliability
- high cost as a percentage of the whole cost for a duplex part
- high requirement on the machine and holding systems due to high cutting forces and vibrations

## **1.5 OBJECTIVE OF THE PROJECT**

Iron-based hardfacing materials are widely used in industry but the machining, especially turning and milling of these materials is one of the most important factors when considering their application. Lack of detailed knowledge of these processes is a problem and the present work is intended to provide information for both the users and the manufacturers of hardfacing materials and the cutting tool inserts.

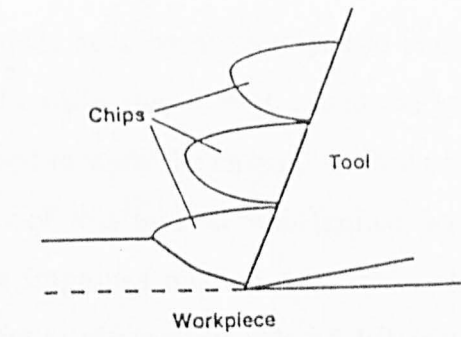
## **CHAPTER 2 LITERATURE REVIEW**

### **2.1 METAL CUTTING PROCESS**

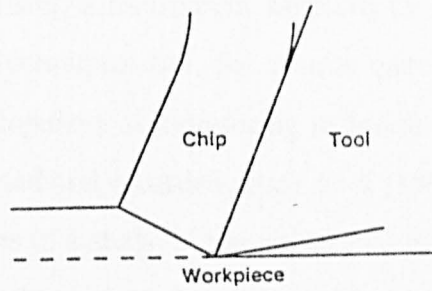
Metal cutting involves a process of removing a thin layer of material from the surface of a workpiece by driving a harder wedge shaped tool symmetrically into the workpiece. The thin layer, known as a chip or swarf, is deformed throughout its volume and impinges upon the rake-face of the tool, moving over it in a direction away from the direction of the motion of the workpiece. The variety of metal cutting processes is very large and includes turning, milling, boring, drilling, forming, shaping and planing. Of these, turning is mostly often employed in fundamental studies of metal cutting.

#### **2.1.1 CHIP FORMATION PROCESS**

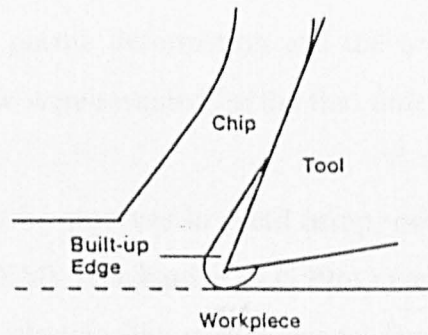
Generally, metal cutting is a process of chip formation and the mode of chip formation is perhaps the most important aspect of the cutting operation. The formation of chips involves the deformation of the workpiece material in the region of a plane (the shear plane) extending from the tool cutting edge to a position where the upper surface of the chip joins the workpiece surface. Different type of chips may be formed depending on the workpiece material and the cutting conditions as shown in Figure 2.1 (Trent, 1991, Stephenson and Agapiou, 1996). The consumption of energy in a cutting process occurs mainly in the formation and movement of the chip. For this reason, the main economic and practical problems concerned with the rate of removal and tool performance can be understood only by studying the behaviour of work material as it formed into a chip and moved over the tool. Many aspects of the cutting process, such as tool forces and temperatures, tool wear, and workpiece surface finish are associated with the chip formation process (Nabhani, 1991). In addition, the size, shape and continuity of chips are very important considerations in automated manufacturing, e.g. collection and disposal.



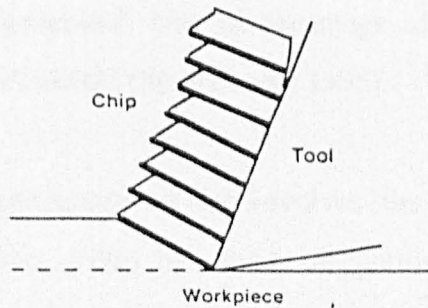
a)



b)



c)



d)

Figure 2.1 Four basic types of chips: a) discontinuous, b) continuous without built-up edge, c) continuous with built-up edge, d) shear localized (Stephenson, 1996).

A number of techniques have been developed to study the chip formation process experimentally. In the early stages, high speed cine-photography at relatively low magnification was used to study the changes in external shape during chip formation but the effectiveness of this method was limited because it could not detect the internal changes. An improved method used by Tonshoff et al (1979) involved a transparent silica plate to observe the role of different phases in the work material during the cutting and, in further research, the movement of the chip across the rake face was studied by using a transparent sapphire tool material. Some success was achieved with these techniques but, the results were far from satisfactory (Trent, 1991). With the development of monitoring techniques, much more information on cutting could be detected and recorded. Back et al (1994) reported the application of high speed videographs in a study of the orthogonal machining of aluminium. In this work, a high speed video camera system with high magnification (1000×) and recording rate (1000 frames/sec) was used to observe the metal cutting process. By this means, the actual plastic deformation and the origin of the shear fronts that comprise the shear plane were revealed for the first time.

Chip formation can also be observed in detail using special devices inside a scanning electron microscope (SEM). Afaghani et al (1996) investigated the deformation of a SiC whisker-reinforced plastic using such a device. The cutting took place inside the SEM chamber to allow observation of the process. The machining behaviour of the whiskers with different orientation was successfully captured and, based on this, cutting models were generated. One disadvantage of this method was that it was limited to relatively soft metals (Stephenson, 1996).

The most effective procedure so far involves the so called quick-stop device (Trent, 1991, Stephenson, 1996) by which the cutting was stopped suddenly and details of the chip formation process were kept undisturbed with the chip attached to the workpiece. The 'frozen chip' can then be separated from the parent workpiece, moulded into plastic, ground and polished for examination in a microscope or for other tests (e.g. micro hardness measurement) (Vorm, 1976). The quick-stop method can satisfactorily arrest the cutting process such that small scale phenomena can be

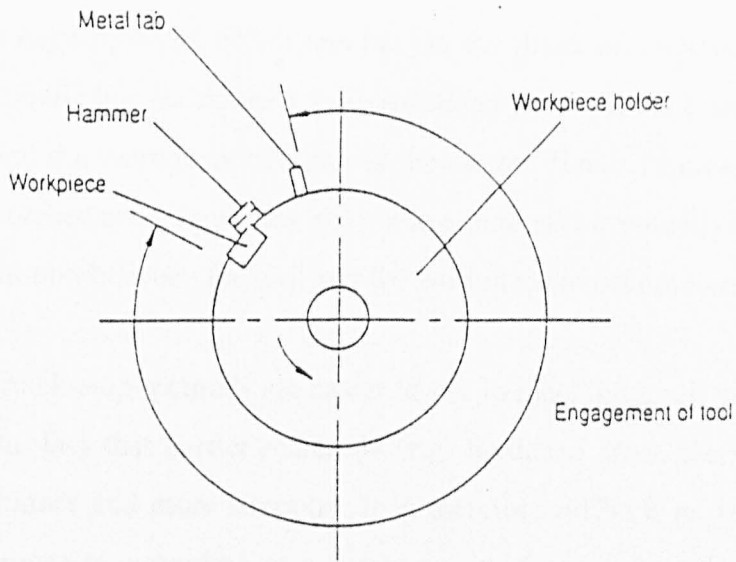
studied, which would be impossible by stopping the cutting process in the normal way. The quick-stop method was first developed for turning operations, but it has been extended to other cutting conditions, e.g., milling (Wager, 1980, Kovac and Sidjanin, 1997), and drilling (Hosoi et al 1980, Griffiths, 1986).

Many types of quick stop device have been developed since the early 70's (Brown, 1974, Vorm, 1976, Nabhani 1991, Yeo et al, 1992). Generally, two mechanisms have been employed in these devices to stop the cutting quickly. One is to reduce the velocity of the cutting tool relative to the workpiece to zero by removing the tool (Yeo et al, 1992) or the workpiece (Vorm, 1976) from the cutting zone using an impact bar or a hammer; while the other mechanism uses an external power source, i.e. the pressure generated by explosives (Brown, 1974) to remove the tool from the cutting zone. This latter method applies extremely high pressure to the tool, breaks the supporting pin and accelerates away from the cutting action.

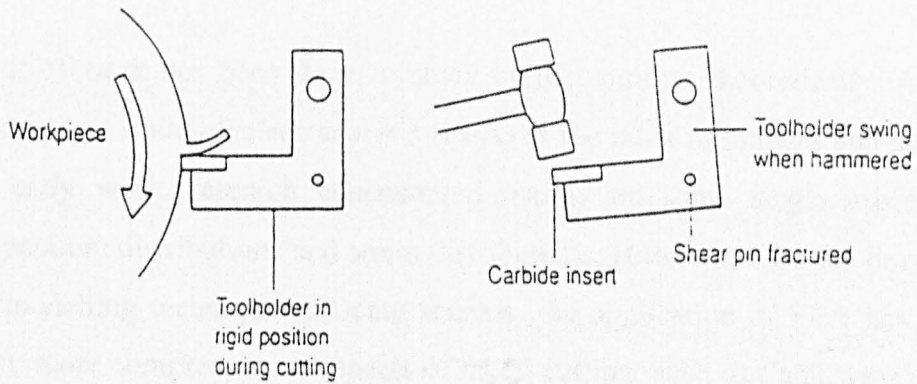
Yeo et al (1992) reported a quick-stop device for orthogonal machining using the hammer and pin method (Figure 2.2). At a pre-determined cutting position, that is, at about the mid-point of the workpiece, the tool-holder was disengaged by breaking the two pins via the impact of a hammer. One improvement to the device was its use with a CNC lathe with a modified turret for a dynamometer system, to allow monitoring of the cutting forces during the cutting process.

In research into machining metal matrix composites, a quick stop facility, based on a modified impact strength tester, has been successfully developed to study the tool wear mechanisms in intermittent cutting (Bergman et al, 1994). By mounting an extra head on the pendulum, trailing the cutting edge, the workpiece will be suddenly knocked out of its holder and the cutting action stopped. Similarly, Quigley et al (1994) reported a quick-stop device used to study the machining mechanisms of Al/SiC metal matrix composite and this device was mounted on a shaping machine.

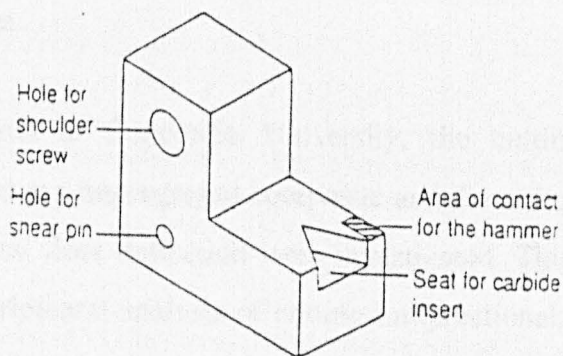
Recently, Byrne et al (1997) reported a newly-developed quick-stop method in studying the machining of aluminium alloys. In the test, the workpiece was bolted to



a) Engagement of the tool



b) The cutting process



c) The tool holder

Figure 2.2 Schematic to show the set-up of a quick-stop device using a hammer to remove the tool from the cutting positions (Yeo et al, 1994).

a large flywheel which was held in the chuck of a manually-operated lathe. Once the spindle has accelerated to a predefined position, the contact between the cutting tool and the workpiece occurs. As the cutting forces increases with cutting distance, the notched area supporting the cutting zone will eventually fracture, causing the relative motion between the tool and the workpiece to become zero, i.e. cutting stops.

Quick-stop methods are easier to use in machining relatively ductile materials due to the fact that harder materials (e.g. hardened steel, etc.) are brittle and the chip is thinner and more irregular. It is therefore difficult to get good quick-stop samples. However, according to a recent report, the technique has been successfully used to study the chip formation process of the hardened 100Cr6 steel (Poulachon et al, 1998). The test results provided very valuable evidence in understanding the cutting mechanism, especially the role of shear and cracking in the chip formation process.

A lot of work has been done to study cutting process theoretically. Among these approaches, finite element analysis (FEA) is the most prominent and successful. In the early work, research concentrated mainly on some single aspects, such as temperature distributions and stress distributions. However, with the development of the modelling technique and data sources, the application of FEA has spread into many more comprehensive aspects of metal cutting, such as flank wear and sticking behaviour on the chip-tool interface (Zone, et al 1995), plastic flow of the workpiece material and friction at the tool-workpiece interface and wear of the tool (Komvopoulos et al, 1991), deformation temperature distribution (Stephenson, 1991), etc..

In research at Concordia University, the cutting mechanics of graphite fibre reinforced pre-impregnated composite and the effect of tool geometry on the cutting quality and fibre deflection were investigated. This work dealt with the theoretical and experimental analysis of cutting unidirectional, cross-ply and woven composite prepregs. Results showed that the cutting mechanism of prepreg was essentially a material failure due to bending-induced fracture and also due to shearing and compressive stresses in which the prepreg resin was ploughed and the reinforced fibres of prepreg were cracked (Wang, 1995).

### 2.1.2 CHIP TYPES

Generally, chips can be divided into four basic groups: discontinuous, continuous, continuous with built-up edge and shear localised (Figure 2.1). The first three types have long been identified while the fourth has been considered as a separate type only in the recent years (Stephenson and Agapiou, 1996).

When brittle materials like cast iron or bronze is cut, it is broken along the shear plane and forms segmented chips (Figure 2.1a), these discontinuous chips of appreciable size were formed by a fracture mechanism. During cutting, a very large amount of strain takes place in the primary deformation region in a very short time and a brittle material like cast iron or bronze can not withstand this strain without fracture (Trent, 1991). In addition, a secondary phase (e.g. graphite flakes) may make the chip easier to fracture (Hooper and Brookes, 1984). At very low speeds, the chips of more ductile materials may also be produced in this form.

Under the majority of cutting conditions, ductile metals and alloys do not fracture on the shear plane and a continuous chip is produced. Such chips could be formed without a built-up edge (Figure 2.1b) or with a built-up edge on the tool (Figure 2.1c).

Built up edge (BUE), or built up nose, is an important feature of metal cutting under seizure conditions. It adheres around the cutting edge and the rake face of the tool, displacing the chip from direct contact with the tool. Its existence mainly depends on the cutting condition, the work material being cut and the tool material used. Favourable conditions for BUE formation include intermediate cutting speed and workpiece materials with more than one phase in their structure. At higher cutting speed, as temperature increases, the form of the BUE changes, decreasing in size or forming a built up layer. Built up edge is one of the principle factors affecting surface finish and can have a considerable influence on the cutting-tool wear. However, certain benefits can be derived, for example, under certain conditions a small stable BUE may be maintained, which can protect the tool without producing an

unacceptably poor surface finish. Another positive effect is that the effective rake angle becomes quite large with a BUE and the energy consumption drops.

The fourth type of chip (Figure 2.1d) was only widely observed as cutting speeds increased and new work materials were introduced. It was macroscopically continuous, consisting of narrow bands of heavily deformed material alternating with larger regions of relatively undeformed material. This type of chip was obtained when machining hardened steel, stainless steel, titanium alloys at high speed, and nickel based super alloys (Shaw and Vyas, 1998). The fundamental mechanism for the segment formation is still not well understood (Davies et al, 1997). Some researchers (Komanduri and Schroeder, 1986, Hou, et al, 1995) attributed the chip formation to catastrophic thermoplastic instability on the shear plane, where the flow stress due to thermal softening associated with an increase in strain more than offsets the associated strain hardening. Others have suggested that the crack is initiated at the free surface and runs toward the tool tip (Shaw and Vyas, 1998).

### **2.1.3 THE CHIP-TOOL INTERFACE**

The movement of the chip and the work material across the faces and around the edges of the tool is of great importance in a cutting process. Initially, it was treated as a classical friction process. However, detailed studies of the tool/work surface have shown that this approach was inappropriate for most cutting conditions. Much research has been undertaken using different techniques to study the interface under different cutting conditions (Trent, 1991). The most important conclusion from these observations was that the contact between tool and work surfaces was so nearly complete over a large part of the total area of the interface that sliding at the interface is impossible under most cutting conditions. It has been observed that seizure occurs on the flank surface under some conditions, particularly close to the edge. Sliding occurs under certain cutting conditions and at a certain position on the tool surface as shown in Figure 2.3.

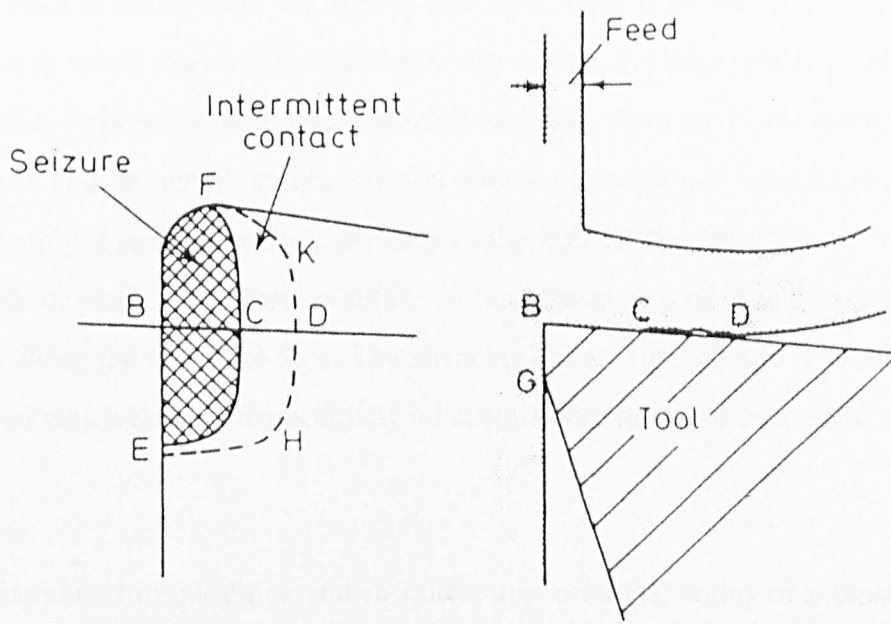


Figure 2.3 Area of seizure on cutting tool (Trent, 1991).

In metal cutting relative movement continues under conditions of seizure and this is possible because the area of seizure is small and sufficient force is applied to shear the work material near the seized interface. Tool materials must have high yield stress to avoid destruction under the very severe stresses which seizure conditions impose. Relative motion under seizure involves shearing in the weaker of the two bodies and in metal cutting this is the work material. The shear strain is not uniformly distributed across the chip as the bulk of the chip formed by shear along the shear plane is not further deformed but moves as a rigid body across the contact area along the tool rake face. The shear resulting from seizure is confined to a thin region which may lie immediately adjacent to the interface or at some distance from it.

### 3.3.1 SURFACE RUGGINESS

In sections through chips and in quick-stop sections, zones of intense shear strain near the interface were normally observed, except under conditions where sliding took place. There is a flow zone near the interface where the behaviour of the work material is in many ways more like that of viscous fluid than solid metal. Hence there is no sharp line separating the flow zone from the body of the chip but a gradual blending in. There is, in fact, a pattern of flow in the work material around the cutting edge and across the tool face, which is characteristic of the metal or alloy being cut and the conditions of cutting. Therefore, a pattern of flow and velocity gradient within the work material, with velocity approaching zero at the tool/work interface, is the basis of a model for relative movement under seizure, to replace the classical friction model of sliding conditions.

## **2.2 SURFACE QUALITY**

Machining aims to create a part of given geometry, specified dimensions and dimensional tolerance. Beyond geometrical considerations, it is also important that the surface produced should be free of defects such as cracks, have no harmful residual stresses, and not to be subjected to undesirable metallurgical changes (Trent, 1991). Error of form and waviness are two other characteristics of the surface geometry. A turned surface usually shows a uniform roughness distribution without significant waviness (Stephenson and Agapiou, 1996) and, therefore, surface quality should be measured in terms of surface roughness and surface integrity.

### **2.2.1 SURFACE ROUGHNESS**

The contact between the flank face and the new workpiece is responsible for the surface roughness. There were two components to the machined surface: the geometry finish and the natural surface (Stephenson and Agapiou, 1996). The concept of geometry finish refers to the ideal surface roughness related to tool nose radius, tool angle and feed rate. A smoother surface could be generated by using a lower feedrate, a larger nose radius and a lower lead angle. The natural part of the roughness results from tool wear, errors in the machine motion, inconsistencies in the workpiece material, discontinuous chip formation, errors in the machine motion, and machining system vibrations. Damage to the cutting edge results in a replication of this in the newly formed surface but the effect can be modified by further contact with the unworn flank face of the tool.

There are many methods used for the measurement of the surface roughness. These include; the use of a mechanical stylus, microscopy, reflectivity measurements and even some manual methods (Shaw, 1984). Two common parameters used in measuring surface finish are the Centre Line Average (Ra) and the Root Mean Square (RMS) values (Stephenson and Agapiou, 1996).

The Rank Taylor Hobson Talysurf is a typical stylus instrument, which provides a selection of roughness and waviness parameters, together with profile graphs. The measurement data are obtained via the movement of a stylus, at constant velocity, across the surface of the specimen. This movement is amplified electronically and the data automatically analysed. The parameter values are then selectable at will from the stored information.

### **2.2.2 SURFACE INTEGRITY**

Surface integrity has been introduced to indicate the absence of undesirable features in the surface as well as in the subsurface region of the workpiece. It usually includes: strain hardening of a surface layer, cracking, phase transformations and residual stresses (Neailley, 1988). Some of these characteristics may be beneficial while most of them are harmful. Some aspects of surface integrity can be evaluated only by destructive techniques (metallography), whereas others can be explored under the microscope, particularly, the SEM. On the basis of such tests, cutting conditions that ensure good surface integrity can be specified (Trent, 1991, Stephenson and Agapiou, 1996). For the most critical applications, non-destructive test (NDT) techniques including x-ray analysis for residual stress have been employed (Brinksmeier et al, 1982).

Abrao et al (1996) found that, when machining hardenable alloy steels, two main types of microstructural change might occur, depending on the maximum temperature reached at the workpiece surface and subsurface. If the temperature exceeds the austenitisation limit, austenite will transform to produce an untempered martensitic structure after quenching, which is very hard and brittle, and generally referred to as a white layer. An overtempered martensitic structure is observed underneath this white layer when the temperature in the region exceeds the original tempering temperature. Such a region is usually dark in colour and possess low hardness and wear resistance.

Both tool materials and workpiece materials may influence the subsurface structure. In finishing AISI H13 steel, the depth of the white layer appeared slightly larger for

samples cut with DBC50 than those cut with ceramic tools, but there was no obvious overtempered martensitic layer. However, in finishing and roughing AISI E52100 steel, a dark overtempered martensitic layer could be seen in all the specimens (Abrao et al 1996). It has also been reported that the thickness of the white layer is related to the size of the cutting tool wear flat and with wear flats up to 0.06 mm no white layer could be observed (Konig et al, 1994). Recently, in machining EN24 steel, Barry and Byrne (1998) found that no white layer was observed in specimens machined with new tools (Alumina, PCBN), while white layers with a maximum depth of 6  $\mu\text{m}$  were formed using worn tools.

It is known that surface sensitive mechanical properties such as creep and fatigue are greatly influenced by the stress condition of the machined surface. Abrao et al (1996) compared the residual stress variations of hardened bearing steels, after turning with both new and worn PCBN cutting tools and grinding. It was found that compressive stresses induced in each specimen and the depth of the compressive residual stresses zone was much shallower with a new insert. With turned samples the highest stress value was obtained at approximately 5-20  $\mu\text{m}$  below the machined surface. In contrast, the highest stress value given by the ground specimen was measured on the surface. Fleming et al (1998) reported similar results when machining forged QS32 steel (similar to EN31) using DBC50 tools.

### 2.3 FORCES IN METAL CUTTING AND STRESSES ON THE TOOL

The forces acting on the tool are important aspects of machining. For those concerned with the manufacture of machine tools, a knowledge of these forces is needed for estimation of power requirement and for design of structures adequately rigid and free from vibration. The cutting forces vary with the tool angles, and accurate measurement of forces is helpful in optimising tool design (Trent, 1991). In addition, cutting forces are also an indicator of the machinability of the workpiece material. Lower cutting forces generally imply lower tool wear rates, better dimensional accuracy and increased machine tool life (Stephenson and Agapiou, 1996).

For a semi-orthogonal cutting operation in lathe turning, the force components can be measured in three directions (Figure 2.4) and the force relationships are relatively simple. The component of the force acting on the rake face of the tool normal to the cutting edge, in the direction OY is called here the “cutting force”,  $F_c$ . This force, which tries to bend the tool, is usually the largest of the three force components, and acts in the direction opposite to the workpiece rotation. The force component acting on the tool in the direction OX, which opposes the feed, is referred as the “feed force”  $F_f$ . The third component, acting in the direction OZ, which tries to press the tool backwards, is called the “radial force”,  $F_r$ . This is the smallest of the force components in semi-orthogonal cutting and, for purposes of analysis of cutting forces in simple turning, it is usually ignored and often not even measured.

The magnitude of these forces depends primarily on the cutting parameter (feedrate, speed and depth of cut), cutting rake angle, workpiece material and tool material. The forces increase in direct proportion to increments in the feed and the depth of cut and an increase in rake angle gives rise to a decrease in both the cutting and the feed forces. However, increase in the rake angle will weaken the tool edge which may well lead to its premature failure.

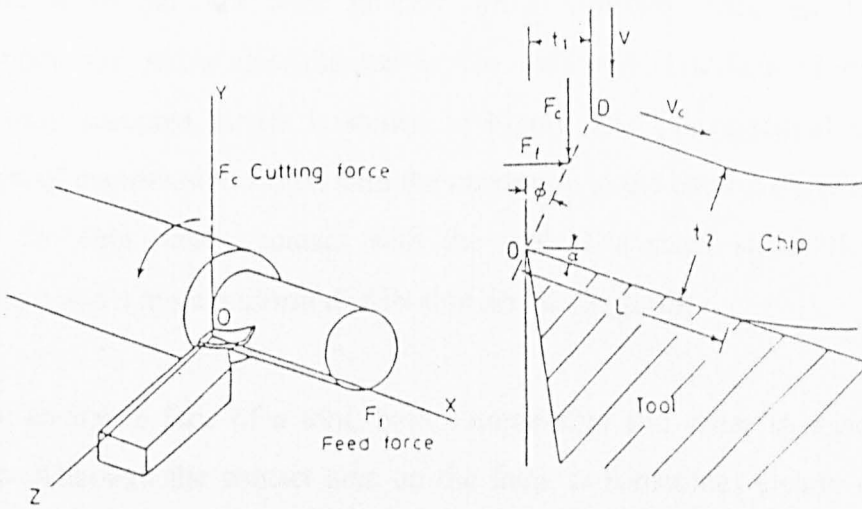


Figure 2.4 Forces acting on cutting tool (Trent, 1991).

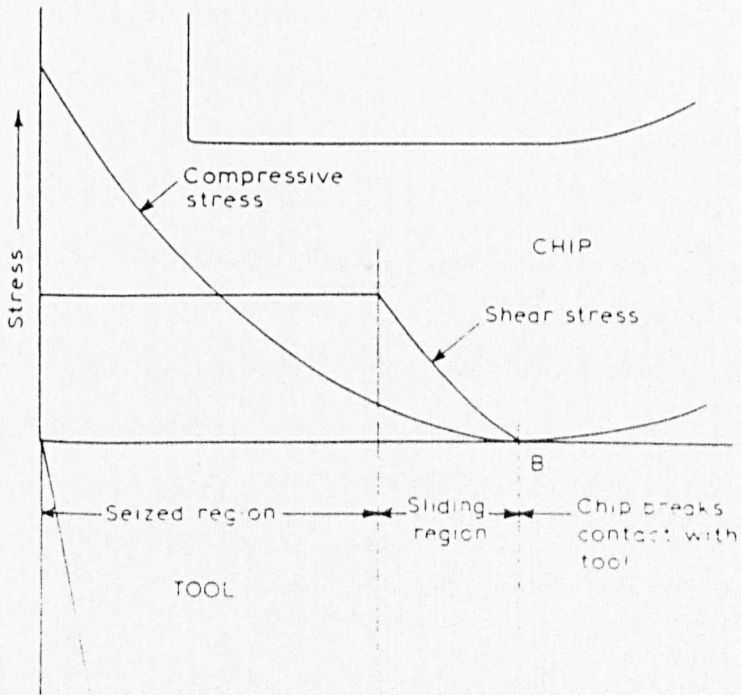


Figure 2.5 Model of stress distribution on tool during cutting (Zorev, 1963).

The stress distribution on the tool in the chip formation process is of great importance in the tool wear process. Much research work has been done to investigate the stress distributions at the tool:work interface (Trent, 1991). A commonly accepted model is shown in Figure 2.5. The essential feature is the gradient of compressive stress, with the maximum at the cutting edge, falling to zero where the chip breaks contact with the tool. The shear stress shows a lower maximum and a more uniform distribution across the surface.

On the clearance face of a tool, both compressive and shear stresses act on this surface. Although the contact area on the flank is sometimes clearly defined, it is very difficult to arrive at values for the forces acting on it, and there are no reliable estimates for the stress on the worn flank surface (Trent, 1991).

## 2.4 THERMAL EFFECTS IN METAL CUTTING

### 2.4.1 HEAT GENERATION IN METAL CUTTING PROCESSES

During cutting by shearing, heat is generated in the primary and secondary shear zones due to plastic deformation of the workpiece material and also at the tool/chip interface (rake and flank faces) due to friction (Figure 2.6). Most of the heat generated is carried away by the chip while the rest is conducted through the tool and the workpiece.

The power consumed in metal cutting is largely converted into heat near the cutting edge of the tool and many of the economic and technical problems of machining are caused directly or indirectly by this heating action. The cost of machining is very much dependent on the rate of material removal and may be reduced by increasing the cutting speed and/or the feed rate. However, these factors are strongly constrained by the effects of high temperature associated with the increase of these parameters. It was noted as early as 1907 by F.W. Taylor that increased cutting speeds resulted in increased tool temperature and, hence, lower tool life. When machining ferrous alloys at moderately high cutting speeds, high temperatures are generated and tool wear is activated by mechanisms such as diffusion and dissolution. Deformation due to compressive stresses also plays a part when machining using conventional tool materials. Excessive heat generation and high temperature gradients may also reduce the integrity of the finished surface. However, a lower limit of cutting speed and feed is also required when cutting some very hard materials, in order to generate sufficient heat to soften the work material (Heath, 1986).

The temperature generated during a machining operation is influenced by the properties of the work materials to be cut and the machining parameters used. Higher temperatures are to be expected in cutting stronger materials at higher speeds, especially when the workpiece material is a poor heat conductor, of low density, and low specific heat. This is one of the reasons why materials such as titanium and

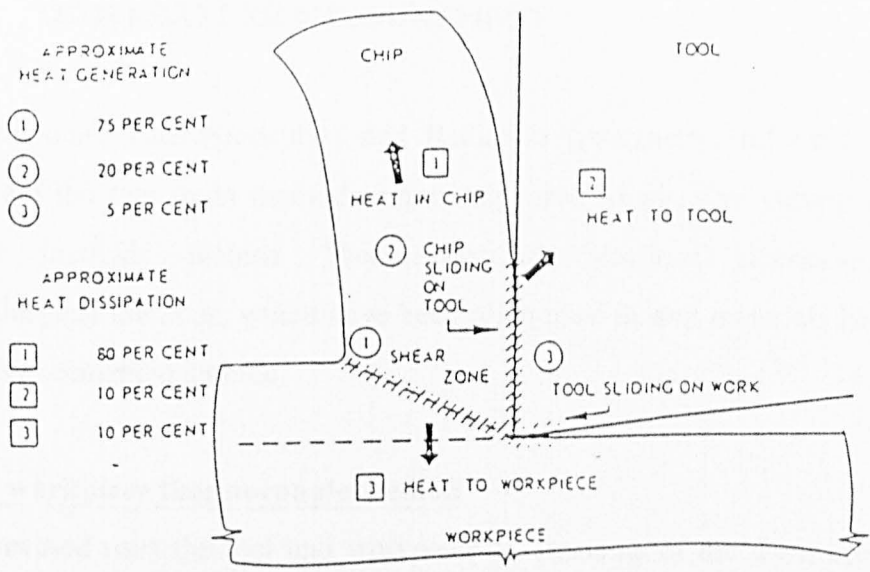


Figure 2.6 Energy partition (heat generation and heat dissipation) in the machining of steel (Komonduri, 1982).

superalloys are difficult to machine, whereas aluminium and magnesium are easy (Trent, 1991, Shaw, 1984).

## 2.4.2 TEMPERATURE MEASUREMENT

Thermo-e.m.f (thermocouples) and Radiation (pyrometry, infra-red photography, etc.) are the two main methods commonly used to measure cutting temperatures. Other methods include Thermo-chemical reactions (thermo-colours) and metallurgical methods, which have been often used in tool materials like high speed steel and cemented carbide.

### Tool: workpiece thermocouple method

This method uses the tool and workpiece as elements of the thermocouple (Figure 2.7). The hot junction is the interface between the tool and the workpiece, the cold junction is formed by a remote section of the tool and workpiece, which must be connected electrically and held at a constant reference temperature (Stephenson and Agapiou, 1996). Due to the fact that the e.m.f. generated is the sum of the individual e.m.f.'s which are generated at all the contacting points between chip and tool, the measured temperature is the average of the temperature field which acts over the whole chip-tool contact zone (Barrow, 1973). This method can only be used when the tool and the workpiece are electrical conductors and thus cannot be used with many ceramic cutting tools. The main advantages of this method include: repeatable results, good correlation with tool wear, quick time response, etc..

### Embedded thermocouple

This method is also known as the conventional thermocouple method (Stephenson and Apegiou, 1996) or implanted or remote thermocouple method (Abrao et al, 1996). In this method, one or more conventional thermocouples are embedded in the tool or workpiece to measure the temperature very near the cutting zone. Figure 2.8 shows schematically a typical set-up for measuring the cutting of PCBN and ceramic tools in machining of AISI E52100 bearing steel. The K-type (nickel-chromium/nickel-aluminium) thermocouple is the most popularly used detector. It

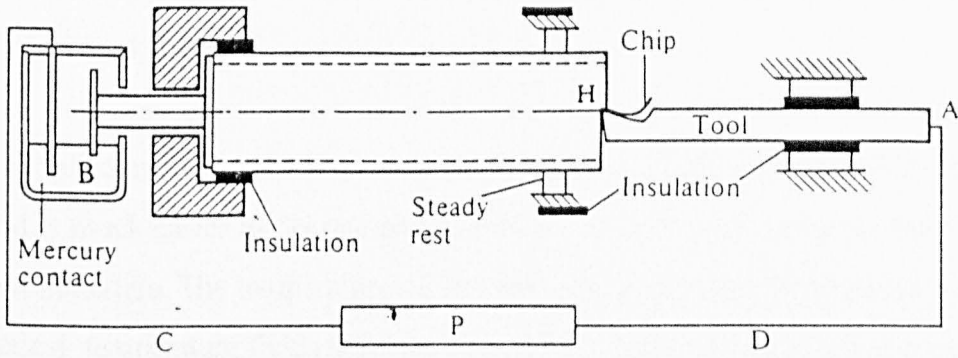


Figure 2.7 Schematic to show the set-up of a tool-chip interface method (Shaw, 1984).

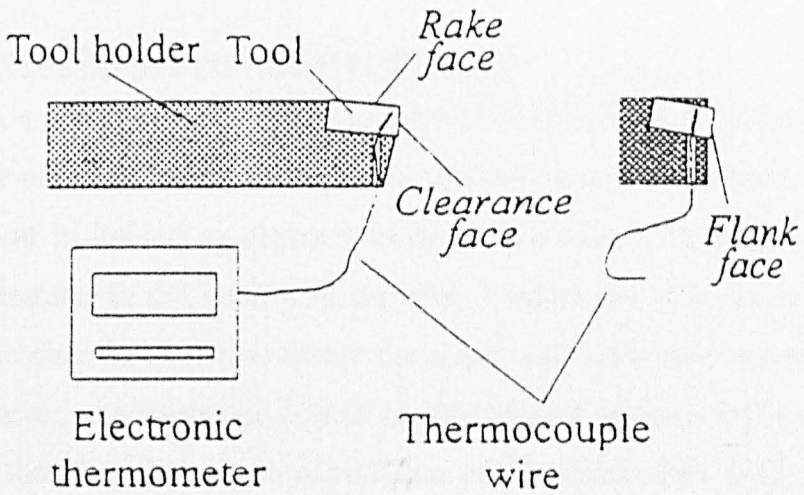


Figure 2.8 Schematic to show the set-up of an embedded thermocouple method (Abrao et al, 1997).

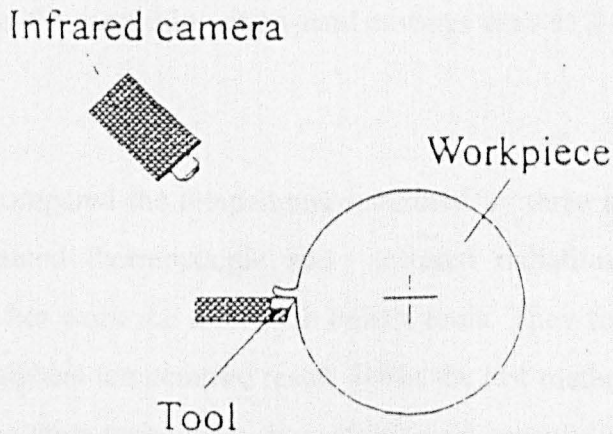


Figure 2.9 Schematic to show the set-up of radiation method (Abrao et al, 1997).

has an operating temperature range between  $-200^{\circ}\text{C}$  to  $1100^{\circ}\text{C}$  and has an almost linear e.m.f. response to temperature rise, as well as good resistance to oxidation (Michalski et al, 1991).

The thermocouple can also be positioned at the back of the cutting tool insert. This method is much easier to operate and avoids the difficulty of producing the holes in the tool materials. The temperature of the real cutting edge can be deduced based on theoretical temperature fields (Lipman et al, 1967). This method is not as accurate as the other method when the thermocouple is much closer to the cutting zone. However, the required thermocouples can be built into the tool holder, making the method attractive for routine measurements and process monitoring.

### **Radiation (pyrometry, infra-red photography, etc.)**

In this method, a pyrometer, also called an infrared thermometer, is used to measure the temperature of a body based on its emitted thermal radiation. As shown in Figure 2.9, this method is limited to exposed surfaces and cannot be used to directly measure temperatures in the interior of the chip. Furthermore it is not possible to measure the interface temperatures where the actual tool/workpiece cutting zone is obscured. However, one advantage offered by this method is that it is a non-contact technique and therefore there is no disturbance of the temperature field. With the development and application of ultrahard tool materials, this method is more likely to be chosen due to the fact that these tool materials are extremely difficult to machine (e.g. drilling a hole for a thermocouple). For example, it has been used to measure the cutting temperature in the machining of Ni-hard castings with PCBN tools (Crooks et al, 1988)

Abrao et al (1996) compared the temperature measured by three methods: tool/chip thermocouple, implanted thermocouple and infrared radiation technique when machining hardened hot work die steel with PCBN tools. They found that the first method yielded the highest temperature result whilst the last method give the lowest value. In addition, the three techniques showed different sensitivity to the change of cutting parameters, i.e. cutting speed, feed rate and depth of cut (Table 2.1)

**Table 2.1** Significance of the effect of cutting parameters on the temperature measured using different techniques (Abrao et al, 1996)

Technique \ Cutting parameters	Cutting speed	Feed rate	Depth of cut
Infrared radiation	***	**	*
Implanted thermocouple	*	***	**
Tool/chip thermocouple	***	*	**

\*\*\* : Most significant

\* : Least significant

## 2.5 CUTTING TOOL MATERIALS

### 2.5.0 DEVELOPMENT OF CUTTING MATERIALS

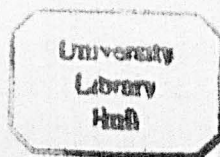
The continual developments in metal cutting tool materials have played a significant role in advancing machining technology. The improved performance and increased tool life made possible by such new materials have been instrumental in achieving the strict dimensional tolerances and surface finishes required to ensure interchangeability of mass-produced components (Bossom and Hoffmann, 1993). As shown in Figure 2.10, advanced tool materials have made it possible to cut at much higher speeds. In another respect, new materials are expected to replace some readily-machinable materials in many areas of the automotive industry and in most cases these new difficult-to-machine materials will require harder and stronger tool materials.

Cutting tool materials can be classified into five groups (Roebuck, 1995, Stephenson and Agapiou, 1996)

- Carbon Tool Steel / HSS
- Sintered Tungsten Carbide (WC)
- Cermets
- Ceramics
- Superhard PCBN and PCD

Cutting processes are very complicated, and no single material exhibits all the desirable properties for a cutting tool (Stephenson and Agapiou, 1996). However, some important considerations must be taken into account when assessing a tool material. These include: 1) High temperature physical and chemical stability; 2) Resistance to fracture; 3) Abrasive wear resistance (Edwards, 1993).

High temperature stability could be represented in terms of hot hardness, thermal shock resistance and adhesion and diffusion resistance at elevated temperatures. It has been shown that, at high temperatures developed in cutting hard materials at high



speed, the hardness of almost all the cutting tool materials decreases to some extent. However, some materials (e.g. PCBN) can retain their hardness to a very high temperature. Thermal shock resistance is determined by the coefficient of thermal expansion and thermal conductivity of the tool material and is of particular importance for alumina-based materials. Adhesion and diffusion resistance is difficult to assess, but, some techniques have been successfully applied to study these properties of tool materials.( Nabhani, 1991, Konig et al, 1993).

The most important property to resist brittle fracture is toughness. Two commonly used items to represent the toughness of a material are Fracture Toughness ( $K_{IC}$ ) and Transverse Rupture Strength ( $Nmm^{-2}$ ) (Clark et al, 1993). Figure 2.11 shows the hardness and toughness of the tool materials and developing trends. This shows the complexity in selecting a tool material, e.g. very hard materials tend to be brittle and thus have poor fracture toughness. The best tool material for a given application depends on not only the tool itself but also on other factors, such as the workpiece, the machine and the tool holder etc..

The hardness of a tool material has a significant effect on its abrasion resistance. It had been thought that abrasion resistance was not a problem with ultrahard tools materials but this has had to be reconsidered in the light of advanced workpiece materials such as fibre and particle-reinforced composites.

### **2.5.1 HIGH SPEED STEEL (HSS) AND RELATED MATERIALS**

High speed steels (HSS) are self-hardening steels alloyed with W, Mo,Co,V and Cr. They exhibit “red hardness” which permits tools to cut at dull red heat without loss of hardness or rapid blunting of the cutting edge. HSS has a hardness range from HRC60-65, however, this decreases rapidly at temperatures above 540 to 600°C (Shaw, 1984). In addition, HSS’s have limited wear resistance and chemical stability and greater tendency to form a built-up-edge than other tool materials. Therefore they are only suitable at relatively low speeds (>50 m/min) (Stephenson and Agapiou,

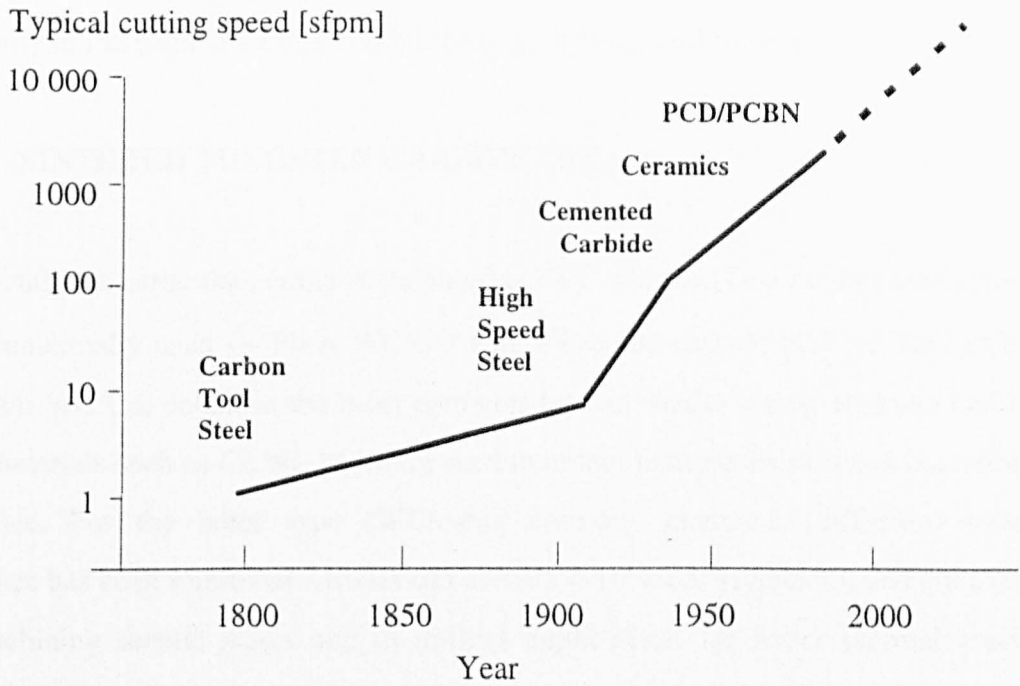
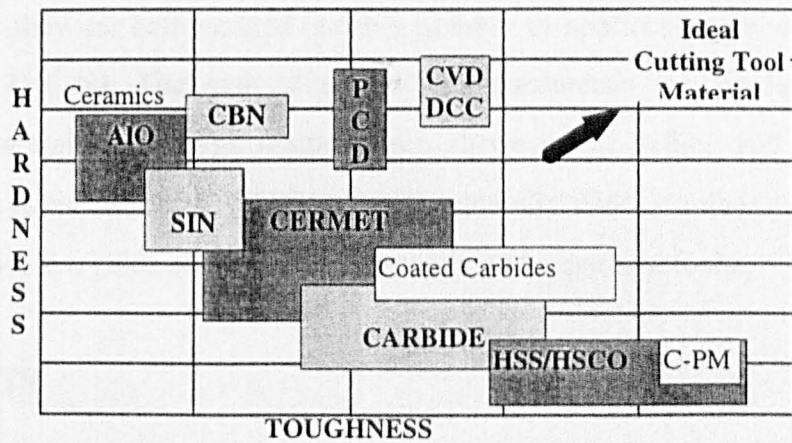


Figure 2.10 Development of tool materials (Bossom and Hoffmann, 1993)



DCC: Diamond coated carbide,  
SiN: Silicon nitride ceramic,

C-PM: Coated powder metallurgy steel  
AIO: Aluminium oxide ceramic

Figure 2.11 Improvement of the toughness and hardness of the cutting tool materials (Stephenson, 1996)

1996). HSS's are inexpensive, easy to shape or resharpen, and have excellent fracture toughness and fatigue and shock resistance. Thus they are still commonly used, especially in interrupted cutting conditions (e.g. drilling, end-milling).

### **2.5.2 SINTERED TUNGSTEN CARBIDE (WC)**

Hardmetals are particulate composites based on WC and Co. Two fundamental types are commercially used — Plain WC/CO and WC/cubic carbide (TiC or TaC )/Co. For plain WC/Co, cobalt is the most common type of binder phase. In some cases, other materials such as Cr, Ni, Mo were used to obtain better corrosion and oxidation resistance. For the latter type (WC/cubic carbide), chemical (diffusion) wear resistance has been improved. Grades can contain 4-16% TiC (typically) and are used for machining ferritic steels and in milling applications for better thermal crack resistance. TiC and TaC also improve the creep strength in substrates for coated hardmetals (Roebuck, 1995).

In cutting tool markets hardmetals, either coated or uncoated, are the technological work-horses, but they are being edged out in a number of applications by ceramics, superhards and Ti(C,N). The main drawback of hardmetals include lower hot hardness and low stability at high temperatures. However, in milling and drilling, where toughness is required, the WC-Co alloy is generally used. Another advantage of hardmetals is its low price compared with ceramic and superhard tools.

### **2.5.3 CERMETS**

Cermets are TiC-, TiN- or TiCN-based hardmetals, consist of hard particles (TiC or TiN) sintered with a refractory metallic binder (e.g. Ni, Co, W, Ta, or Mo). Cermets have better diffusion wear resistance, but lower resistance to fracture and higher thermal expansion coefficient than sintered tungsten carbide materials. Cermets are generally used in semi-finishing to finishing applications and are especially suitable for high speed finishing applications. The speed range is 200m/min to 400 m/min, i.e. higher than that of WC but lower than that of ceramics. Cermets perform well

when machining most superalloys, malleable irons, carbon and alloy steels, hardened steels, stainless steels and non-ferrous alloys, e.g. brass, zinc and copper (Stephenson and Agapiou, 1996).

#### 2.5.4 CERAMICS

Ceramic cutting tool materials, made by sintering, offer great resistance to wear and show little tendency towards diffusion. However, their brittleness and low thermal shock resistance lead to fracture, which often ends tool life prematurely. This has limited the application of ceramic tools in some conditions and they are not usually recommended for interrupted cutting (Trent, 1991). Sufficient rigidity of the machine, workpiece and the tool, together with high machine power and a suitable arrangement of the cut-in and cut-out conditions are all pre-conditions for economic use of these tools.

There are three main types of ceramic tools (Roebuck, 1995): —

- a)  $\text{Al}_2\text{O}_3$  based — including monolithic  $\text{Al}_2\text{O}_3$ , and those with either whisker additions for increased toughness or particulate additions for increased strength.  $\text{SiC}_w$ , TiC and  $\text{ZrO}_2$  are three commonly used additions.
- b)  $\text{Si}_3\text{N}_4$  based — including monolithic  $\text{Si}_3\text{N}_4$ , Sialons, and  $\text{Si}_3\text{N}_4$  reinforced by whiskers of  $\text{SiC}_w$  or TiC particulates.
- c) SiC based — this type is more for wearing parts than cutting applications.

Cast iron and superalloys account for half of all materials machined by ceramics. In the automotive sector, ceramic tools are used to machine grey cast-iron brake drums, discs and cylinder blocks (Roebuck, 1995). They were used for finishing operations and produced surfaces similar to those produced by grinding when cutting cast irons. When machining nickel-based alloys, the risk of premature tool failure, and the possibility of subsequent component failure, restricted the application of ceramic tools to intermediate/semi-finishing operations (Richard and Aspinwall, 1989). Application to machining steels was mainly limited to mild steel in the early stages,

but more recently their application has been extended to hardened alloy steels (Mehrotra, 1998).

Alumina tools can be used to cut steel at speeds much higher than can be used with conventional cemented carbides. Negative rake throw-away tool tips are nearly always used and it is not difficult to demonstrate that cutting speeds of 600-700m/min can be sustained at a feed of 0.25mm/rev for long periods without excessive flank and crater wear (Brandt, 1986). Gradual failure was observed involving flaking of thin fragments from the rake or clearance faces. It seems to be an advantage of alumina tools that such fracture does not always lead to sudden and massive failure of the whole tool edge with major damage to the work-piece, such as would occur after the fracture of the edge of carbide tools. However, unpredictable and variable tool life is still a major problem when using ceramic tools. Ceramic tools are generally recommended for use at high speed only since at lower speeds such tools tend to fail because of their poor toughness and transverse rupture strength (King et al, 1984). However, according to some researchers (Chattopadhyay et al, 1983), when cutting C-15 steel with a series ceramic cutting tools, grooving wear was almost absent at low speed ( $75\text{m min}^{-1}$ ) which suggested that modern ceramic tools also can be used at lower speeds if required.

The recent developments in ceramic tool materials have focused on improving fracture resistance so they can be used in a tougher conditions (Mehrotra, 1998). With the development of reinforced materials, the application of ceramic tools has been increased. Composite ceramics such as 30% TiC- $\text{Al}_2\text{O}_3$ , can be used for uninterrupted cuts on hardened steels, chilled cast irons and cast irons with hard scales.  $\text{SiC}_w$ -  $\text{Al}_2\text{O}_3$  ceramics have better hot edge toughness, hot hardness and thermal shock resistance than conventional ceramics. They can therefore withstand the high stresses incurred when cutting high temperature aerospace alloy turbine parts.  $\text{Al}_2\text{O}_3$ -SiC reinforced cutting tools are in general the best tool for cutting Nimonic and other aerospace materials at high cutting speeds where the high temperatures tolerated by the tool allows the workpiece to be softened and cut more

easily. SiC is attacked by iron at 1200°C to form iron silicide, so these tools cannot be used to machine low/medium strength steels (Billman et al, 1988)

Sialons ( $\text{Si}_3\text{N}_4 + \text{Al}_2\text{O}_3 + \text{sintering aids}$ ) are mainly used in rough machining of superalloys and cast iron (Edwards, 1993). The most important property of Sialons is their low coefficient of thermal expansion and high thermal conductivity, so that the stresses between hot and cool parts of a cutting tool insert are minimised, giving good thermal shock resistance. Other beneficial properties also include high hardness, high bend strength and high toughness. Sialons cannot be used for general steel machining because they are not chemically stable in contact with Fe and suffer rapid diffusion wear (Reobuck, 1995).

### **2.5.5 POLYCRYSTALLINE CUBIC BORON NITRIDE**

Polycrystalline Cubic Boron Nitride (PCBN) cutting tools were developed in the 1970's and have gained an important position in the cutting tool industry because of their excellent performance. PCBN has high hardness and fracture toughness compared with ceramic tools and good thermal stability and better chemical stability with ferrous elements than diamond.

PCBN tools compete with ceramic tools, especially with  $\text{SiCw-Al}_2\text{O}_3$  tools (Roebuck, 1995). No apparent advantage of PCBN over hardmetal has been found at medium speed. The superior performance of PCBN tool material in terms of higher material removal rate has been shown in many areas. Materials suitable for machining with PCBN tools include hardened alloy steel, cobalt-base alloys, nickel-base alloys and tool steels. In addition, cast irons and nickel/chromium cast iron can be machined at very high speeds.

### **2.5.6 POLYCRYSTALLINE DIAMOND (PCD)**

Diamond is the hardest material known and has long been employed as a cutting tool although its high cost has restricted its use to operations where other tool materials

cannot perform effectively. There are two groups in terms of their composition: type a) contains cobalt metal binder and type b) contains a ceramic binder, based on SiC. PCD is made by a two step process in high pressure (6-7GPa)-high temperature (1500 °C) equipment (Nabhani, 1991). In the first stage, graphite is transformed to diamond powder. In the second stage, this powder is compacted and grown together with a binder (Wentorf et al, 1980).

PCD has a number of superior physical and mechanical properties compared with other tool materials.

### 1) High hardness

The hardness of both single crystal diamond and PCD decreases as the temperature increases as with other tool materials. Brookes and Lambert (1982) have shown that the high temperature hardness of diamond is still much higher than that of other tool materials.

### 2) Thermal Conductivity

PCD has a comparatively high thermal conductivity of about 560 W/m°C. This is slightly lower than that of natural diamond (665 W/m°C)

### 3) Abrasion Resistance

PCD tooling has higher abrasion resistance than natural diamond. The high abrasion resistance of PCD with its high resistance to loading enables it to be used for effective machining of non-ferrous materials.

The polycrystalline diamond tools are aggregates of randomly orientated diamond particles, which behave as an isotropic material in many applications. The main advantages of sintered polycrystalline tools over natural single crystal tools are better control over amounts of inclusions and imperfections, higher quality, greater toughness and wear resistance resulting from the random orientation of diamond grains and the corresponding lack of simple cleavage planes. In cutting operations, their wear behaviour demonstrates that the edges are less sensitive to accidental

damage, while maintaining exceptional resistance to wear. Therefore, PCD tools can maintain an accurate cutting edge for very long periods of time and this has made them successful competitors in specific areas of machining.

The use of PCD in commercial quantities started in the early 1970s. PCD tools commercially available as Compax tools were produced by the General Electric company, USA, and Syndite produced by De Beers. Composite tools can be clamped or brazed, ground, lapped and polished. Worn composite tools can be reground but the grinding taking longer than for carbide tools (Nabhani, 1991).

In the early years, PCD was introduced very much on a one-off basis, usually only in operations which caused particular problems for conventional carbide tooling. However, this situation has changed with the widespread demand for high productivity in industry. Now, PCD tools are being used in a much wider field of application, especially in automotive industry. The distinct advantages offered by PCD tooling compared to carbide include superior tool life and surface finish, higher cutting speeds, reduced cycle times and minimal machine down time (Roebuck, 1995).

Diamond tools are not suitable for cutting ferrous workpieces due to their reactivity with these workpieces. The tool are smoothly worn by a mechanism which appears to involve transformation of diamond to a graphitic form and/or interaction between diamond and iron at the atmosphere. Diamond is not a stable form of carbon at atmospheric pressure, but does not revert to the graphitic form in the absence of air at temperatures below 1500°C. In contact with iron, however, graphitisation begins just over 730°C (Hitchener et al, 1981) and oxygen begins to etch a diamond surface at about 830°C. Diamond tools are rapidly worn when cutting nickel also and generally they have not been recommended for machining high melting point metals and alloys where high temperatures are generated at the interface.

They are therefore better suited to cutting non-ferrous (Al, Cu, Brass, Bronze) alloys, abrasive advanced composite materials including graphite, carbon/carbon, carbon-



## 2.6 CUTTING TOOL WEAR

### 2.6.1 TOOL WEAR FORMS

In terms of the position of wear on the tool or the shape of the wear, tool wear can take the following forms:

#### **Flank wear**

Intense rubbing of the flank of the tool over the freshly formed surface of the workpiece results in the formation of a wear land. The rate of wear can be measured by interrupting the cut and measuring the average width of the wear land  $VB$ . After rapid wear during the first few seconds, wear settles down to a steady-state rate only to accelerate again toward the end of tool life (Figure 2.12). Flank wear is due usually to both abrasive and adhesive mechanisms and is generally undesirable because dimensional control is lost, surface finish deteriorates and heat generation increases.

Flank wear can be measured in terms of the time to reach a certain amount of flank wear ( $VB$ ). Another way to assess flank wear was to measure the width of the wear land within a certain period of time. Scanning electronic microscopy is commonly used to measure flank wear and it also can be readily determined by means of a tool-maker's microscope. Other methods, such as profile projection, have also been used by some researchers. (Lin et al, 1995).

#### **Crater wear**

Crater wear or rake face wear produces a damage some distance away from the tool edge on the tool face (Figure 2.12). The high temperatures generated on the rake face combine with shear stresses to create a crater. Moderate crater wear usually does not limit tool life. In fact, crater formation increases the effective rake angle of the tool and thus may reduce cutting force (Stephenson and Agapiou, 1996). Under very high speed cutting conditions crater wear is often the factor that determines the life of the cutting tool, since the cratering becomes so severe that the tool edge is weakened and

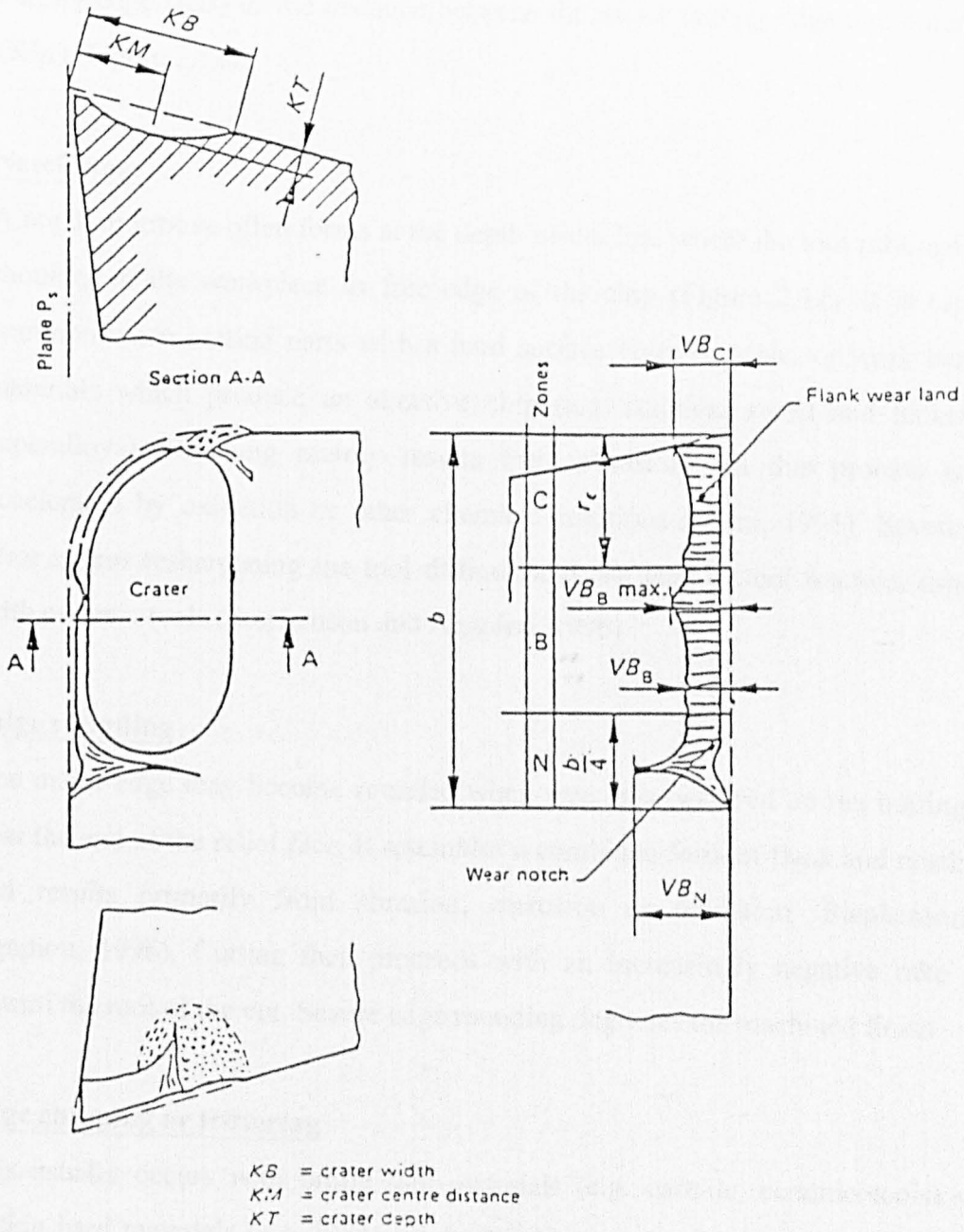


Figure 2.12 Types of wear on turning tools after BS 5623 (1979).

eventually fractures. Crater wear progresses linearly under the influence of abrasion, adhesion, followed by dragging out of tool materials, diffusion, or thermal softening and plastic deformation. Crater wear can be minimised by increasing the chemical stability of the tool material or by decreasing the tool's chemical solubility in the chip, e.g. applying coating on the tool surface. Crater wear is usually quantified by measuring the depth  $K_T$ , the cross-section area of the crater perpendicular to the cutting edge ( $K_B$ ) or the distance between the major cutting edge and crater centre ( $K_M$ ) (Figure 2.12).

### **Notch wear**

A notch or groove often forms at the depth-of-cut line where the tool rubs against the shoulder of the workpiece or free edge of the chip (Figure 2.12). It is especially common when cutting parts with a hard surface layer or scale, or work hardening materials which produce an abrasive chip (e.g. stainless steels and nickel-based superalloys). Notching mainly results from abrasion and this process is often accelerated by oxidation or other chemical reactions (Trent, 1991). Severe notch wear makes resharpening the tool difficult and can lead to tool fracture, especially with ceramic tools (Stephenson and Agapiou, 1996).

### **Edge rounding**

The major edge may become rounded when wear has occurred on the trailing edge near the end of the relief face. It resembles a combined form of flank and notch wear and results primarily from abrasion, corrosion or oxidation (Stephenson and Agapiou, 1996). Cutting then proceeds with an increasingly negative rake angle toward the root of the cut. Severe edge rounding degrades the machined finish.

### **Edge chipping or frittering**

This usually occurs with brittle tool materials (e.g. carbide, ceramic tools) when cutting hard materials (e.g. hardened steel) or materials with hard spots (e.g. metal matrix composite). Interrupted cuts also increase the possibility of edge chipping. This form may occur on a small scale (e.g. a few particles) or on a large scale (e.g. a segment of the cutting edge). In addition, periodic break-off of the BUE may also

cause edge chipping (Trent, 1991). Chipping results in poor surface finish and can lead to tool breakage.

### **Edge cracking**

When a tool is subjected to cyclic mechanical loading (e.g. interrupted cutting) or thermal loading (e.g. when cutting with coolant), cracking of the cutting edge may occur. The crack may be parallel or perpendicular to the cutting edge of tools (comb cracks). The former type results from the mechanical loading while the latter type results from thermal loading. This cracking leads to rapid tool fracture or chipping.

### **Catastrophic failure**

Tools made of brittle materials are subject to sudden failure (breakage). This is a problem with all brittle materials such as ceramics and cemented carbides, especially with interrupted cuts. The likelihood of cutting tools fracturing under exit conditions are much higher than under steady cutting or entry conditions based on tests using tungsten carbide tools (WC+6%Co) (Lee et al, 1984). Improved tool manufacturing processes, zero or negative rake, and selection of the proper machining conditions all help in the avoidance of catastrophic failure.

## **2.6.2 Tool wear mechanisms**

The most common wear mechanisms encountered in metal cutting are described below.

### **Abrasive wear**

This type of wear occurs when hard particles abrade and remove material from the cutting tool. There are machining operations in which the work-piece material contains hard particles, such as non-metallic inclusions (e.g. carbides) or adhering sand in sand-cast parts. Particles pulled out from the cutting tool material itself may also abrade the tool surface and result in so-called self-abrasive wear (Nabhani, 1991, Chen 1993). In addition, the hard particles may also result from the chip or from a

chemical reaction between the chips and cutting fluid, as in the case of sintered steel (Stephenson and Agapiou, 1996). Abrasive wear by hard particles entrained in the cutting fluid is sometimes called erosive wear. Abrasive wear is usually the primary cause of flank wear, notch wear and edge rounding. As such, it is often the form of wear which controls tool life, especially at low cutting speeds.

### **Adhesive wear**

When surfaces rub together, particularly in the absence of lubricant films, some adhesion occurs at the points of rubbing contact. The friction force is primarily the force required to shear the junctions so formed. The adhesion junctions will be subsequently broken and a relatively large fragment may be removed from the tool by fracture. One example of this is the interaction between a soft metal like copper and a hard brittle material like sapphire. Buckley (1967) has shown that under conditions of strong adhesion the copper can pluck pieces of sapphire out of the harder surface.

Adhesive wear rates are usually low, so that this form of wear is not usually significant. However, significant adhesive wear may occur with built-up edge formation, since the BUE can result in chipping of the tool.

### **Attrition wear**

Attrition describes a wear process in which the tool shape is changed by the periodic removal of distinct small fragments of the tool material. These fragments are usually a few microns in size, or possibly just less than a micron. In certain cutting conditions, the high contact stresses and the high temperatures generated together with some other favourable conditions make it difficult to prevent seizure between tool and work materials at the interface (Trent, 1991). In many operations, conditions are such that the two surfaces are not completely bonded together for the whole cutting time, but are periodically separated over part of the interface. This is particularly true if the tool is ploughing in and out of the workpiece material, if a

built-up edge is formed on the tool and is periodically broken away, or if the machine tool lacks rigidity so that vibration occurs. Under these conditions, small fragments are frequently removed from the tool surface as work material bonded to it is pulled away or flows unevenly across the tool. This is most likely to occur at relatively low speeds and it subjects very small local areas of the tool to tensile stresses. High speed steel tools are found to be resistant to attrition wear better than carbide tools in many conditions (Trent, 1991).

### **Diffusion wear or solution wear**

In this type of wear, a constituent of tool material (e.g. metal or carbon atoms) diffuses into or forms a solid solution with the chip material. This weakens the tool surface and contributes to the formation of a crater on the rake face of the tool.

The rate of diffusion wear depends on temperature and also on the rate of solution of the tool in work material. This is particularly important for cemented carbide tools. Tungsten carbide (WC) is dissolved easily in hot steel and for this reason WC-Co tools fail as a result of rapid crater wear when cutting steel at high speeds. TiC and TaC are much less readily dissolved and the rate of crater wear of cemented carbides based on these two materials is much lower (Trent, 1991).

Diffusion wear is most clearly demonstrated in relation to cratering at the hottest part of the tool. It is also a major factor in flank wear during the high speed cutting of cast iron and steel. As the cutting speed is raised, the rate of flank wear increases. The rate of flank wear also can be reduced by addition of TiC and TaC to WC-Co alloy tools. Where tool life depends on diffusion wear, the chemical composition of the tool material is of more importance in relation to wear resistance than mechanical properties such as hardness.

## **Plastic deformation**

Plastic deformation is classified as a permanent change in shape or size of a solid body without fracture. This process is a direct result of the application of sustained stress beyond the elastic limit. It differs from tool wear in that no tool material is actually removed. Plastic deformation occurs when there is a high concentration of compressive stress at the tool rake face ( close to the cutting edge ) making the tool edge deform downwards and causing an acceleration of various wear processes which ultimately reduce the life of the tool.

## **Chemical wear**

In contrast to the wear processes controlled by the mechanical behaviour of materials, cutting tools can wear by the chemical dissociation of hard materials and the chemical dissolution of the dissociated materials in the workpiece. Chemical effects may contribute to both flank wear and crater wear and the wear scars are smooth compared to wear scars produced by other mechanisms. This type of wear is commonly observed when machining highly reactive materials (e.g. titanium alloys) (Hartung and Kramer, 1982).

## 2.7 MANUFACTURING PROCESS OF PCBN MATERIALS

### 2.7.1 FORMATION AND PROPERTIES OF CUBIC BORON NITRIDE

Cubic boron nitride is transformed from hexagonal boron nitride (HBN) at high temperature and high pressure (Wentorf et al, 1980). With boron and nitrogen, the two elements on either side of carbon in the Periodic Table, HBN could be formed using the reaction (Heath, 1986):



HBN is a slippery, friable substance with a hexagonal, graphite-like structure with approximately equal numbers of boron and nitrogen atoms arranged alternatively. It has good chemical inertness, excellent electrical insulating properties and also a low coefficient of friction (Gardinier, 1988)

In the synthesis of CBN, hexagonal boron nitride is dissolved into the solvent/catalyst within the high temperature and high pressure region (Figure 2.13), CBN then begins to nucleate and grow. Control of the nucleation and growth processes in the system is used to vary the physical properties of the CBN. The solvents used are metals (Mg) or metal nitride (AlN) and by enhancing the rate at which transformation occurs, they effectively reduce the pressure and temperatures required for synthesis to more easily attainable levels of about 60 kilobar and 1500 °C (Wentorf, 1980). CBN can readily be synthesised by the direct conversion of HBN to CBN in high-pressure equipment. By dissolving the unwanted matrix, the crystals of CBN can be liberated and recovered for subsequent processing.

CBN is made up of two inter-penetrating face-centred-cubic lattices, one of boron atoms and the other of nitrogen atoms. The structure of CBN is very rigid although not all the bonds between neighbouring atoms are covalent, about twenty five per cent of the bonding is ionic (Brookes and Lambert, 1982). This makes CBN the next hardest substance to diamond. The cleavage plane was suggested to be {110} while possible active slip system to {111}<1-10>. The Knoop hardness of CBN crystal, with a load of 500g, has been reported as 43.12GPa(001)[100], 29.89GPa(001)[110],

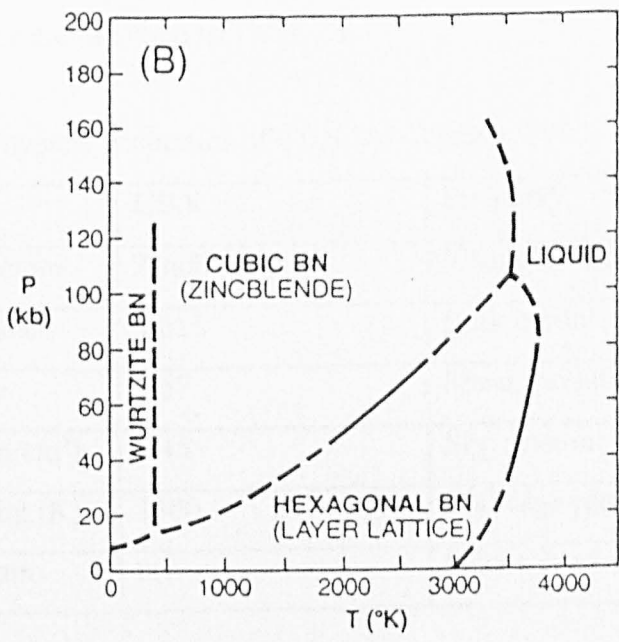


Figure 2.13 Pressure-temperature phase diagrams for boron nitride systems (Gardinier, 1988).

41.50GPa(111)[11-2] and 39.45GPa(111)[1-10] (Brookes, 1995). The physical properties are summarised in Table 2.2.

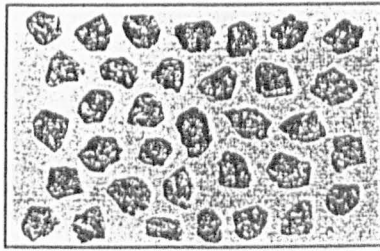
**Table 2.2** Physical properties of CBN (Al-Watban, 1996)

Property	CBN	Property	CBN
Crystal structure	Zincblende	Young's modulus (GPa)	730
Lattice constant	3.615	Bulk modulus (GPa)	290
Ion distance	1.57	Shear modulus (GPa)	332
Density (gm/cm <sup>3</sup> )	3.45	Slip system	{111}<1-10>
Melting point (K)	3500	Cleavage plane	{011}
Poisson's ratio	0.1	Knoop hardness (GPa)	HK30-45

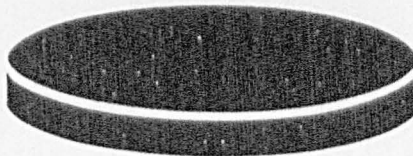
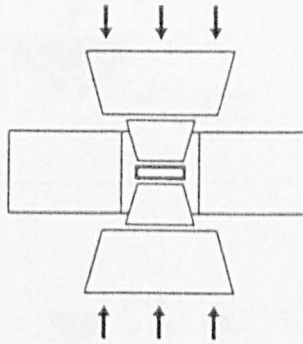
### 2.7.2 MANUFACTURE OF PCBN TOOLS

Polycrystalline cubic boron nitride is formed by sintering the cubic boron nitride particles together at high temperature and high pressure with addition of a solvent (Figure 2.14) and, in this process, the whole mass must be maintained in the cubic region to prevent the reverse transformation to hexagonal boron nitride (Figure 2.13) (Gardinier, 1988). The sintering process is resisted by the limited plasticity of CBN, which prevents the achievement of the applied pressure over whole grain surface (Pullman and Lewis, 1990). It was found that, in general, this type of ceramic has a di-phasic microstructure, whereby the individual grains are held within a secondary binder (or matrix) phase. Typically, the secondary phase found in industrial boron nitride tool materials is from the incomplete reaction of aluminium with individual cubic boron nitride grains and it is generally accepted that all nitride and boride forming metals react with cubic boron nitride (Walmsley and Lang, 1987).

The sintered products then can be processed into the following types of tool blanks/ inserts : solid inserts, full-face inserts and brazed inserts by laser cutting or EDM cutting (Figure 2.15).



CBN grits  
+  
Binder



PCBN disc

Figure 2.14 Manufacture process of PCBN materials (Seco Ltd, 1996).

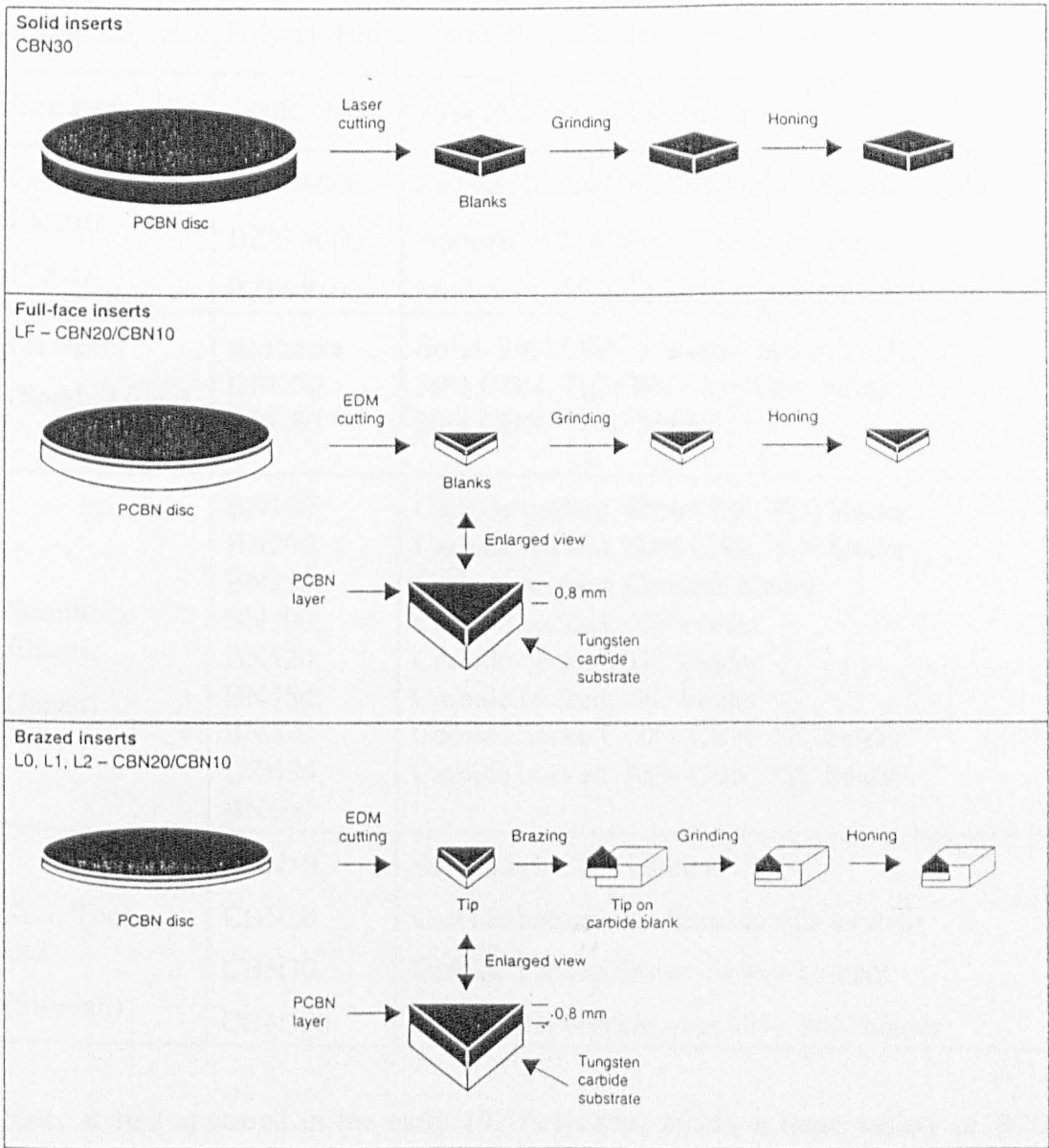


Figure 2.15 Types of PCBN tools and the shaping processes (Seco Ltd, 1996).

## 2.8 STRUCTURE AND PROPERTIES OF PCBN MATERIALS

**Table 2.3** Main Polycrystalline Cubic Boron Nitride (PCBN) Products

Company	Trade name	Type, Composition and structure
General Electric (USA)	BZN-6000,	Carbide backed, 90-95%CBN, Metallic binder
	BZN-8000	Approx. 50% CBN, Ceramic binder
	BZN-8100	Medium CBN content, Ceramic binder
De Beers (South Africa)	Amborite	Solid, 90% CBN, Ceramic binder (AlN)
	DBC50,	50% CBN, TiC+WC+Al+AlB <sub>2</sub> binder
	DBC80	80% CBN, Ti-Al binder
Sumitomo Electric (Japan)	BN100,	Carbide backed, 85% CBN, TiN binder
	BN200,	Carbide backed, 60% CBN, TiN binder
	BN250,	Carbide backed, Ceramic binder
	BN300,	Carbide backed, TiN binder
	BN520,	Carbide backed, TiC binder
	BN550;	Carbide backed, TiC binder
	BNX4,	Carbide backed, 70% CBN, TiC binder
GZB34 BN600	Carbide backed, 85% CBN, TiC binder	
Seco Tools Ltd (Sweden)	CBN10	Solid, high CBN content
	CBN20	Carbide backed, medium carbide content
	CBN30	Carbide backed, lower carbide content
	CBN300	Solid, CBN content over 90%, AlN binder

Since it first appeared in the early 1970's (Hibbs, 1974), a large variety of PCBN materials have been developed. Most commercial products are synthesised with various catalyst materials. Table 2.3 lists the characteristics of the main PCBN products from different companies. The concentration of CBN grit ranges from 30% up to 95%. (Aspinwall, 1984). The grain size of individual crystals varies from less than 1µm to 20µm. Some products contain wurtzite BN (WBN) (Figure 2.13) in addition to CBN and the binder and this results in tougher compact tools at the expense of hardness and thermal stability (Momper, 1988).

Generally, PCBN products can be classified into two types (Stephenson and Agapiou, 1996); one type has relatively low CBN content (< 60%) and variable

binder phase and they are commonly used in smooth or finish cutting; The other type has higher CBN contents with either a ceramic binder (e.g. AlN) or a metallic binder (e.g. cobalt). Products of this type have high hardness, toughness and thermal conductivity and are used in rough cutting conditions or for some extremely difficult-to-machine materials, e.g. Ni-hard, hardmetals and some engineering ceramics.

For a cutting application, the most important property of PCBN is its hot hardness (Figure 2.16). The hardness of PCBN (BZN) at 750°C is approximately equal to that of oxide ceramics and tungsten carbide at room temperature. The lattice structure of CBN does not revert to the hexagonal form at temperature below 1200°C under atmospheric pressure and it can withstand edge temperatures up to 1300°C (Wentorf, 1980). In addition to its hardness, PCBN also has very good fracture toughness compared with other tool materials as shown in Figure 2.17. It is clear that PCBN is very tough. Its fracture toughness ( $K_{IC}$ ) approaches that of tungsten carbide, is four times greater than that of  $Al_2O_3$  ceramics and twice that of the Sialon-type material. This good combination of hardness and toughness provides PCBN with unique properties as a cutting tool material. It can be used at high speed or in very tough conditions, effectively increasing productivity. In some cases (e.g. machining hardened steel) it can replace the grinding process.

PCBN tools have excellent thermal stability and this has made it possible to cut hard ferrous materials at very high speed. It is superior to Polycrystalline Diamond tools, which are known to react readily with elemental carbide formers such as Fe, Co, Ni, Al, Ta and B at about 1000°C (Gardinier, 1988). PCBN materials also have very good thermal conductivity compared with ceramic tools as shown in Figure 2.18. This maintains the temperature of the tool at a lower level while the workpiece is thermally softened (Narutaki et al, 1979).

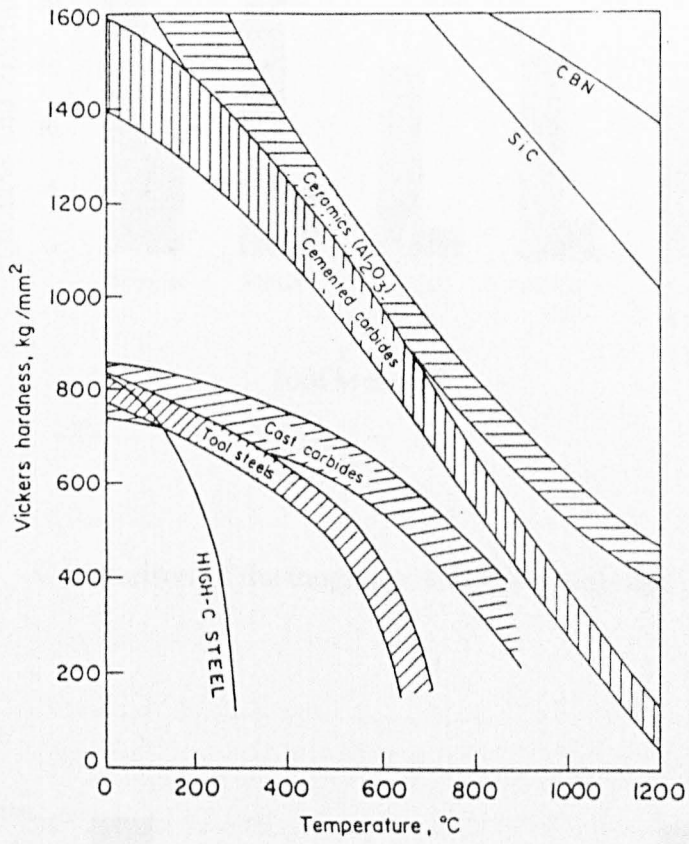


Figure 2.16 Hardness of cutting tool materials at elevated temperatures (Schey, 1987)

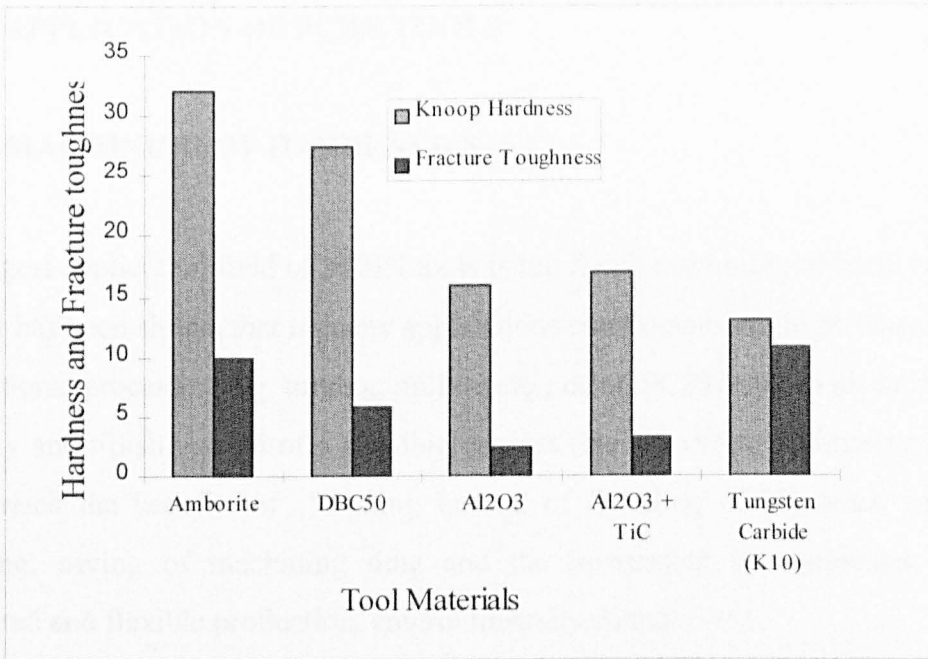


Figure 2.17 Comparison of the toughness of PCBN tools and other tool materials

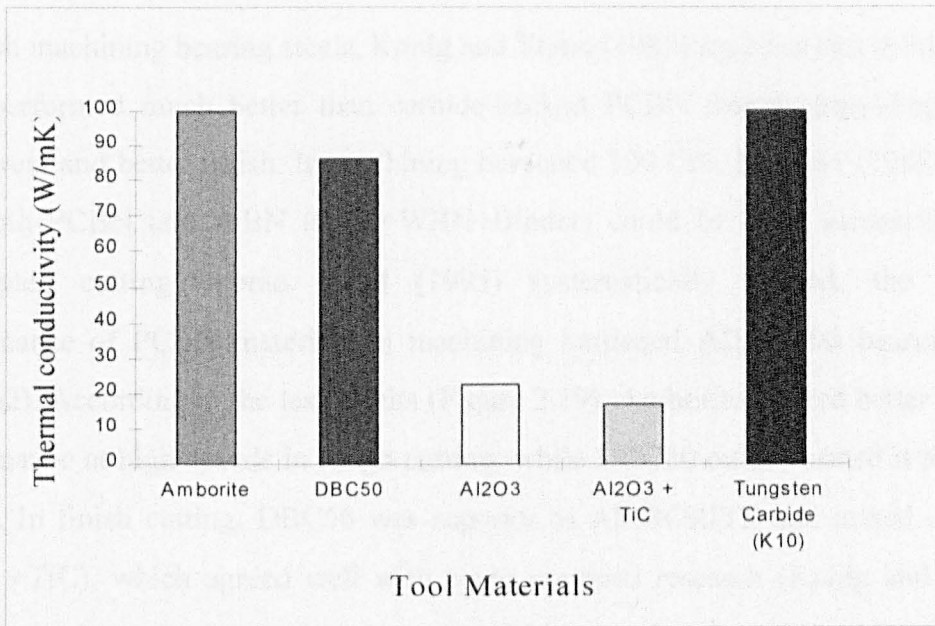


Figure 2.18 Thermal conductivity of PCBN tools and other tool materials

## 2.9 APPLICATION OF PCBN TOOLS

### 2.9.1 MACHINING OF HARDENED STEELS

The largest application field of PCBN tools is the finish machining of hardened steel parts. It has been shown that in many applications components could be machined by conventional processes (e.g. turning, milling etc.) using PCBN tools with satisfactory accuracy and finish instead of a grinding process (Heath, 1986). Ordinartsev (1984) summarised the benefits of “Cutting Instead of Grinding of Hardened Steel” as including: saving of machining time and the investment in equipment, highly automated and flexible production, environmentally friendly, etc..

A large range of hardened steels are capable of being machined with PCBN, e.g. bearing steel, tool steels, case hardened steels, etc.. Machining operations include turning, facing, boring, milling and threading.

In finish machining bearing steels, Konig and Wand (1987) reported that solid PCBN tools performed much better than carbide-backed PCBN inserts, providing lower flank wear and better finish. In machining hardened 100 Cr6, Momper (1988) found that both PCBN and WBN (CBN+WBN+Binder) could be used successfully for interrupted cutting. Abrao et al (1995) systematically studied, the cutting performance of PCBN materials in machining hardened AISI52100 bearing steel (HRC62). According to the test results (Figure 2.19), Amborite offered better cutting performance at high speeds in rough cutting, while DBC50 outperformed it at lower speeds. In finish cutting, DBC50 was superior to AMBORITE and mixed ceramic ( $Al_2O_3 + TiC$ ), which agreed well with some previous research (Konig and Wand, 1987)

Case hardened steels can be cut effectively by PCBN compacts. In general, titanium carbide bonded PCBN (e.g. BN200) outperformed a metal-bonded PCBN due to its ability to maintain a higher hardness at elevated temperature (Abrao et al, 1993). PCBN tools can also be used successfully in the interrupted machining of case

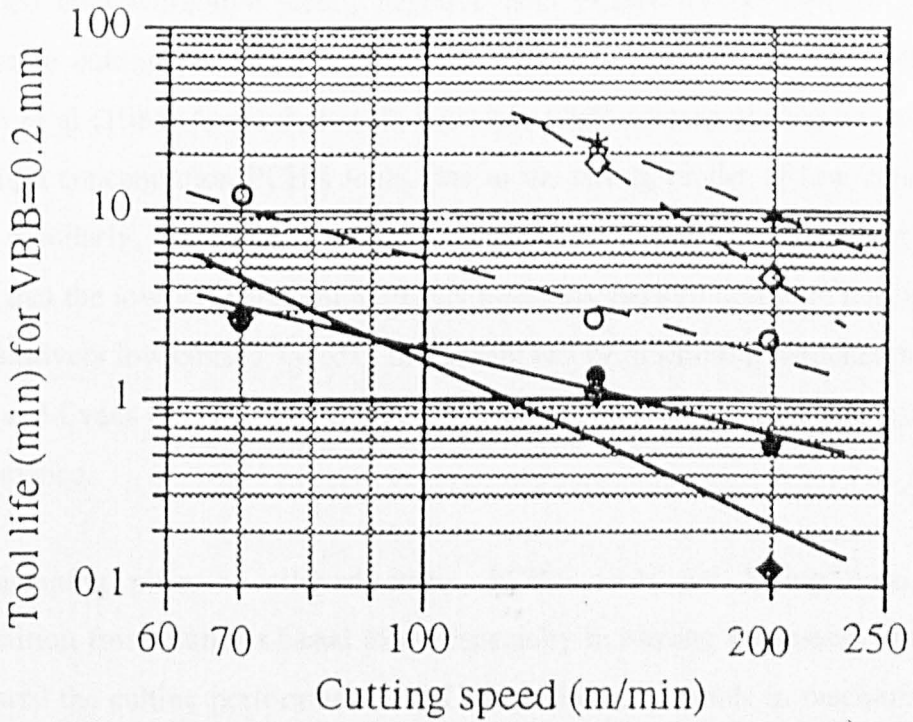
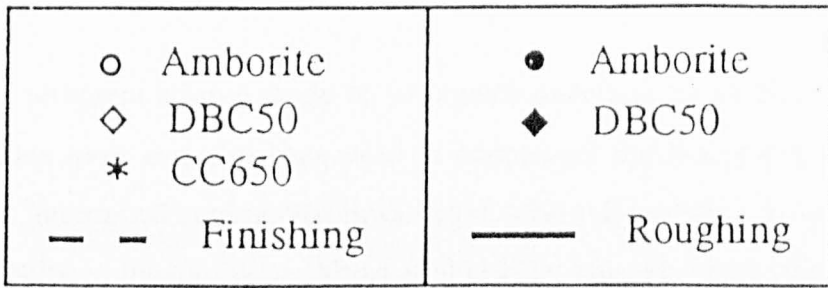


Figure 2.19 Cutting performance of PCBN tools with high and low cBN content. (Abrao et al, 1995)

hardened steels at high cutting speeds (Shintani et al 1989, Abrao et al, 1993). Shintani et al (1989) reported that a proper negative land on the tool insert could effectively increase the cutting tool life both in continuous and interrupted cutting.

Tool steels represent a large range of workpiece materials for PCBN tools. In this field, alumina tools can also be used in continuous machining but they are not suitable for interrupted cutting (Aspinwall et al, 1991). Based on a review of several research results on the tool wear, Abrao et al (1993), suggested that when machining hardened cold work tool steels, negative land PCBN inserts were necessary for acceptable cutting performance. In a test of continuous turning die steel SKD11, Kohno et al (1986) found that tools with low CBN content performed much better than high concentration PCBN tools, due to the strong binder of low concentration tools. Similarly, when PCBN tools were used in milling of H13, Dewes et al (1997) found that the lower concentration PCBN materials showed optimum performance at comparatively low cutting speeds. In a recent test of machining hardened tool steels, Chou and Evans (1997) found that, PCBN tools with smaller grain size had the best performance.

In machining plain or alloyed steels, PCBN tools are facing even stronger competition from alumina-based tools, especially in turning processes. Chen (1993) compared the cutting performance of PCBN and ceramic tools in machining carbon steel (BS 070M55) hardened to HRC45-55. In most of the cases, mixed alumina tools performed better than the PCBN tools used. Recently, Barry and Byrne (1998) studied the finish cutting performance of PCBN and Alumina-based tools in machining EN24 (4340, alloyed steel). They found that the relative performance of the tools was strongly dependent on the cutting speed. For cutting speeds greater than 250m/min, the Alumina-based tools exhibited better performance than the PCBN tools.

## **2.9.2 MACHINING OF CAST IRONS**

High speed machining of cast iron using cubic boron nitride in industry started in the 1980s. The machinability of cast iron mainly depends on its structure rather than its

hardness. Two important criteria have been indicated by Heath (1986): 1) the microstructure must contain little, if any, ferrite i.e. be fully pearlitic; and 2) cutting speeds should be excess of 500 m/min, if machine capability permits. Ferrite is highly reactive and produces rapid wear on CBN tools, as a consequence, an uneconomical tool life. Research has shown that at lower cutting speeds, the performance of ceramic tools is superior to PCBN tools; while at higher cutting speeds, the tool life of PCBN is approximately twenty times that of the ceramics (Heath, 1986). In similar research (Kohno et al, 1986), it was found that two PCBN tools (CBN+TiN) with CBN concentration of 60% and 85% respectively showed similar cutting performance, while another one (CBN+TiC) performed much better. They also found that 400 -500m/min were the best cutting speed range for the tools.

Haldin et al (1993) found that DBC80 showed better cutting performance than DBC50, during long cuts in machining grey cast iron. The surface finish achieved with DBC80 over its total life was 1.6 $\mu$ m, and the required diameter tolerance was maintained. Deming et al (1993) pointed out that among BZN products, BZN 6000 is the most suitable tool for cast iron due to its high abrasion resistance. In addition, as listed in Table 2.4, they also recommended the optimum tool geometry including: lead angle, rake angle and edge preparation of the inserts.

**Table 2.4** Optimum geometry for BZN6000 in machining cast irons (Deming et al, 1993)

Material	Lead angle	Rake angle	Edge preparation	
Grey cast iron	15-45 degrees	negative 5-7 degrees	20° × 0.008" (Roughing)	20° × 0.004" (Finishing)

Hyatt (1997) reported the application of PCBN tools in dry milling of cast iron. They found that the solid PCBN tools performed better than brazed-on inserts and PCBN tools showed much more advantage over carbide and ceramics tools, with longer tool life and less inserts needed.

Nickel/chromium white cast iron is produced by chilling during casting. This martensitic iron is much harder (45 to 65 HRC), more brittle and wear resistant than grey iron because of the presence of carbides instead of graphite. PCBN tools have been used successfully in both rough and finish cutting of this material showing great improvement over carbide and ceramic tools. Mansfeld et al (1982) reported application of PCBN tools in machining chill cast rolls. They found that Amborite enabled more than a hundred times as much chilled iron to be machined as that with carbide form tools. Notter and Heath (1980) found that Amborite could be used with much higher speeds and feedrates than ceramic tools. At 60m/min and 0.16 mm/rev, the tool life of ceramic material was only 0.6 minutes against an extrapolated tool life of 200 minutes for Amborite.

It has been shown that Ni-Hard is one of the most difficult-to-machine materials (BS4844, 1972). Its microstructure consists of a white, discontinuous, carbide ((CrFe)<sub>7</sub>C<sub>3</sub>) phase in martensitic matrix. This microstructure makes Ni-Hard an ideal, abrasive-resistant material for ore- and coal-crushing equipment. In many cases, the design of the components required interrupted cutting in the manufacturing process. Conventional tool materials, such as ceramics, tend to have insufficient toughness, whilst carbide tools can only be used at slow cutting speeds because of their inadequate hardness at high cutting temperatures (Heath, 1986). PCBN tools with high CBN concentration had been successfully applied in this field. Fillmore and Ladd (1981) reported the application of BZN in machining Type 4 Ni-Hard PUMP components. The insert used consisted of a layer of polycrystalline Borazon CBN on a cemented tungsten carbide substrate. By changing from grinding to a turning process, the manufacturing time was reduced by 60%. Amborite Compacts have also been reported as being successful in machining different kinds of Ni-Hard components, e.g. augers (Nicolis, 1984), crushing rings (Muller and Steinmetz, 1983) and pump sleeves (Silveri, 1985). In most of the cases, round inserts were used because of their higher strength. Typical operating conditions were cutting speeds from 66 to 80 m/min at a feed rate of 0.25 mm/rev and depth of cut 1.5-3 mm.

### **2.9.3 MACHINING OF COBALT AND NICKEL BASED SUPER ALLOYS**

Cobalt and nickel based super alloys with hardness above HRC 35 are difficult to machine because they maintain a major part of their strength during cutting and work harden during machining. They are usually machined with tungsten carbide tools at low cutting speeds ( $< 30\text{m/min}$ ). PCBN tools can be used with these alloys at much higher speeds. Richard and Aspinwall (1989) reviewed all the practical problems when machining these super alloys, and indicated that the cutting speed should be high enough to soften the workpiece but not the PCBN tool. They also found that some superalloys can be machined effectively with PCBN tools with flood coolant. The effect of CBN content of the tool has been studied by Takatsu et al (1983) and Kono et al (1980). They found that PCBN tools with a volume fraction between CBN55%-60 % gave the best cutting performance.

### **2.9.4 MACHINING OF HARDFACING MATERIALS**

Hard facing alloys are designed to be applied as a welded surface layer to improve the wear resistance of a component and normally contain large quantities of carbide in a softer matrix. The nature of their microstructure makes them difficult to machine. In addition, the surface of the welded layer is often very rough and irregular and hence present more difficulties in the cutting process.

It has been found that PCBN is a suitable tool material for machining hardfacing materials, and, in some cases, the productivity can be increased dramatically. Klimenko (1992) reported that when machining flame-sprayed alloys (Colmony No.43), a PCBN tool could finish 3,000 pieces while a cemented carbide tool could only finish 9 pieces.

For nickel-based and cobalt-based hardfacing alloys, speed is the key to a successful machining and some guidelines are listed in Table 2.5. It is generally recommended that speeds in range 200-250 m/min be used and, because of the work hardening nature of these alloys, feed rates should be not less than 0.2 mm/rev. Round,

chamfered inserts should be used wherever possible and the depth of cut should be sufficient to penetrate into the solid underlying material to avoid the abrasiveness of the as-cast or as-deposited alloy skin.

**Table 2.5** Guidelines for the turning and milling of hard facing alloys (Heath et al, 1986)

MATERIAL	PARAMETERS	EXAMPLES
Nickel Based (turning and milling)	v=80-120m/min a=1.0mm s=0.2-0.3mm/rev	Colmonoy 5,6,75
Cobalt Based (turning only)	v=200-250m/min a=1.5mm s=0.2-0.3mm/rev	Stellite No.4, 6, 12, 20, 21

The application of PCBN tools in machining iron-based hardfacing alloys are very limited. Some applications have been reported but many tool companies claim that their products are not suitable for all kind of hardfacings. Bossom and Hoffmann (1993) suggested that PCBN tools were suitable for machining some iron-based hardfacings with a hardness over HRC35, operating in the speed range 60-120 m/min.

### 2.9.5 MACHINING OF OTHER DIFFICULT -TO-MACHINE WORKPIECE MATERIALS

In addition to the materials mentioned above, PCBN tools have also been used to machine some other difficult-to-machine materials including sintered HSS, tungsten carbide and new engineering materials (e.g.  $\text{Si}_3\text{N}_4$ ) (Kitagawa and Maekawa, 1990, Wang, 1996,). According to Zhou et al (1997), powder metallurgy high speed steel could be machined using PCBN tools, and showed better machinability than the conventionally-produced steels with similar composition. When machining tungsten carbide, the cutting was usually at low speed (about 30m/min) and using tools with high CBN concentration (Abrao et al, 1993).

The application of PCBN tools in machining ceramics is still at the research stage. Turning or milling have only limited application to advanced ceramics in their fully sintered state because of high rates of tool wear (Wang et al, 1996). Many efforts have been made to heat the workpiece material ahead of the insert by an external heating source like a laser or gas torch (Kitagawa and Maekawa, 1990), while others have tried to cool the cutting zone (Wang et al, 1996). In many of these tests, PCBN was used as the tool material due to its high toughness and hardness.

Kitagawa and Maekawa (1990) used turning to investigate the effect of laser heating on the cutting forces and tool wear. They used a PCBN tool to machine alumina ceramic. The cutting forces were measured by a piezoelectric transducer. The cutting forces were compared with those obtained by turning without laser heating. The cutting forces were higher when laser heating was applied. The tool wear was also measured. The tool wear was lower when laser heating was applied. The authors concluded that laser heating can reduce the cutting forces and tool wear when machining advanced ceramics with PCBN tools. Wang et al (1996) used turning to investigate the effect of laser heating on the cutting forces and tool wear. They used a PCBN tool to machine alumina ceramic. The cutting forces were measured by a piezoelectric transducer. The cutting forces were higher when laser heating was applied. The tool wear was also measured. The tool wear was lower when laser heating was applied. The authors concluded that laser heating can reduce the cutting forces and tool wear when machining advanced ceramics with PCBN tools.

Kitagawa and Maekawa (1990) used turning to investigate the effect of laser heating on the cutting forces and tool wear. They used a PCBN tool to machine alumina ceramic. The cutting forces were measured by a piezoelectric transducer. The cutting forces were higher when laser heating was applied. The tool wear was also measured. The tool wear was lower when laser heating was applied. The authors concluded that laser heating can reduce the cutting forces and tool wear when machining advanced ceramics with PCBN tools. Wang et al (1996) used turning to investigate the effect of laser heating on the cutting forces and tool wear. They used a PCBN tool to machine alumina ceramic. The cutting forces were measured by a piezoelectric transducer. The cutting forces were higher when laser heating was applied. The tool wear was also measured. The tool wear was lower when laser heating was applied. The authors concluded that laser heating can reduce the cutting forces and tool wear when machining advanced ceramics with PCBN tools.

Tool wear also affects the cutting forces in both turning and milling. Kitagawa and Maekawa (1990) used turning to investigate the effect of laser heating on the cutting forces and tool wear. They used a PCBN tool to machine alumina ceramic. The cutting forces were measured by a piezoelectric transducer. The cutting forces were higher when laser heating was applied. The tool wear was also measured. The tool wear was lower when laser heating was applied. The authors concluded that laser heating can reduce the cutting forces and tool wear when machining advanced ceramics with PCBN tools. Wang et al (1996) used turning to investigate the effect of laser heating on the cutting forces and tool wear. They used a PCBN tool to machine alumina ceramic. The cutting forces were measured by a piezoelectric transducer. The cutting forces were higher when laser heating was applied. The tool wear was also measured. The tool wear was lower when laser heating was applied. The authors concluded that laser heating can reduce the cutting forces and tool wear when machining advanced ceramics with PCBN tools.

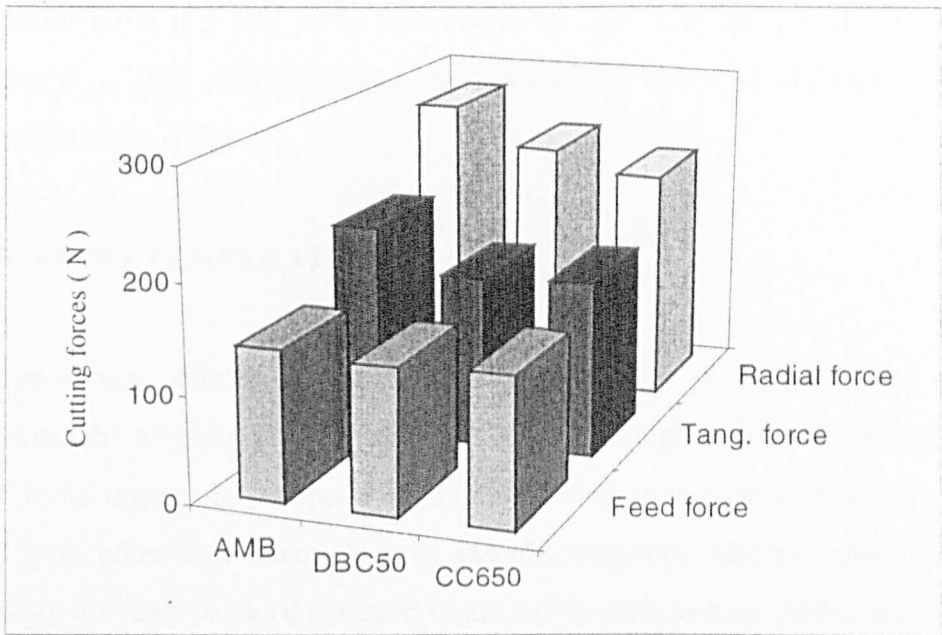
## 2.10 CUTTING FORCES AND TEMPERATURES OF PCBN TOOLS

### 2.10.1 CUTTING FORCES

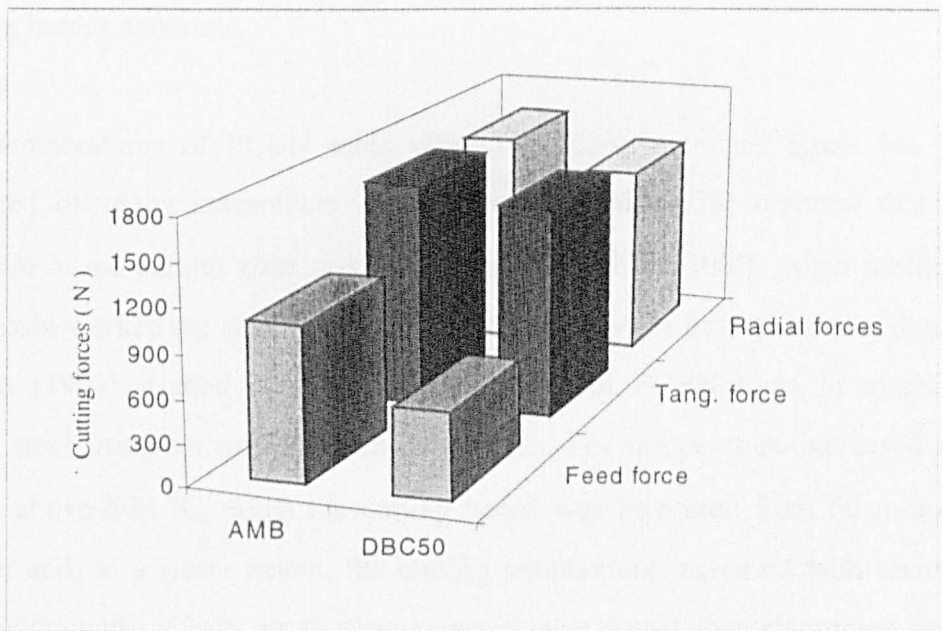
Cutting parameters have a great influence on cutting forces in hard machining. Konig and Wand (1987), when machining hardened bearing steel using PCBN tools, found that the cutting forces decreased with increasing cutting speed up to 200m/min, then remained constant. In a machining tests with hardened AISI E52100 (HRC62), Abrao et al (1995) found cutting forces increased linearly with increasing feed rate and depth of cut, with the tangential forces having the largest gradient. They also found that the cutting forces in a rough cutting conditions was much higher than that in finish cutting, as shown in Figure 2.20. The thrust forces (radial forces) were greater than the tangential forces with light cutting while the tangential forces were greater than the radial forces in heavy cutting, which showed good agreement with the work by Lin et al (1995).

Cutting forces are affected by the tool material and geometry. When machining a hardened high speed steel, Bossom (1991) found that low CBN content tool produced lower cutting forces and, similarly, Abrao and Aspinwall (1995) found that the cutting forces produced using Amborite was higher that that when using DBC50 and CC650 (Figure 2.20). When machining a hardened steel (HRC 45-55), it was found that the cutting forces with a chamfered round insert were higher than those of an insert without a chamfer, especially the radial thrust forces (Chen, 1993).

Tool wear also affects the cutting forces in both roughing and finishing cuttings when using PCBN tools. With longer cutting times, as the tool wear increased, so did the cutting forces. It was also found that tool wear had greater effect on feed force than the other two forces (Abrao et al, 1995). Chipping of the cutting edge also resulted in higher cutting forces. In research into continuous turning of carburized steel using PCBN tools, Shintani et al (1989) found that a step-wise increase in the cutting force occurred as a result of chipping.



Finish cutting (S200m/min, F0.06mm/rev, DOC0.5mm/side)



Rough cutting (S70m/min, F0.25mm/rev, DOC2.0mm/side)

Figure 2.20 Cutting forces in rough and finish cutting condition using different tool materials (Abrao et al, 1995)

In machining welded Co-based alloys with PCBN tools (Weinert, 1994), it was found that the radial force ( $F_r$ ) was more than twice as high than the usually-dominant cutting force ( $F_c$ ). They also found that minima for both tool wear and cutting force occurred at the same speed.

### 2.10.2 CUTTING TEMPERATURES

Thermal properties, especially the thermal conductivity of PCBN, have great influence over the temperature of the cutting edge. The higher thermal conductivity of PCBN tools means the temperature of the cutting tool edge is relatively low compared with other tool materials (e.g. carbide, ceramics) under similar cutting conditions. In the early work of Narutaki et al (1979), various heat-treated tool steels (SK 3) and high speed steel, with hardnesses in the range of HRC 20-65, were machined using PCBN tools. It was found that the average cutting temperature of PCBN tool was lower than that of carbide tools and the difference increased when machining harder materials.

Cutting temperatures of PCBN tools when machining hardened steels has been investigated by many researchers. Bhattacharyya et al (1978) reported that the temperature in the cutting zone was in the region of 1275-1300°C when machining AISI D3 cold worked die steel at 60m/min, 0.12 mm/rev feedrate and 2 mm depth of cut. Chen (1993) studied the cutting temperature of PCBN tools in machining hardened steel using an implanted thermocouple. The temperature increased from 300°C to above 800 °C, when the cutting speed was increased from 60 m/min to 150m/min and, to a lesser extent, the cutting temperature increased with increased feedrate and depth of cut. In the same test it was found that chamfered inserts generated lower cutting temperatures than unchamfered inserts at low speed, while at higher speed the situation was reversed. Similarly, in later work when machining bearing steel (Abrao and Aspinwall, 1997), cutting temperature was found to increase with cutting speed (Figure 2.21). Amborite gave the lowest temperature than other tools due to its high thermal conductivity but cutting temperatures increased greatly with tool wear after longer cutting times (Figure 2.22).

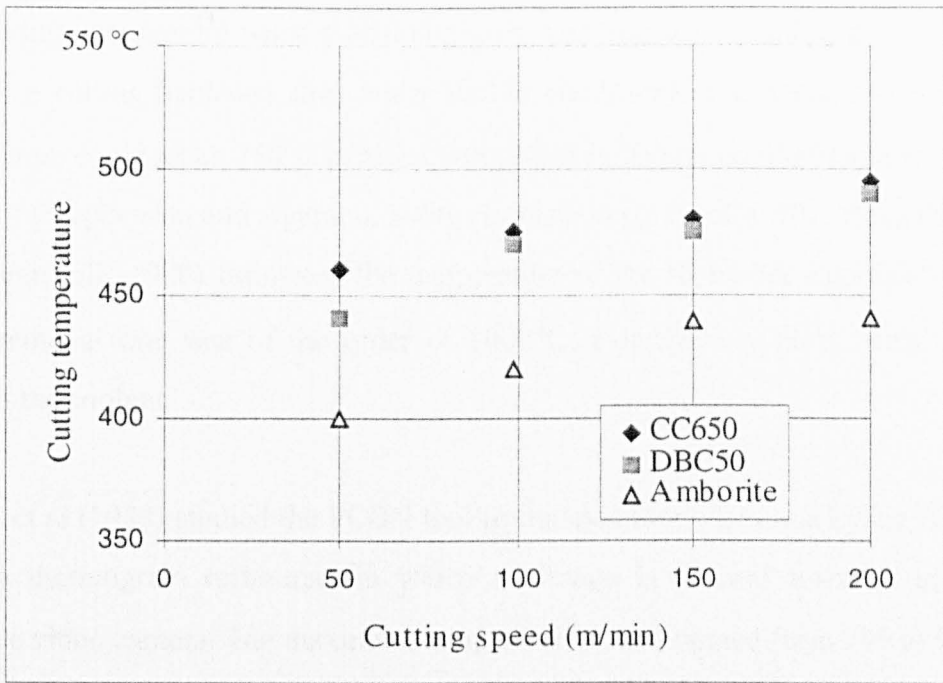


Figure 2.21 Effect of cutting speed on temperature of swarf leaving cutting zone of given inserts: feedrate 0.06 mm/rev, depth of cut 0.5mm (Abrao et al, 1997)

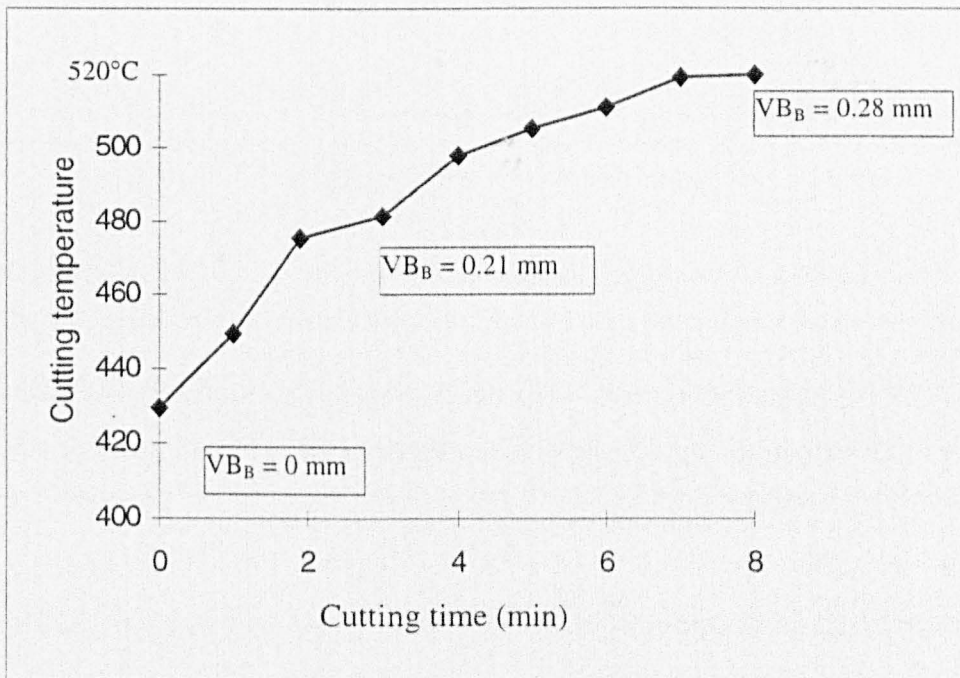


Figure 2.22 Effect of tool wear on temperature of swarf leaving cutting zone of Amborite inserts: cutting speed 100 m/min, feedrate 0.06 mm/rev, depth of cut 0.5mm (Abrao et al, 1996)

The cutting temperature when machining grey cast iron was found to be lower than that when cutting hardened steel under similar conditions. The average cutting tool temperature could reach 750°C at high cutting speed (300m/min, F0.05mm/rev, DOC 0.2 mm) (Stephenson and Agapiou, 1996). In machining Incoloy 901, Bhattacharyya and Aspinwall (1980) estimated the temperature of the tool/work interface at high metal removal rate was of the order of 1000°C, a red/yellow glow being visible through the coolant.

Crooks et al (1988) studied the PCBN tool tip temperature when machining Ni-Hard using a thermogram technique, in which an image is derived from an infra-red sensitive video camera. The maximum temperature found ranged from 745 to 817 °C when the surface speed increased from 200 to 300 m/min at feedrate of 0.5-1.0 mm/rev and depth of cut 1.0 mm.

## 2.11 FAILURE MODES OF PCBN TOOLS

Figure 2.23 (Seco, 1996) shows the failure modes of PCBN commonly encountered in machining, including excessive flank wear, excessive crater wear, notching, edge chipping, cutting edge breakage, rake face flaking and insert breakage.

Flank wear is the most common tool life limit for all types of inserts, especially under finish cutting conditions. Excessive flank wear leads to high cutting loads and temperatures and therefore deterioration in the surface finish and the subsurface structure.

Crater wear is another wear type of PCBN tools commonly found in finish cutting (Kohno et al, 1986, Xiao, 1990). Xiao (1990) found that, in machining hardened alloy steel, PCBN tools show more distinctive and deeper crater wear than ceramic tools, and the failure of BZN was caused by heavy cratering which led to a very sharp edge and, hence, fracture. In the work on milling welded 56NiCrMoV die steel, Bieker (1995) found that crater was the main failure mode at lower speeds (20-30m/min) while chipping occurred on the lip of the crater at higher speeds (over 400m/min) due to the excessive stress on the tool material.

It has been reported (Notter and Heath, 1980) that when machining M2 steel using AMBORITE, a notch often developed on the leading edge of the insert. Notching is more commonly found in machining super alloys due to the high degree of work hardening and large cutting forces. Severe notching could develop ahead of the flank wear and determine the tool life (Bhattacharyya et al, 1980, Richard and Aspinwall, 1989).

Edge chipping is more commonly found in machining workpieces with high hardness, in rough cutting or in interrupted cutting (Xiao 1990, Stephenson and Agapiou, 1996). Bhattacharyya et al (1980) reported that micro-chipping was one of the failure modes of a PCBN tool in machining hardened SUJ2 steel (HRC65). Xiao (1990) found that in machining hardened AISI H13 steel(HRC43-48), Amborite

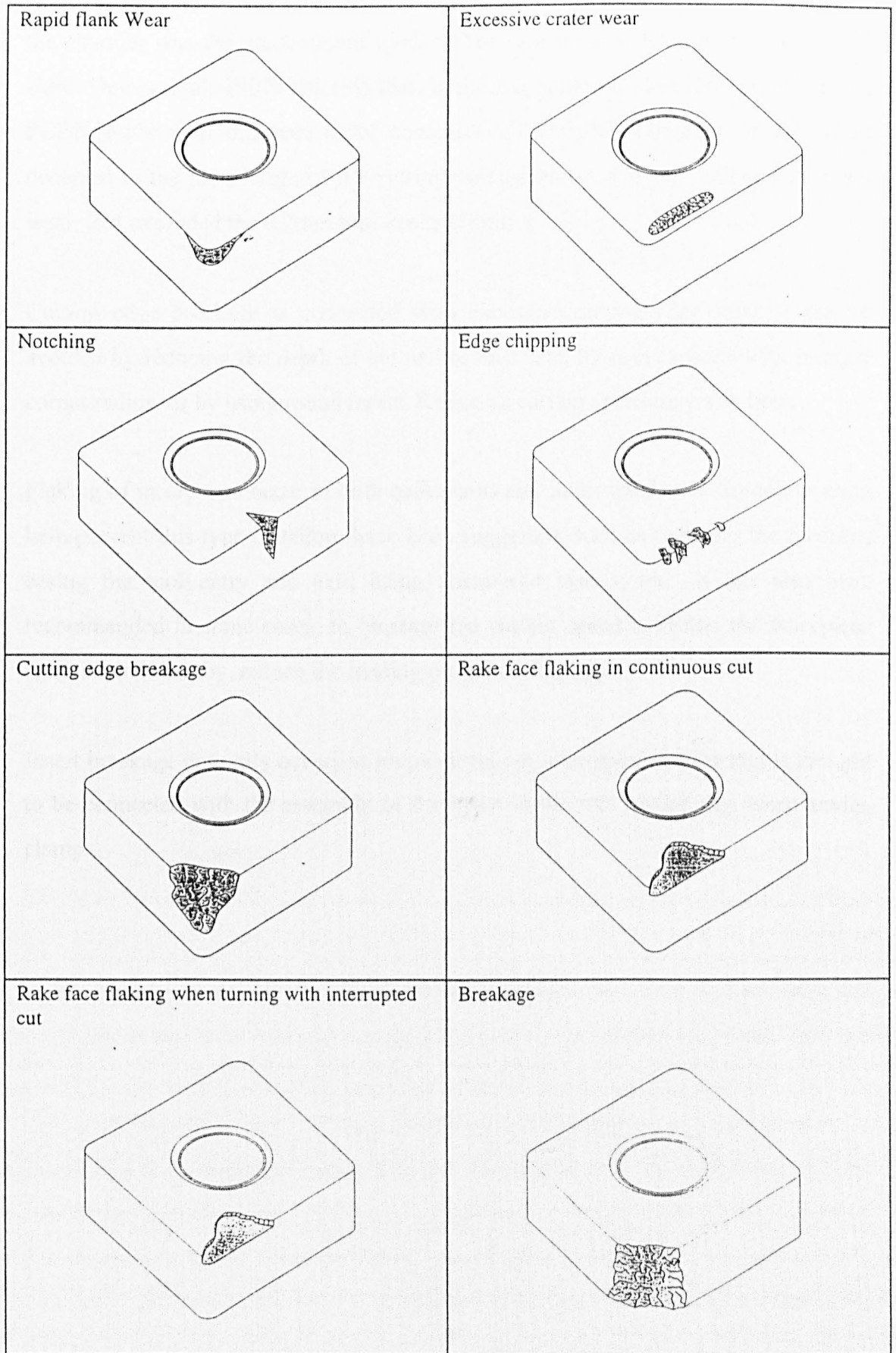


Figure 2.23 Wear mode of PCBN tools (Seco Ltd, 1996)

failed by edge chipping. Fillmore (1981) found that chipping on the lower edge of the chamfer was the predominant mode of the tool wear of BZN in machining Ni-Hard. Dewes et al (1997) reported that, in milling hardened steel (HRC51-54) using PCBN tools with different CBN content (vol 50-90%), chipping of the insert occurred in the latter stage of the cutting process and it was this, rather than flank wear, that exceeded the 0.2mm tool life criterion.

Cutting edge breakage is connected with excessive cutting edge load. It can be avoided by reducing the depth of cut and/or feed rate, by using inserts with a larger corner radius, or by using round insert. Reducing cutting speed may also help.

Flaking of inserts can occur in both continuous and interrupted cuts. Some means to help prevent this type of failure have been suggested, such as reducing the feedrate, easing the tool entry and exit, using chamfered inserts, etc.. It has also been recommended in some cases, to increase the cutting speed to soften the workpiece material and thereby, reduce the loading on the cutting edge.

Insert breakage normally occurs in rough cutting or interrupted cutting and is thought to be connected with the assembly of the insert in the tool holder, e.g. worn anvils, clamps.

## **2.12 WEAR MECHANISMS OF PCBN TOOLS**

The wear mechanisms of PCBN materials have long been the subject of concern and research attention. Extensive cutting tests, either in industrial fields or in the laboratory, have been performed to investigate the operating mechanisms resulting in tool wear under different cutting conditions. In addition, many techniques, e.g. high temperature wear testing, adhesion tests etc. (Hooper and Brookes 1984, Brookes et al, 1992, König and Neises, 1993), have been jointly used for looking into the fundamental aspects of the tool wear.

### **2.12.1 WEAR MECHANISMS OF PCBN IN MACHINING STEELS**

In machining tests of case hardened steel SCM21(HRC65) and die steel SKD11(HRC63), Kono et al (1980) found that CBN1 (60% CBN + TiN) showed less flank wear than the other two materials CBN2 (85% CBN + TiN) and CBN3 ( $\approx$  80% CBN +Co). SEM examination revealed many micro-cracks and striations on the flank wear land of the tools. They suggested that the micro-cracks and striations were due to removed CBN grains rubbing on the flank surface. Based on this suggestion, they attributed the better performance of CBN1 to the fact that the CBN grains were firmly held by the matrix and therefore more difficult to pull out. This so called self-wearing of tools has also been reported by other researchers (Klimenko et al, 1992).

In diffusion experiments with PCBN tools (Narutaki et al, 1979), it was found that CBN grains are stable with Fe at temperatures up to 1200°C but when they are sintered, boron (B) and cobalt (Co), contained in the sintered material, tend to diffuse into Fe. Eda et al (1980) found that the wear of PCBN tools increase when the hardness of the workpiece material is low, and at around HRC 60, the wear on a BZN tool became markedly greater than on a BN200 tool. They identified the operating mechanism as attrition, accompanied by plastic deformation.

Hooper and Brookes (1984) studied the fundamental wear mechanism of PCBN tools when cutting a cold-worked steel. In this work, a wear process was identified

involving the rapid chemical attack of those highly dislocated areas developed close to the cutting edge and their subsequent removal as an oxide.

Xiao (1990) found that the crater surfaces of BZN and AMBORITE were smooth and polished with fine scratches in the direction of flow of the chip. This showed that diffusion wear was the operative mechanism. He also found that voids formed on the edge and flank face of the tool insert as the result of particles being plucked out. The significant particle loss was possibly due to the brittleness of the ceramic binding phase. In similar research (Chen, 1993), it was found that CBN6000 tools were susceptible to abrasive wear at low cutting speeds due to loss of CBN crystals and chemical wear at high cutting speed.

Klimenko et al (1992) studied the possible chemical wear mechanisms in PCBN tools when machining hardened IIIIX15 bearing steel (60-62HRC). Based on detailed composition and phase identification analysis of the coating formed on the cutting tool face, they suggested that new chemical compounds were formed (e.g.  $Fe_2B$ ) at the tool-workpiece interface. The new compounds are of lower melting point than the materials in contact and possibly in liquid form at the high cutting temperatures. This was continuously being removed from the tool surface by the chips and therefore contributing to the tool wear process.

Konig and Neises (1993) investigated the basic wear mechanisms of PCBN by diffusion and abrasion tests. Particular attention was paid to the effect of the diffusion mechanism on the abrasion resistance of PCBN during cutting processes. It was found that the PCBN samples, exposed to diffusion with steel at temperatures up to 950 °C, suffered significant changes in the structure of the binder. It was also suggested that this could be one of the reasons for the reduction of the abrasive wear resistance of the tool materials at high temperatures.

Recently, Chou and Evans (1997) studied the wear mechanism of PCBN tools in machining AISI M50 manufactured by different processes, including conventional ingot, vacuum induction melting and vacuum arc re-melting (VIMVAR) and powder metallurgy (PM). The three PCBN tools used were of grain size 3.0 $\mu$ m, 1.0 $\mu$ m and

0.5 $\mu$ m, respectively. They found an adherent layer appeared on the tool flank in machining conventional and VIMVAR and this layer was repeatedly built-up and broken off during cutting, which therefore resulted in delaminated fracture of the flank face.

In most of the cases, PCBN tools exhibit normal wear modes. However, severe damage may occur even in continuous cutting conditions. Takatsu et al (1983) found that in turning hardened high speed steel and die steel, flake-like chipping was generated on the face when the CBN content of the tool was low. The chipping occurs after a short cutting time and it determines the tool life. They suggested that the chipping was due to mechanical loading (e.g. cutting forces). Therefore the inherent wear and fracture resistance will be an important feature of the tool.

Billman et al (1988) reported that, in machining hardened D3 steel, PCBN tools with metallic binder suffered from premature fracture, while other tools with a relatively large volume of ceramic binder showed normal wear modes and higher resistance to fracture. This again suggested that over-loading of the cutting edge was the main reason for chipping or breakage of PCBN tools.

In the research on optimum tool geometry of PCBN tools for continuous turning of carburized steel (Shintani et al, 1989), it was found that in the earlier stages, frequent chipping occurred caused by high stresses generated on the tool edge. In the later stages, a type of adhesive wear was involved in the development of the chipping process, as shown in Figure 2.24. As a result of chipping, a step-wise increase in the cutting force occurred. Another result observed in their experiment was grooving wear of the side cutting edge due to oxidation when using narrow negative land tools.

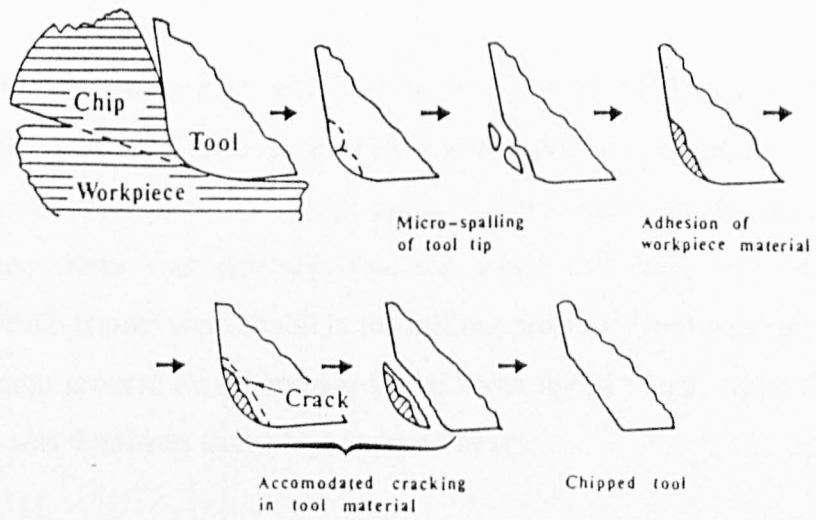


Figure 2.24 Schematic representation of chipping process of PCBN tools (Shintani et al, 1989)

## 2.12.2 WEAR MECHANISMS OF PCBN TOOLS IN MACHINING CAST IRON, SUPER ALLOYS AND TITANIUM ALLOYS

When cutting grey cast iron FC25 ( $C\% = 3.3$ ) with PCBN tools (CBN-TiN composite, 60% cBN), Kohno et al (1986) found that, at 100m/min, crater wear developed on the rake face and small grooves were found on the flank face. At 400m/min, the crater was scarcely observed while the flank wear was getting smoother. Similar results were found in the milling process. From this, they proposed that the abrasion process was dominant in the lower speed range, while the thermal wear process was dominant in the higher speed range.

Deming et al (1993) studied the effect of feedrate on the operating mechanisms of PCBN tools in machining cast irons. They found that the tool wear transition from chemical wear to abrasive wear could occur with increased feedrate at a speed about 850 m/min, which could increase the tool life and productivity. However, when the feedrate was increased, surface finish on the workpiece deteriorated dramatically.

In machining of Ni-Hard (Fillmore and Ladd, 1981), a crater type wear occurred very close to the cutting edge. However, this form of wear tends to make the tool self-sharpening. Another type of the tool wear was edge chipping, especially when taking interrupted cuts, which makes the tool life unpredictable. This chipping was probably due to the cyclic high loading of the cutting edge. The solution to this problem proved to be a chamfered and honed cutting edge to eliminate the previous sharp corner, which was vulnerable to the chipping damage.

In machining INCOLOY 901(Kono et al, 1980), a notch was formed on both the flank and the rake faces. At speeds of 122 - 153m/min, the rate of notch growth exceeded that of the flank wear, and coincident with notch growth they found that burr formed on the leading edge of the workpiece. Lee (1979) observed boron and nitrogen on the serrated underside of an Inconel 718 chip after machining with a cubic boron nitride (CBN) tool. This supported a mechanism that chip-tool welding

and subsequent tool material pullout resulted in the formation of the groove. Some others suggested the notch was formed by the uneven tearing action of the serrated edge of the chip against the top edge of the tool at depth of cut line (Richard and Aspinwall, 1989).

Much research has been undertaken to exploit the possibility of using PCBN tools to machine titanium alloys. Hartung et al (1982) identified a mechanism by which rapid wear can occur in one region of the crater while essentially no wear developed in an adjacent region. They explained that a dead layer formed quickly, due to the adhesion between the tool and the workpiece material, and this layer could limit the mass transport of constituents from the tool surface. When machining aerospace alloy TA48 using AMBORITE (Nabhani, 1991), a similar wear process was found and in a quasi-static adhesion test, it was found that strong adhesion between the tool and a workpiece material occurred at temperatures above 900°C.

### **2.12.3 WEAR MECHANISMS OF PCBN TOOLS IN MACHINING HARDFACING MATERIALS**

In reported investigations (Klimenko et al, 1992) of machining sprayed and overlaid coatings a CBN blade cutting tool was introduced. It was found that, with Amborite cutting tool in combination with preliminary plasma heating of the cutting layer, the cutting time could be reduced 5-6 times in comparison with hard-alloy cutting tools.

When turning weld-deposited cobalt-based alloys with PCBN tools, flank wear was found the main wear mode and there was an optimum of cutting speed (70-80 m/min) to minimise the tool wear (Weinert, 1994). At lower speeds, notches occurred at the end and beginning of the working cutting edge. Two reasons were proposed for the notch formation including high mechanical loading due to the largest undeformed chip thickness and the high gradient of mechanical load and temperature at these two locations. The tools showed similar wear patterns when rough machining the welded skin but the optimum cutting speed was lower (40m/min). In order to study the

influence of interruption of the cut, returned shafts with Co-based alloy deposited layers were produced with three slots milled parallel to the turning axis. An optimum cutting speed of 330 m/min was found. When cutting at lower speeds the tool wear was uneven and chipping at the cutting edge occurred. With an increase of cutting speed, the wear became progressively smoother.

Iron-based hardfacing is more difficult to machine for the following reasons. Firstly, the structure of the alloy, i.e. shrinkage, inhomogeneous parts of the welding, or the presence of large carbides, which increase the danger of tool fracture with the increases in cutting speed. Secondly, the problems associated with diffusion of iron. There is a high tendency for reaction between PCBN, and other tool materials, with the soft (non-martensitic) phases of iron at the high temperatures developed under cutting conditions (Heath, 1986).

A recent successful application of PCBN (Bieker, 1995) in cutting welded die material has suggested the possibility of development of cutting techniques for iron based hardfacing materials. A weld alloy F41 ( 56 NiCrMoV ) was used as a wear resistant hardfacing. The layer has a very irregular surface, in the form of parallel ridges. The resulting variation in depth of cut, the structural differences in the edge zone and the associated variations in hardness all make substantial demands in terms of toughness and wear resistance of cutting tools. Testing carried out with a variety of carbide and PCBN grades showed that the PCBN materials DBC80 and AMBORITE offered considerable benefits. A strongly negative cutting edge geometry results in high cutting forces which must be absorbed by the milling machine. So, statically and dynamically stable machining conditions are essential. These conditions were achieved by using a cutter specially adapted for use with PCBN and a cutter arrangement which ensures consistent cutting conditions.

## CHAPTER 3 EXPERIMENTAL WORK

### 3.1 INTRODUCTION

In the current work, the process of turning chromium carbide based hardfacings using PCBN tools is studied, including chip formation, tool wear and cutting temperatures. Cutting performance of PCBN tools from different suppliers were compared in field cutting tests; hardness, microstructure and the adhesion of the workpiece material are examined in relation to the cutting performance of these tool materials.

A quick stop technique was employed to investigate the chip formation process, with particular attention to the deformation of the carbides within the hardfacing material and their interaction with the cutting edge. In addition, chip morphology was also studied.

Controlled cutting tests were conducted in the laboratory to study the failure process of the PCBN tools and the wear mechanisms involved in the early stages of cutting. Field cutting tests with PCBN tool inserts from different suppliers were also performed in an industrial workshop to compare their cutting performance and the failure mechanisms of the inserts after longer cutting periods.

In the laboratory cutting tests, cutting temperature was monitored by means of a thermocouple located between the tool insert and its supporting shim. As a comparison, the temperatures when machining of mild steel and titanium alloy were also measured by the same technique. Based on the measured temperature, A ANSYS Finite Element Analysis (FEA) model was generated to simulate the temperature at the chip-tool interface and the temperature distribution within the tool material.

Detailed hardness tests were performed to compare the hardness of the PCBN materials at different loads, and microstructure of the PCBN materials was investigated by an etching technique. Finally, a quasi-static adhesion test technique

was used to investigate the adhesion between the hardfacing workpiece material and different PCBN tool materials.

## **3.2 EXPERIMENTAL EQUIPMENT AND SETUP**

### **3.2.1 MACHINING EQUIPMENT**

The machining tests in the laboratory were conducted using a Churchill 'Compturn' 290 CNC lathe, with a left-hand tool holder mounted in the rear tool turret. The lathe spindle was driven by a 16 kw DC motor *via* a separate gearbox and had an operating speed range of 20 - 2000 rev/min. The carriage and cross slide were located in front of the spindle with the carriage above the cross slide. The lathe was equipped with an hydraulically indexing tool post with double tool holding fixtures and each unit accommodated eight tools.

Industrial field tests were conducted on a Universal-315 CNC machining centre with a 12 tool stations tool turret. The machine was driven by a 44 kw DC Motor, and could operate between 33-2000 rev/min. The machine could perform turning and facing at one set-up. The cutting process was controlled by a computer program but the operator could alter the process via a pendant control panel. The infinitely variable manual feedrate override is 0-120% and the infinitely variable spindle speed override is 50-120%.

### **3.2.2 QUICK STOP DEVICE**

The quick-stop facility was mounted in place of the front tool post of the Churchill 'Compturn' 290 CNC lathe used for the cutting tests. It utilises a humane killer gun to rapidly disengage and remove the tool from the cutting position so that the chip remains attached to the workpiece, i.e. the cutting action is effectively frozen. Rapid acceleration of the tool away from the workpiece is achieved when an explosive charge is fired. According to Williams et al (1970), the mean acceleration of the tool from the chip bottom could reach over  $32.5E7$  mm/sec. Hence, for the cutting speed

used in this test, the removal of the tool no longer affects the chip flow after a very short distance from the tool root (Nabhani, 1991).

Figure 3.1 shows, schematically, the quick stop system. The humane killer gun was positioned above the tool holder supported by a notched brass shear pin. The tool holder was manufactured to reproduce the tool geometry in normal cutting conditions. In a quick stop test, once the gun is fired, the solid captive bolt is projected at high speed to strike against the tool holder, breaking the shear pin and the tool accelerates rapidly away from the cutting position. The tool holder allows the tool to clear the workpiece at an angle of  $8^\circ$  as it moves downwards. This avoids any contact between the tool and workpiece once the pin is broken. The plasticine packed in the hollow quick-stop block traps the broken shear pin pieces and arrests the tool holder to prevent it from rebounding back into the workpiece. The sample, in the form of the chip and the adjacent part of the workpiece, is removed from the workpiece using an Electro-discharge Machine (EDM).

### 3.2.3 QUASI-STATIC ADHESION EXPERIMENTS

The adhesion between the workpiece and the tool material was assessed by pressing a workpiece cone at high temperature (Figure 3.2a) onto the rake face of a tool insert enclosed within a vacuum chamber. The cone was machined from a thick layer of hardfacing deposited on a mild steel substrate, with an included angle of  $120^\circ$  at the hardfacing end. The set-up of the equipment is shown in Figure 3.2b. It consists of a vacuum system, a heating and cooling system and a loading system. The tool insert was positioned on a graphite susceptor, which was directly heated by a radio frequency coil within the chamber. Due to the difference between atmospheric pressure and the vacuum, a loads of 115N could be transmitted to the tool *via* the cone at the working vacuum pressure of approximately  $10^{-5}$  mbar (Nabhani, 1991).

Naturally, during the application of the load, the cone flattens to form a contact area sufficient to support the applied load. Subsequently, after measuring the area of the

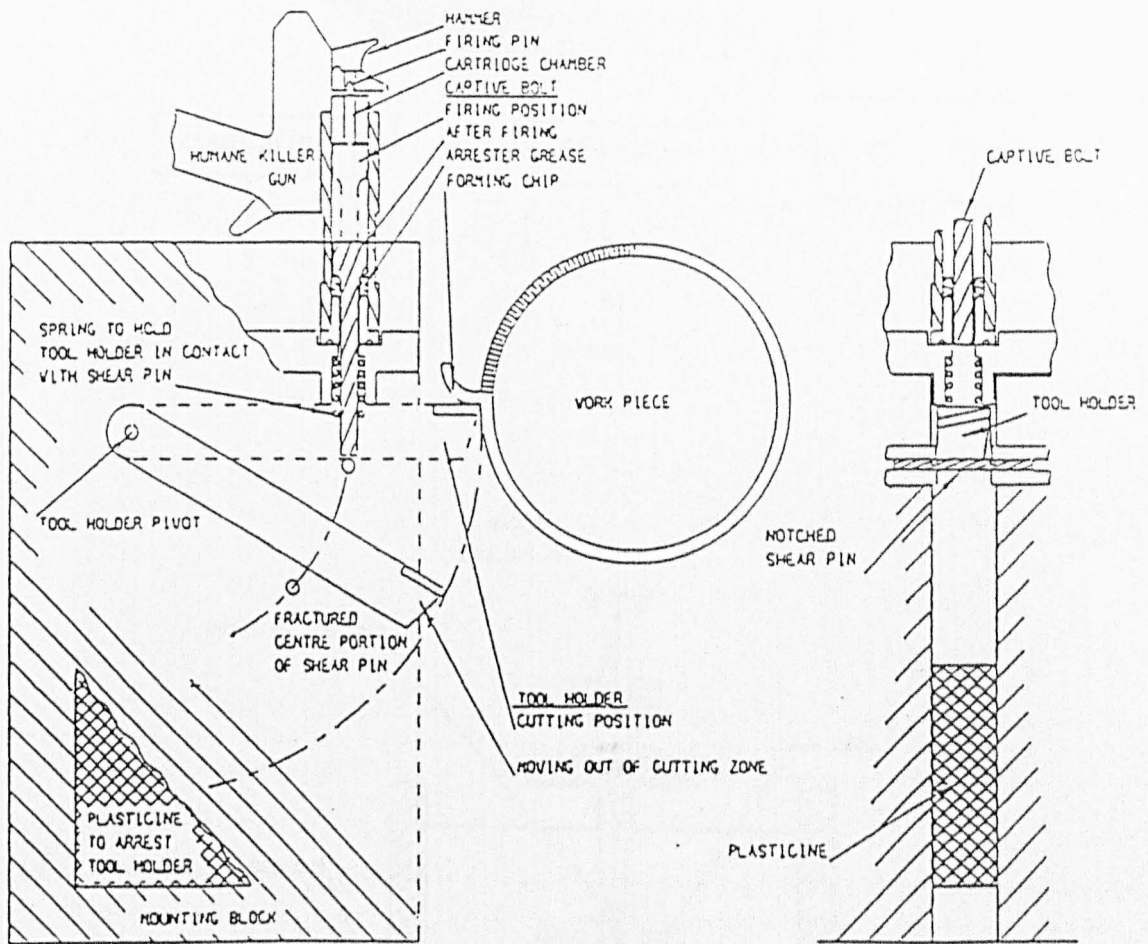
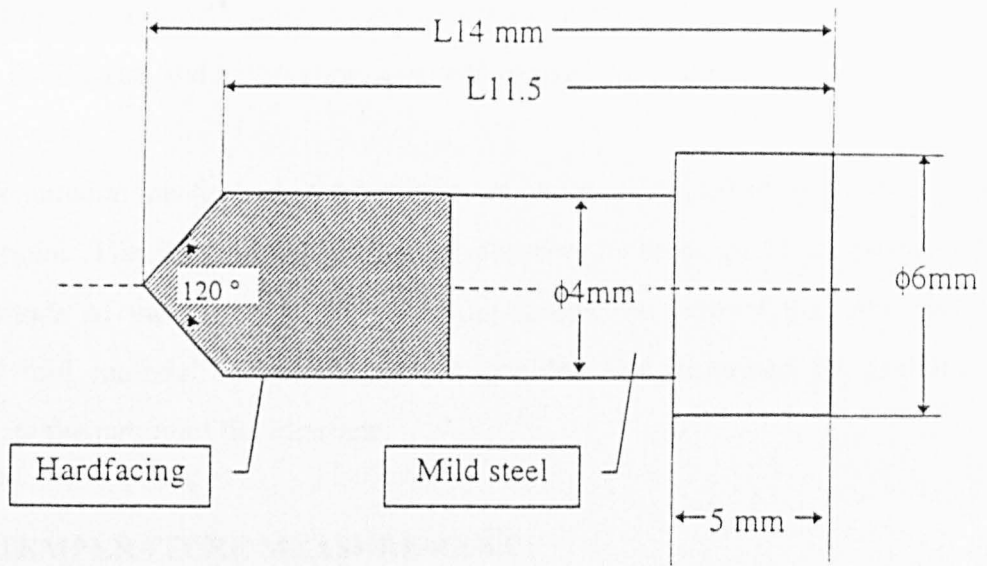
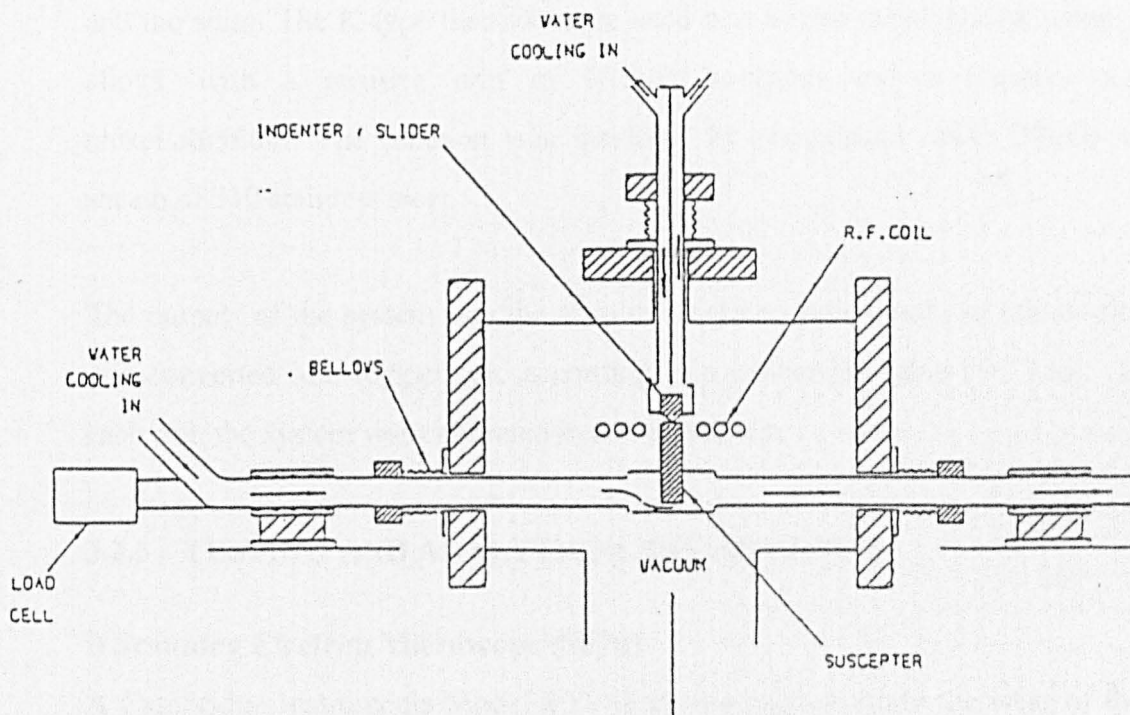


Figure 3.1 The quick stop device utilising a humane killer to disengage the tool from the workpiece rapidly leaving the flow of the metal in the chip undisturbed.



a)



b)

Figure 3.2 a) Schematic section of the cone, b) Schematic cross section of the high temperature adhesion tester.

flattened tip the nominal contact pressure was calculated. The time of contact was 30 minutes in all cases and a new cone was used for each experiment.

Once the junction has formed, it was separated under conditions of room temperature and pressure. The fracture surfaces were observed with an SEM to establish the failure mode of the materials. Some of the sample in form of the cone and the attached tool material, were mounted in Araldite and sectioned by grinding to investigate the nature of the interface.

### **3.2.4 TEMPERATURE MEASUREMENT**

Figure 3.3 shows the set-up of the temperature measurement system. A thin thermocouple ( $\phi 0.5\text{mm}$ ) was mounted in a shallow groove on the silver steel shim, so it could detect the average temperature developed at the interface of the tool insert and the shim. The K-type thermocouple used was a base metal system using nickel alloys, with a positive arm of Nickel/Chromium and a negative arm of nickel/aluminium. The junction was insulated by magnesium oxide (MgO) with a sheath of 310 stainless steel.

The output of the system was the absolute thermocouple e.m.f., in microvolts, and was converted into temperature according to a conversion table (TC Ltd). Before each test, the system was calibrated in the laboratory.

### **3.2.5 TESTING AND ANALYTICAL INSTRUMENTS**

#### **i) Scanning Electron Microscope (SEM)**

A Cambridge Instruments Model 200 SEM was used to study the wear of the tool and the microstructure of the workpiece and tool materials. Elemental analysis was carried out on a QX200 X-Ray Microanalysis System (Link SYSTEMS Ltd.) integrated with the SEM machine. Due to the limited electrical conductivity of the PCBN materials, some of the samples were coated with gold before being examined with the SEM.

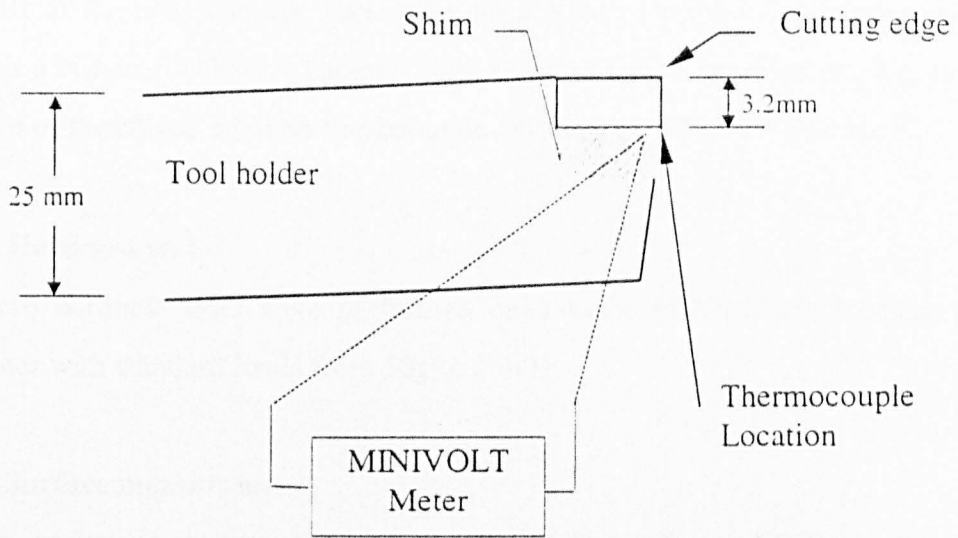


Figure 3.3 Schematic to show the set-up of the temperature measurement system.

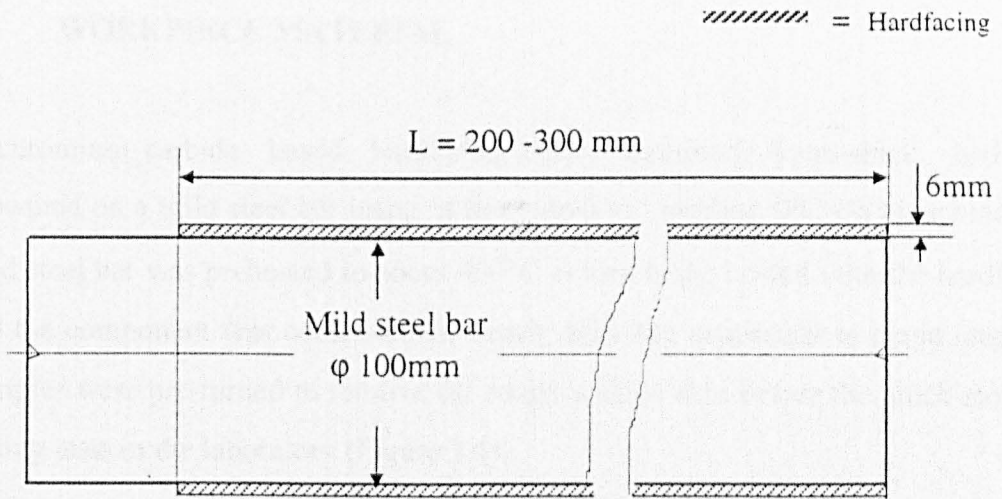


Figure 3.4 Schematic to show the hardfaced workpiece used in the laboratory cutting tests.

## **ii) Optical microscope**

Most of the observations were made on a Nikon Optiphot-2 Microscope equipped with a Nikon FX-35WA camera. For study at low magnification, e.g. the general form of the chips, a Nikon Stereoscopic Microscope SMZ-2T was used.

## **iii) Hardness test**

Micro hardness tests were performed on a Leitz MINILOAD 2 Micro Hardness Tester with standard loads from 50g to 2000g.

## **iv) Surface measurement**

The workpiece surface roughness achieved by different PCBN materials in the industrial tests was measured by a Model 3 Rank Taylor Hobson 'Talysurf'. The measured result was Roughness Average (Ra) which is the centre line average (CLA) height of all irregularities within a standard length of surface.

### **3.3 WORKPIECE MATERIAL**

A chromium carbide based hardfacing layer, nominally 6mm thick, had been deposited on a mild steel bar using a flux cored arc welding (FCAW) machine. The mild steel bar was preheated to about 400°C before being coated with the hardfacing and the component was cooled down slowly after the deposition to avoid cracking. Samples were pre-turned to remove the rough welded skin before the quick-stop and cutting tests in the laboratory (Figure 3.4).

The hardfacing materials used in these tests belong to the Fe-Cr-C composition system. The solidification begins with the formation of primary  $(Cr, Fe)_7C_3$  carbides, the residual liquid decomposing eventually by a ternary eutectic reaction into a mixture of austenite and more  $(Cr, Fe)_7C_3$  (Atamert et al, 1990). Normally, the primary carbides are much larger than the carbides in the eutectic reaction. As shown in Figure 3.5, hardfacing with two types of microstructure were used as the workpiece materials in the current work, Hardfacing A and Hardfacing B. They were deposited from a similar raw material but under different welding process conditions

to achieve different dilution rates, and therefore exhibit different microstructures (Atamert et al, 1990).

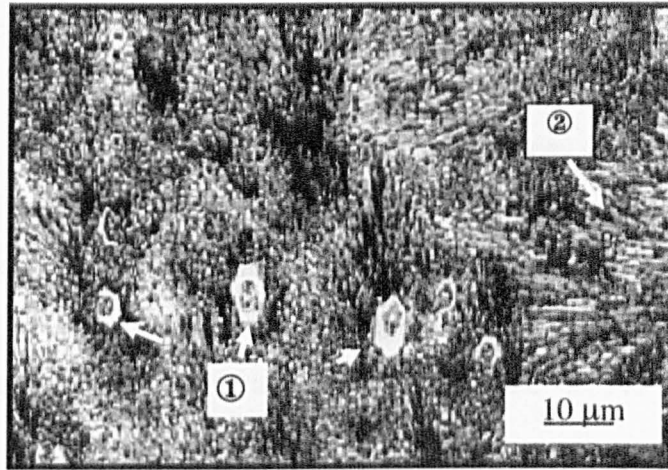
As shown in Figure 3.5a, Hardfacing A is characterised by a relatively fine structure. The needle-like bright image and the tangled structure is the eutectic of fine carbides (1-3  $\mu\text{m}$  in diameter) in an austenite matrix. The much larger grains are the primary carbides (8-15  $\mu\text{m}$  in diameter).

Hardfacing B, is characterised by a very coarse structure (Figure 3.5b). A large portion of primary carbides has formed with the remaining part transformed into mixture of austenite and fine carbides. The primary carbides are much bigger than those in Hardfacing A, up to 20-35  $\mu\text{m}$  in cross-section. In the solidification process, the primary carbides have exhibited columnar growth with an hexagonal cross-section (Lee et al, 1996), so the carbide shows different sections depending on the sampling plane. As shown in the microstructure, there is a carbide-free region around the large carbides due to a chromium depletion process (Lee et al, 1996). It also should be noted that, the hexagonal cross-section shows that the carbide is not perfectly dense in the centre, i.e. some defects exist within the carbide and this could reduce their fracture toughness (Lee et al, 1996).

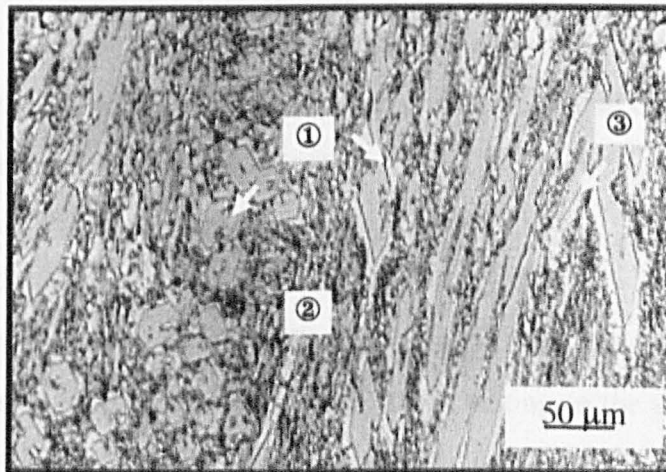
**Table 3.1** Bulk hardness of the hardfacing materials and the carbides (Load = 200g)

Materials \ Hardness	Hardfacing A	Hardfacing B	Carbides
Knoop hardness (GPa)	6.69	7.12	14.57

Table 3.1 lists the bulk hardness of the two hardfacing materials, together with the hardness of the individual carbides. Knoop hardness of the hardfacings is quoted, so it can be easily referred to the hardness of the carbide and, later to the tool material. The Rockwell hardnesses of the two hardfacings are approximately 57 HRC and 59 HRC for Hardfacing A and B respectively. Both hardfacings have high bulk hardness due to the high volume fraction of discrete carbides.



a) Hardfacing with fine structure (Hardfacing A), ① Primary carbides, ② Fine carbides carbides in  $\gamma$  matrix.



b) Hardfacing with coarse structure (Hardfacing B), ① Primary carbide, ② Fine carbides carbides in  $\gamma$  matrix, ③ Carbide free region

Figure 3.5 Microstructures of the hardfacing workpiece materials.

Both structures should provide excellent abrasion resistance and are widely used in industry under a variety of service conditions. However, more attention was paid to the machining of hardfacing with finer structure (Hardfacing A) in this work, and Hardfacing B was specially designed to study the effect of the very large carbide grains in the chip formation process and wear of the tools.

In the industrial cutting tests, hardfaced components were machined under normal production conditions. All the components were round parts, and some were tapered. The size of the components was larger than the workpieces used in the laboratory tests and some were as large as 200 mm in diameter. The basic microstructure of the hardfacings, turned in the industrial tests, was similar to the microstructure of Hardfacing A.

### **3.4 TOOL MATERIALS AND TOOL GEOMETRY**

Generally, PCBN products can be sorted into two types (Stephenson et al, 1996); one type has relatively low cBN content (<60%) and various binder phases and is commonly used in smooth or finish cutting; The other type has a higher cBN content and with either a ceramic binder (e.g. AlN) or a metallic binder (e.g. cobalt). Products of this type have high hardness, toughness and thermal conductivity and are used in rough cutting conditions or for some extremely difficult-to-machine materials e.g. Ni-hard, hardmetals and some engineering ceramics.

In this work, three PCBN materials (CBN1- 6) designed for rough cutting conditions were used for turning the hardfacings. All of them belong to the second group with the higher cBN volume fraction and with high hardness. The materials are all commercially available but from different suppliers. Detailed investigation of their microstructures has been carried out in the current work and the results will be presented in Chapter 4.

As listed in Table 3.2, most of the inserts used in this work were solid because of the arduous nature of the task. The inserts of CBN6 were single-sided, but the insert size

( $\phi$  10 mm) is larger than the other inserts ( $\phi$  7 mm/9mm). This may increase the strength of the cutting edge. Edge preparation is also very important for a successful application and a proper chamfer may well increase the strength of the cutting edge (Stephenson, 1996). The size and edge preparation of the inserts used in these tests were commercially available and no special designs have been used. The tool holder, 25 × 25 mm in section, was also commercially available and had a screw top clamp. It was available in both left or right hand orientation to meet the requirements of the machining conditions.

**Table 3.2** Tools used in the test.

Parameter Material	Insert type	Geometry*	Chamfer	Tool holder
CBN1	Solid	RNGN070300	0.1mm × 10°	CRSNL2525
CBN2	Solid	RNMN090400	0.15mm × 10°	CRSNL2525
CBN3	Solid	RNGN070300	0.1mm × 10°	CRSNL2525
CBN4	Solid	RNMN070300	0.15mm × 10°	CRSNL2525
CBN5	Solid	RNMN070300	0.15mm × 20°	CRSNL2525
CBN6	Sided	RNMN100300	—	CRSNL2525

\* R: Round insert, N: Clearance angle = 0°, G/M: Tolerance, N: Solid insert.

# CHAPTER 4 MICROSTRUCTURE AND FUNCTIONAL CHARACTERISTICS OF TOOL MATERIALS

## 4.1 MICROSTRUCTURE AND HARDNESS OF THE TOOL MATERIALS

The six PCBN tool materials were mounted, ground and polished using standard metallographic techniques to reveal their structure. The process was difficult due to the high hardness of the material and the difference between the hardness of the CBN particles and the binding phases. The polished samples were examined on the Optical Microscope and SEM. Some general information on the materials, including particle size, volume fraction is summarised in Table 4.1. Elementary analysis revealed that CBN1, CBN2, CBN3 and CBN4 are based on ceramic binders, while CBN5 and CBN6 were manufactured with metallic binders.

**Table 4.1** Microstructural factors of the six PCBN tool materials.

Material \ Properties	Grain size	Volume fraction	Binder
CBN1	5-8 $\mu\text{m}$	>95%	AlN
CBN2	15-20 $\mu\text{m}$	>90%	AlN
CBN3	8-10 $\mu\text{m}$	>90%	AlN
CBN4	2-5 $\mu\text{m}$	>90%	AlN
CBN5	10 $\mu\text{m}$	>90%	Co
CBN6	10-15 $\mu\text{m}$	>90%	Co, Ni, Zn

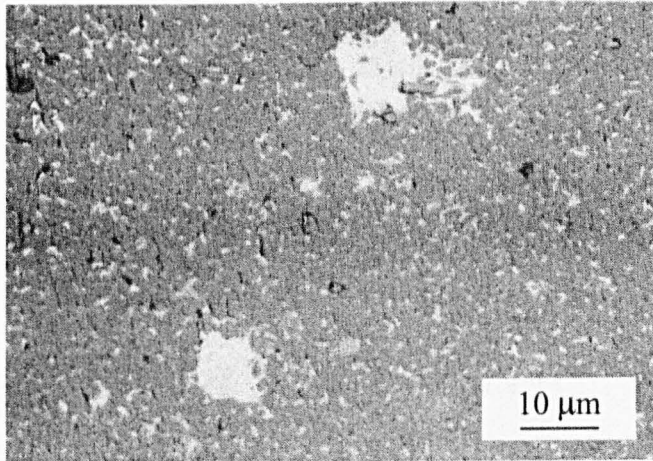
PCBN is formed by sintering cubic boron nitride particles together at high temperature and high pressure with the addition of a solvent or binder. As shown in

Figure 4.1, the microstructure of polished sections could be clearly distinguished with an optical microscope. The binding phase produces a bright image, while the bulk of the image comprises the cBN particles sintered together.

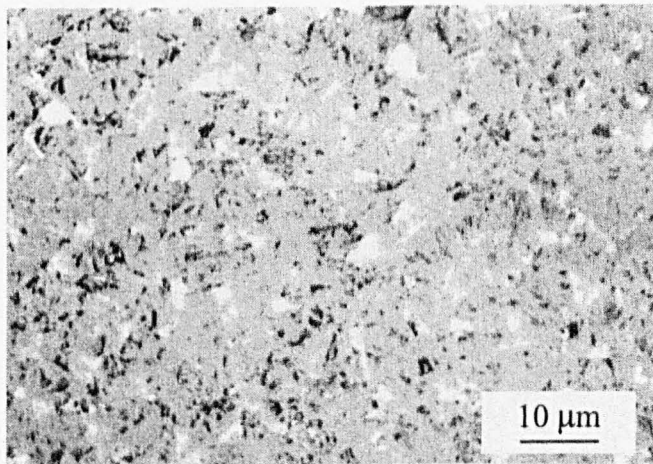
The difference in the six materials under microscopy are reflection of differences in the constituents and the manufacturing process, e.g. sintering temperature and pressure. CBN1 exhibits a dense structure with very little binding phase. The structure of CBN2 and CBN3 is similar, however, less binding phase was apparent in CBN2. CBN4 consists of a very fine structure with small particle size but the large agglomerates of binder are obvious signs of structural inhomogeneity. CBN5 has a metallic binding phase and, in the polishing process, this phase was readily torn out by the abrasive. This gave rise to the black areas seen under the microscope (Figure 4.1e). CBN6 was manufactured using a multiphase binding system and shows a certain degree of structural inhomogeneity.

In the synthesis of PCBN at high temperature and high pressure, the cBN particles maybe sintered together to form a particle network (Hooper and Brookes, 1984). The way the particles have been sintered together to form the PCBN sketch will have great influence on the mechanical properties of the material. In this work, boiling hydrochloride solution was used to remove the binding phase (AlN) to reveal the structure for CBN1-CBN4. This method was not applicable to CBN5 and CBN6, but examination with the SEM could still reveal much more useful microstructural information.

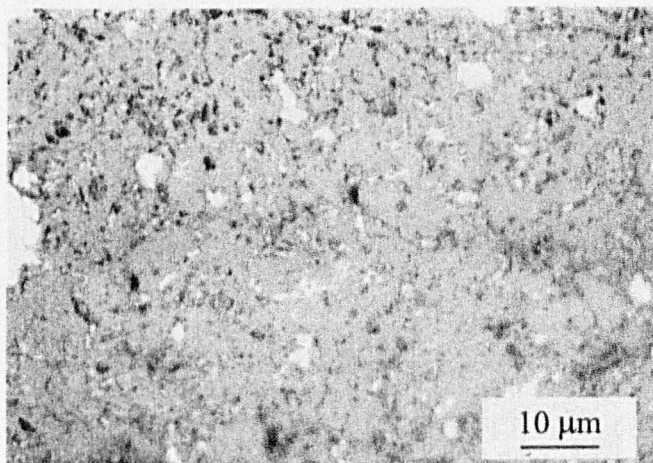
Figure 4.2 shows the SEM photos of the PCBN materials. It is clearly shown, after leaching off the binding phase, that network of cBN particles have formed within the microstructure of the materials. This continuous skeletal structure of CBN particle inevitably will provide resistance to the deformation of this material under mechanical loading conditions and the random orientation of strong particles make the polycrystalline materials very tough and much stronger than single crystals (Heath, 1986).



d) CBN4

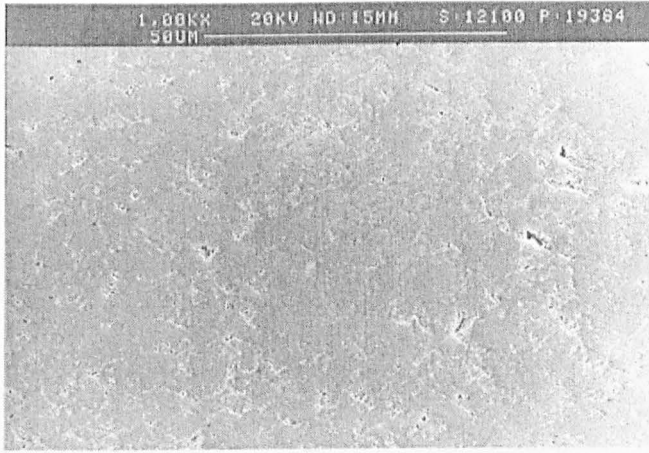


e) CBN5

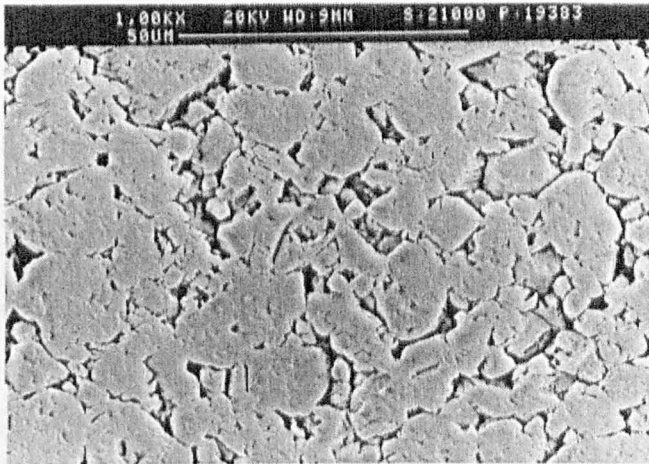


f) CBN6

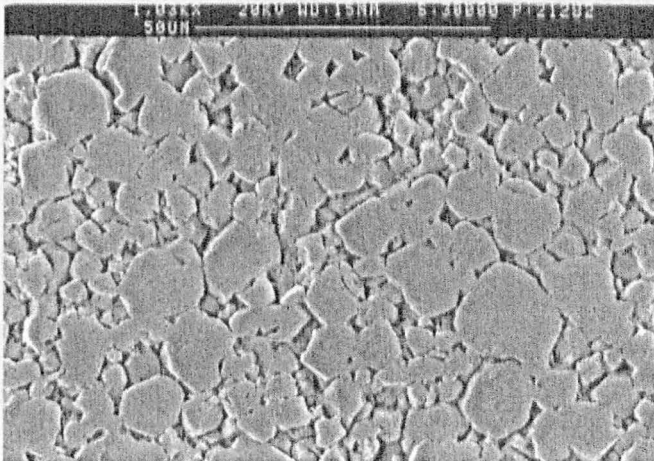
**Figure 4.1** Microstructure of the PCBN tool materials.



a) CBN1 (leached)

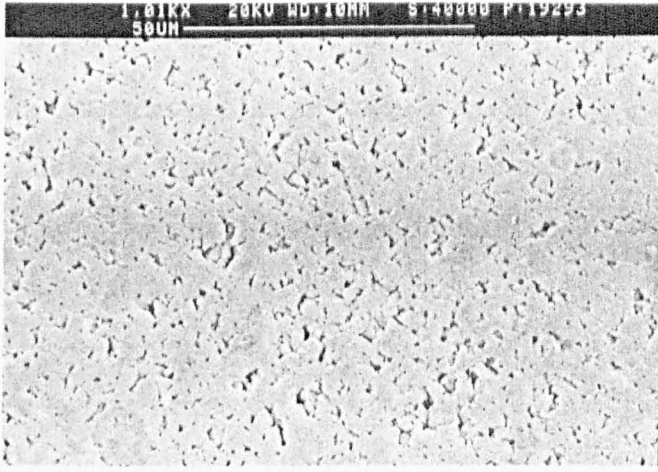


b) CBN2 (leached)

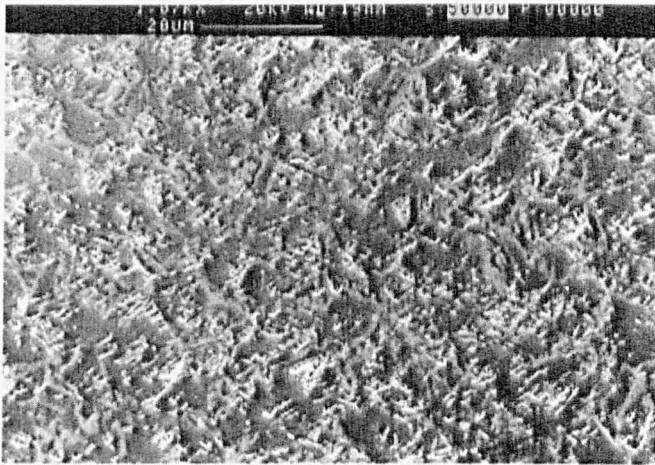


c) CBN3 (leached)

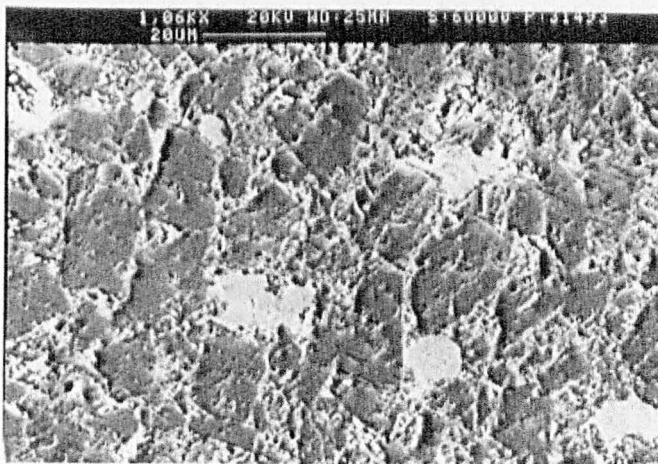
Figure 4.2 SEM photos showing the CBN network of the tool materials (Continued)



d) CBN4 (leached)



f) CBN5



g) CBN6

Figure 4.2 SEM photos showing CBN network of the tool materials

As shown in Figure 4.2a, CBN1 is very dense with regular-sized particles strongly sintered together. Figure 4.3 shows the microstructure of the material at higher magnification. It suggests that plastic deformation of the particles has occurred to some extent in the sintering process, which helped to form this very dense structure. The gaps between the particles (filled with the binding phase before leaching) are typical of pores in conventional sintering processes.

CBN2 has the large-size particles, and these are closely bonded but internal pores could be observed in some particles. The size of the external pores is largely due to the packing influence of the larger particles during the ceramic powder compaction. The particles are of regular size but the shape of the particles varies slightly. Some smaller particles filled in the gaps between the main particles, thus making the particle network more continuous.

CBN3 has the most homogeneous structure under the optical microscope (Figure 4.1c). SEM observation of the materials, after leaching out the binders revealed that the cBN particles are regular both in shape and size (Figure 4.2c). This will inevitably improve the structure in terms of homogeneity and probably will increase the reliability of the product. Some particles of smaller size have filled in the gaps between the CBN particles, thereby improving the sintering process. The particle size of PCBN4 is much more smaller than that of the other tool materials and the particles were closely bonded together (Figure 4.2d).

Figure 4.2 e-f shows the SEM photos of CBN5 and CBN6, without leaching the binding phases. CBN 5 has medium particle size and the particles have been closely sintered together. The damage that occurred to the binder in the polishing process can again be seen. CBN6 consists of very large CBN particles with a multiphase binding system. The main particles appear to be more loosely packed than the other PCBN materials and many internal defects could be observed.

The difference between the microstructures and possible differences between the intrinsic hardness of the raw materials resulted in different hardness values of the

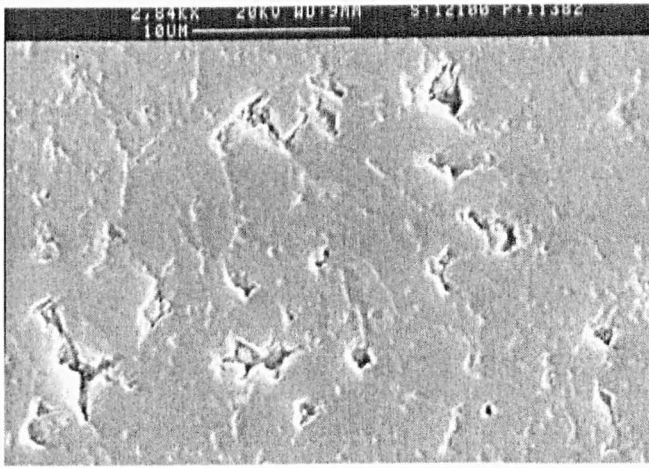


Figure 4.3 Close-up view of Figure 4.2a showing the detail of CBN1

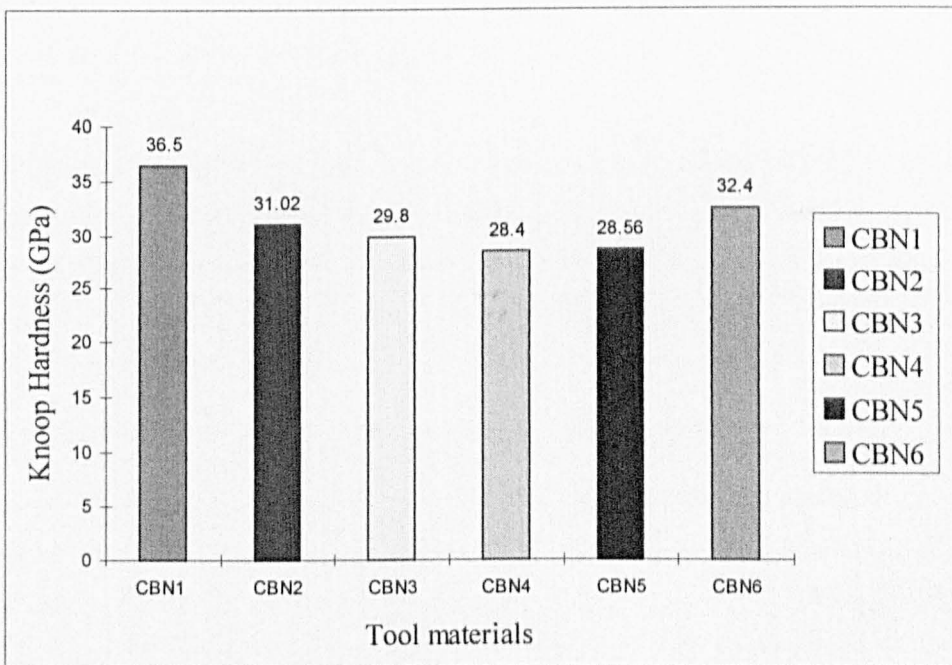


Figure 4.4 Knoop hardness of the tool materials (load = 2000 g)

materials, as shown in Figure 4.4. All the materials have high hardness values due to their high volume fraction and strong bonding between particles. This is an important characteristic of PCBN materials for their application in hard machining. Among these materials, CBN1 has the highest hardness while the other CBN materials all have similar hardness values.

Figure 4.4 shows the hardness of the materials at different temperatures. The hardness of the materials decreases as the temperature increases. This is due to the fact that the materials become softer as the temperature increases. The hardness of the materials is also affected by the grain size of the materials. The smaller the grain size, the higher the hardness of the materials. The hardness of the materials is also affected by the sintering temperature. The higher the sintering temperature, the higher the hardness of the materials. The hardness of the materials is also affected by the volume fraction of the materials. The higher the volume fraction, the higher the hardness of the materials.

Table 4.2 Summary of the relationship between the grain size and the hardness of the materials at different temperatures.

Material	850-850 °C	750-850 °C	650-850 °C
CBN1	~18 GPa	~18 GPa	~18 GPa
CBN2	~18 GPa	~18 GPa	~18 GPa
CBN3	~18 GPa	~18 GPa	~18 GPa

As the grain size of the materials increases, the hardness of the materials decreases. This is due to the fact that the materials become softer as the grain size increases. The hardness of the materials is also affected by the sintering temperature. The higher the sintering temperature, the higher the hardness of the materials. The hardness of the materials is also affected by the volume fraction of the materials. The higher the volume fraction, the higher the hardness of the materials.

## 4.2 ADHESION TEST RESULTS

The adhesion tests were carried out in an enclosed chamber, evacuated to a pressure of approximately  $10^{-5}$  mbar at temperatures representative of the temperatures generated during cutting. The lowest temperature at which adhesion occurred was determined by increasing the test temperature in increments of  $50^{\circ}\text{C}$  from an initial temperature of  $800^{\circ}\text{C}$ . The separation of the junction was carried out at room temperature in normal atmosphere.

Normally, during the application of the load, the tip of the cone flattened by plastic flow to form a contact area sufficient to support the applied load (Nabhani, 1991). The contact pressure was obtained by dividing the load by the measured contact area. With increased the temperature, the area of the contact surface increased and consequently, the contact pressure decreased.

**Table 4.2** Summary of the interaction between the cone and tool surfaces at different temperatures

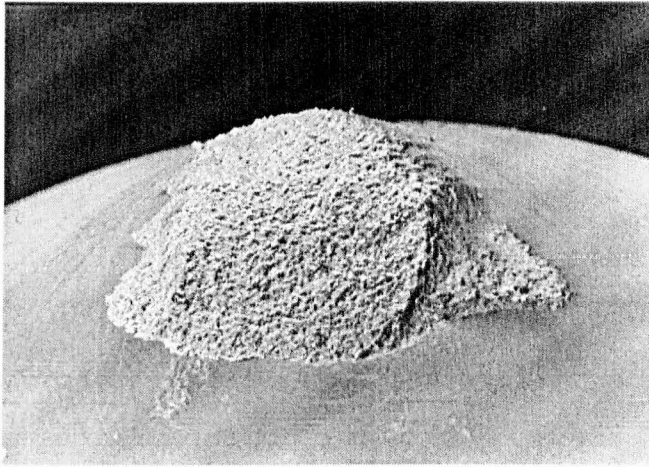
	800 - 850 °C	900 -1000 °C	1050 °C
CBN1	×	×	×
CBN2	×	Strong adhesive junction	
CBN3	×	×	Particles pulled out

x: no adhesion occurred

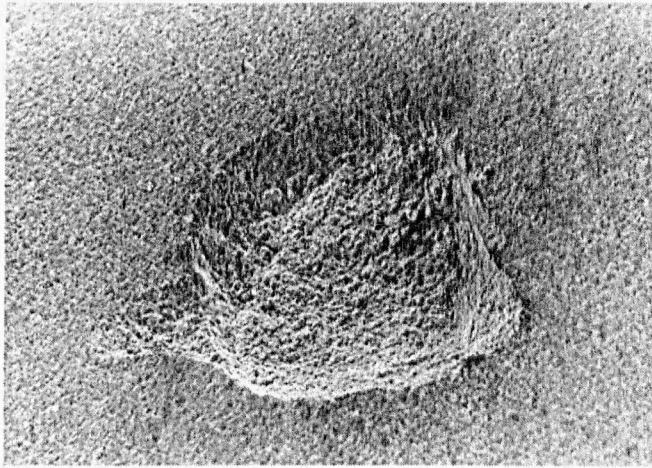
Table 4.2 summarises interaction between the cone and the workpiece at different temperatures. At temperatures of  $800^{\circ}\text{C}$  and  $850^{\circ}\text{C}$ , no adhesion occurred between the cone and any of the three CBN materials. In each case, the contact face of the cone and the CBN was smooth and clean.

At 900°C and a mean contact pressure of 0.23 GPa, strong adhesion occurred between the workpiece cone and CBN2 material, the junction having sufficient strength to lift the tool insert up from the recess of the susceptor when removing the load. The subsequent separation of the cone and the CBN2 material resulted in fracture within the CBN, over the whole contact area. Figure 4.5 shows the result of separation of the junction formed between the hardfacing and the tool material. A hemispherical fragment has been transferred to the cone (Figure 4.5a), and a crater has been left in the original surface the CBN2 (Figure 4.5b). SEM observation of the crater surface has shown that the basic fracture mode was transgranular, which agreed well with the observations by Hooper and Brookes (1984). Their fractography studies showed that fracture occurs through the primary particles and across the inter-particle bridges in a number of aggregates of cubic boron nitride and of diamond.

Further increases in experimental temperature, up to 1050°C, were insufficient to form a strong welded junction with either CBN1 or CBN3. However, a number of particles of the hard phase i.e. cubic boron nitride, were pulled out from the tool material at the temperature.



a) CBN2 tool material adhering to the workpiece cone



b) Crater formed in CBN2 material

**Figure 4.5** An adhesive junction between the workpiece cone and CBN2 at 900°C (separated at room temperature).

## CHAPTER 5 QUICK STOP TEST RESULTS

### 5.1 INTRODUCTION

The cutting conditions in the quick stop tests were set as: S65-70m/min, F0.25mm/rev and depth of cut 0.5 -0.7 mm to simulate the conditions used in the cutting tests. The RNGN070400 insert of CBN1 was held in the quick stop tool holder with a negative rake of 6°. All the cutting was performed without using a coolant or lubricant and a tailstock was used in all the tests in order to make the system sufficiently rigid.

In a quick stop test, once steady-state cutting had been established, the cutting action was suddenly stopped by firing the gun. Figure 5.1 shows schematically the chip attached to the workpiece after a quick stop test. It is difficult to produce good quick-stop chips with these hardfacing materials due to the nature of the chip formation process and the presence of carbide particles within the material, which may lead to microscopic cracking.

In the sampling process, a quick-setting epoxy resin (Araldite) was poured into a plasticine mould around the chip to embed it and protect it from possible damage in the sample preparation process. The sample, in the form of the chip and the adjacent part of the workpiece covered by the resin, was separated from the parent bar on an Electro Discharge Machine (EDM). The sample was then re-mounted in Araldite and sectioned about half way through its width, to reach the whole longitudinal section of the chip, by grinding away the excessive Araldite and the workpiece material. After fine grinding and polishing, the specimen was etched in Marble's reagent (10g  $\text{CuSO}_4$ , 50 ml HCl, 50ml  $\text{H}_2\text{O}$ ) to reveal the microstructure.

In a machining process, the chip is separated from the workpiece on the transient, newly formed, surface (Figure 5.1), which is under direct contact with the cutting edge and the flank face of the insert. Therefore, the subsurface structure of the transient surface may well reflect the deformation behaviour of the constituents of

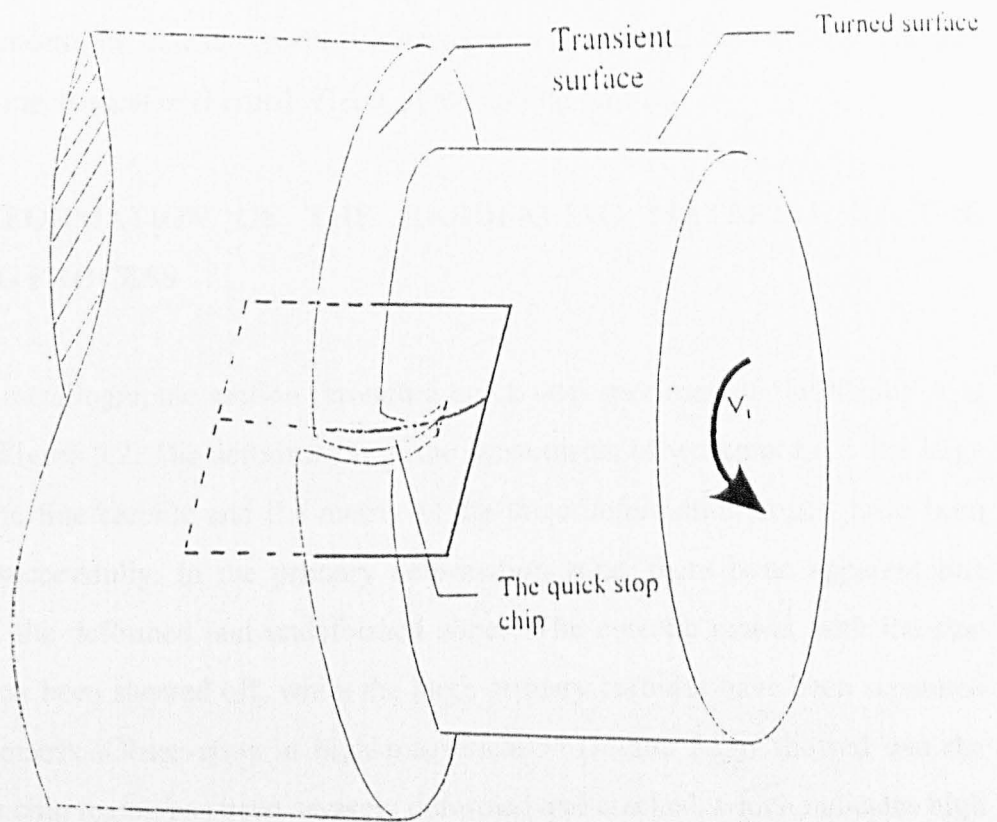


Figure 5.1 Schematic to show the chip attached to the parent workpiece after the quick stop.

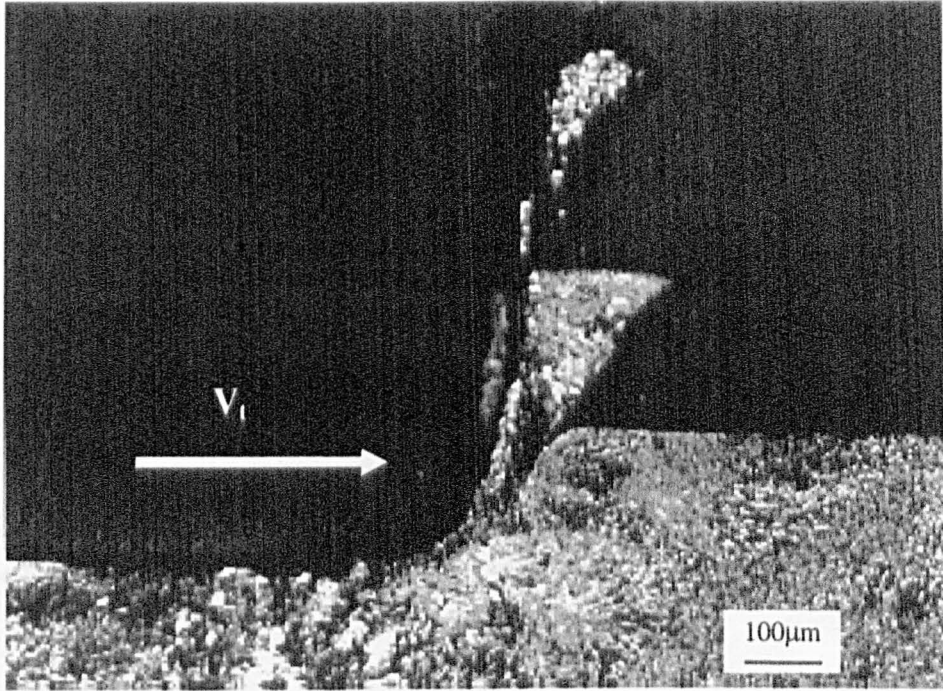
the workpiece, especially the carbides, which is of great importance in understanding the wear of tool inserts in the cutting process. The sample was obtained by sectioning the transient surface, as shown in the Figure 5.1. After grinding and polishing, the sample was etched to reveal the subsurface structure. In addition, micro-hardness profiles beneath the transient surface were measured to reveal the hardness changes due to the mechanical or thermal effects of the cutting process.

## **5.2 DEFORMATION OF THE HARDFACING MATERIAL IN THE CUTTING PROCESS**

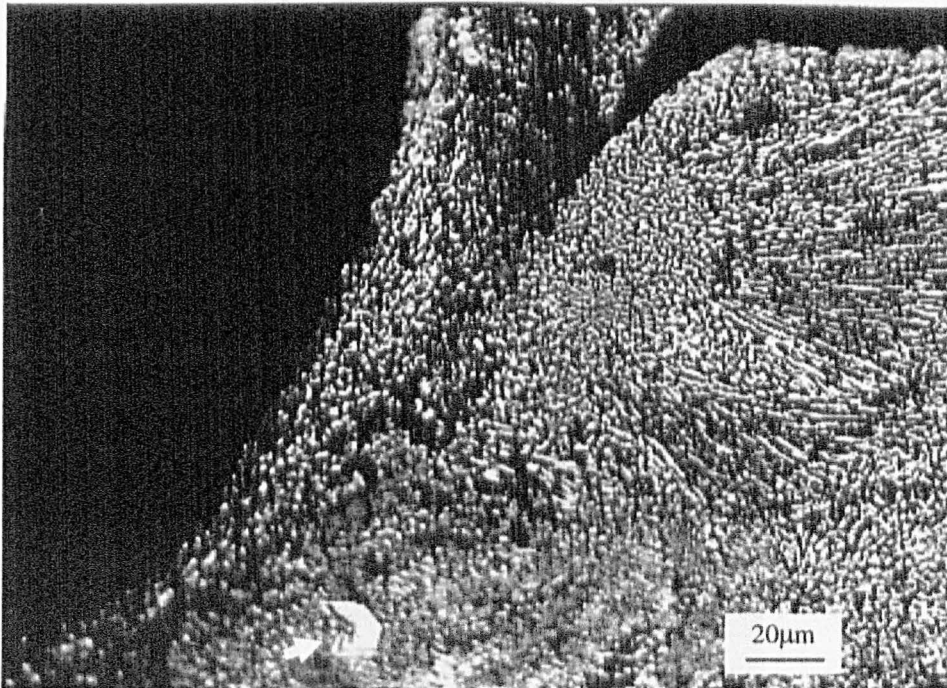
A typical metallographic section through a quick-stop specimen of Hardfacing A is shown in Figure 5.2. The deformation of the constituents of workpiece, i.e. the large carbide, the fine carbide and the matrix in the three deformation zones, have been captured successfully. In the primary deformation zone, there is an apparent line separating the deformed and undeformed zones. The eutectic matrix with the fine carbides has been sheared off, while the large primary carbides have been separated from the matrix. Observation at high magnification (Figure 5.2b) showed that the root of the chip region has been severely deformed and cracked, which indicates high loading in this region in the cutting process.

During the cutting, most of the primary carbides appear to move into the chip segment without contacting the tool but those under direct contact with the tool material become fractured. The large carbide (Figure 5.2b) right ahead of the cutting has cracked under the very high loading in advance of the tool, which indicates the high stress generated around the cutting edge. Detailed observation showed that the cracking started from the centre of the carbide due to its inherent structural defects.

Figure 5.3a shows a typical quick-stop sample of Hardfacing B. On the orthogonal plane, the primary carbides shows different section shapes in relation to their orientation to the cutting edge. The columnar grains (A) are carbides roughly perpendicular to the cutting edge, while the hexagonal grains (B) are representative of those roughly parallel to the cutting edge. In the workpiece, most of the primary

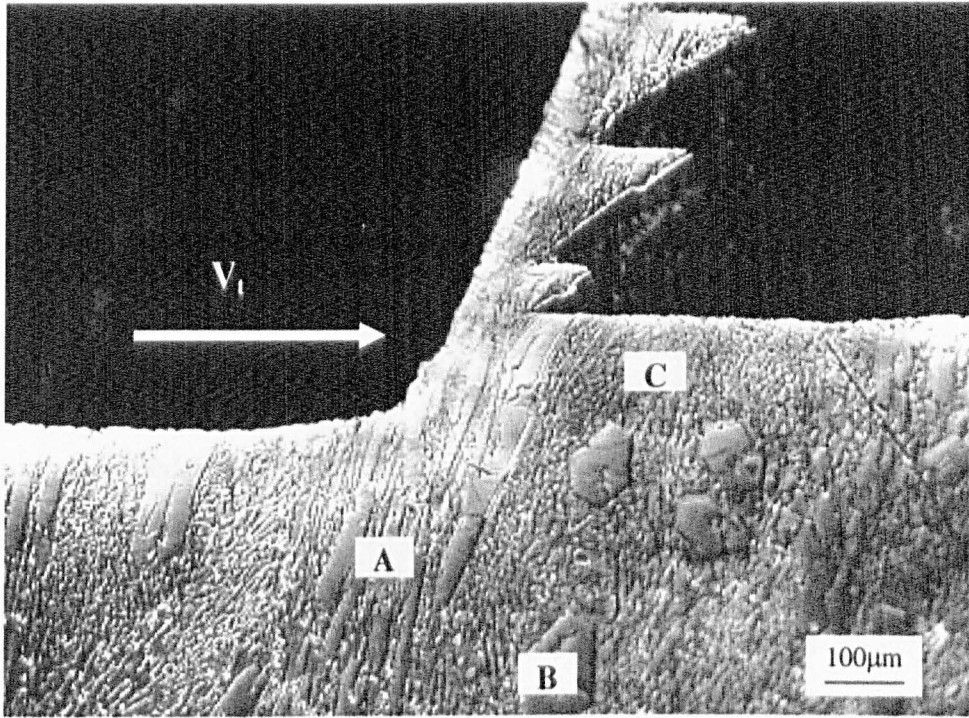


a) General view

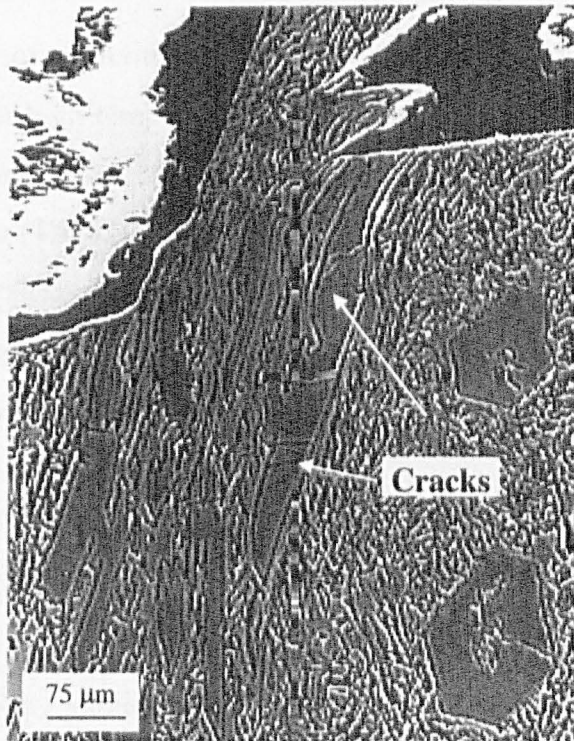


b) Enlarged view of the base of the the chip

**Figure 5.2** Metallographic section through a quick-stop specimen of Hardfacing A (fine structure, S65m/min., F0.25mm/rev, DOC0.65mm)



a) General view



b) Enlarged view showing cracking of primary carbides around the cutting edge.

**Figure 5.3** Metallographic sections through a quick-stop specimen of Hardfacing B (coarse structure, S65m/min, F0.25mm/rev, DOC0.65mm).

carbides were columnar, due to the preferential cooling from the mild steel substrate in the welding process. As shown in the microstructure, the cross sections of the large carbides were not regular and exhibited significant structural defects.

Figure 5.3b shows a close-up view of the deformation of the large carbides around the cutting edge. Some large, columnar, primary carbides have cracked ahead of the cutting edge and cleavage is the main fracture mode. In addition, separation of the carbide and matrix has occurred along the boundary of the carbide and the chromium-depleted zone. After fracture, fragments of the carbides have moved into the chip in the subsequent chip formation process but no obvious movement (e.g. rotation), of these large fractured carbide segments was observed. The eutectic structure (fine carbide in matrix) has severely deformed in this process but no cracking of the eutectic matrix was observed. The fracture toughness of the fine structure is much greater than that of the brittle carbide (Lee et al, 1996).

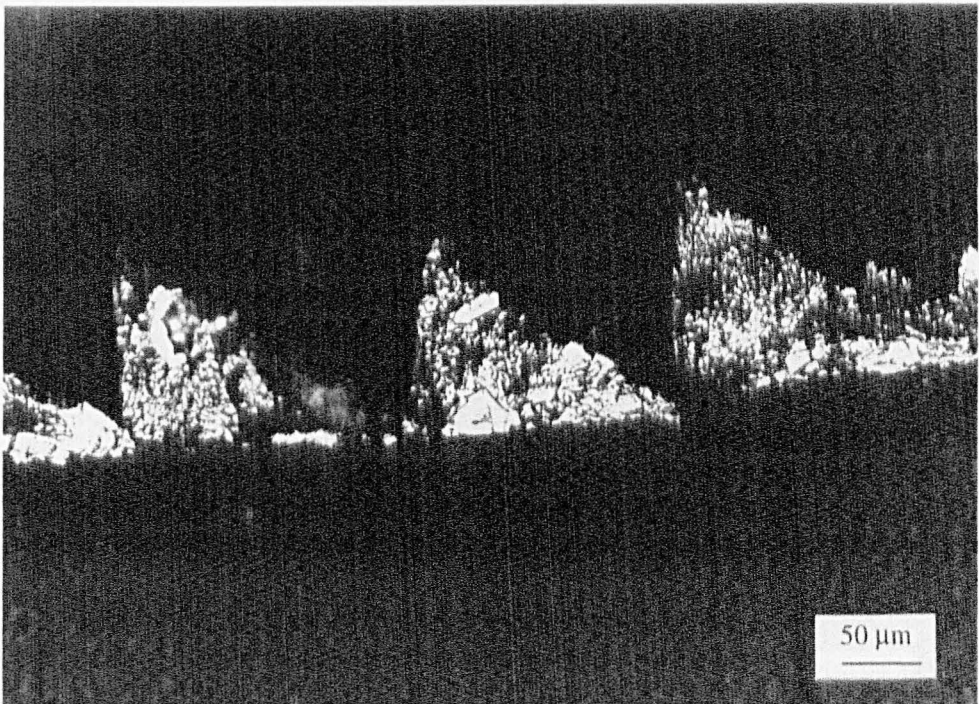
In machining some soft materials, e.g. mild steel, the high compressive stresses on the clean material at high temperatures can produce friction welding of the chip to the tool. A flow zone could form with a steep velocity gradient away from a zero value at the rake face (Trent, 1991). However, in the machining of both Hardfacings A and B, the underside of the chip was free from welding to the tool face. No apparent flow zone could be observed in the quick stop samples. This is possibly due to the poor plasticity of the workpiece and lack of adhesion between the workpiece material and the tool material.

### **5.3 CHIP MORPHOLOGY**

In the cutting process, similar forms of chip have been produced for the two hardfacing materials (Figure 5.4a and Figure 5.5a). The basic form of the chips is semi-circular with the side near the minor cutting edge severely segregated. The chip for Hardfacing A was a golden colour while the chip of Hardfacing B was a similar colour but brighter. The chips of Hardfacing B, generated under similar cutting conditions, were much more regular than those of Hardfacing A. The general form of

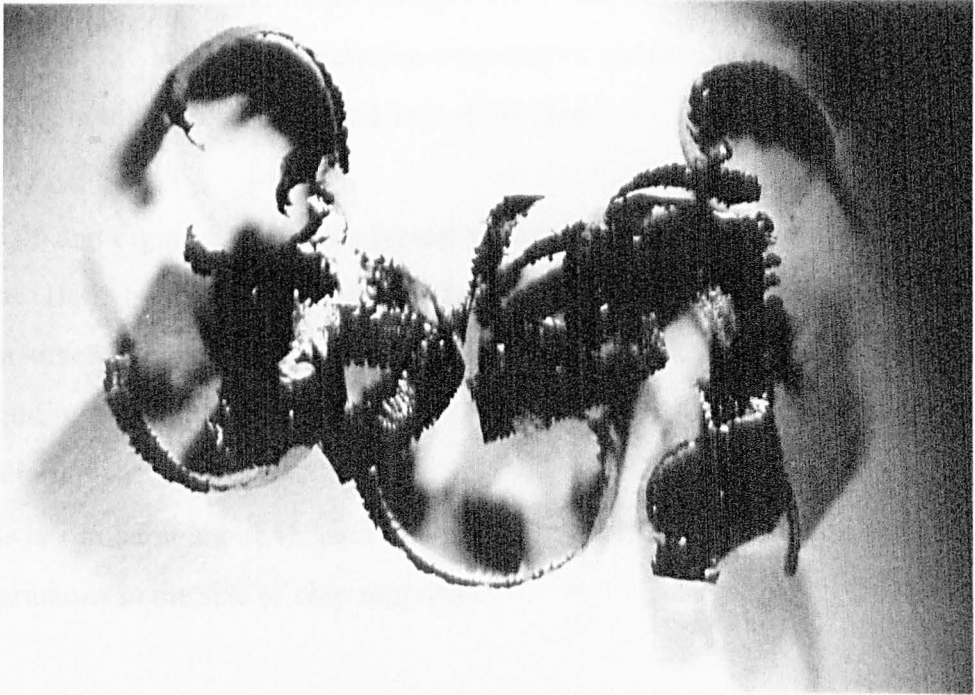


a) General chip form

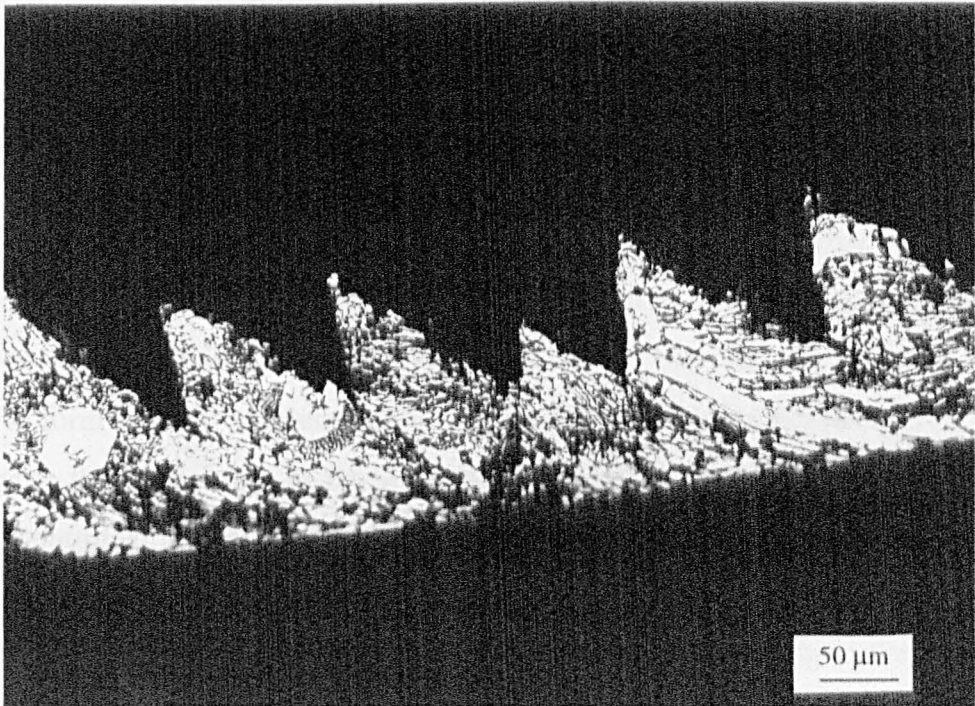


b) Longitudinal section of the chip

**Figure 5.4** Typical chips of Hardfacing A (fine structure, S65m/min, F0.25mm/rev, DOC0.65mm).



a) General chip form



b) longitudinal section of the chip

**Figure 5.5** Typical chips of Hardfacing B (Coarse structure, S65m/min, F0.25mm/rev,DOC0.65mm).

the chips did not vary significantly with changes of cutting speed or feedrate. However, the colour of the chips changed from brighter to darker with increased cutting speed. This reflected the cutting temperature increase with cutting speed and the consequent higher oxidation tendency of the chip.

Figure 5.4b and Figure 5.5b show a typical views of the longitudinal cross sections of the chips. Both hardfacings produced typical saw-tooth chips, which have been found in other engineering materials e.g. Hardened steel, titanium alloys, etc. at certain cutting conditions (Stephenson and Agapiou, 1996). The angle of the primary deformation plane with respect to the cutting direction for the two workpiece materials is similar at about  $45^\circ$  and this angle has kept roughly constant irrespective of the variations in the size of chip segments.

The tool face side of the chips is regular and, as in the case of the quick-stop samples, no apparent flow of the workpiece has occurred. However, observation at high magnification revealed severe deformation at the base of the chip; cracking or fracture of the fine carbide could be observed at the base of the chips of Hardfacing A.

For both of the two materials, much less deformation has occurred in the bulk of the chip segment than in primary and secondary deformation zones. The large quantity of fine carbides and the primary carbides or the fragments of the carbides will inhibit further deformation within the chip segment. Hence, the shearing and cracking process to form the chip segment was limited to a narrow region extending from the tool edge to the free surface of the workpiece. In addition, the large carbides have strongly controlled the chip formation process as shown in Figure 5.5b. A carbide, which is large enough cover the one or more chip segments, has kept its original form, thus restraining the ability of the material to deform. According to Stephenson and Agapiou (1996), this localised chip formation characteristic will inevitably increase the cutting forces.

Apparently, the cutting edge will suffer from very high loading due to the deformation character of the workpiece material in the cutting and result in high tool wear rates. In addition, it should be noted, compared with the fine carbide in some other engineering materials like steel, the carbide size in the hardfacing materials is much larger. As a consequence more severe damage to the tool material will occur in the cutting process. As shown in the cross-sections of the chips, the matrix of the workpiece material is not continuous enough to avoid the direct contact between the carbides and the tool surface. When large carbide fragments are encountered, the carbide may impact on the CBN particle when the chip is moving over the tool surface, thus increasing the wear of the tool.

#### **5.4 HARDNESS PROFILE AND SUBSURFACE STRUCTURE OF THE TRANSIENT SURFACE**

Hardness samples were sectioned from different locations of the transient surface and the measurements were made without etching the samples. A relatively high load (200g) was used to reduce the effect of individual particles. Each result was the average value of at least five readings.

Figure 5.6 plots the subsurface hardness profile of the two hardfacing materials. It is clearly shown that, there is a soft layer about 30-40 $\mu$ m deep right beneath the transient surface of the workpieces. The figure also shows that the hardness decreases more towards the transient surface in Hardfacing B than in Hardfacing A.

Figure 5.7 shows the structure of the cross-section of Hardfacing A. In the region beneath the transient surface (arrowed), a disturbed microstructure exists. The fine carbides have been bent slightly in the cutting direction by the action of the tool. In addition, the carbides had been fragmented at the surface region. The mechanically-disturbed layer is much shallower than the region with lower hardness, as shown in Figure 5.6. This demonstrates that the thermal effects involved in the cutting process have determined the depth of the affected layer. Observation of the larger carbides at

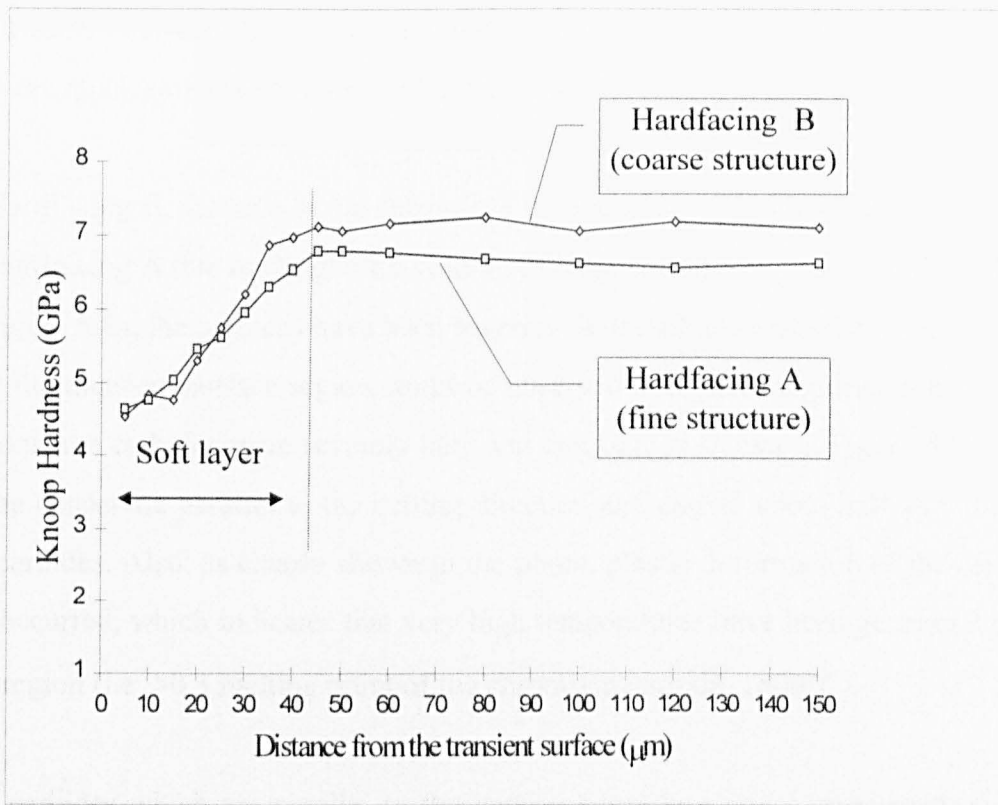


**Figure 5.6** Hardness profile beneath the transient surface (load = 200g).

the transient surface shows that they have cracked or fractured, which is consistent with the quick stop result shown in Figure 5.2b.

In Hardfacing B, damage of the subsurface is much more significant than in the case of Hardfacing A due to the greater volume of large carbides in the former. As shown in Figure 5.8a, the carbides have been severely deflected and cracking of the carbides near the transient surface region could be observed at higher magnification. In some regions, the carbides were severely bent and cracked, as shown in Figure 5.8b. Most of the cracks are parallel to the cutting direction and extend about half way through the carbides. Also, as clearly shown in the photo, plastic deformation of the carbides has occurred, which indicates that very high temperatures have been generated in the this region (i.e.  $>0.3$  melting point of the chromium carbide,  $1800^{\circ}\text{C}$ ).

The carbides which are parallel to the cutting edge (hexagonal cross-section) have undergone more severe interaction with the tool in the material removal process. These carbides have either fractured or cracked and this damage would have been initiated at the centre of the carbide due to the existence of defects. The greater microstructural disturbance in Hardfacing B suggests that the flank of the tool insert has suffered much less abrasion in machining Hardfacing A than in machining Hardfacing B.

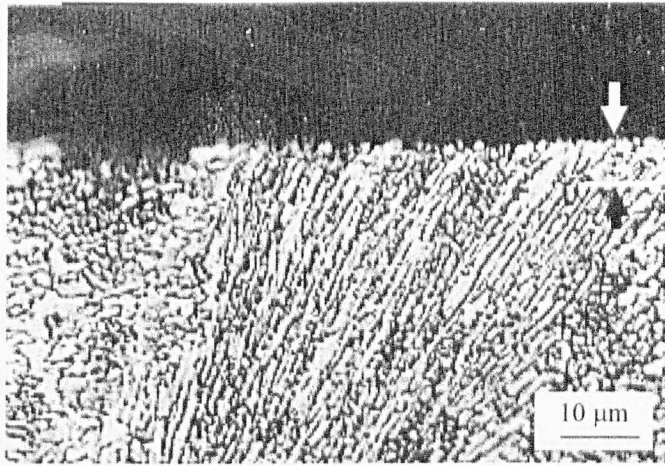
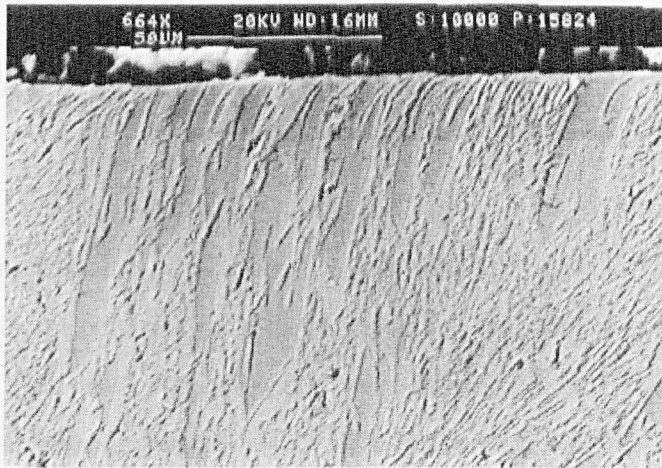


**Figure 5.7** Cross section of the transient surface of Hardfacing A (S65m/min).



a) Deflection + bending of the carbides



b) Cracking of large carbides

**Figure 5.8** Cross section of the transient surface of Hardfacing B (S65m/min).

## CHAPTER 6 CUTTING TESTS RESULTS

### 6.0 INTRODUCTION

This chapter contains the results of cutting tests both in the laboratory and in industry. In the laboratory tests, tool wear processes and the effect of cutting time, cutting speed and the feedrate was studied. In the field cutting tests, the cutting performance of six PCBN products from different suppliers was assessed, and the failure modes and wear mechanisms of different PCBN materials were examined.

### 6.1 LABORATORY CUTTING TESTS

#### 6.1.1 INTRODUCTION

Machining tests were conducted on the CNC lathe with a left-hand tool holder mounted in the rear tool turret. Table 6.1 lists the cutting conditions for the tests. Depth of cut was kept constant in order to minimise the effects of the microstructure inhomogeneity. The used tool inserts were observed on a scanning electron microscope (SEM) after cleaning in 50%-50% hydrochloride solution. Some samples were observed without cleaning in order to investigate the interaction between the cutting tool and the workpiece. Contact length, width of the flank wear land and chipping dimension of the engaged edge were measured and compared between the tools under different cutting conditions.

**Table 6.1** Conditions for the laboratory cutting tests.

Cutting speed (m/min)	32, 45, 65, 85
Feed rate (mm/rev)	0.15, 0.25, 0.35
Depth of cut (mm)	0.65
Cutting time (mins)	0 - 8
Tool material	CBN1

Extensive cutting tests were undertaken using Hardfacing A to investigate the tool wear process and the effects of the cutting time and cutting parameters. Limited cutting tests have been undertaken with Hardfacing B to study the effect of the large carbides in the workpiece material on tool wear mode and rate.

## 6.1.2 MACHINING OF HARDFACING A (FINE STRUCTURE)

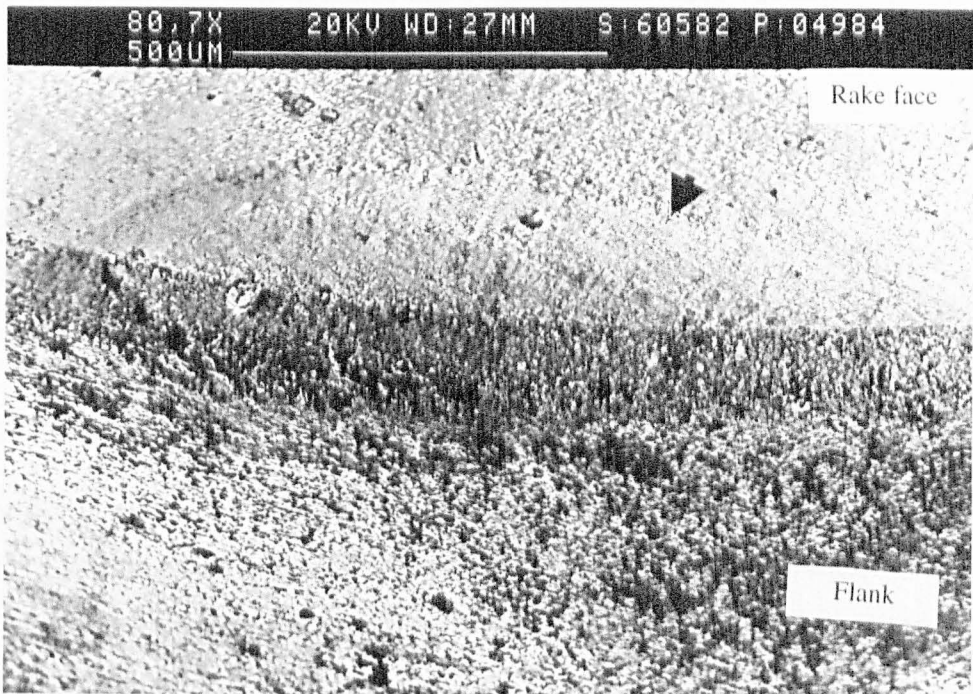
### 6.1.2.1 Chip-tool contact in the cutting process

Figure 6.1a shows a typical view of the tool face in which the main contact area can be clearly distinguished. The main cutting force involved in the chip formation process was applied on this region. The contact length varied with the undeformed chip thickness along the cutting edge. The average contact length, after 1 min. cutting in machining of workpiece A under different cutting conditions, are listed in Table 6.2. It is clear that with increased feed rate, the contact length has significantly increased and on the other hand, contact lengths have slightly reduced at higher cutting speed. Within the cutting times in this test, no large variations in contact length were found with different cutting duration, which agrees well with early work (Balazinski, 1993).

**Table 6.2** Contact length (mm) at different cutting conditions.

Feedrate Speed	F0.15 mm/rev	F0.25 mm/rev	F0.35 mm/rev
40 m/min	0.14	0.245	0.30
60 m/min	0.13	0.23	0.29
80 m/min	0.125	0.19	—

Figure 6.1b shows a close-up view of the main contact region. In the cutting process, the adhesion between the chip and tool rake face is very limited. No sign of a built-up layer or edge has been observed for inserts under different cutting conditions. X-ray analysis showed very limited signs of the workpiece elements (Fe, Cr, C) on the



**Figure 6.1a** Chip-tool contact area in the cutting process.

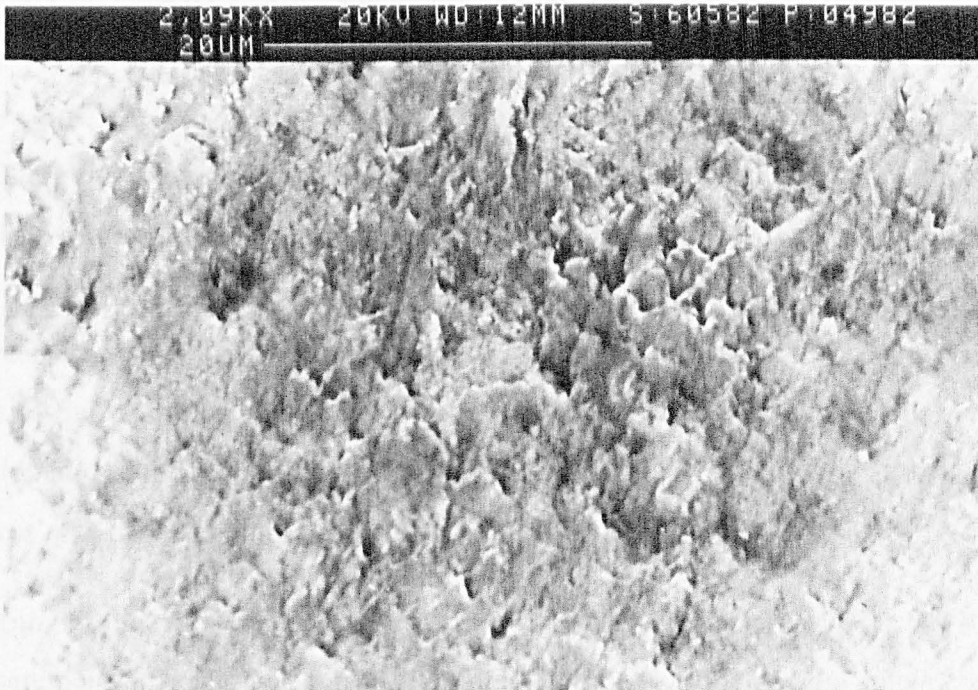


**Figure 6.1b** Enlarged view of a) showing the detail of the main contact area on the tool rake face.

contact surface. The binding phase has been eroded away at some locations, but no grooving or cratering is apparent.

### 6.1.2.2 TOOL WEAR PROCESSES

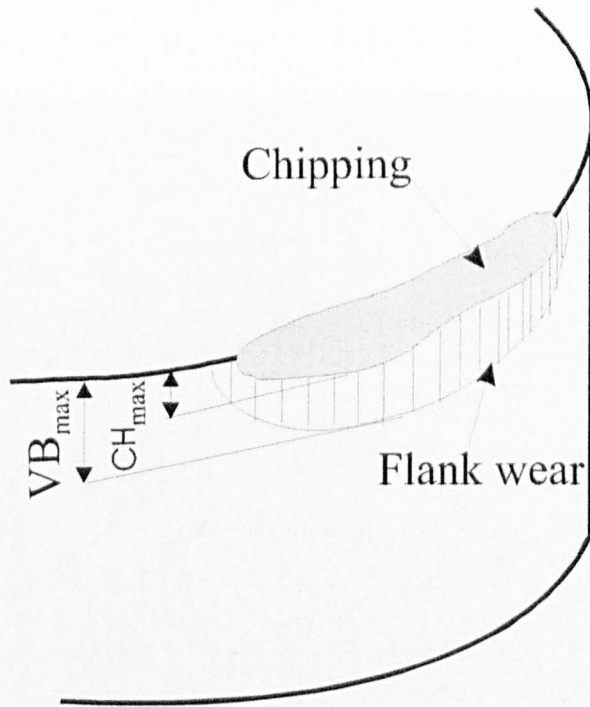
#### Tool wear vs. cutting time

Figure 6.2 shows, schematically, typical wear on the edge and the flank face of a tool insert. In addition to  $VB$  and  $VB_{max}$  (the average and maximum width of the flank wear land), the average and maximum width of the chipping, designated  $CH$  and  $CH_{max}$ , respectively, have also been monitored. As shown in the model,  $CH$  and  $CH_{max}$  represent the decrease of the engaged cutting edge and, roughly, reflect the lost volume of the cutting edge. According to Wright and Bagchi (1981) and Shintani et al (1989), the decrease of the cutting edge is an important additional tool wear parameter.

Figure 6.3 is a plot of tool wear as a function of cutting time at fixed feed rate (F0.25mm/rev) and depth of cut (0.65mm). The flank wear land width has increased steadily with the cutting time. The consistency of  $VB$  and  $VB_{max}$  indicates that the tool flank face has experienced a regular wear process. In the later stage, the gap between the  $VB$  and  $VB_{max}$  has increased, which indicates that the contact between the tool flank and the workpiece has formed in such a way that the tool wear has developed preferentially in some locations. This also indicates that the cutting process may have become less stable.

Chipping of the cutting edge occurred at an early stage but on a limited scale, making measurement difficult. The consistency of  $CH$  and  $CH_{max}$  indicated a stable chipping process, in which the chipping was on a small scale and damage to the cutting edge progressive.

Figure 6.4 shows the chipping and flank wear of the insert after 1 and 8 minutes cutting. Chipping has started at the lower edge of the chamfer and developed on the



**Figure 6.2** Schematic to show typical tool wear mode and the definition of  $VB_{max}$  and  $CH_{max}$ .

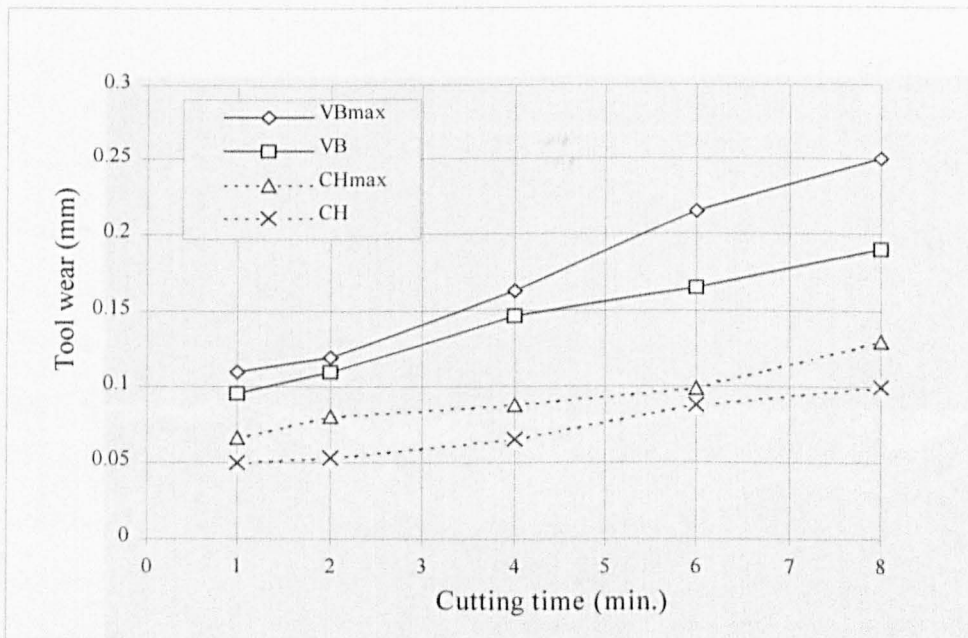


**Figure 6.3** Tool wear vs. cutting time (S65m/min, F0.25mm/rev, DOC0.65mm).

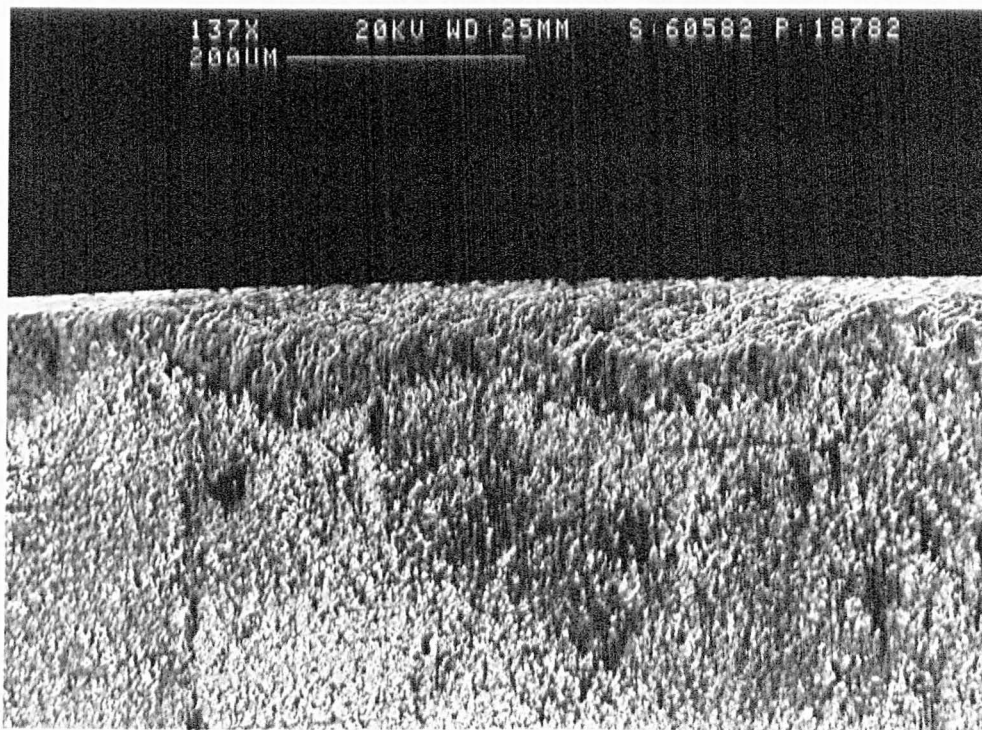


**Figure 6.4a** Chipping and flank wear of tool insert after 1 minute cutting (S65m/min, F0.25mm/rev, DOC0.65mm).

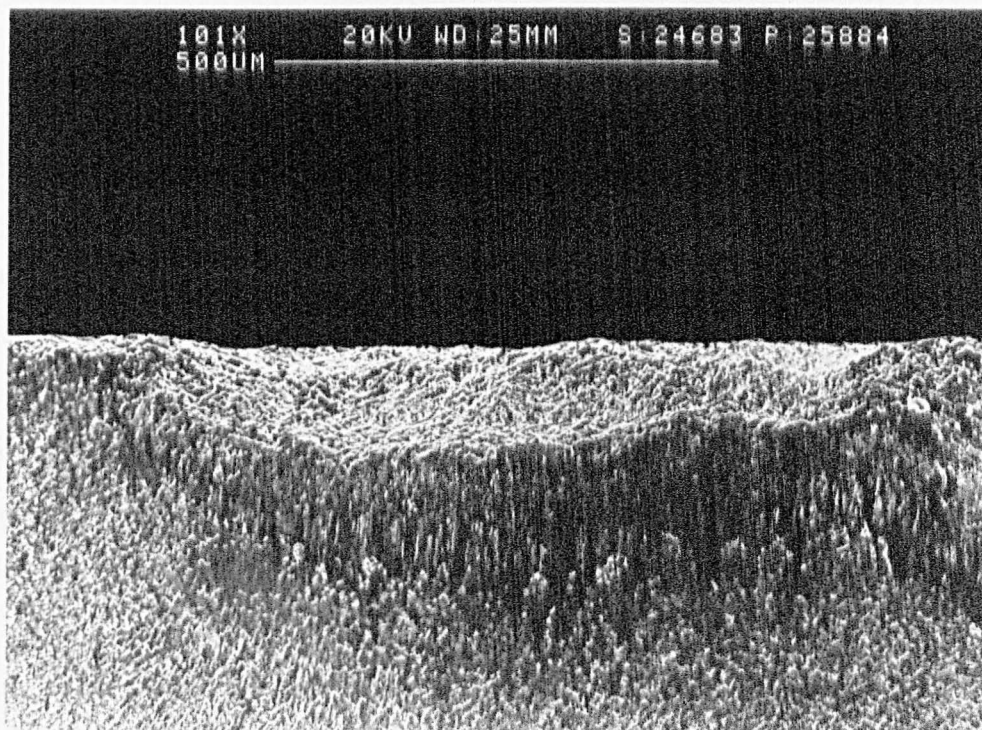


**Figure 6.4b** Chipping and flank wear of the insert after 8 minutes cutting (S65m/min, F0.25mm/rev, DOC0.65mm).

flank face of the insert. In the later stage, it developed further along the cutting edge in addition to developing further down the tool flank, leading to large portion of the cutting edge being lost.

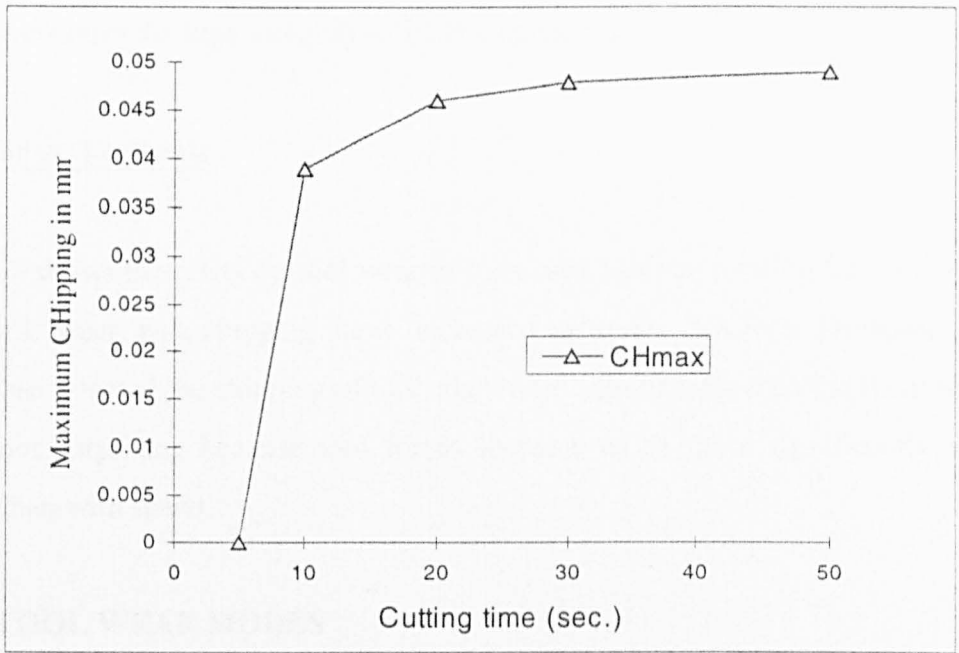
### **Initiation of chipping after short time cutting**

A series of short cutting tests (<1minute) were performed to study the initiation of tool wear, especially in terms of the chipping of the cutting edge. The results in the form of a tool wear curve is plotted in Figure 6.5. The chipping process started after cutting for about 10 secs, and was limited to very small scale, i.e. a few CBN particles. As shown in the curve, there is an incubation period (about 5 sec.), during which no chipping seems to have occurred. This indicates that the chipping process is time-dependent, and there is accumulation of damage in the tool before material is finally removed from the cutting edge.

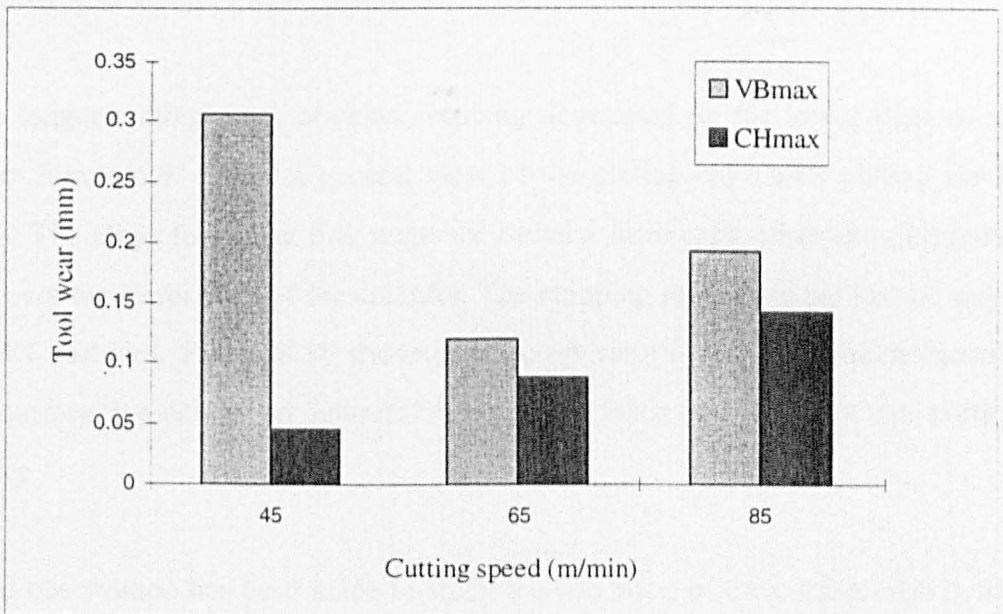
### **Tool wear vs. Speed**

Figure 6.6 compares the flank wear and chipping of CBN tools at three cutting speeds (cutting for 1 minute). Cutting speed appears to affect flank wear and chipping in different ways. At higher and lower cutting speeds, the tool has suffered higher flank wear. In other words, there appears to be an optimum speed in terms of the flank wear. This agrees with many results when machining hard materials, e.g. hardened steel, cobalt-based hardfacing materials, with PCBN tools. This phenomenon is connected with the opposite effect of cutting speeds over factors enhancing wear e.g. increased temperature, and those reducing wear, e.g. decrease of the strength of the workpiece material (Weinert, 1994). This will be discussed in detail later.

Chipping of the cutting edge increased with cutting speed. This suggests that the mechanism of chipping process is different from that involved in flank wear. Possibly, the interaction between the carbides and individual CBN particles within the tool material has played an important role the chipping process. In all the tests,



**Figure 6.5** Initiation and development of chipping in early stages of cutting (S65m/min, F0.25mm/rev, DOC0.65mm).



**Figure 6.6** Tool wear vs. cutting speed (1 minute, F0.25mm/rev, DOC0.65mm).

the chipping was on a small scale and no gross fracture of the cutting edge occurred. This demonstrates the high integrity of PCBN materials.

### **Tool wear vs. Feed rate**

Figure 6.7 shows the effect on tool wear of increased feedrate (cutting for 1 minute). Both flank wear and chipping have increased with the feedrate. However, the feedrate has affected the chipping of tool edge more significantly than the flank wear. This is not surprising because tool forces increase much more significantly with feedrate than with speed.

#### **6.1.2.3 TOOL WEAR MODES**

Figure 6.8 shows the edge of a tool after cutting for 5 secs. At this very early stage, only minor damage to the tool has occurred. The cutting edge is clean and no flank wear land is apparent. Observation at high magnification showed no cracking of the CBN network or of individual particles.

After a longer cutting time, obvious chipping developed on the lower edge of the chamfer. Figure 6.9 shows a general view of the cutting edge after cutting for 20 seconds. The chips formed at this stage are isolated from each other and distributed evenly over the lower edge of the chamfer. The chipping represents the loss of only a few CBN particles. Figure 6.10 shows a close-up view of a chip, which shows a rough surface typical of an intergranular failure mode, i.e. through the particle boundary.

Detailed observation has been made to study the condition of the cutting edge before the chipping occurs to determine the fundamental failure process of the edge or the CBN particles. Figure 6.11 shows the detail of part of the lower edge of the tool chamfer before chipping occurs. Severe cracking has developed on the cutting edge and most of the cracking was through the bridging part of the particles, however,

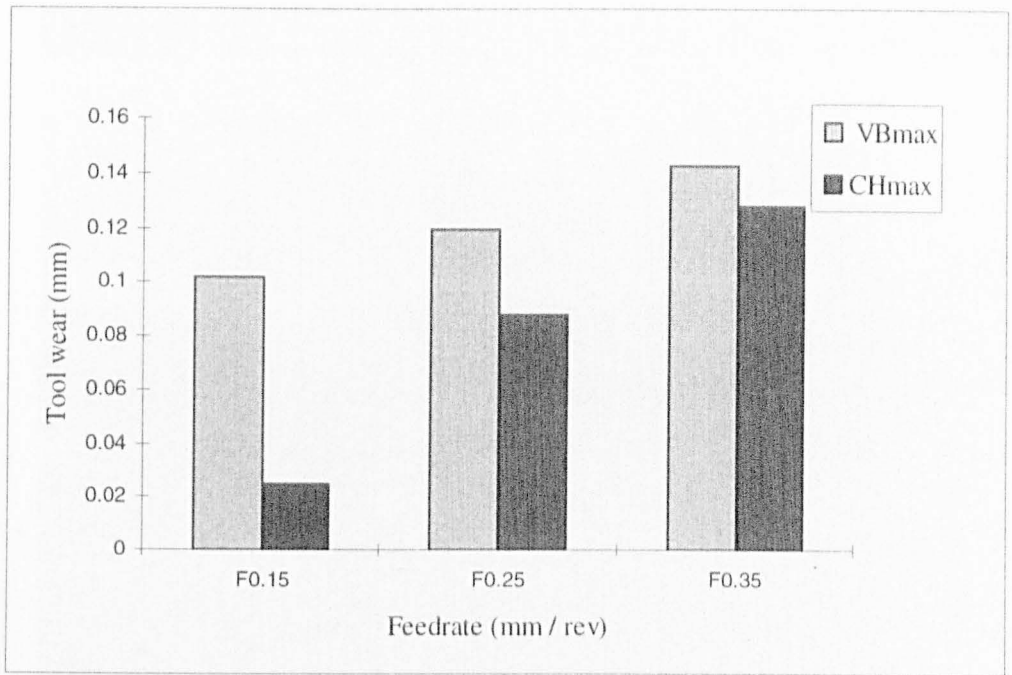


**Figure 6.7** Tool wear vs. feed rate on the tool wear (1 min., S65m/min, DOC0.65).

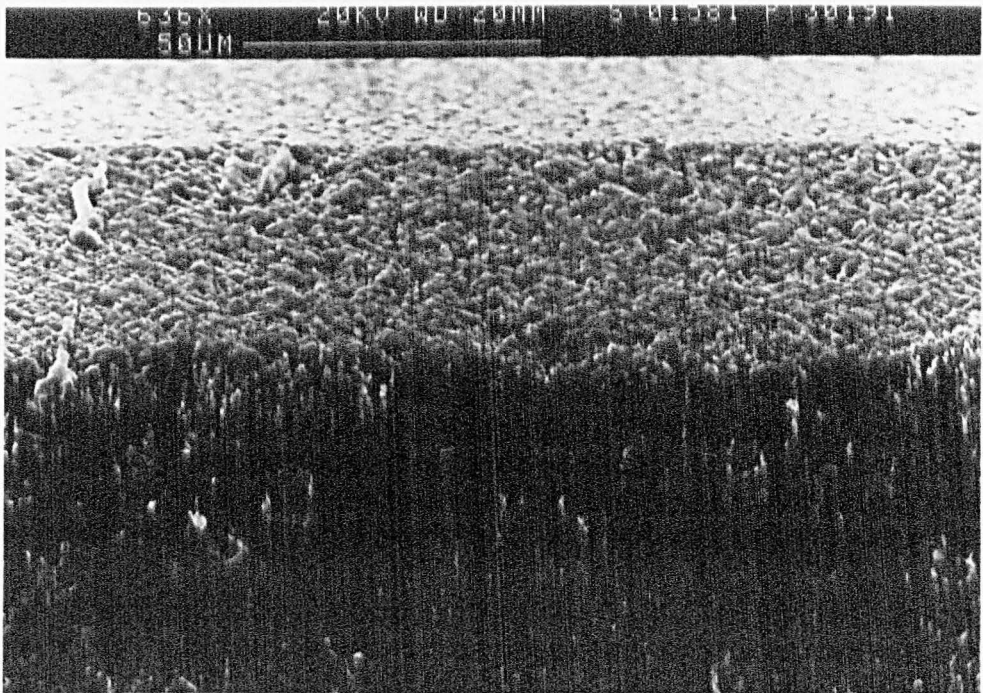


**Figure 6.8** Cutting edge after a very short cutting time cutting (5 secs) showing no chipping damage (S65m/min, F0.25mm/rev, DOC0.65mm).

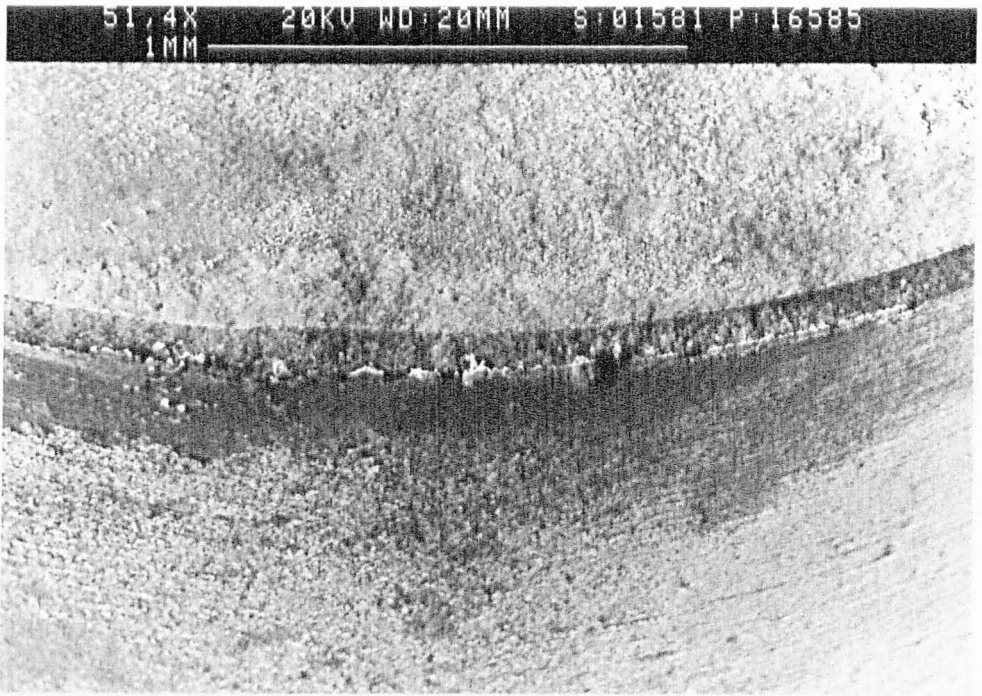


**Figure 6.9** Chipping of the cutting edge after a cutting time of 20 sec (S65m/min, F0.25mm/rev, DOC0.65).

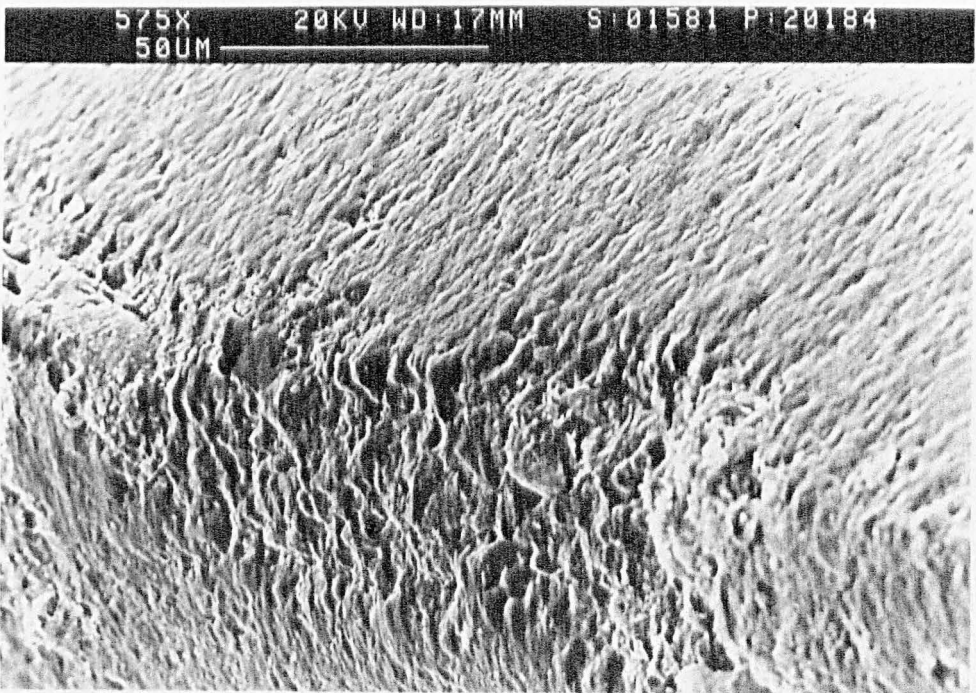


**Figure 6.10** Close-up view to show the detail of the chipping in Figure 6.9.

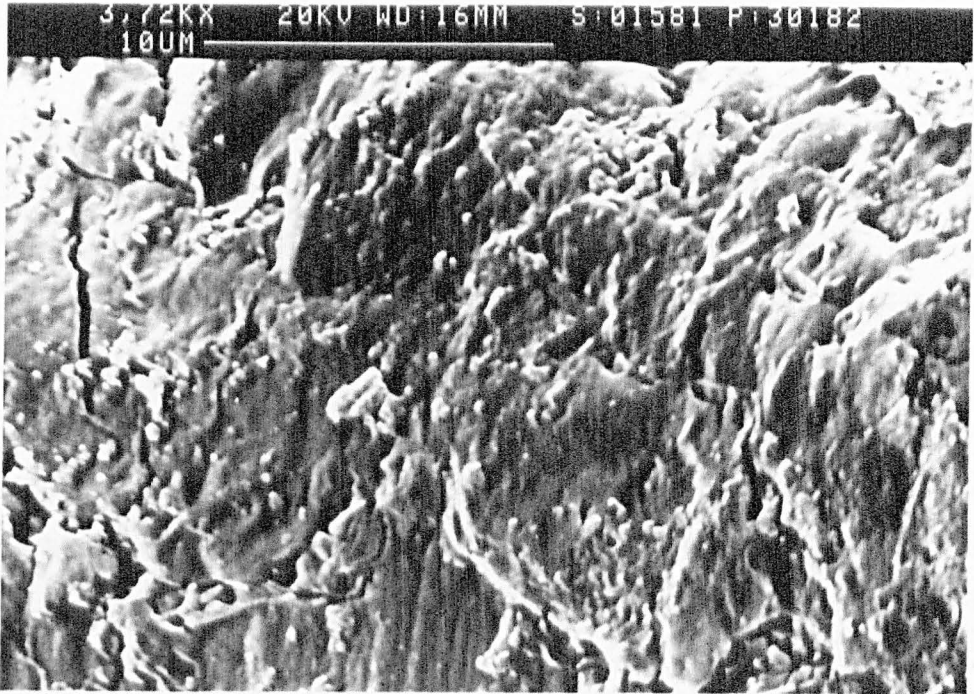


**Figure 6.11** Cracking on the lower edge of the tool chamfer before the edge chipping.



**Figure 6.12** General view of the cutting edge showing chipping developed over the cutting edge (1 minute, S65m/min, F0.25mm/rev, DOC0.65mm).

some cracks have gone through the whole particle. In addition, some shallow rubbing marks or grooves have appeared on the CBN particles.

Later in the cutting process, chipping has developed on the cutting edge and individual chips have joined up to give more intensive damage. In other words, the chipping has developed laterally (Figure 6.12). However, the chipping was still concentrated on the lower edge of the chamfer. In addition, a wear land has formed below the chipping on the flank face of the tool.

Figure 6.13a shows the chamfer of a cutting edge after 1 minute cutting. The chipping has spread along the lower edge of the chamfer and developed onto the chamfer itself. However, the chamfer has still kept its geometry at this stage. The chipped location is rough and shows individual particle loss. High magnification observation (Figure 6.13b) showed that transgranular fracture had also been involved in the chipping process at some locations. As shown in the picture, the base of the chipping is flat which indicates that the crack has gone through the CBN particles and the binding phase.

After longer cutting times, both chipping and flank wear has developed on the cutting edge and the flank land as shown in Figure 6.14a. It shows clearly that the flank wear land has developed ahead of chipping of the cutting edge. At higher magnification, observation of the flank wear land revealed a ridged surface (Figure 6.14b).

As shown in Figure 6.14a, delamination failure of the flank face has also occurred at this stage. The accumulation of chipping has caused the cutting edge to lose its geometry and thus a higher cutting force will be generated. This, together with shear stresses acting on the flank surface (Trent, 1991) may have contributed to the delamination process. Study of the surface after delamination showed no obvious sign of transgranular fracture, which suggests that a progressive process has been involved in the subsurface crack propagation. This eventually causes the layer to separate from the tool when it is not strong enough to support the load. It should be noted that no delamination has developed out of the flank wear region.

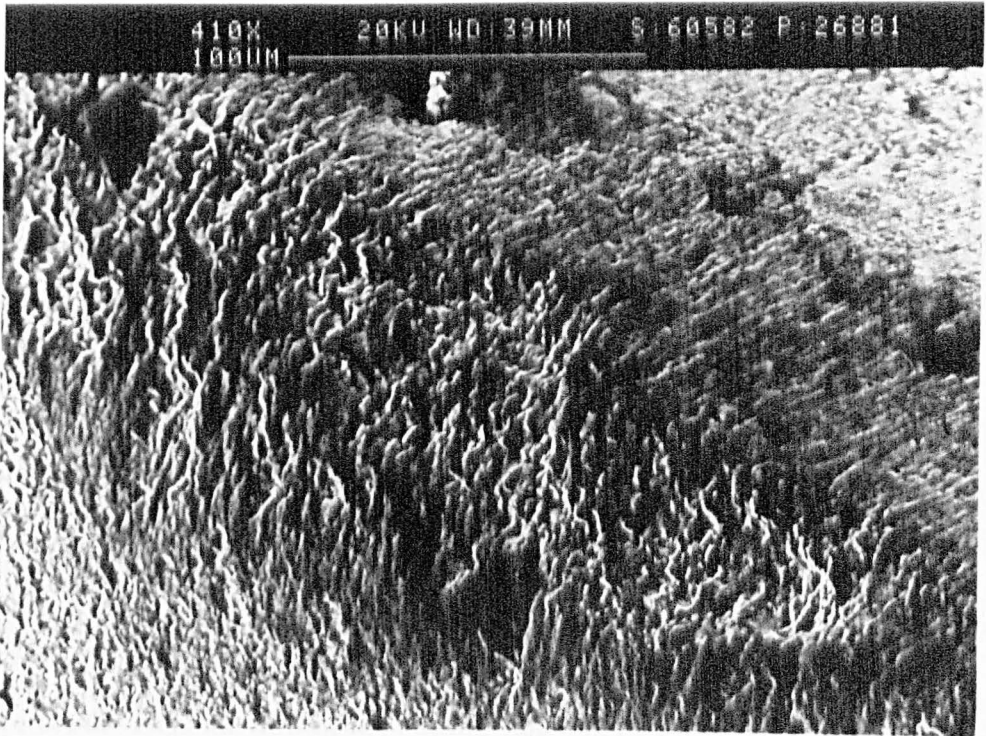


**Figure 6.13a** Chipping developed on the lower edge of the chamfer.

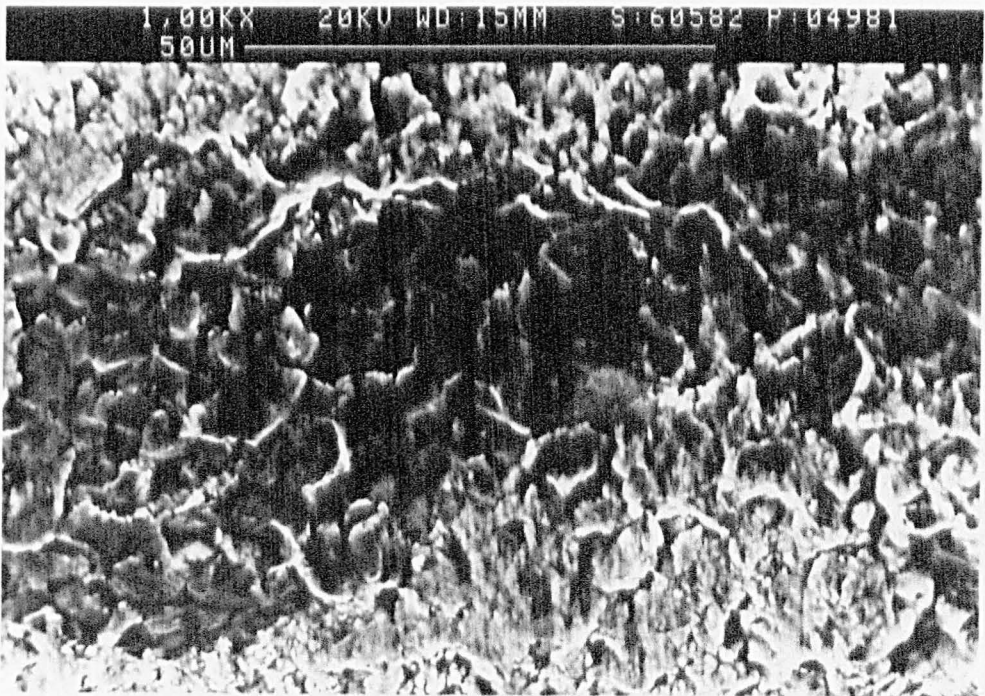


**Figure 6.13b** Enlarged view of one chipped location in a) showing transgranular fracture involved in the chipping process.

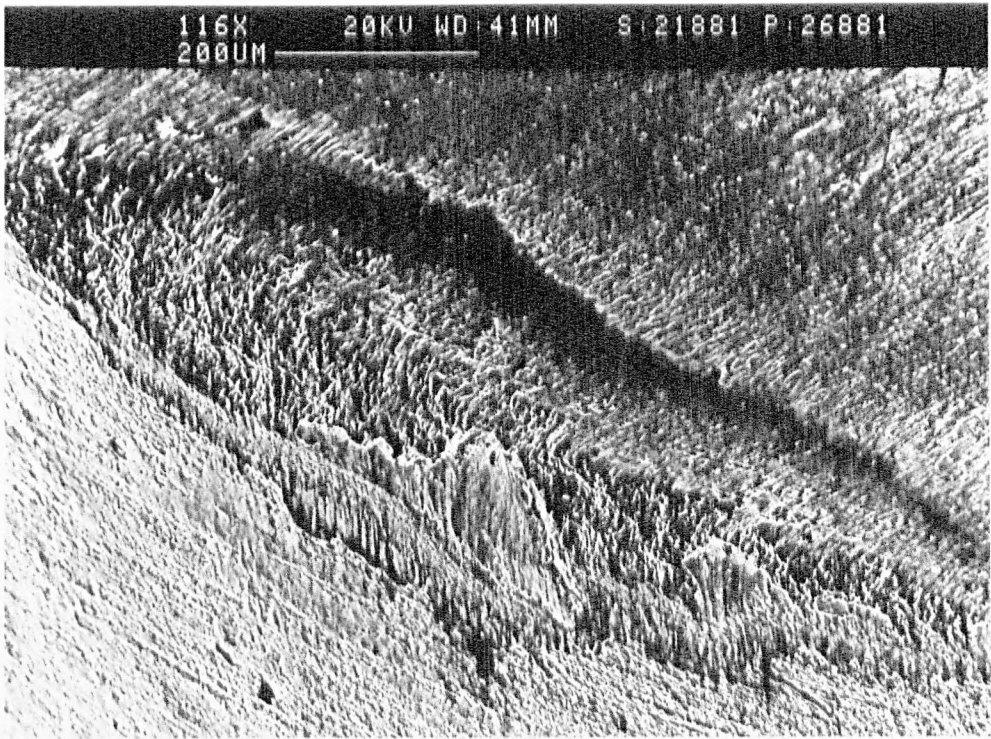


**Figure 6.14a** General view of the cutting edge after cutting for 4 minutes  
(S65m/min, F0.25mm/rev, DOC0.65mm).

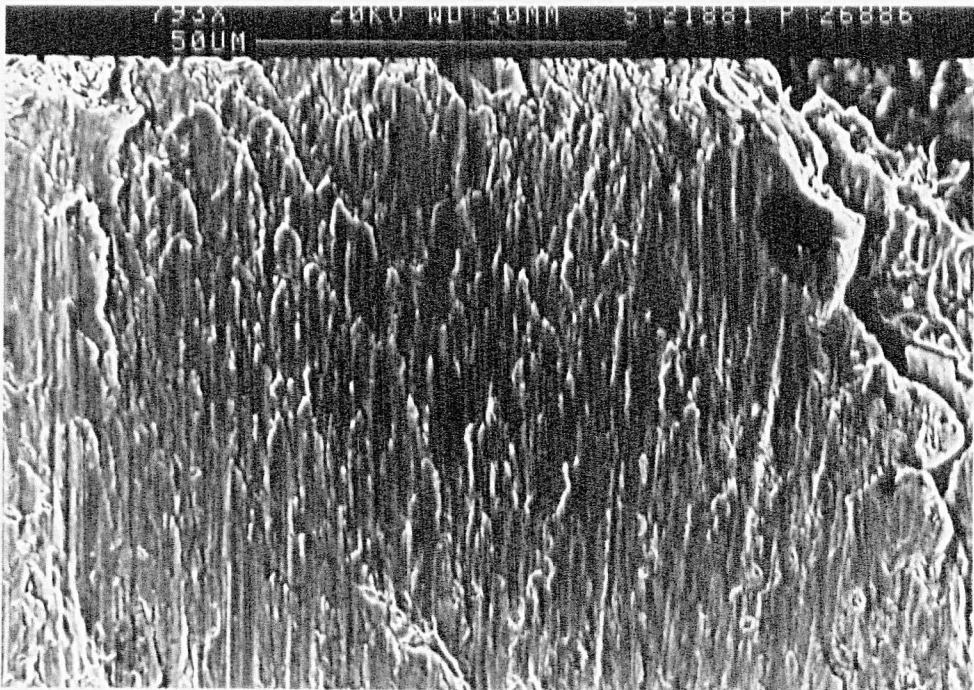


**Figure 6.14b** Enlarged view of a) showing the ridged surface of the flank wear land.

Figure 6.15a shows the cutting edge after 6 minutes cutting and chipping has developed onto the whole chamfer. The chipped surface, as shown in Figure 6.15b, is rough and shows individual CBN particles lost due to high mechanical loading in the cutting process and the action of abrasive particles in the workpiece.

In the later stages, accumulation of chipping has damaged the geometry of the cutting edge to an extent that the movement of the chip will exert higher mechanical forces on the edge of undamaged region resulting in further loss of the chamfer (Figure 6.15c). It is clearly shown that particle loss is the main mode for development of chipping damage at this location.

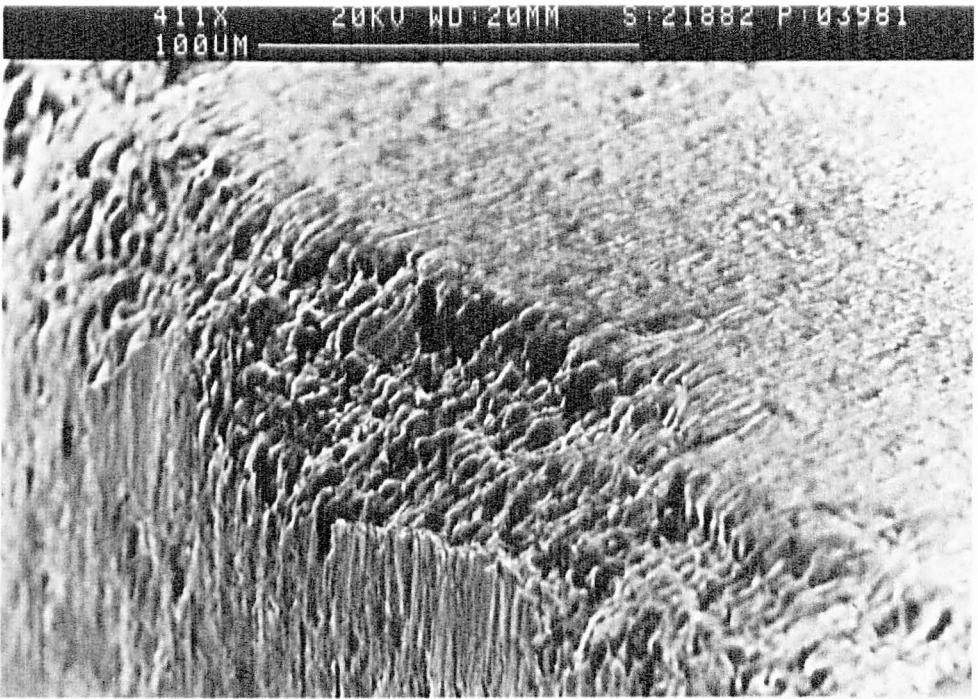
### **6.1.3 MACHINING OF HARDFACING B (COARSE CARBIDES)**

As shown in quick stop study, the large carbides of Hardfacing B have greatly affected the cutting process. This has resulted in a different tool wear mode and wear rate.

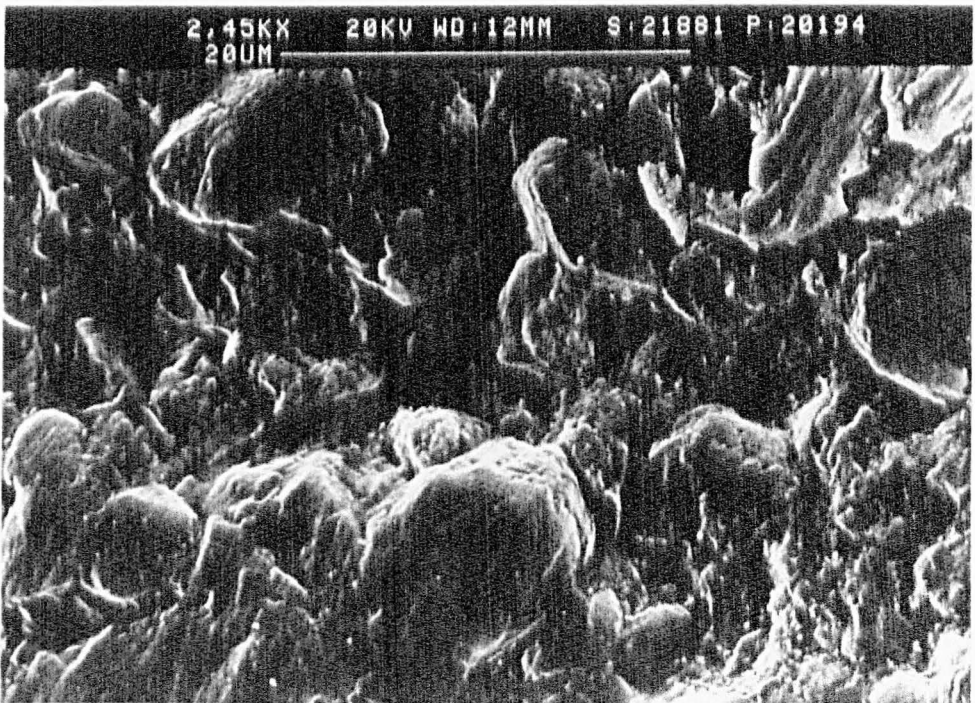
Figure 6.16 plots the wear of the tools at different cutting speeds (cutting for 1 minute). As was the case for Hardfacing A, the chipping has increased with cutting speed while flank wear was lowest at 45 m/sec. Compared with Figure 6.6, the rate of both the flank wear and edge chipping of the edge is much higher when machining Hardfacing B.

Figure 6.17 shows the tool wear after cutting for 2 mins at 45 m/min. Both flank wear and edge-chipping has occurred. The shape of the flank wear land is regular, the insert has locally lost the chamfer due to chipping but the rake face is relatively damage-free.

Figure 6.18 shows the cutting edge after cutting at 65 m/min (cutting for 2 minutes). Severe damage has occurred on the cutting edge, which has lost its original geometry and has been lowered by the chipping process. The chipped surface is much rougher



**Figure 6.15a** Wear of the cutting edge showing chipping has developed over the whole chamfer (6 minutes, S65m/min, F0.25mm/rev, DOC0.65mm)



**Figure 6.15b** Enlarged view of a) showing individual CBN particles lost on the chipped surface.

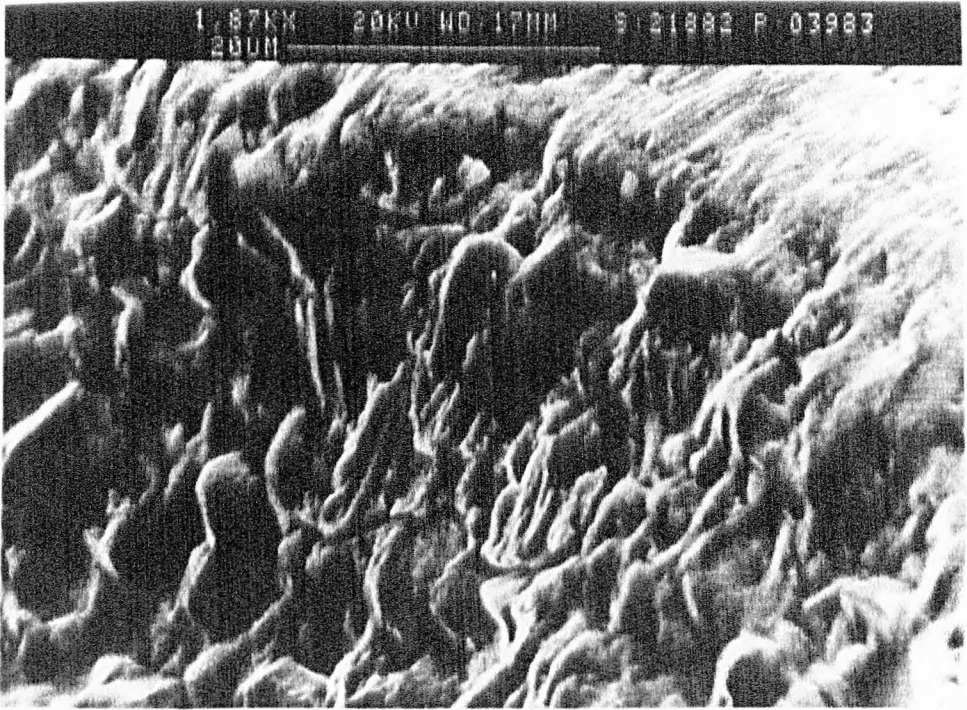


**Figure 6.15c** Enlarged view of a) showing the development of chipping into the undamaged region.

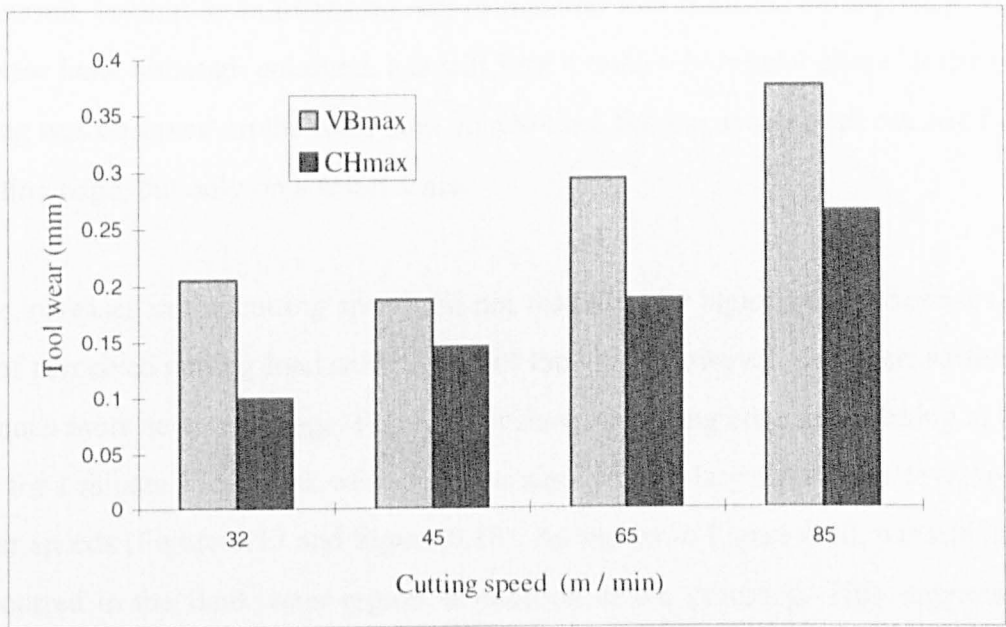


**Figure 6.16** Tool wear vs. cutting speed when machining Hardfacing B (F0.25mm/rev, DOC0.65mm).

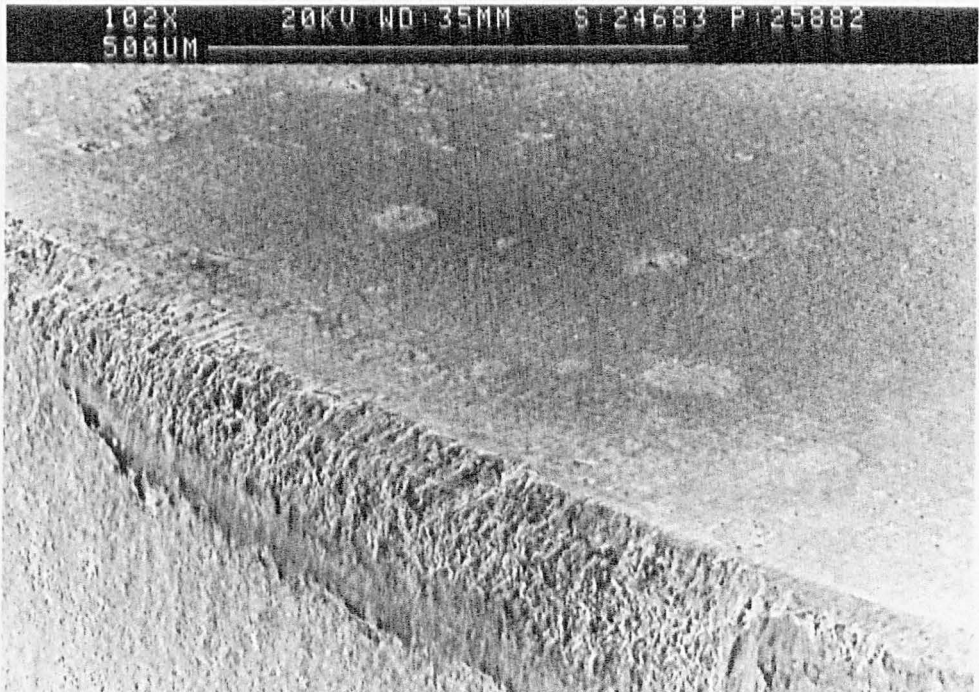


**Figure 6.17** Tool wear mode when machining Hardfacing B at a cutting speed of 45m/min (F0.25mm/rev, DOC0.65mm).

and, in addition to losses of individual particles, fragmentation of the tool material has occurred, leading to an increased rate of material loss from the cutting edge. The flank wear land, although enlarged, has still kept a relatively regular shape. Intensive grooving was observed on the wear land. In addition, flaking damage has occurred on the cutting edge, but only on a small scale.

Further increases in the cutting speed did not result in any significant differences in terms of perceived cutting load or vibration of the lathe. However, the insert suffered from much more severe damage. Figure 6.19 shows a cutting edge after cutting at 85 m/min for 1 minute. The flank wear land was significantly larger than that developed at lower speeds (Figure 6.17 and Figure 6.18). As shown in Figure 6.20, particle loss has occurred in the flank wear region in addition to the grooving. This suggests a much higher contact loading from the large carbides and at this speed the abrasiveness of the carbides is probably the main cause of the flank wear.

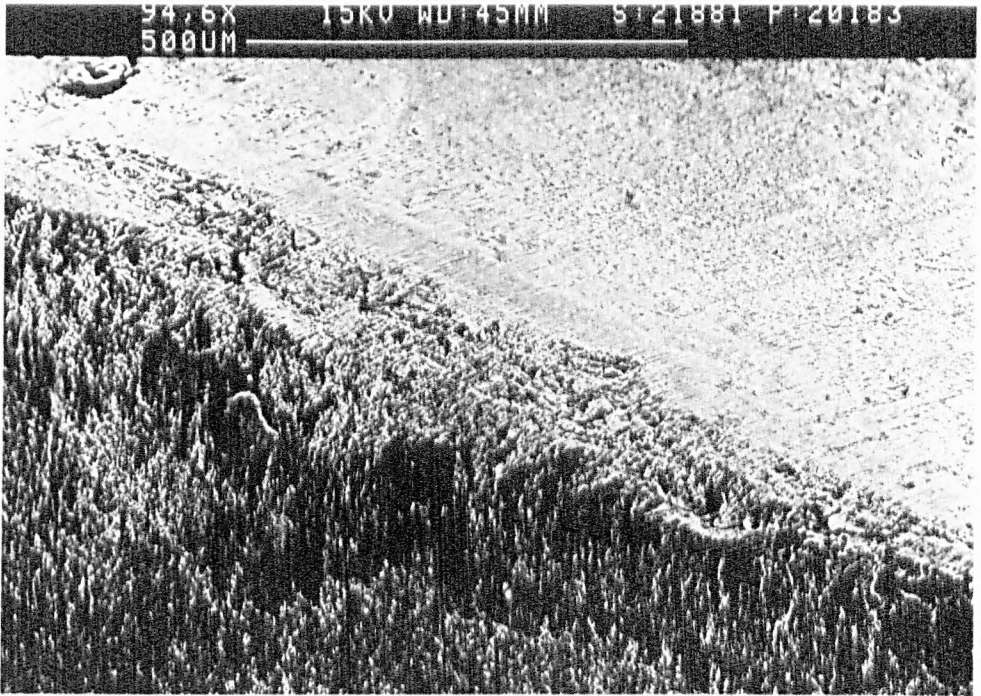


**Figure 6.18** Tool wear when machining Hardfacing B at 65 m/min (F0.25mm/rev, DOC0.65mm).



**Figure 6.19** Tool wear when machining Hardfacing B at higher speed (85m/min.) showing severe damage of the cutting edge and the flank of the tool (F0.25mm/rev, DOC0.65mm).

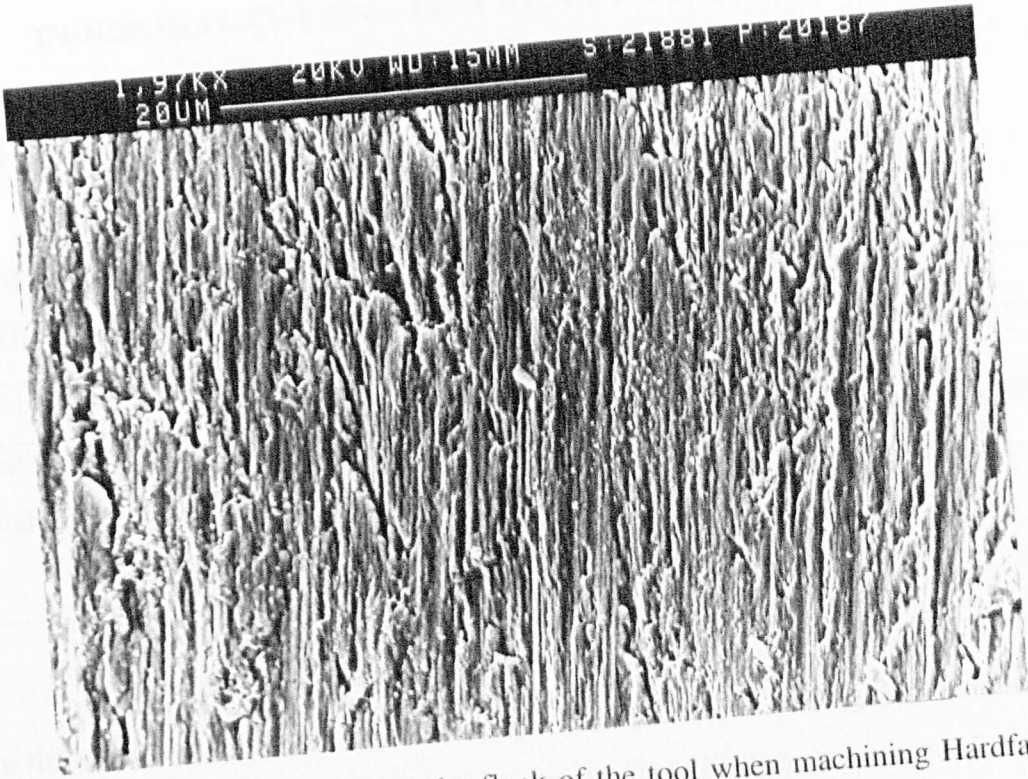


**Figure 6.20** Ridged surface on the flank of the tool when machining Hardfacing B showing abrasive wear process.

## 6.2 INDUSTRIAL CUTTING TEST RESULTS

### 6.2.1 INTRODUCTION

**Table 6.3** Cutting conditions for the industrial tests.

Tools	CBN1, CBN2, CBN3, CBN4, CBN5, CBN6
Tool holder	CRSNL2525
Cutting condition	Rough cutting: S50-75m/min, F0.15-0.25mm/rev, DOC 0.5-0.75 mm Smooth cutting: 65-100m/min, F0.25 mm/rev, DOC 0.75-1.0 mm Finish cutting: 80-100m/min, F0.1 mm/rev, DOC 0.1 mm

In these tests, inserts were used for rough cutting, smooth cutting and finish cutting as listed in Table 6.3. In rough cutting, the rough weld skin was removed and, as a consequence, the cutting was rough and intermittent and lower cutting speeds were used. In smooth cutting, a thick layer of workpiece material was removed to meet the required geometry. In these two processes, the insert life was determined empirically by the observation of the operator, e.g. the portion of the lost cutting edge, the vibration and loading condition, etc..

In order to explore the possible potential of each material, the cutting was stopped whenever the insert appeared to have lost its cutting capability. This was empirically determined by sensing the cutting force and vibration of the machine. Some fixed time cuttings was undertaken with CBN1 in order to investigate the tool failure process. The cutting life of each insert was recorded and the average value was used to represent the tool life. Some of the used cutting tool inserts were thoroughly cleaned and coated with gold before being examined in the SEM. In addition, the performance of various tool materials under finish cutting conditions was assessed in terms of the average surface finish they achieved.

## 6.2.2 CUTTING PERFORMANCE OF PCBN MATERIALS

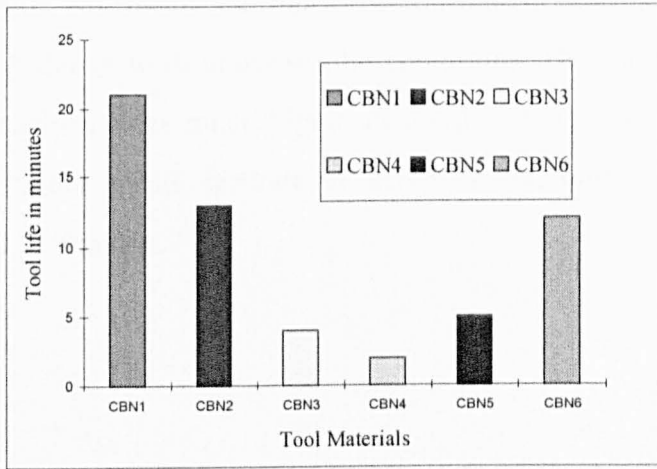
### Tool life

Figure 6.21 shows the average cutting tool life of various CBN inserts. CBN1 achieved the longest tool life but about 5% of these inserts suffered from premature failure (failed within 1 minute). CBN2 achieved reasonable tool life and showed much better performance in the smooth cutting or smaller components than in rough cutting or large components. In addition, the CBN2 tools demonstrated very consistent performance, i.e. good reliability. CBN3, and CBN5 only lasted a few minutes and therefore could not meet the required standard for production machining. CBN4 lasted only a very short time and suffered from gross fracture. CBN6 achieved a similar tool life to CBN2 but some inserts suffered from premature failure.

Figure 6.22a shows a typical used CBN1 showing the decrease in the cutting edge. The extent of the decrease of the cutting edge was measured and the average value for each material is presented in Figure 6.22b. This roughly reflects the lost volume of the tool edge. CBN1 has much lower edge decrease than other tools, while CBN2, CBN3 and CBN5 showed similar edge decrease. CBN4 fractured totally, so no measurement was made.

### Cutting temperature and cutting forces

In the cutting process, the temperature of the cutting zone is very high. Glowing of the cutting tip and red-hot chips were observed even when a new insert was used. With increased cutting time, as tool wear increases, the temperature gets higher. An on-site measurement using an infrared pyrometer showed that local temperatures in the region of 750-800°C were developed during the cutting process when using CBN1 and CBN2, irrespective of the tool material



**Figure 6.21** Average cutting tool life of the CBN inserts.

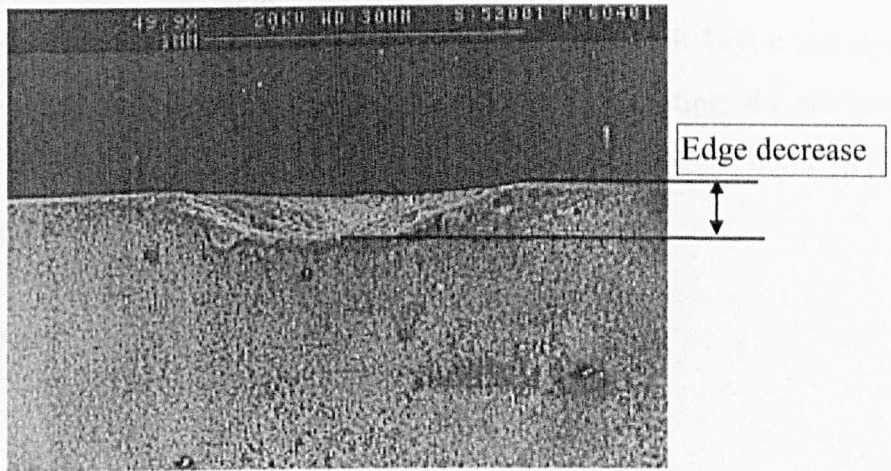


**Figure 6.22a** A typical used insert showing the decrease of the cutting edge.

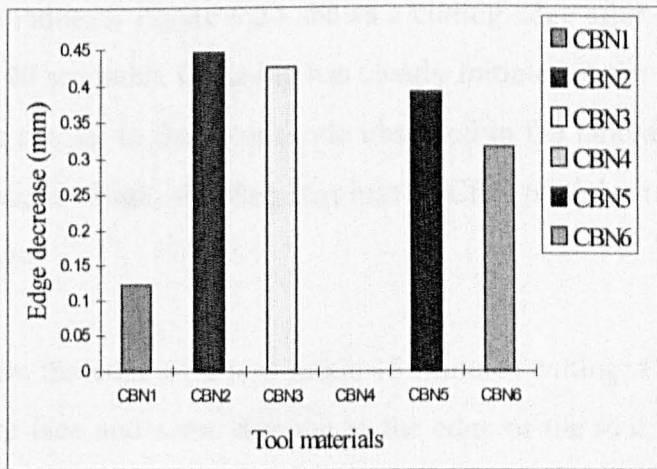


**Figure 6.22b** Decrease in the cutting edge of the PCBN tools.

Cutting forces were not measured but it was apparent that these forces were comparable using different tools under similar conditions. The cutting forces and the vibration of the machine were much higher in rough cutting than in finish cutting. When cutting at higher speed, feedrate or depth of cut, both cutting forces and vibration appeared to increase.

### **Surface finish**

The hardfaced parts are normally used in environments where they are exposed to the abrasive wear and the surface requirement is 2.5-3.2  $\mu\text{mRa}$ . This range of surface finish could be checked visually by the operator. However, the surface finish achieved with some CBN inserts was measured using a portable Rank Taylor hobson 'Talysurf' and the results are shown in Figure 6.23. Under light cutting, the surface finish achieved by the four inserts met the engineering requirements but CBN1 produced the roughest finish.

## **6.2.3 TOOL FAILURE MODE**

### **CBN1**

In rough cutting, because the process is rough and intermittent, the cutting speed and feed are normally reduced. Figure 6.24 shows a cutting edge after cutting for a very short time (about 40 seconds). Chipping has clearly initiated at the lower edge of the chamfer, which is similar to the wear mode observed in the laboratory cutting tests. The chipped surface is rough, showing that loss of CBN particles is the predominant damage at this stage.

Figure 6.25a shows the edge of a tool insert 15 minutes cutting. Despite significant flaking of the rake face and some damage to the edge of the tool, it was still sharp enough to cut effectively. Detailed examination of the flaked face damage revealed transgranular cracking had occurred (Figure 6.25b) and cleavage steps can be

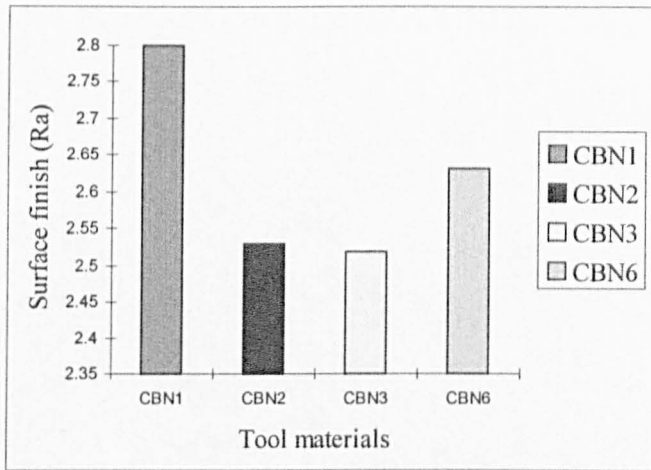


**Figure 6.23** Surface finish achieved by the PCBN tools.

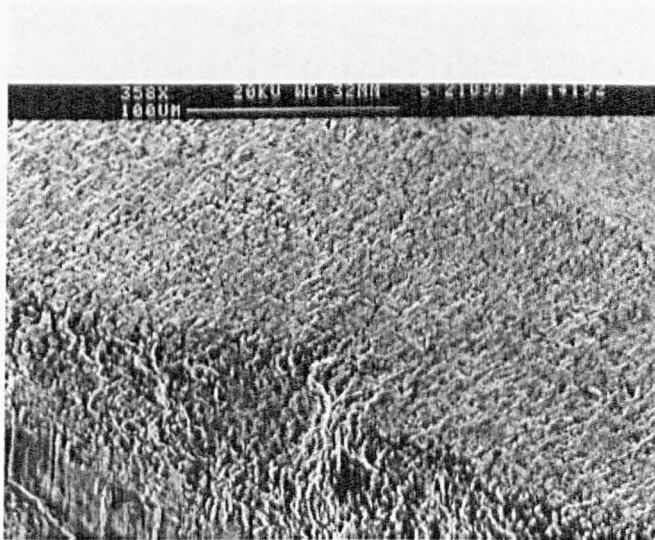


**Figure 6.24** Chipping on the lower edge of the chamfer of CBN1 insert in the early stages of cutting.

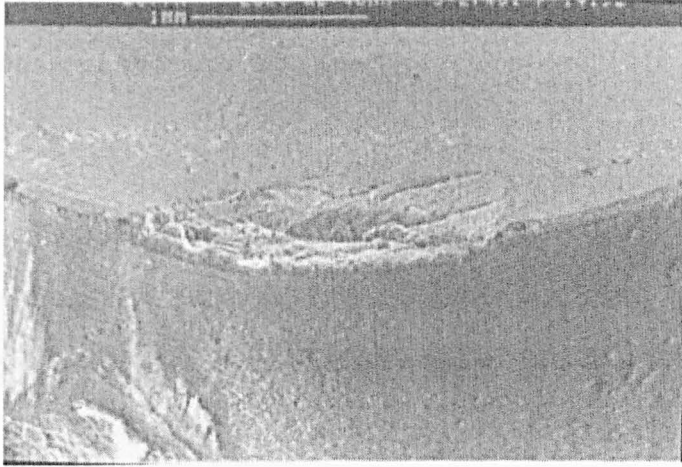


**Figure 6.25a** General view of CBN1 insert showing flaking of the rake face.

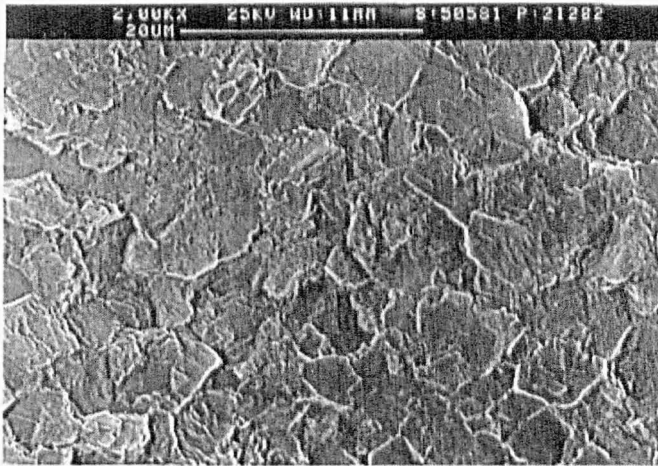


**Figure 6.25 b** Details of the flaking surface showing transgranular fracture.

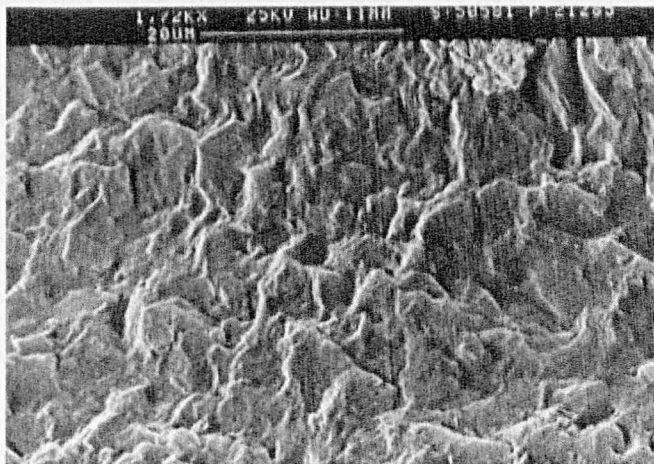


**Figure 6.25c** Close-up view of the near edge region of Figure 6.25a showing intergranular failure.

observed. Damage to the flank, however, (Figure 6.25c) is typical of intergranular fracture and the whole particle has been removed.

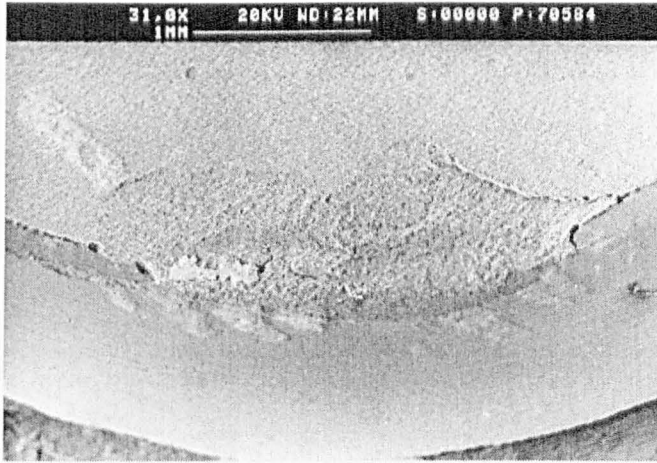
After longer cutting time, the effect of higher cutting forces and temperatures could be observed and the failure of the cutting edge became much more unpredictable and irregular. As shown before in Figure 6.22a, larger portions of the cutting edge were removed by chipping and fracture until it lost the ability to cut effectively.

## CBN2

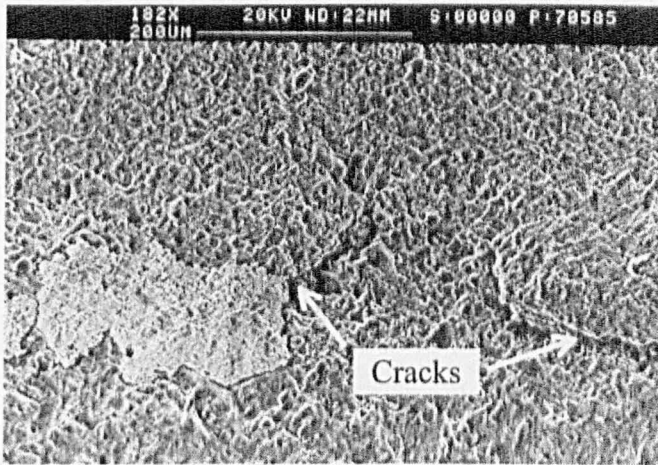
Figure 6.26a shows the cutting edge of a CBN2 insert after controlled cutting for 8 minutes. Flaking has occurred on a much larger scale compared to CBN1 (Figure 6.25a). As shown in the photo, patches of the workpiece have adhered to the fractured surface. This agreed well with the quasi-static adhesion test results, in which a strong adhesive junction formed between the workpiece cone and CBN2. Other tool materials showed very limited adhesion to the workpiece.

Figure 6.26b shows a close up view of the adhered workpiece material and local cracking of the tool can be clearly seen as indicated by the arrow. It is also possible that, once strong adhesion has occurred, the tool material may be torn away when the adhered material is removed by the moving chip.

Figure 6.27a shows a typical failed cutting edge of a CBN2 insert. A much larger portion of the edge has been lost which indicates that lateral fracture of the cutting edge has occurred. Figures 6.27 b and c show the near-edge region and the flaked surface. The flaked surface is flat indicating transgranular fracture, while in the near edge region, a lot of loose CBN particles could be observed due to particle bonding failure.



**Figure 6.26a** General view of CBN2 insert showing flaking of the rake face and adhered workpiece material.



**Figure 6.26b** Close-up view of a) showing workpiece material adhering to the tool surface. The arrow indicates crack development into the tool material.

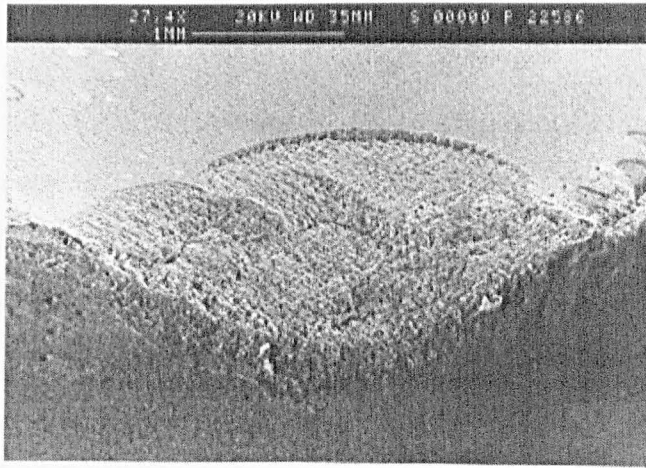


**Figure 6.27a** A typical cutting edge of a used CBN2 tool.

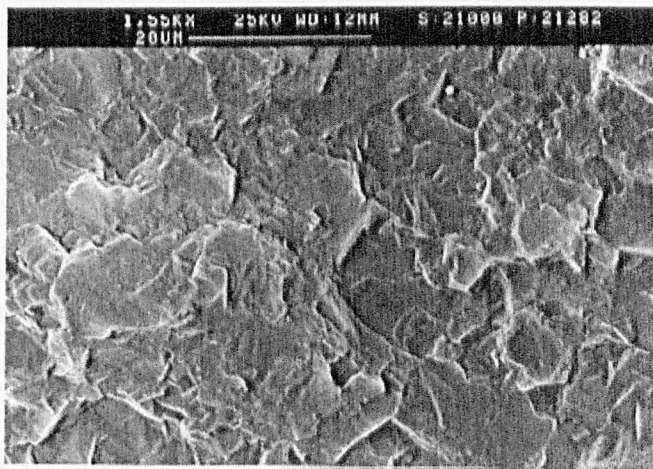


**Figure 6.27 b** Detail of the flaking surface.

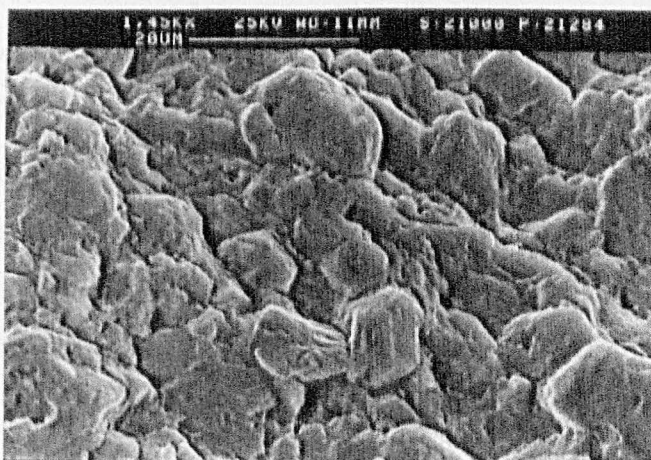


**Figure 6.27c** Close-up view of the near edge region of Figure 6.25a showing the loose particles due to intergranular failure.

### CBN3

In the cutting process, CBN3 inserts lasted only a very short time. The failure mode of the insert, as shown in Figure 6.28a, is clearly flaking of the rake face. The flaked surface is very flat with very limited crack deflection as shown in Figure 6.28b. Figure 6.28c shows the detail of the near-edge region, where failure along the particle boundary appears to have been the main failure mode. In addition, it is also clear that the binding phase has been eroded away, which will leave the CBN particles unsupported and therefore easier to be removed from the tool surface.

### CBN4

The two CBN4 inserts tested both fractured under the clamp after a short time cutting (Figure 6.29a). The inserts fractured into large fragments with irregular shape and the curved fracture path is typical of failure of an aggregate e.g. rock (Figure 6.29b). Detailed observation revealed that the cracks have preferentially gone through particular orientations of particles instead of evenly through the particles and the binding phase, as in the flaking process (Figure 6.29c).

### CBN5

Figure 6.30a shows a general view of cutting edge of a CBN5 insert. As was the case with CBN1-CBN3, flaking and chipping of the cutting edge are the main wear modes. In addition, obvious delamination of the flank face has occurred. Figure 6.30b shows a close-up view of the delamination. The surface is flat and indicates a fast fracture process. Cracking (arrowed) has occurred some distance from the cutting edge and goes parallel to the rake face, which will possibly cause flaking of the rake face later in the cutting process. Figure 6.30c shows the detail of the flaking on the rake face. The basic failure mode is transgranular fracture but much more crack deflection has occurred as it goes through individual particles.

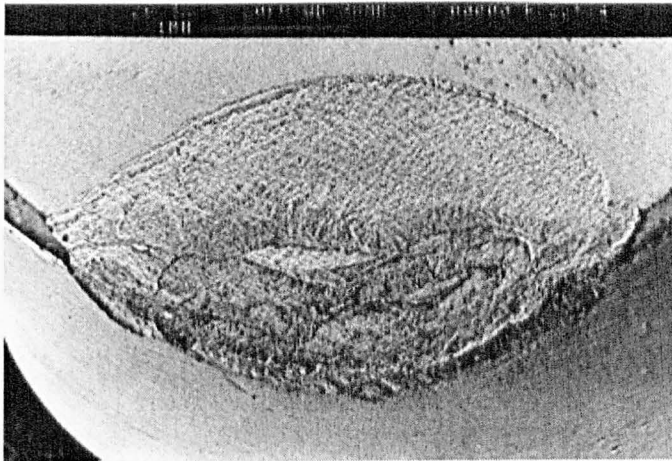


**Figure 6.28a** Failure mode of CBN3.

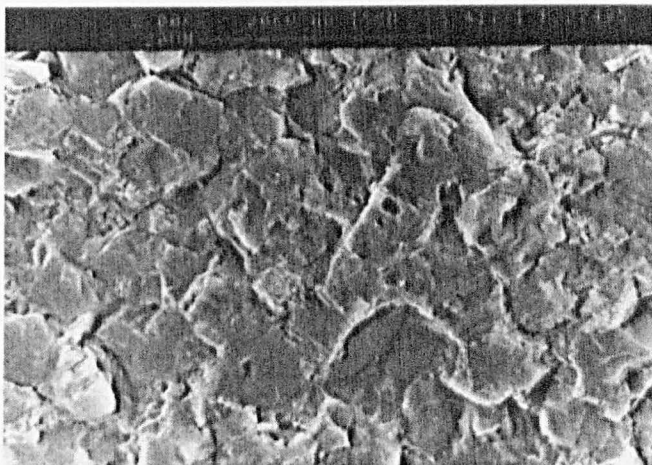


**Figure 6.28b** Detail of the flaked surface.

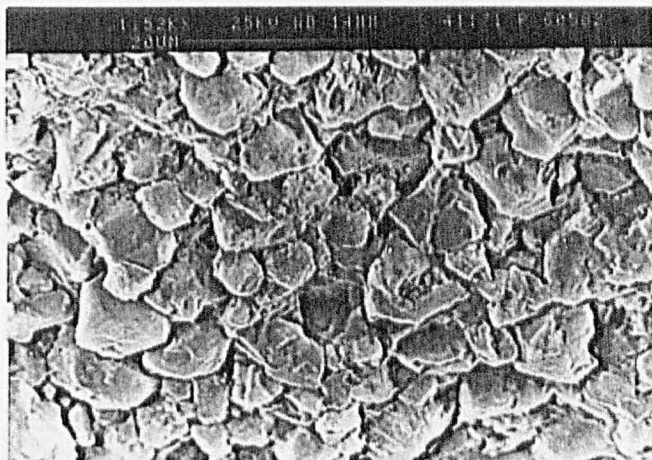


**Figure 6.28c** Close-up view of the near edge region showing the loose CBN particle and the binder phase being eroded away.

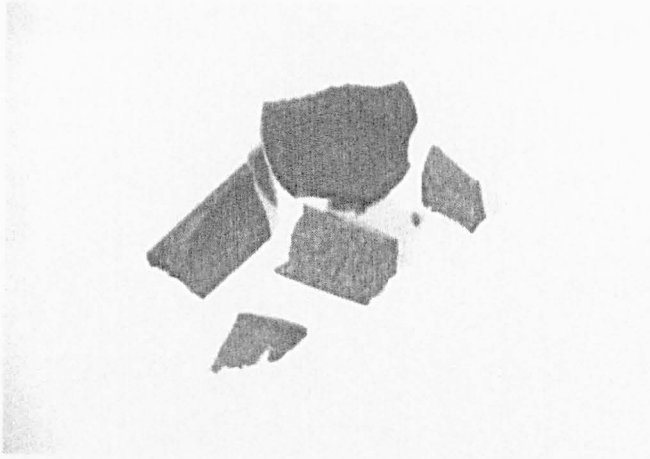


**Figure 6.29a** Fragments of the CBN4 tools fractured underneath the clamp.

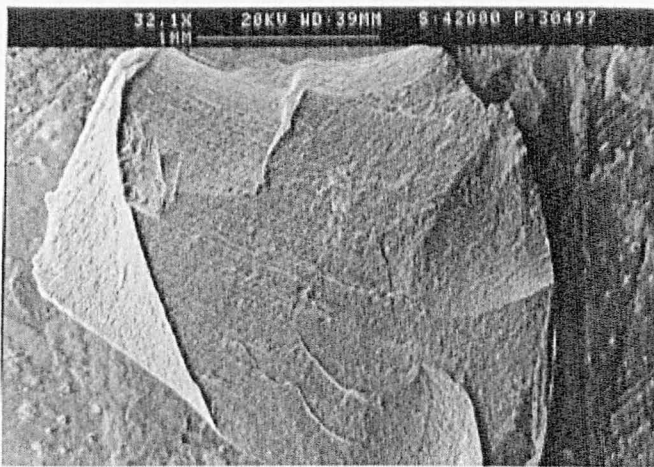


**Figure 6.29 b** Enlarged view of the fragment surface

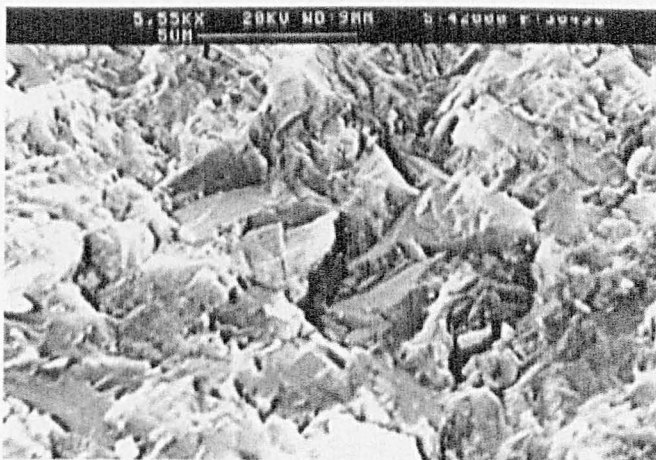


**Figure 6.29c** Close-up view of b) showing the fracture of the CBN particles.

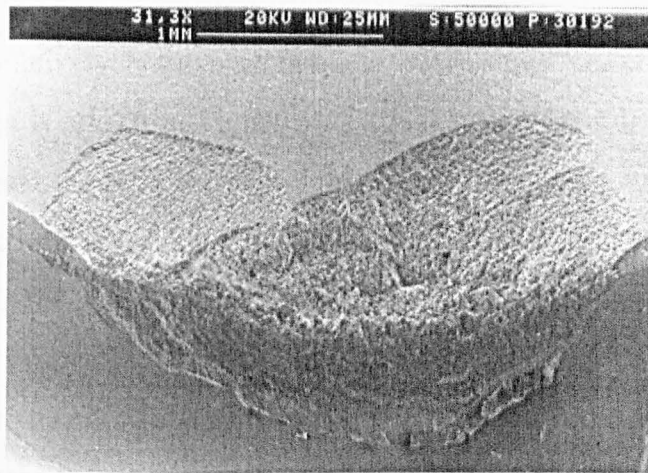


**Figure 6.30a** General view of a failed cutting edge of CBN5 showing flaking of the rake face and the delamination of the flank face

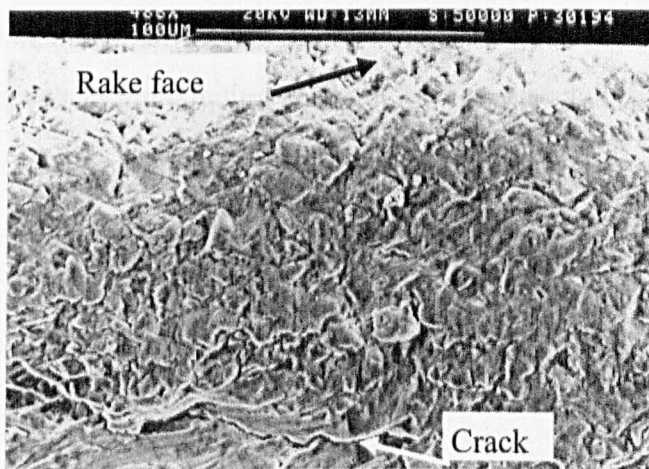


**Figure 6.30b** Detail of the delaminated surface and cracking of the cutting edge

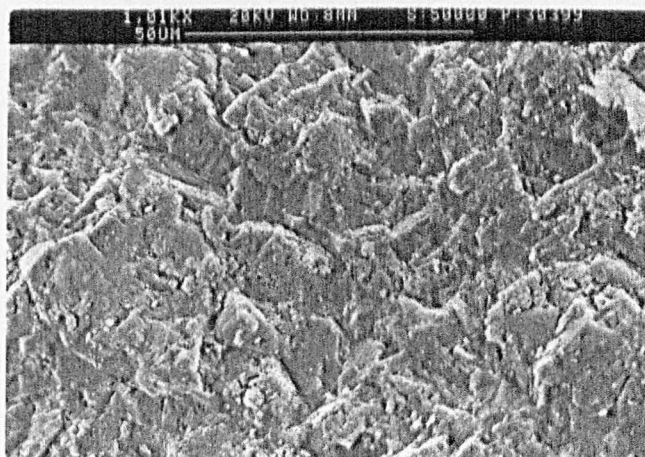


**Figure 6.30 c** Detail of the flaking surface

## CBN6

CBN6 lasted a relatively long time and give satisfactory performance. A typical failed cutting edge is shown in Figure 6.31a. Flaking on the rake face is again the main wear mode and Figure 6.31b shows the detail of the flaked surface. The surface is flat with limited crack deflection. The flaking surface also shows that porosity existed both within the particles and the boundary regions.

Another characteristic of CBN6 is the delamination of the flank face and it has extended down to the tungsten carbide substrate. Figure 6.32c shows a close-up view of the flank face near the cutting edge. The delaminated surface is flat indicating transgranular fracture. It can also be seen that severe cracking has developed over the cutting edge, which would probably cause flaking of the rake face later in the cutting process. In addition, not many loose particles could be observed in the near-edge region, which suggests strong bonding between the particles and the binder.

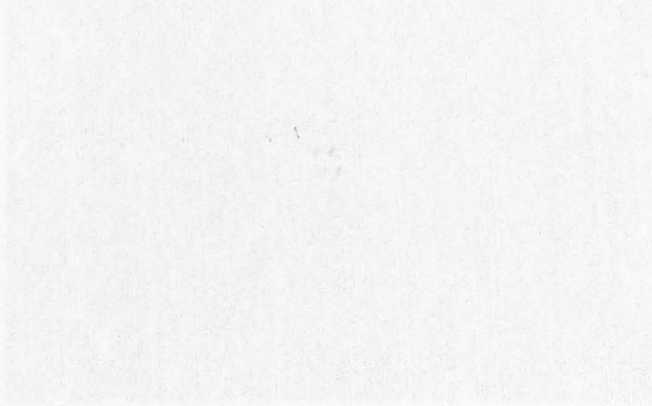


Figure 6.31b. Detail of the flaked surface.

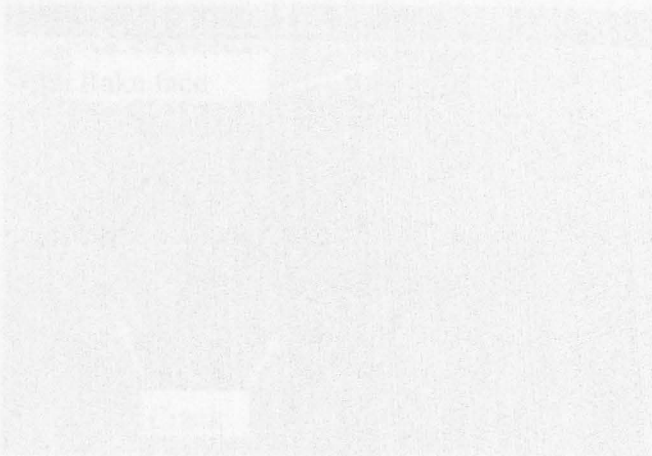
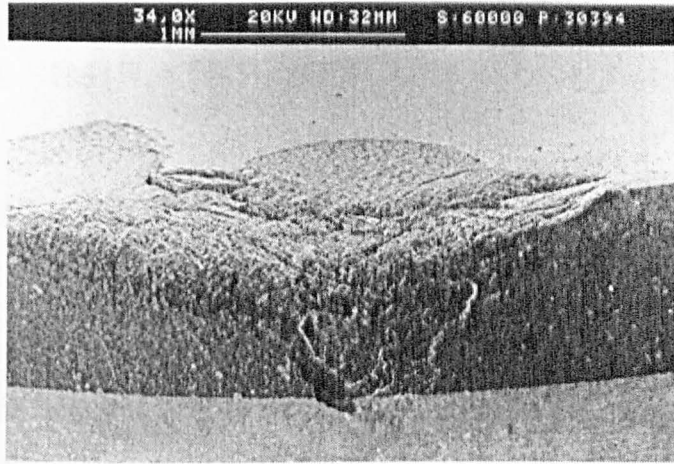
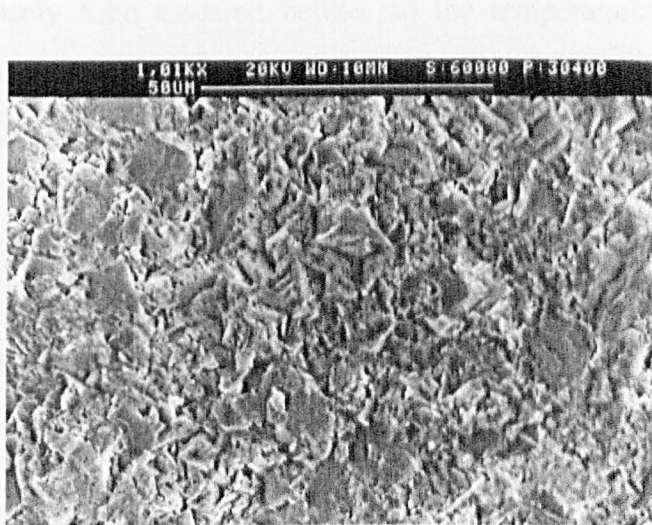


Figure 6.31a. Close-up view of the cutting edge showing cracking.



**Figure 6.31a** A general view of a failed cutting edge of CBN6 showing flaking of the rake face and the delamination fracture of the flank face extending down to the substrate.



**Figure 6.31b** Detail of the flaked surface.

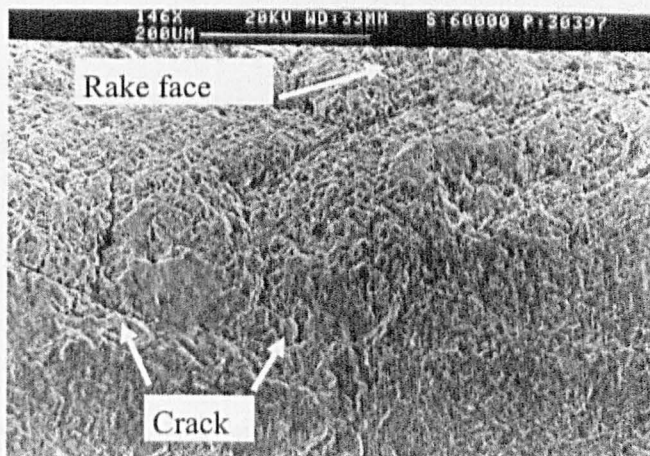


**Figure 6.31c** Close-up view of the cutting edge showing cracking.

# CHAPTER 7      TEMPERATURE      MEASUREMENTS      AND NUMERICAL SIMULATION RESULTS

## 7.0      INTRODUCTION

This chapter contains the temperature measurement results using the set-up described in Chapter 3. The remote thermocouple method is not as sensitive as when the thermocouple is put closer to the cutting zone. However, it is more flexible and yields more consistent results (Chow and Wright, 1988). In addition, both the tool material and the workpiece material in these tests are very difficult to machine e.g. drilling a hole for an embedded thermocouple. The temperature when machining hardfacing has rarely been assessed before, so the temperatures generated when machining titanium alloy and mild steel were also measured under similar cutting conditions as a basis for comparison.

The heat transfer process involved in the cutting operation has been analysed by means of the finite element method, using ANSYS software, which is able to take into account the dependence of temperature on the thermal conductivity coefficients of the tool materials. The temperature - time distribution at any location in the tool for a given tool-chip interface temperature could be determined. Therefore the average tool-chip interface temperature could be predicted using the measured tool-shim temperatures.

## 7.1 THE MEASURED TOOL-SHIM INTERFACE TEMPERATURE

Figure 7.1 shows the increase of the measured temperature at the tool-shim interface with cutting time, when cutting at a speed of 65m/min and a feedrate of 0.25mm/rev. When the cutting started, the temperature at the tool-shim interface increased very quickly. After 15 - 20 seconds, the temperature increased more gradually. The

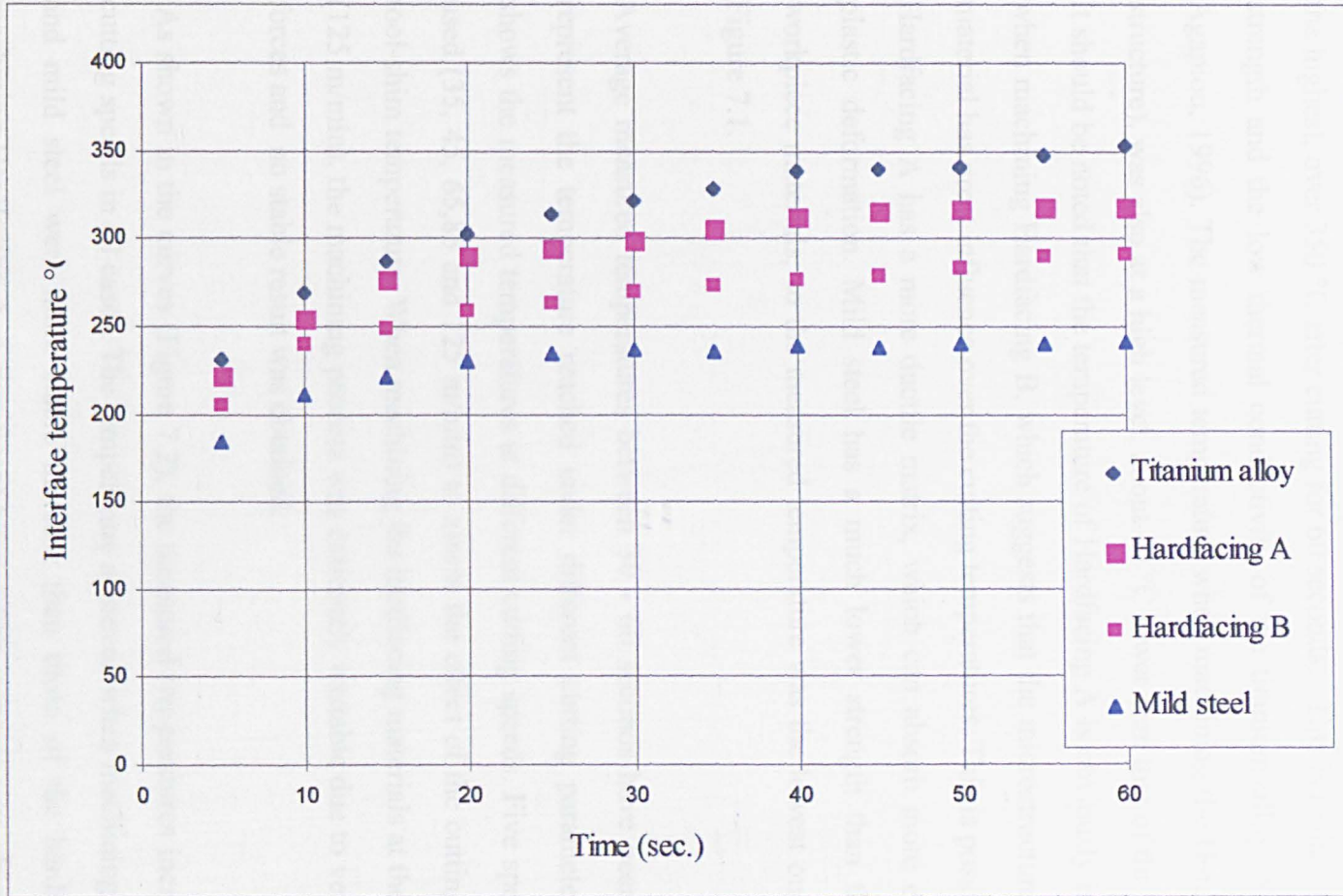


**Figure 7.1** Temperature increases at the tool-shim interface with cutting time (S65m/min, F0.25mm/rev, DOC0.65mm).

temperature when machining the four workpiece materials all showed the same trend, with similar periods of rapid increase before reaching a stable stage.

Different temperatures were generated at the tool-shim interface for each of the workpiece materials. The measured temperature when machining titanium alloy was the highest, over 350 °C after cutting for 60 seconds. This is mainly due to the high strength and the low thermal conductivity of the titanium alloy (Stephenson and Agapiou, 1996). The measured temperature when machining the Hardfacing A (fine structure), was also at a high level, about 40 °C lower than that of the titanium alloy. It should be noted that the temperature of Hardfacing A is obviously higher than that when machining Hardfacing B, which suggests that the microstructure of hardfacing material has great influence over the cutting temperatures. This is possibly due to that Hardfacing A has a more ductile matrix, which can absorb more energy through plastic deformation. Mild steel has a much lower strength than the other three workpiece materials, so the measured temperature was the lowest one, as shown in Figure 7.1.

Average measured temperatures between 30 - 60 seconds have been calculated to represent the temperature reached under different cutting parameters. Figure 7.2 shows the measured temperatures at different cutting speeds. Five speeds have been used (35, 45, 65, 85 and 125 m/min) to assess the effect of the cutting speed on the tool-shim temperature. When machining the hardfacing materials at the highest speed (125 m/min), the machining process was extremely unstable due to very high cutting forces and no stable result was obtained.

As shown in the curves (Figure 7.2), the measured temperatures increased with the cutting speeds in all cases. The temperature achieved when machining titanium alloy and mild steel were more stable increase than those of the hardfacings. When machining Hardfacing A, a significant temperature increase was observed when the speed increased from 45 m/min to 65 m/min.

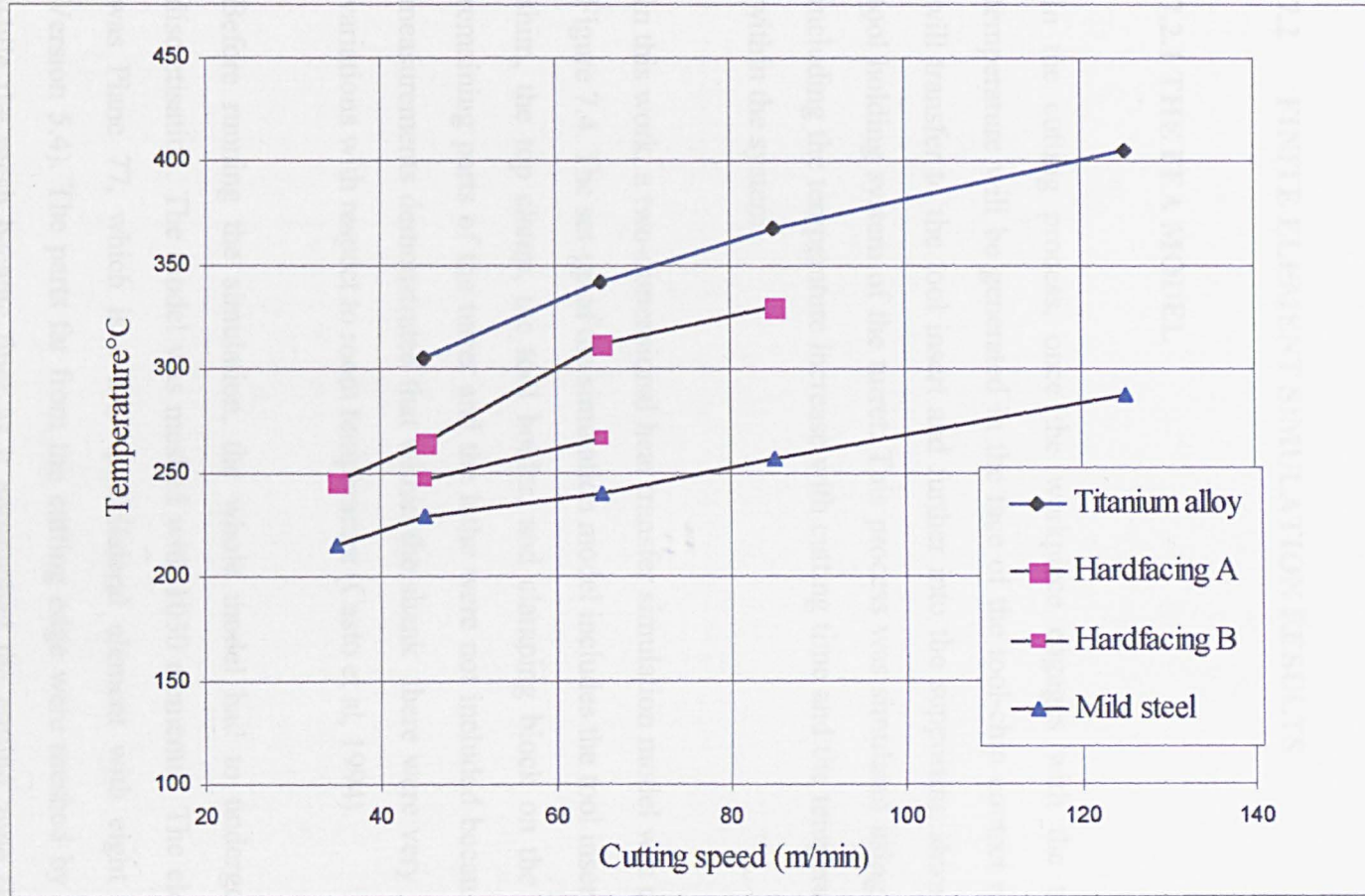


**Figure 7.2** Measured tool-shim interface temperature vs. cutting speeds (F0.25mm/rev, DOC0.65mm).

Figure 7.3 shows the temperatures measured at different feed rates. All the measured temperatures increased smoothly with feed rate. The temperature when machining titanium alloy has showed the most significant increase and at a feedrate of 0.35 mm/rev, reached over 400 °C. The two hardfacing materials exhibited similar trends, but the higher rate of increase was found when machining Hardfacing A.

## **7.2 FINITE ELEMENT SIMULATION RESULTS**

### **7.2.1 THE FEA MODEL**

In the cutting process, once the workpiece engages with the tool tip, a high temperature will be generated in the face of the tool-chip contact region. This heat will transfer to the tool insert and further into the supporting shim, top clamp, the tool holding system of the turret. This process was simulated using an FEA model, including the temperature increase with cutting time and the temperature distribution within the system.

In this work, a two-dimensional heat transfer simulation model was used as shown in Figure 7.4. The set-up of the simulation model includes the tool insert, the supporting shim, the top clamp, the tool holder, and clamping block on the tool turret. The remaining parts of the turret and the lathe were not included because thermocouple measurements demonstrated that within the shank there were very low temperature variations with respect to room temperature (Casto et al, 1994).

Before running the simulation, the whole model had to undergo finite element discretisation. The model was meshed with 1030 elements. The element type used was Plane 77, which is a 2-D quadrilateral element with eight nodes (ANSYS Version 5.4). The parts far from the cutting edge were meshed by coarse elements while the mesh became finer as it approached the cutting zone (Figure 7.5). The reason for this is that the closer to the cutting zone, the more intense will be the heat exchange between the elements, and the finer mesh is needed to increase the accuracy. For the tool holder and the clamping block of the turret, the heat exchange

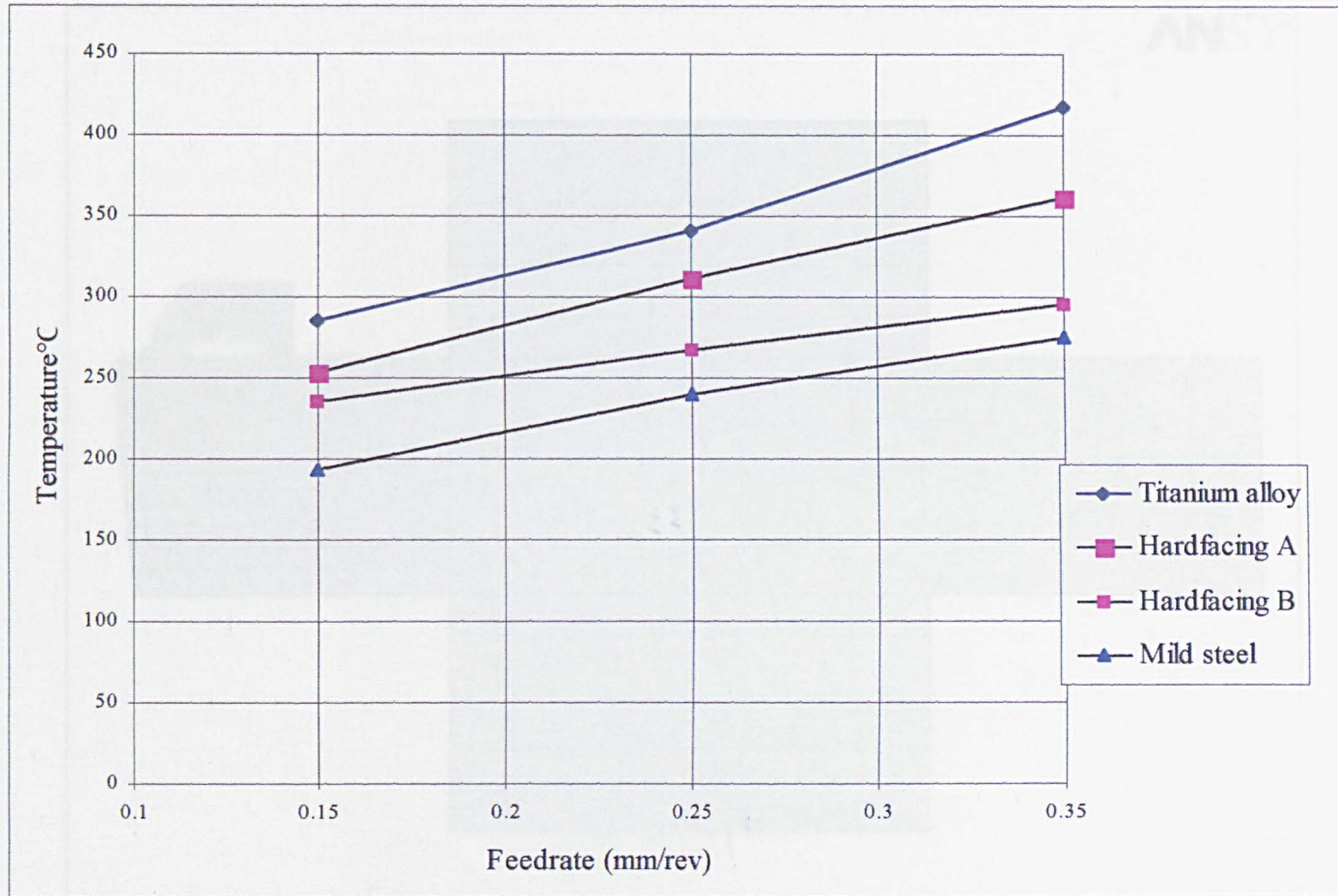


**Figure 7.3** Measured tool-shim interface temperature vs. feedrate (S65m/min).

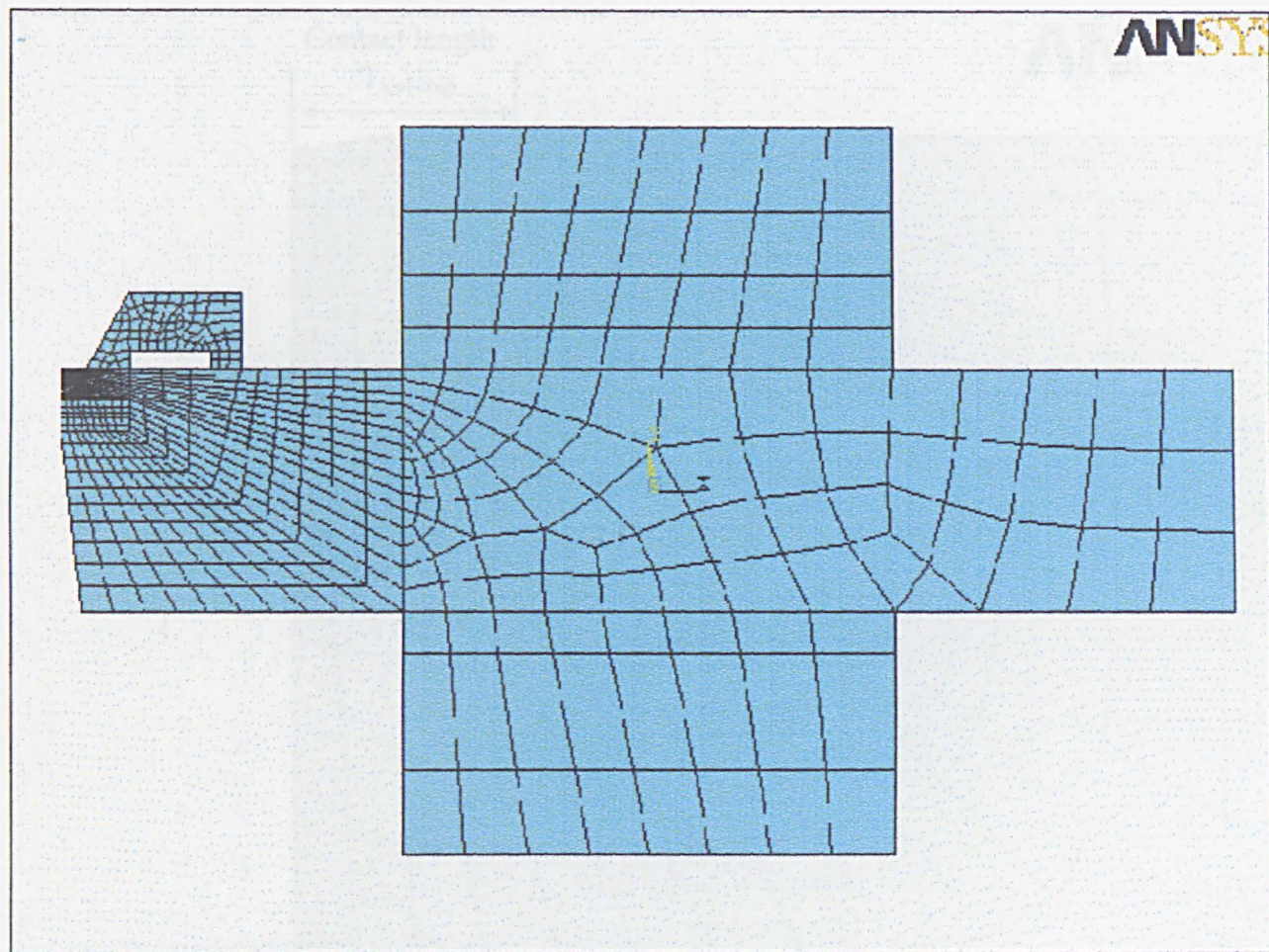


**Figure 7.4** The set-up of the simulation model and the mesh method.

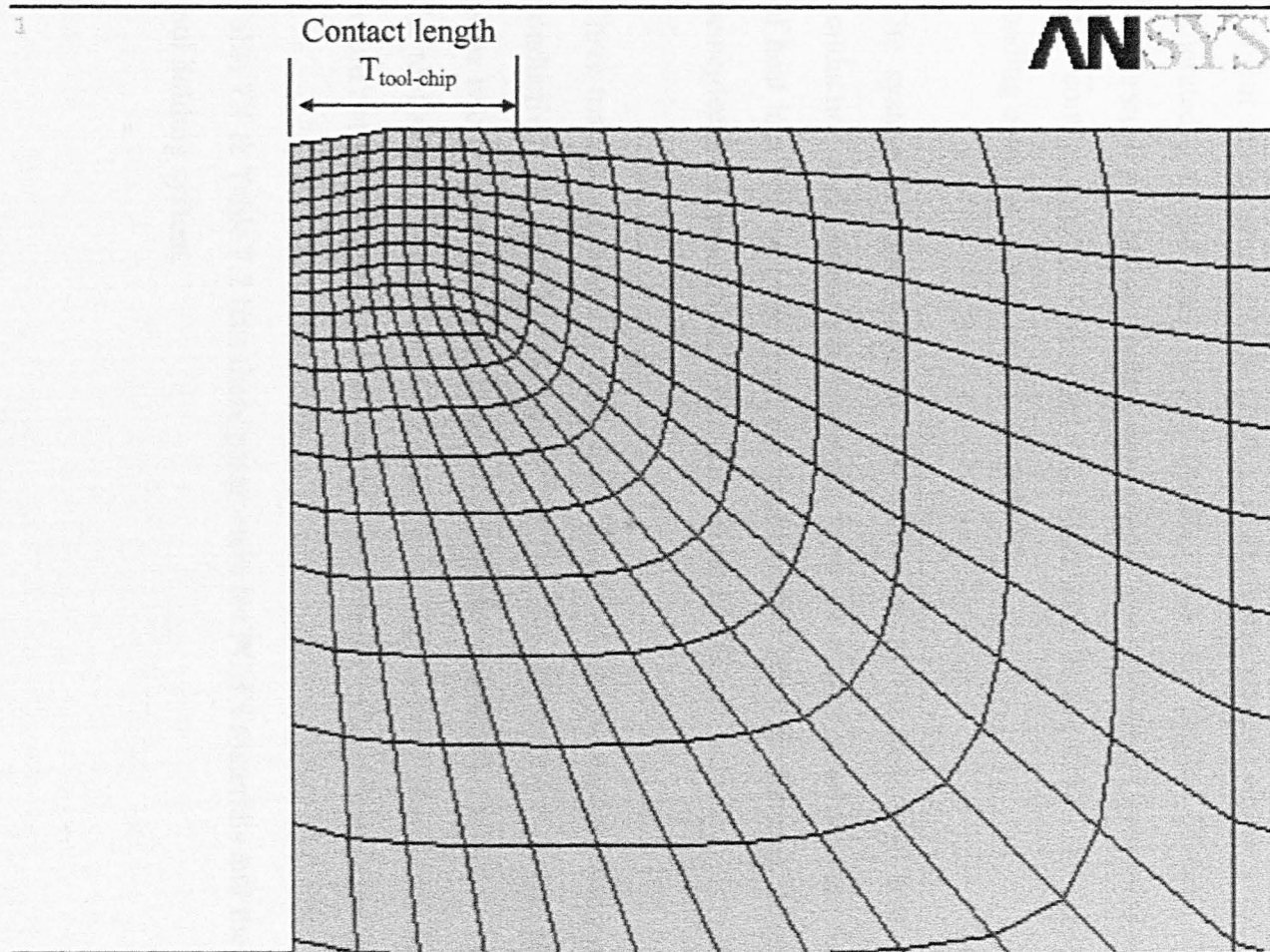


**Figure 7.5** Meshing of the cutting tip and the temperature applied on the contact length.

will not as significant as in the parts near the insert and therefore a coarser mesh was applied to reduce processing time and increase efficiency.

## 7.2.2 BOUNDARY CONDITIONS AND MATERIAL PROPERTIES

In the initial stage, i.e. at time zero, the whole system was assumed at a constant ambient temperature 293 K (20°C). In the early stages (within 1 minute) the heat generated over the flank face of the tool was very limited (Younis, 1992), so the temperature rise of the system was mainly due to the heat generated over the tool-chip contact length. This input was simulated in the model by applying thermal loading onto the contact region (Figure 7.5).

The system is surrounded by air and some of the heat will be lost by radiation, conduction and convection. However, since air is very good heat insulator, this part of heat loss will be very small compared to that through the tool, therefore, it could be neglected (Lipman et al, 1967, Tieu et al, 1998).

Three materials properties need to be specified for the model; density ( $\rho$ ), thermal conductivity ( $k$ ) and specific heat ( $C_p$ ). Density is assumed to be constant, while the other two properties are temperature dependent, especially for the tool material. For the tool steel, constant thermal conductivity and specific heat were used since they would not vary significantly within the temperature range encountered in the tests.

Table 7.1 & Table 7.2 lists these parameters for PCBN materials and the steel for the tool holding system.

**Table 7.1** Properties of PCBN at different temperatures (DeVries, 1972)

	$k$ (W/mm K)	$C_p$ (J/kg K)	$\rho$ (kg/mm <sup>3</sup> )
293.15 K (20 °C)	100e-3	1000	3.12 e-6
373.15 K (100 °C)	100e-3	1045	
573.15 K (300 °C)	110e-3	1496	
773.15 K (500 °C)	120e-3	1618	
973.15 K (700 °C)	125e-3	1914	
1173.15 (900 °C)	130e-3	1966	

**Table 7.2** Properties of toolholder steel (Younis, 1992)

	$k$ (W/mm K)	$C_p$ (J/kg K)	$\rho$ (kg/mm <sup>3</sup> )
Tool steel	47 e-3	486	7.8e-6

### 7.2.3 SIMULATED TEMPERATURE DISTRIBUTIONS AND TOOL - CHIP TEMPERATURE

In the simulation process, the temperature of the tool insert and its holding system increases with cutting time. For an input average temperature on the contact length, the temperature distribution of the system at any time could be determined. Figure 7.6 shows a typical temperature distribution for the system (at time = 30 seconds). The temperature contours are represented by different colours, which allow the temperature regions to be clearly distinguished. It should be noted however that the regions with similar colour are not necessarily all at the same temperature because explicit values of the temperature of each node or element could be read out by the program.

As shown in the Figure 7.6, significant temperature rise has occurred in the tool and the supporting shim (red, yellow and green in colour). The temperature of top clamp and a small part of the tool holder has also increased (light blue). However, the tool holder and the turret clamp are basically still in their original temperature (dark blue).

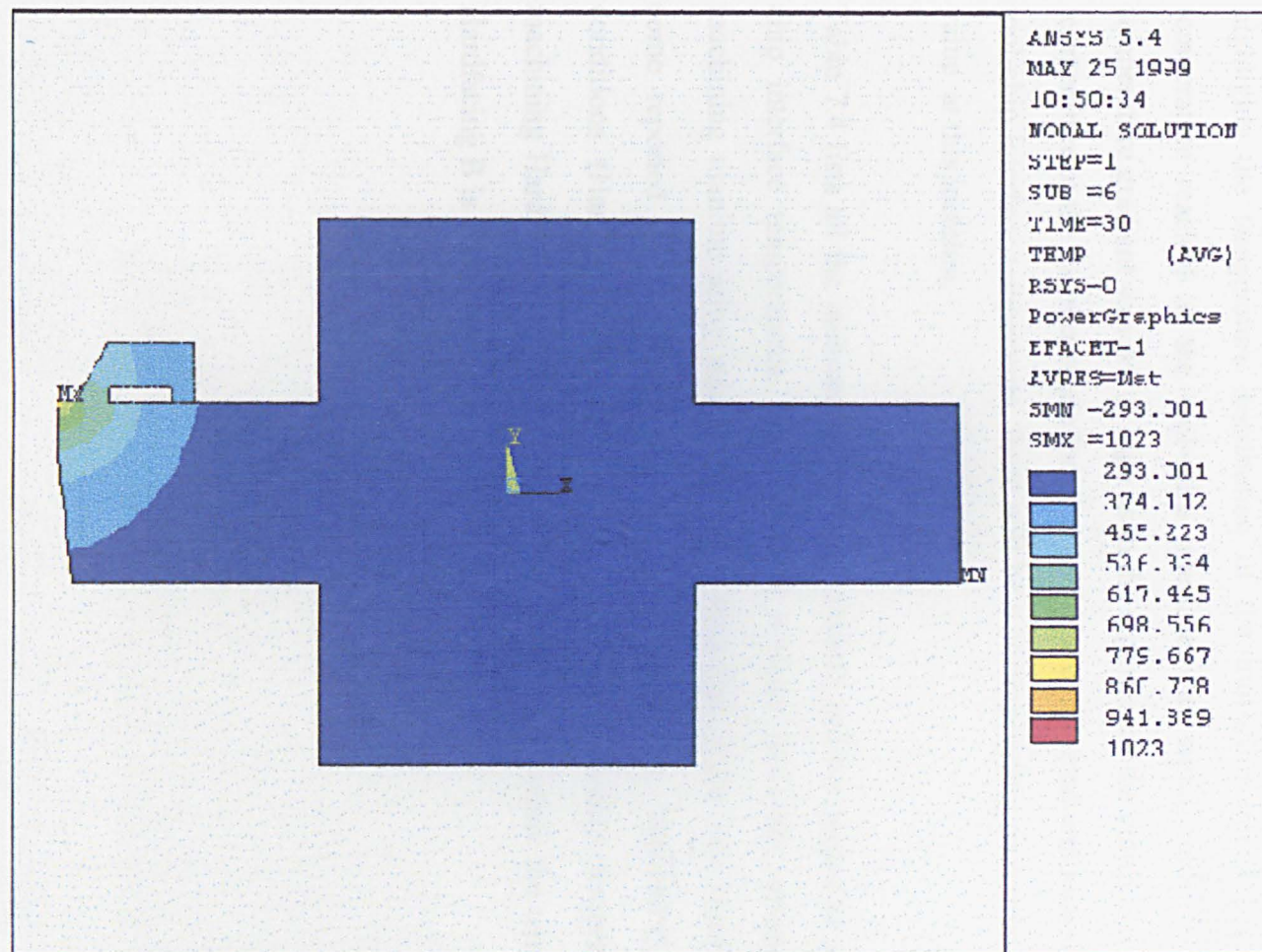


Figure 7.6 Temperature distribution of the system (K).

This shows that the original assumption to model this sub-system instead of the whole machine as a heat sink was valid.

Figure 7.7 shows the temperature distribution of the tool tip. The high temperature was concentrated on a small portion of the tip (red in colour). The temperature dropped quickly from the tool surface into the bulk of the tool insert. Figure 7.8 highlights the temperature distribution of the tool-shim interface region. The temperature reached at the tool-shim interface was significantly lower and the temperature gradient was not as high as in the region near the cutting zone. The node temperature at the thermocouple location could be easily read and recorded. For each tool-chip interface temperature, there will be a corresponding tool-shim temperature value at this location.

Table 7.4 lists all the measured insert temperatures and the predicted average tool-chip interface temperatures. The predicted average tool-chip temperature when machining titanium alloy was much higher than that of the two Hardfacings. The some reported average tool-chip interface temperatures, 700-900°C, at similar conditions (Hartung et al, 1982). The simulated tool-chip temperature when machining Hardfacing A is ranged between 600-700 °C, while the temperature for Hardfacing B is lower (600°C).

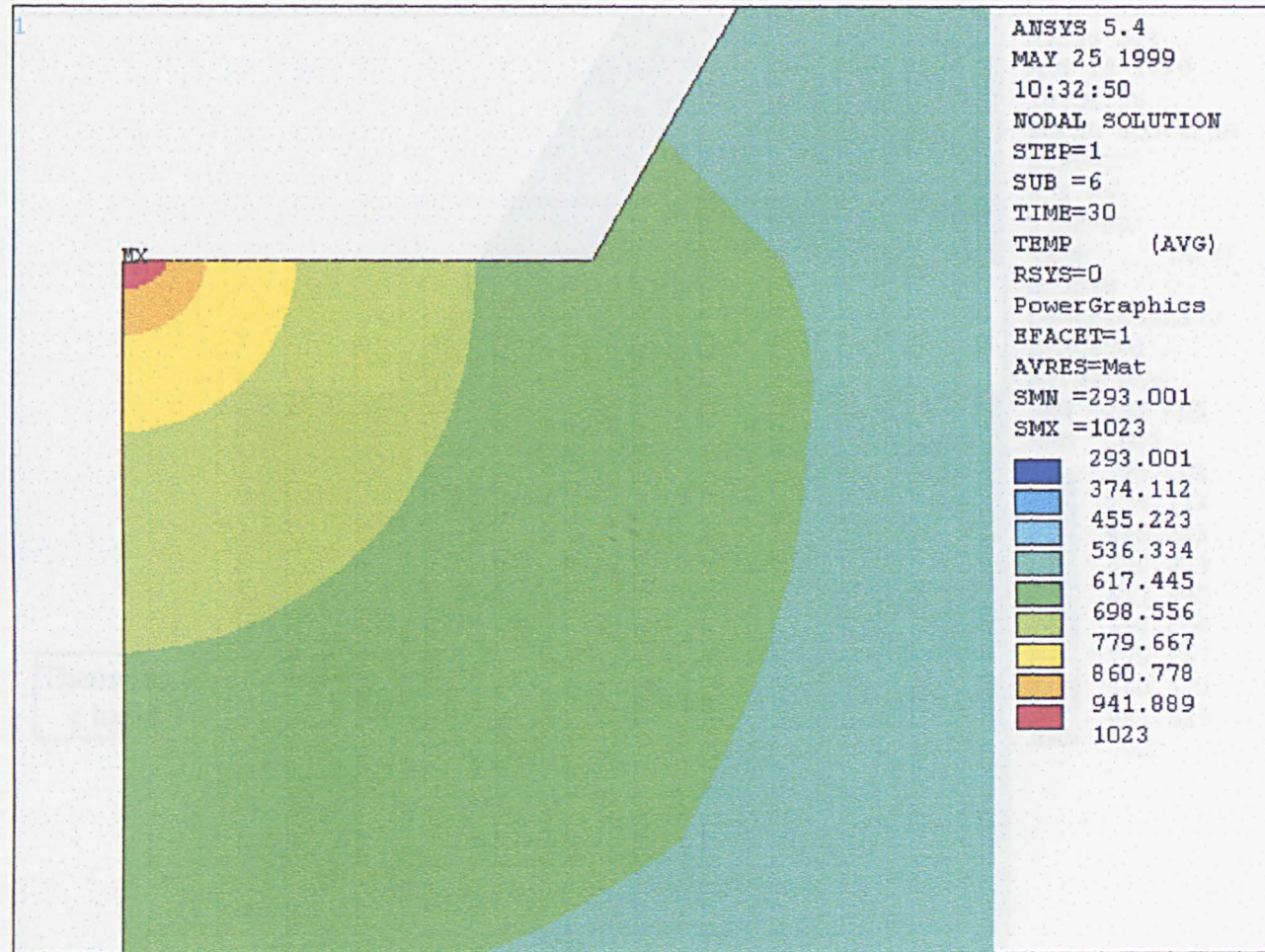
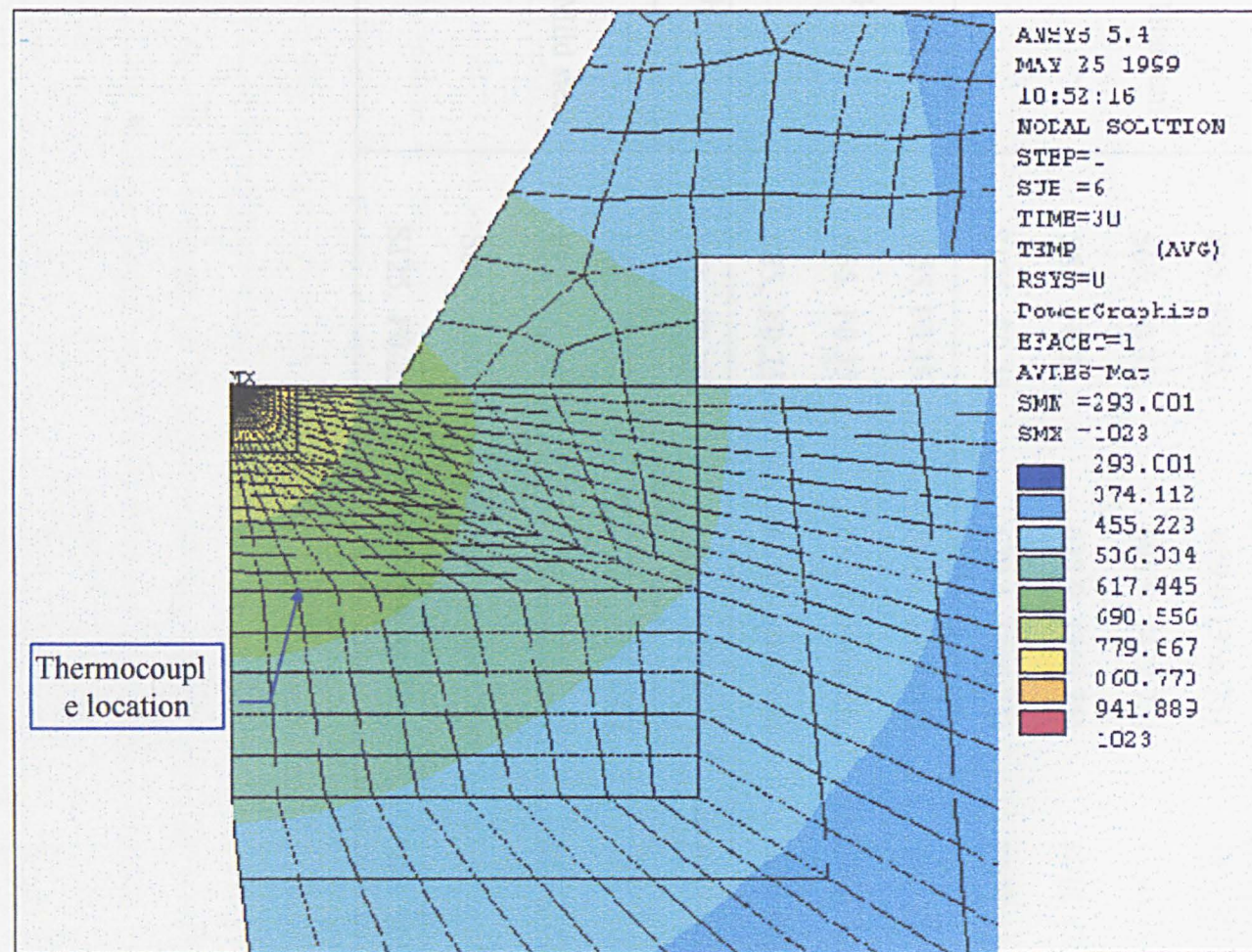


Figure 7.7 Temperature distribution of the cutting tool tip (K).



**Figure 7.8** Temperature distribution at the tool-shim interface (K).

**Table 7.5** Simulated tool-chip interface temperatures

	Cutting parameters	Measured	Predicted
	(m/min, mm/rev)	$T_{\text{tool-shim}}$ K (°C)	$T_{\text{tool-chip}}$ K (°C)
Titanium	S65, F0.15	571.3 (298.15)	880 (606.85)
	S65, F0.25,	629.9 (356.75)	991 (717.85)
	S65, F0.35,	695.9 (422.75)	1130 (856.85)
	S85, F0.25	637.9 (364.75)	1012 (738.85)
	S125, F0.25	679.4 (406.25)	1097 (823.85)
HF-A	S65, F0.25	589.1 (315.85)	915 (641.85)
	S65, F0.35	633.4 (360.25)	998.4 (724.85)
	S85, F0.25	611.9 (338.75)	960 (686.85)
HF-B	S65, F0.25	568.6 (295.45)	874 (600.85)
Mild steel	S65, F0.25	517.7 (244.55)	773 (499.85)
	S65, F0.35	529.8 (256.65)	797.4 (524.25)
	S85, F0.25	529.4 (254.25)	797 (523.85)
	S125, F0.25	587.8 (314.65)	912 (638.85)

## CHAPTER 8 DISCUSSIONS

### 8.1 CHIP FORMATION OF THE HARDFACING MATERIALS

As shown in the quick-stop and chip samples, saw tooth chips formed with the hardfacing materials. It is clear that the separation of the chip segment from the workpiece was limited to a narrow region. This type of saw tooth, or cyclic chip, has been found with some workpieces such as titanium alloys, hardened 4340 steel, case carburized steel and Inconel 718 (Shaw and Vyas, 1998, Stephenson and Agapiou, 1996).

This type of chip formation depends on the thermal and physical properties and the metallurgical state of the workpiece material, as well as on the dynamics of the machine structure and cutting process (Stephenson and Agapiou, 1996). Thus, high hardness, hexagonal close-packed structure and a low thermal conductivity are determining factors as in the case of titanium alloys. The overall effect of these thermomechanical-metallurgical characteristics of the work material is to concentrate deformation in a narrow region and resist deformation in the bulk of the segment (Komanduri and Schroeder, 1986). In addition, inhomogeneity of the workpiece microstructure and low rigidity of the tool or workpiece will also encourage the formation of this type of chip. For the hardfacing materials in this work, the microstructure contains large quantity of carbides, which inhibit deformation within the chip segment. Thus, the shearing or cracking process to form the chip segment was limited to a narrow region extending from the tool edge to the free surface of the workpiece. In addition, the carbides retain their hardness at high temperatures and this will decrease the tendency to bulk deformation of the chip segment.

Figure 8.1 shows, schematically, the chip formation mechanism for a hardfacing material, which consists of two stages. In the first, crack initiation occurs at the free surface of the workpiece and proceeds downwards along the shear plane towards the tool tip. In the second stage, the segment is displaced and separated from the workpiece material.

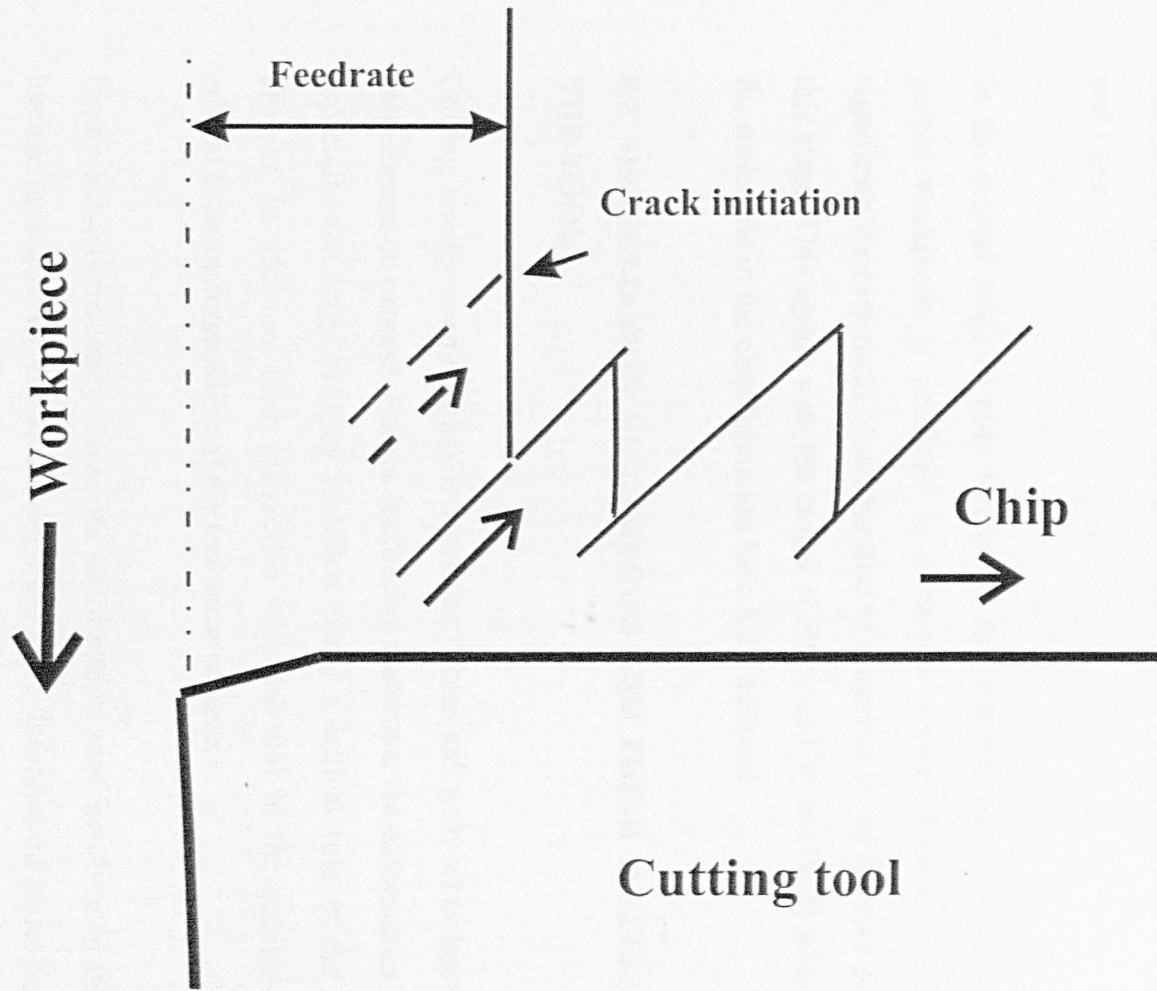


Figure 8.1 Schematic to show the mechanism of the chip formation process of the hardfacing materials

As a result of lower level of compressive stress and, at the same time, high shear stresses, a crack is formed in the surface of the workpiece at the point where the critical shear stress is first exceeded (Konig et al, 1994, Shaw and Vyas, 1998). For a homogenous workpiece material, e.g. titanium alloy, cracks was regularly formed on the surface in front of the cutting tool thereby resulting in regular-segmented saw-tooth chips (Shaw and Vyas, 1998). However, for the hardfacing materials in this work, the microstructure is extremely heterogeneous and this will alter the stress distribution and lead to variations in the chip segment size, as shown in Figure 5.4 and Figure 5.5.

In the second stage of chip formation, the material between the segment and the parent workpiece is confined in a narrow region, shown in Figure 8.1. One significant characteristic of the hardfacing materials is the fracture of the carbides in this stage. This agrees with the model of Shaw and Vyas (1998) where fracture plays the main role in the chip formation for a hard material.

## **8.2 DEFORMATION OF CARBIDES AND THEIR INTERACTION WITH THE TOOL**

Cutting energy consumption is basically connected with what happens during the chip-formation process. For the hardfacing materials, the deformation of the carbides, especially the large primary carbides, plays a critical role in the chip formation process. In addition, their interaction with the tool in the cutting process is also critical to an understanding of the tool wear process.

Figure 8.2 schematically shows the deformation zone involved in the cutting of the hardfacing materials. Besides the normal three deformation zones for homogeneous materials (Shaw, 1984, Trent, 1991,), a large deformation zone exists, ahead of the cutting edge, deep into the workpiece when large carbides are present.

In the primary deformation region, carbide fracture was identified in the quick-stop samples. The fine carbides were fractured and moved into the base of the chip. When

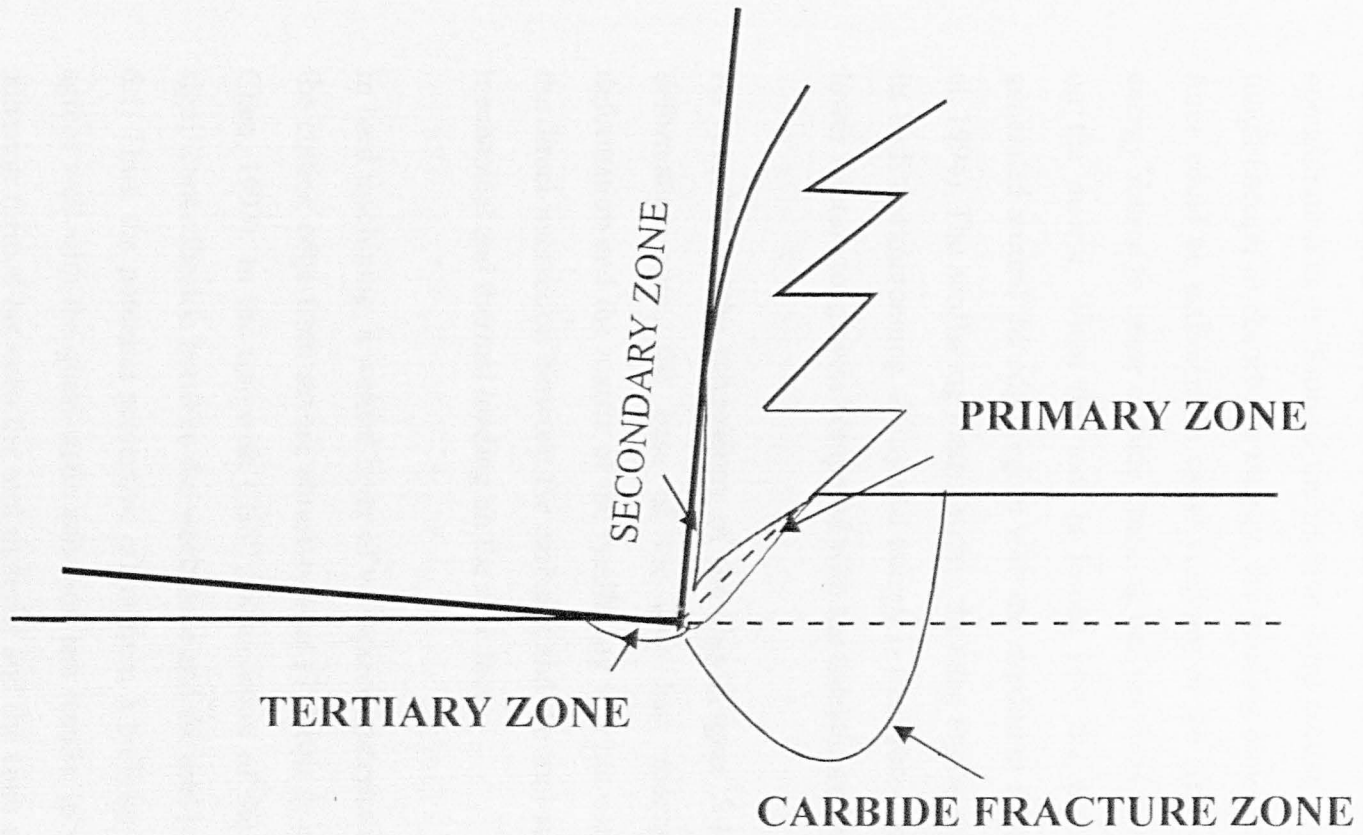


Figure 8.2 Deformation zone of the cutting process

large primary carbides were encountered, they cleaved ahead of the cutting edge and the subsequent chip formation process actually progressed within the eutectic matrix and these carbide segments.

Two possible processes may have contributed to fracture of the large carbides. In cutting, there is a steep stress gradient in front of the tool and a strong stress concentration in the form of the relative sharp cutting edge. When the matrix is not tough enough to absorb the energy, the bending moment resulting from the cutting force could be sufficient to cause cracking of the large carbides. Another possible energy source to cause carbide cracking derives from the action of the tool chamfer on the matrix. When the tool is forced into the workpiece, a stress pattern is generated around the edge region with the maximum stress at the chamfer (Konig et al, 1994). The hardfacing matrix within the edge region will be highly strained due to its high workhardening ability and energy is transferred to the carbides, which are of lower fracture toughness compared with the eutectic matrix (Lee et al, 1996).

As revealed by the microscopy of the chip (Figure 5.4 & 5.5), in the secondary deformation zone, the base of the chip has undergone very limited plastic deformation and the matrix of the hardfacing was not continuous enough to prevent the direct interaction between the carbides and the tool surface. This will exert high mechanical and thermal loading on the rake face.

In hard machining, a welded layer of workpiece material on the tool surface protects the cutting edge from severe abrasive wear (Takatsu et al, 1983, Oishi et al, 1992, Chen, 1993). In the test with CBN1, observation of the cutting edge indicated no significant adhesion between the workpiece and the tool material, as shown in Figure 6.1. Thus, the potential protective effect from a built-up layer is very limited. This agrees well with the quasi-static adhesion test results, in which it was found that no adhesion formed between the tool material and the cone of chromium-carbide-based materials at temperatures up to 1050°C. The reason for this is possibly the very high carbide content of the workpiece and the high CBN content of the tool material (Takatsu et al, 1983).

Another characteristic connected to the secondary deformation zone is the short chip contact length with the hardfacing materials. Comparing the measured contact length in this work with published results involving machining other engineering materials (Trent, 1991, Balazinski, 1993), the deformation characteristics of the hardfacing material resulted in relatively short contact length between the chip and the tool. Thus, for a given cutting force, higher unit stress will be involved on the tool face, especially in the chamfer region (Takatsu et al, 1983).

In the tertiary deformation zone, interaction of the fractured carbides and the flank face of the tool insert occurred, as shown in the quick-stop pictures and the subsurface study. The deformation of the carbides indicates that high mechanical and thermal loading occurs in this region. The hardness profile under the transient surface showed that a high temperature region existed and the way the carbides have been deformed suggests that, possibly, the temperature has exceeded the brittle/ductile transition temperature (BDT) of the carbide at around 600°C i.e. 0.3 T<sub>m</sub>, about 1800 °C for chromium carbide crystals (Kosolapova et al, 1971).

### **8.3 CUTTING FORCES AND TEMPERATURES**

#### **8.3.1 CUTTING FORCES AND STRESSES ON THE TOOL**

No direct measurements of cutting forces were made in this work but the spindle power required when machining hardfacing materials was monitored and compared with that for case hardened steels. In machining process, on the same machine and at similar cutting conditions, the cutting energy required was much higher when machining hardfacing materials than when machining the hardened steel.

The spindle power  $P_s$  is

$$P_s \approx Q \cdot \mu_s,$$

where 'Q' is the material removal rate per unit time and is given by the product of the feed rate, cutting speed, and depth of cut ( $Q = V \cdot f \cdot d$ ). ' $\mu_s$ ' is the power required to cut a unit volume of workpiece material. Among many engineering materials,

hardened steel has the highest unit power requirement (Stephenson and Agapiou, 1996). Therefore, it suggests that hardfacing materials have even higher unit power requirements.

A major reason for the high cutting forces is related to the high strength of the carbides. According to Weinert (1994), the hardness of the carbides will slightly decrease at 600°C and decrease rapidly above 900°C. However, the average cutting temperatures as listed in Table 7.5 were lower than this level. In other words, the cutting temperatures were not high to significantly soften the carbides. As discussed above, the deformation of the carbides plays a dominant part in the chip formation process and their retained high strength at the cutting temperature will result in higher cutting forces.

The high cutting forces, applied via a short contact length, will result in high stress at the tool tip. In addition, according to Davies et al (1997), discontinuous chip formation is inherently unsteady and produces periodic cutting forces. At low cutting speeds, the amplitude of the force variations is large, especially with negative rake tool geometry. As a consequence, the cutting edge is under cyclic loading and this is damaging to the tool especially in the near edge regions.

### **8.3.2 CUTTING TEMPERATURE AND ITS EFFECT ON THE CUTTING PROCESS**

As shown in Figure 7.1-7.3, the temperatures generated in cutting hardfacings are higher than when machining mild steel under similar cutting conditions but lower than those with titanium alloy. It was also clearly shown that the temperature when cutting Hardfacing A was much higher than with Hardfacing B (which contained coarse carbides). This is probably due to that more matrix being involved in the shearing process during chip formation.

Cutting temperatures may have affected the cutting process in two respects: the deformation of the workpiece material and the wear of the tool. In the chip formation

process, a higher temperature will usually soften the work piece and thus easing the cutting process, i.e. reducing the strength of the workpiece and hence the cutting forces. In the machining of the hardfacing in this work, even though the cutting temperature will not significantly soften the carbide it will soften the matrix and reduce its ability to hold the carbides.

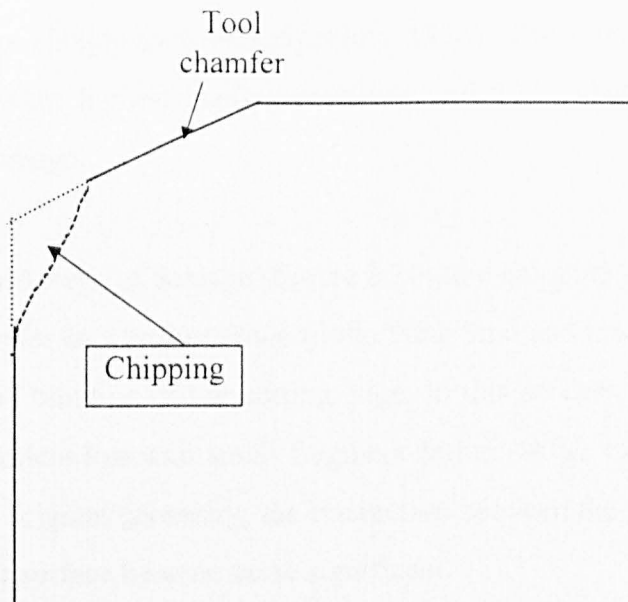
On the other hand, high cutting temperatures will also raise the temperature of the tool but the range of the tool:chip temperatures achieved will not significantly affect the strength of PCBN materials (Figure 2.16). This demonstrates the superiority of PCBN tools in hot machining because the temperatures reached will soften the workpiece but will be below that required for rapid wear for PCBN tools.

#### **8.4 TOOL FAILURE PROCESS**

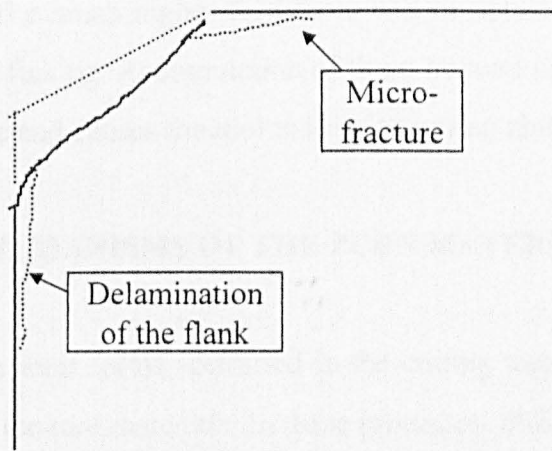
From the laboratory cutting tests and the field cutting tests, the tool failure process was seen to be progressive and starting from micro-chipping which eventually led to large scale fracture. Figure 8.3 schematically shows the main stages involved in the process.

In the early stages (Figure 8.3a), tool wear was concentrated on the lower edge of the chamfer and the main failure mode was clearly micro-chipping, as shown earlier in Figure 6.9 – 6.12. This type of chipping was on a very small scale and started at isolated locations and eventually spread over the whole lower edge of the tool chamfer. By the end of this stage, the lower edge of the chamfer had become chipped. This type of chipping has been reported in machining some other difficult work-piece materials e.g. machining Ni-Hard with BZN tools (Fillmore and Ladd, 1981). It was also found that chipping on the lower edge of the chamfer was the predominant mode of tool wear.

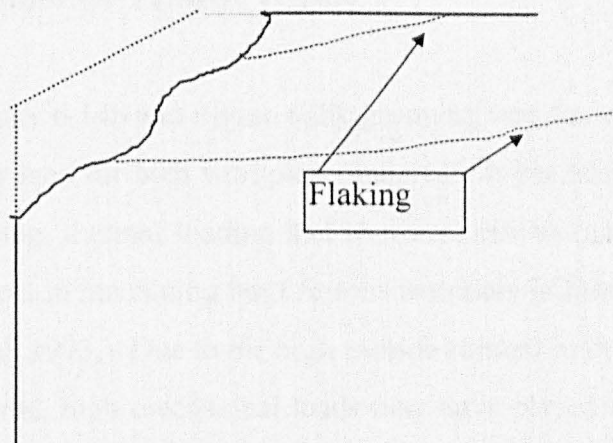
The main reason for this is probably cutting tip overstress. The tool chamfer is incorporated to protect the cutting edge from gross fracture but there is a steep stress gradient in advance of the tool and a high stress concentration at the relatively sharp



a) Earlier chipping of the lower edge of the chamfer



b) Development of chipping and fracture onto the rake face and the flank of the tool



c) Flaking of the rake face in the final stage

**Figure 8.3** Schematic to show the failure process of the PCBN tools.

cutting edge (Stephenson and Agapiou, 1996). The lower edge of the chamfer is subjected to the highest loading condition and this probably leaves it vulnerable to chipping damage.

In the second stage of damage (Figure 8.3b), the chipping has further developed both on the chamfer and further down to the flank land and has resulted in the loss of the chamfer and blunting of the cutting edge. In this process, the most significant wear mode is particle loss and small fragment failure. After the lower edge the chamfer has lost its original geometry, the interaction between the under side of the chip and the chamfer surface become more significant.

In the final stage (Figure 8.3c), the cutting edge has lost its original shape, especially the chamfer and a much higher feed force will be applied to the cutting edge which leads to further flaking. Accumulation of these fracture processes eventually destroys the cutting edge and causes the tool to lose its cutting ability.

## **8.5 WEAR MECHANISMS OF THE PCBN MATERIALS**

The three main wear forms identified in the cutting tests were flank wear, chipping and fracture of the tool materials. In these processes, different mechanisms have been involved and are discussed below.

### **8.5.1 MECHANISM OF FLANK WEAR**

As shown in Figure 6.14b and Figure 6.20, grooving was the most significant feature of the flank wear land for both workpiece materials. It has been well established that mechanical loading, thermal loading and chemical effects may all contribute to the wear of CBN tools in machining hard ferrous materials (Klimenko et al, 1992, Chen 1993, Konig et al, 1993,). Due to the high carbide content in the microstructure of the hardfacing material, high mechanical loads may have played more active roles than with more homogeneous workpieces. Although, the constituents of the tool materials (CBN and AlN) are harder than the carbides and the matrix of the workpiece

material, it is still possible that the tool will suffer 'soft' abrasive wear (Chou and Evans, 1997).

As shown in Figure 6.6, flank wear was at a minimum level at a surface speed of 65 m/min. At speeds higher or lower than this, the wear rate increased. This is due to different influences of cutting speed on the flank wear. At lower speeds, the temperature of the workpiece is relatively low and this results in increased mechanical loading and rapid flank wear. At higher speeds, thermally-induced softening of the workpiece is not sufficient to offset the effect of speed-related mechanical wear.

### **8.5.2 MECHANISM OF THE CHIPPING PROCESS**

Both intergranular and transgranular fracture have been involved in the chipping damage to the cutting tools. However, the two mechanisms have played different roles at particular stages of the damage process.

CBN crystals are made up of two interpenetrating face-centred cubic lattices, one of boron atoms and the other of nitrogen atoms and they show a tendency to cleave on the {110} plane. Transgranular fracture was observed, but only during the initial stages of tool wear. The predicted tool:chip temperatures in machining the hard facing material were well below 900°C, however, the brittle:ductile threshold temperature, above which the dislocation volume rapidly expands, is 900° (Brookes and Lambert, 1982). Therefore dislocation movement is extremely limited below 900°C. When the applied stress, resolved onto the cleavage plane, exceeds the fracture stress and cause crack of CBN particles as shown in Figure 6.11 and illustrated schematically in Figure 8.4.

As revealed by the SEM study (Figures 6.10, 6.11, 6.15b and 6.15c), intergranular failure was the predominant failure mode in the chipping process and it can be seen that this involves the initiation and propagation of cracks at the boundaries between the CBN particles (Figure 8.4). This type of failure results from the micro-structural

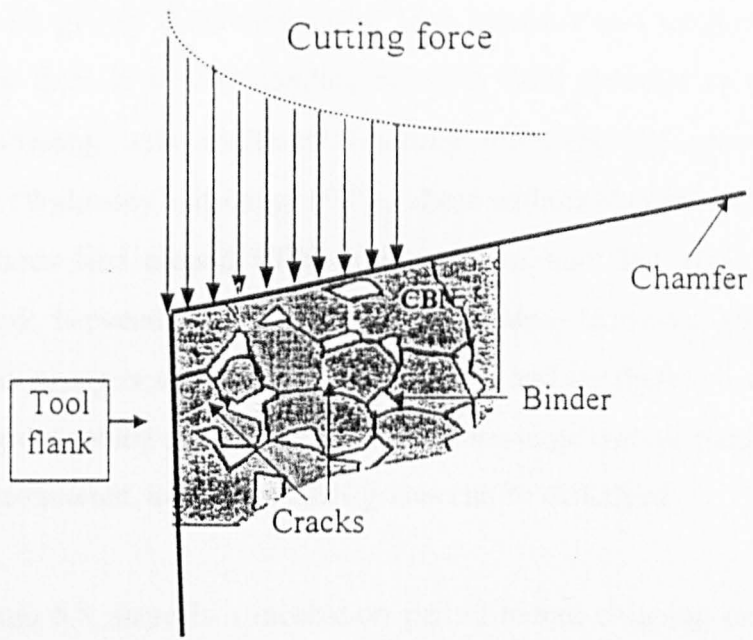


Figure 8.4 Schematic to show the chipping mechanism of the PCBN tool material.

characteristics of PCBN materials. In the sintering process, PCBN materials form a very strong network giving a combination of high hardness and toughness. It has been reported that there is limited bonding between CBN particles as a result of direct contact sintering, with additional bridging following the growth of the secondary phases (Walmsley and Lang, 1987). These authors also showed that AlN formed a continuous rind around CBN grain surfaces and that AlB<sub>2</sub> formed a continuous network between the individual CBN grains. However, the bonding products are not as strong or tough as the bulk material and are therefore susceptible to cracking during the cutting process. In addition, when large carbide particles in the work-piece are encountered, individual CBN grains can be dislodged.

As shown in Figure 6.5, there is a incubation period before chipping occurs. This suggests that the failure process of these tool materials involves the failure of individual connections between the particles. This eventually causes the failure of the tool material when the remaining connections are not strong enough to withstand the cutting load. As discussed before, the saw-tooth type of chip is associated with variation of cutting forces, which will encourage this type of failure mechanism. In addition, when large carbides are encountered, they may impact on the particles and, eventually, tear them out.

As shown in Figure 6.6, the scale of chipping has continuously increased with cutting speed. Cutting speed may enhance the chipping process in two ways. Firstly, it increases the velocity of the workpiece ( $V_c$ ) (Figure 8.4) increase the cutting load. Secondly, it increases the energy of the carbides before they impact on the CBN particles, thereby increasing the tool wear rate. These two effects have offset the beneficial of increased speed on the cutting process by softening of the workpiece material. In other words, 'hot' machining cannot achieve its full potential when machining chromium-carbide based hardfacing materials.

### **8.5.3 MECHANISM OF FRACTURE OF PCBN MATERIALS**

In the later stages of damage, flaking occurred in all the CBN materials used. As has been shown in Figure 6.25-6.31b, the fracture has progressed evenly through the

CBN particles and the binder, i.e. transgranular fracture. This suggests that the flaking process occurred at a rapid rate. In a study of the fracture mechanisms of PCBN materials (Hooper and Brookes, 1984), a single impact test was used to fracture diamond and cubic boron nitride aggregates. Micro-fractography studies showed that, in all cases, the fracture propagated in a transgranular fashion with very little fracture of the interparticle bridges other than in the direction of cracking.

However, it should be noted that the fracture surface of CBN4 showed much more crack deflection than the other CBN materials, as shown in Figure 6.29c. The crack has clearly gone towards a preferential orientation. This orientation is probably on the cleavage plane of CBN single crystals, i.e. (110).

## **8.6 REQUIREMENTS OF THE TOOL MATERIALS**

The requirements of the tool materials are determined by many factors, such as the workpiece material, the interaction between the tool material and the workpiece material, requirements of the machined surface finish etc. (Tonshoff et al, 1986). As shown in the cutting test results and in the earlier discussion, the deformation behaviour of the hardfacing materials and the wear of the tools suggests that for this application, the main requirements of a successful tool material will be abrasion resistance to withstand the effects of the carbide particles and toughness to withstand the cutting loads and so avoid large-scale fracture.

Abrasion resistance is a very important property of a tool material for rough cutting conditions. This is mainly determined by the hardness of the tool material, especially the hardness at the high temperatures generated in the cutting process. The microstructure of the hardfacing materials was designed to provide abrasion resistance in service and this in turn, requires the cutting tool material to have high abrasion resistance itself. In addition, the deformation behaviour in cutting results in short chip contact length, thin chips and, thus, high chip velocity over the tool. These factors will intensify the severity of chip-tool interaction. As described earlier, severe interaction between the workpiece and the tool edge and flank occurs in the tertiary

zone during the cutting process and the tool material needs to have sufficient abrasion resistance to ensure acceptably low wear rates.

High fracture toughness is another very important requirement for a tool material. In this particular application, the high and fluctuating cutting forces require that the tool materials have high toughness to prevent gross fracture and reduced tool life.

In the cutting tests carried in this work, some other tool materials such as tungsten carbide and whisker-reinforced  $\text{Al}_2\text{O}_3$  tools were also tested. However, they lasted only very short times due to excessive wear or fracture and therefore were not able to cope with the demands of production machining. PCBN tools were the only suitable tool materials for this application because of their good combination of high hot hardness and fracture toughness.

In applications such as machining cast iron, the excellent abrasion resistance of PCBN tools has played an important role (Deming et al, 1993). However, in the hardfacing application, large scale of fracture occurred in the cutting process (Figure 6.25-6.31), and the PCBN tools could continue to be used until it has totally lost its cutting ability. In addition, the scale of tool fracture has a direct influence on the number of times an insert can be indexed thus, on the economy of a machining operation. Therefore the fracture resistance of a PCBN material will play a significant role and should be a prime consideration in the future development of PCBN materials for this and similar applications.

## **8.7 EFFECT OF MICROSTRUCTURE OF PCBN MATERIALS ON THEIR CUTTING PERFORMANCE**

An analysis of the mechanical properties of aggregate materials requires a knowledge of the properties of their components, their volume fractions and information on the contiguity or amount of contact between the phases. Although the CBN tools are from different sources, their performance still reflected the influence of different

microstructural characteristics on the cutting performance of the materials in this application.

All the tools used in the tests have relatively high CBN contents and this is essential to meet the requirements for high abrasion resistance and toughness. In materials with lower CBN content, the particles are more isolated and this results in reduced hardness and fracture toughness (Bossom, 1991). As revealed in Chapter 4, most of the PCBN materials used in this work have dense structures but CBN1 has an obviously higher CBN content and a denser structure than the others. This is probably the main reason for its superior cutting performance and higher edge strength. This suggests that materials with a high volume fraction of CBN will be the most suitable for machining hard-facings and similar materials.

Another important aspect of PCBN materials is particle contiguity. This defines the extent of contact between a CBN particle and its neighbours. This is an important characteristic in determining the strength of the CBN network and, thus, the bulk strength of the material. Contiguity depends mainly on two factors; material manufacturing parameters such as temperature and pressure and the ability of particles to deform plastically during the sintering process (Pullum and Lewis, 1990). CBN2 and CBN3 are from similar sources but SEM study of these materials revealed that CBN2 has a stronger skeleton than that of CBN3 and performed much better in machining trials.

The PCBN materials used in this work were produced with particles of different sizes and the machining trials suggest that this may also be a significant factor in determining cutting tool performance. Of the six materials examined, CBN4 had the smallest particle size and showed the worst cutting performance, with the tools suffering gross fracture. CBN2 and CBN6 materials had larger particles and performed better in machining tests, presumably because the larger particles are better able to resist abrasion by the carbide particles in the work-piece.

In summary, it appears that dense structure, large particle size and strong inter-particle bonding are all desirable features of PCBN materials for machining hard-faced workpieces. This is exemplified by the performance of CBN1 in the cutting trials.

## **CHAPTER 9      CONCLUSIONS AND RECOMMENDATIONS FOR FURTHER WORK**

### **9.1      CONCLUSIONS**

The machinability of chromium carbide based hard facing materials appears to be strongly related to their microstructural properties and, in particular, to the presence and deformation characteristics of large carbides. The formation of saw-tooth chips and short chip:tool contact lengths were distinctive features of the material removal process. Quick-stop tests revealed that the presence of large carbides influenced the cutting process in three indentifiable zones. In the primary zone, the machining process involves fracture of the large carbides in advance of the cutting tool. In the secondary zone, the matrix is not sufficiently continuous to form a protecting layer and contact with the under-side of the chip with fractured carbides will exert high mechanical and thermal loading condition to the rake face. In the tertiary zone, interaction of the fractured carbides and the flank face of the tool occurs, when these two surfaces move at very high relative speed, which leads to high mechanical and thermal loading.

Temperature measurements of the cutting process, using a remote thermocouple method, indicated that the average temperature generated at the tool:shim interface was higher than when machining mild steel but lower than when machining a titanium alloy, under comparable conditions. Finite element analysis was used to calculate tool:chip temperatures based on those measured at the tool:shim interface. The predicted average temperature at the tool:chip interface was in the range 600-700 °C. At this level, PCBN material could maintained their high hardness.

The work demonstrated that PCBN cutting tools could be used successfully to machine iron-based welded hardfacings but that the nature and composition of the tool material was strongly influential on cutting performance and tool life. Studies of PCBN materials from various sources, using both optical and scanning electron microscopy, revealed significant microstructural differences and these clearly

influenced cutting performance. It is apparent that a dense structure with strong inter-particle bonding is essential for satisfactory cutting performance in the application considered; other factors e.g. large particle size also improve the performance of the tool material.

Cutting tests revealed the existence of four types of wear with the PCBN materials; flank wear, micro-chipping, flaking of the rake face and delamination of the flank face. Flank wear occurred as the result of abrasion, the severity of which was found to depend on cutting speed and feedrate. The principal mechanism of microchipping was found to be loss of individual CBN particles by the propagation of inter-particle cracks. Flaking of the rake face and delamination of the flank face occurred later in the tool damage process and both involved transgranular cracking of the CBN particles. In most cases, damage was progressive but gross fracture of the cutting tool was observed in materials with relatively small CBN particle size.

## **9.2 RECOMMENDATIONS FOR FURTHER WORK**

The current work has gone some way towards investigating the performance of ultra-hard (PCBN) cutting tools when turning welded iron-based hardfacing materials using several experimental techniques. However, it was not possible to measure cutting forces during the experimental work and it is recommended that further tests be conducted with a tool-post dynamometer attached to the lathe. Furthermore, it was not possible to conduct tests over a sufficiently wide range of machining conditions to investigate the effect of temperature on the cutting process. PCBN materials are known to work well under machining conditions that promote thermal softening of the work-piece ahead of the tool. There is also the possibility of applying heat from an external source, such as a laser, to assist machining of 'difficult' materials. In addition, the effect of carbide size and disposition on cutting performance and tool should also be further investigated.

## REFERENCES

- Abrao A M** and **Aspinwall D K**, 1996, The surface integrity of turned and ground hardened bearing steel, *Wear*, Vol. 196, pp279-284.
- Abrao A M** and **Aspinwall D K**, 1995, Cutting forces assessment when turning hardened bearing steel, *Journal of the Brazilian Society of Mechanical Sciences*, Vol. 17, No. 4, pp 353-359.
- Abrao A M** and **Aspinwall D K**, 1997, Temperature evaluation of cutting tools during machining of hardened bearing steel using polycrystalline cubic boron nitride and ceramic cutting tools, *Materials Science and Technology*, Vol.13, pp445-451.
- Abrao A M**, **Aspinwall D K** and **Ng E-G.**, 1996, Temperature evaluation when machining hardened hot work die steel using PCBN tooling, *Industrial Diamond Review*, Vol.56, No.569, pp. 40-44.
- Abrao A M**, **Aspinwall D K** and **Wise M L H**, 1993, A review of polycrystalline cubic boron nitride cutting tool developments and application, *Proceedings of the 13th International MATADOR Conference*, Manchester, UK, pp169-180.
- Abrao A M**, **Wise M L H** and **Aspinwall D K**, 1995, Tool life and workpiece surface integrity evaluations when machining hardened AISI H13 and AISI E52100 steels when conventional ceramic and PCBN tool materials, *NAMRC XXIII*, Houghton, Michigan, MR95-159, pp1-9.
- Afaghani J E D**, **Yamaguchi K**, **Horaguchi I** and **Nakamoto T**, 1996, Whisker behaviours and tool wear in cutting unidirectional SiC whisker-reinforced plastic, *Wear*, Vol. 195, pp223-231.
- AL-Watban A**, 1996 PhD Thesis, University of Hull.
- Aspinwall D K** and **Tunstall M**, 1985, Cutting tool life comparison, in: S.A. Tobia (Ed.), *Proc. 24th MTDR. Conf.*, Birmingham, Macmillan, London, pp269-277.
- Aspinwall D K**, 1984, Superhard tooling ten years on, *Metalworking Production*, Vol.129, No. 11, pp72-77.
- Aspinwall D K**, **Radford M** and **Wise M L H**, 1991, Machining of hardened AISI H13 hot work die steel using advanced ceramic tool materials, *IMEchE*, C412/055, pp221-225.
- Atamert S** and **Bhadeshia H K D H**, 1990, Microstructure and stability of Fe-Cr-C hardfacing alloys, *Material Science and Engineering*, A130, pp101-111.

- Back J T** and **Briggs N D**, 1994, High speed videographs of the orthogonal machining of aluminium, *Proceedings of the Energy-Sources Technology Conference*, Tribology Symposium American Society of Mechanical Engineers, Petroleum Division (Publication) PD Vol. 61, Pub. by ASME, pp 41-54.
- Balazinski M**, **Litwin J** and **Fortin C**, 1993, Influence of the feed variation on tool wear when machining Inconel 600, *Transaction of CSME*, Vol.17, No. 4A, pp659-669.
- Barrow G**, 1973, A review of experimental and theoretical techniques for assessing cutting temperature, *Annals of CIRP*, Vol.22, No.2, pp203-211.
- Barry J** and **Byrne G**, 1998, Ceramic and CBN cutting tool wear in finish turning of hardened EN24 steel, *4<sup>th</sup> International Conference on Behaviour of Materials in Machining: Opportunities and prospects for Improved Operations*, Straford-upon-Avon (UK), pp57-66.
- Bergman F** and **Jacobson S**, 1994, Tool wear mechanisms in intermittent cutting of metal matrix composites, *Wear*, Vol. 179, pp.89-93.
- Bhattacharyya S K**, **Aspinwall D K** and **Nicol, A W**, 1978, The application of polycrystalline compacts for ferrous machining, *Proc. of the 19<sup>th</sup> Int. MTDR Conf.*, pp425-434.
- Bhattacharyya S K** and **Aspinwall D K**, 1980, Aspects of Machinability using polycrystalline diamond and CBN compact tooling, *Proceeding of an International Conference on Cutting Tool Materials*, Ft. Mitchell, Kentucky, pp249-262.
- Bieker R**, 1995, High speed die milling with PCBN, *Industrial Diamond Review*, Vol. 55, No. 564, pp1-3.
- Billman E R**, **Mehrotra P K**, **Shuster A F** and **Beeghly C W**, 1988, Machining with Al<sub>2</sub>O<sub>3</sub>-SiC-Whisker cutting tools, *Am. Ceram. Soc. Bull.*, Vol.67, No.6, pp1016-1019.
- Bordui D**, 1988, Hard-part machining with ceramic inserts, *Am. Ceram. Soc. Bull.*, Vol.67, No.6, pp998-1001.
- Bossom P K** and **Hoffmann**, 1993, Turning and milling with PCBN in the automatic industry, *Diamond & CBN Ultrahard Materials Symposium*, IDA, pp99-114.
- Bossom P K**, 1991, The selection of high and low CBN cutting tool materials for automotive applications, *Proceeding of Superabrasive 91*, Society of Manufacturing Engineer, Chicago, IL, USA, pp1139-1160.

- Brandt G**, 1986, Flank and crater wear mechanisms of Alumina-based cutting tools when machining steel, *Wear*, Vol. 112, pp39-56.
- Brinksmeier E, Cammett J K, Konig W, Leskovar P, Peters J and Tonshoff H K**, 1982, Residual stresses — measurement and causes in machining process, *Annals of the CIRP*, pp491-509.
- British Standard B.S. 4844: Prat 2**: 1972, Abrasion Resisting White Cast Irons, Part2: Nickel-Chromium.
- Brookes C A**, 1995, Hand-out for the MSc on Advanced Materials & Manufacturing, University of Hull.
- Brookes C A, James R D, Nabhani F and Parry A R**, 1992, Structure, composition, and integrity of workpiece:tool interfaces in metal cutting and grinding, *IMEchE Seminar on Tribology in Metal cutting & grinding*, April, pp41-48.
- Brookes, C. A. and Lambert, W. A.**, 1982, Ultra Hard Material Application Technology, (De Beers), Hornbeam Press LTD.
- Brown R H**, 1974, A double shear-pin quick-stop device for very rapid disengagement of a cutting tool, *Int. J. Mach. Tool Des. res.*, Vol. 16, pp115-121
- Buckley**, 1967, Machining, Institute of metallurgist, No. 9.
- Byrne G, Heinz J, Barry J and Eitzenberger H**, 1997, Chip root tests using PCD and MCD cutting tools, *Industrial Diamond review*, No.3, pp96-101.
- Casto L S, Valvo L E, Piacentini M, Ruisi V F, Lucchini E, and Maschio S**, 1994, Cutting temperatures evaluation in ceramic tools; experimental tests, numerical analysis and SEM observations, *CIRP Annals*, Vol. 43, No.1, pp73-76.
- Chattopadhyay A K and Chattopadhyay A B**, 1983, Wear characteristics of ceramic cutting tools in machining steel, *Wear*, Vol.93, pp347-359.
- Chen W Y**, 1993, The machining of hardened steel using superhard CBN tooling and CBN tipped rotary cutting tools, PhD Thesis, University of Birmingham.
- Chou Y K and Evans C J**, 1997, Tool wear mechanism in continuous cutting of hardened tool steels, *Wear*, vol. 212, pp59 - 65.
- Chow J G and Wright P K**, 1988, On-line estimation of tool-chip interface temperatures for a turning operation, *Journal of Engineering for Industry*, Vol.110, February, pp56-64.
- Clark I E and Hoffmann J**, 1993, PCD tooling in the automotive industry, *Diamond & CBN Ultrahard Materials Symposium*, IDA, pp115-130

- Crooks A G, Jong A DE and Wong W C K**, 1988, Effect of machining parameters on CBN tool tip temperature, *Forth International Conference on Manufacturing Engineering*, Brisbane, pp11-13.
- Davies M A, Burns T J and Evans C J**, 1997, On the Dynamics of chip formation in Machining hard metals, *Annals of the CIRP*, Vol.46, No.1, pp25-30.
- Deming M S, Young B A and Ratliff D A**, 1993, Turning grey cast iron with PCBN cutting tools, *Diamond & CBN Ultrahard Materials Symposium*, IDA, pp132-141.
- Department of Trade and Industry**, 1985, Wear resistant surfaces in engineering, a guide to their production, properties and selection, International Research & Development Co Ltd.
- DeVries R C**, 1972, Cubic Boron Nitride: Handbook of Properties, General Electric Company, pp1-17.
- Dewes R C, Aspinwall D K, Dipple S J, Schoen S and Thielemann**, 1997, Tool wear and surface integrity observations during the high speed milling of hardened die steel, *International Conference and Exhibition on Design and Production of Dies and Moulds*, pp. 131-138.
- Eda H, Kishi K and Hashimoto H**, 1980, Wear resistance and cutting ability of a newly developed cutting tool, *Proceeding of an International Conference on Cutting Tool Materials*, Ft. Mitchell, Kentucky, pp265-280.
- Edwards R**, 1993, Cutting tools, Institute of Materials.
- Fillmore B, Ladd R C**, 1981, Machining Ni-hard: tough, hard and interrupted, *Manufacturing Engineering* (August), pp57-59.
- Fleming M A, Sweeney C, Valentine T J and Simpkin R**, 1998, PCBN hard turning and workpiece surface integrity, *4<sup>th</sup> International Conference on Behaviour of Materials in Machining: Opportunities and prospects for Improved Operations*, Straford-upon-Avon (UK), pp. 43-55.
- Gardinier C F**, 1988, Physical properties of superabrasives, *Am. Ceram. Soc. Bull*, Vol.67, No.6, pp1006-1008.
- Gregory E N**, 1980, Materials for hardfacing, *Weld Surfacing and Hardfacing*, Published by Welding Institute, pp11-22.
- Griffiths B J**, 1986, The development of a quick stop device for use in metal cutting hole manufacturing processes, *International Journal of Machine Tools & Manufacture*, Vol. 26, No.2, pp. 191-203.

- Haldin O, Karttunen A and Pruß P**, 1993, Finish grey cast iron with DBC80, *Industrial Diamond Review*, No. 4, pp187-189.
- Hartung P D and Kramer B M**, 1982, Tool wear in Titanium machining, *Annals of the CIRP*, Vol. 31, No.1, pp75-79.
- Heath P J**, 1986, Structure, properties and applications of polycrystalline cubic boron nitride, *14th North American Manufacturing Research Conference Proceedings*, pp. 66-80.
- Hibbs L E Jr and Wentorf R H Jr**, 1974, Borazon and diamond compact tools, *High Temperature - High Pressures*, Vol.6, pp409-413.
- Hitchener A P, Thornton A G and Wilks**, 1981, (A.S.M.E) *J. Wear of Materials*, p. 728.
- Hodgson T and Trendler P H J**, 1981, Turning hardened tool steels with cubic nitride insert, *Annals of the CIRP*, 30(1), pp63-66.
- Hooper R M and Brookes C A**, 1984, Microstructure and wear of cubic boron nitride aggregate tools, *2nd Int. Conf. Science Hard Mater.*, Rhodes, p907-917.
- Hosoi T, Hosoi R, Asano K, Horiuchi O and Hasegawa Y**, 1980, High rate drilling with a new type of carbide-tipped twist drill, *Proceeding of an International Conference on Cutting Tool Materials*, Ft. Mitchell, Kentucky, pp399-410.
- Hou Z B and Komanduri R**, 1995, On the thermomechanical model of shear instability in machining, *Annals of the CIRP*, Vol.44, No.1, pp69-73.
- Hyatt G**, 1997, High & Dry High-speed dry machining can cut cycle times and cost, *Manufacturing Engineering*, September, pp82-87.
- King A G and Wheildon M**, 1966, *Ceramics in Machining Process*, Academic Press, New York.
- Kitagawa T and Maekawa K**, 1990, Plasma hot machining for new engineering materials, *Wear*, Vol.139, pp251-267.
- Klimenko S A**, 1992, Cutting of components with hard-facing and spraying coatings (in Russian), *Sverkhtverdye Materialy*, No.5, pp55-60.
- Klimenko S A, Mukavoz Y A, Lyashko V A, Vashchenko A N and Ogorodnik V V**, 1992, On the wear mechanism of cubic boron nitride base cutting tools, *Wear*, Vol.157, pp 1-6.
- Konig W and Wagemann**, 1993, Machining of ceramic components: process - technological potentials, *NIST Spec. Publ.* 847, pp3-20.

- Kohno Y, Uchida T and Hara A**, 1986, New application of polycrystalline CBN, *14th North American Manufacturing Research Conference Proceedings*, pp55-65.
- Komanduri R and Schroeder T A**, 1986, On shear instability in machining a nickel-iron based super alloy, *Journal of Engineering for Industry*, Vol.108, pp93-100.
- Komonduri R**, 1982, *Wear*, 76.
- Komvopoulos K and Erpenbeck S A**, 1991, Finite element modelling of orthogonal metal-cutting, *Journal of Engineering For Industry-Transactions of The ASME*, Vol. 113, No. 3, pp. 253-267.
- Konig W and Neises A**, 1993, Wear mechanisms of ultrahard, non-metallic cutting materials, *Wear*, Vol.162-164, pp12-21
- Konig W and Neises N**, 1993, Turning TiAl6V4 with PCD, *Industrial Diamond Review*, Vol.53, No. 555, pp. 85-88.
- Konig W and Wand T**, 1987, Turning bearing steel with Amborite and Ceramic, *Industrial Diamond Review*, No.3, pp117-120.
- Konig W, Berktold A, Liermann J and Winands N**, 1994, Top quality components not only by grinding, *Industrial Diamond Review*, No.3, pp127-132
- Kono Y, Hara A, Yazu S, Uchida T and Mori, Y**, 1980, Cutting performance of sintered CBN tools, *Proceeding of an International Conference on Cutting Tool Materials*, Ft. Mitchell, Kentucky.
- Kopac, J. and Dolinsek, S.**, 1996, Advantages of experimental research over theoretical models in the field of metal cutting, *Experimental Techniques*, Vol. 20, No. 3, pp24-28.
- Kosolapova, T I**, 1971, "Carbides:properties, production, and application", Plenum Press (New York).
- Kovac P and Sidjanin L**, 1997, Investigation of chip formation during milling, *Int. J Production Economics*, Vol.51, pp149-153.
- Lee S, Choo S, Baek E, Ahn S and Kim N**, 1996, Correlation of microstructure and fracture toughness in high-chromium white iron hardfacing alloys, *Metallurgical and Materials Transactions A*, Vol27A, 1996, pp3881-3891.
- Lee Y M, Sampath B and Shaw M.C.**, 1984, Tool fracture probability of cutting tools under different exiting conditions, *Transactions of the ASME, Journal of Engineering for Industry*, Vol.106, pp168-170.

- Lin Z C** and **Chen D Y**, 1995, A study of cutting with a CBN tool, *Journal of Materials Processing Technology*, Vol.49, pp149-164.
- Lipman M P**, **Nevis B E** and **Kane G E**, 1967, A remote sensor method for determining average tool-chip interface temperatures in metal cutting, *Journal of Engineering for Industry*, May, pp333-338.
- Müller-Hummel, P.** and **Lahres, M.**, 1995, Temperature measurement on diamond-coated tools during machining, *Industrial Diamond Review*, Vol. 55, No.565, pp78-83.
- Macleay P M**, 1997, High Temperature Properties of New Superhard Materials, *MEng Thesis*, University of Hull.
- Mansfeld F W**, 1982, Turning of chill cast rolls on CNC production machines, *Industrial & Production Engineering*, No.1, pp69-71.
- Mehrotra P K**, 1998, Machining with ceramic cutting tools, *4<sup>th</sup> International Conference on Behaviour of Materials in Machining: Opportunities and prospects for Improved Operations*, Straford-upon-Avon (UK), pp. 33-42..
- Menon, R**, 1995, New Developments in Hardfacing Alloys, *Welding Journal*, (February), p43-48.
- Michalski L**, **Eckersdorf K** and **McGhee J**, 1991, Temperature measurement, London, Wiley.
- Momper F**, 1988, Take the grind out of hard steel turning, *Metalworking Production*, October, pp72-75.
- Muller H** and **Steinmetz K**, 1983, Machining mineral crushing rings with Amborite, *Industrial Diamond Review*, No.1, pp30-31.
- Nabhani F**, 1991, The Performance of Ultra-hard Cutting Tool Materials in Machining Aerospace Alloy TA48, *Ph.D Thesis*, The University of Hull
- Nakayama K** and **Arai M**, 1992, Comprehensive chip form classification based on the cutting mechanism, *Annals of the CIRP*, Vol. 41, No. 1, pp71-74.
- Narutaki N**, **Yamane Y** and **Takeuchi M**, 1979, Wear of CBN cutting tools, *Journal of the Japan Society of Precision Engineering*, Vol.45, No.2, pp81-87.
- Neailey K**, 1988, Surface integrity of machined components - microstructural aspects, *Metals and Materials* , February, pp93-96
- Nicolis M O**, 1984, Machining Ni-hard augers with Amborite, *Industrial Diamond Review*, no.1, pp28-29.

- Notter A T and Heath P J**, 1980, *Industrial Diamond Review*, July, pp244-251.
- Oishi K, Nishida T and Ono T**, 1992, Study of the fracture characteristics of ceramic cutting tools (first report), *Wear*, 154, pp. 361-370.
- Ordinartsev I A**, 1984, Widening the use of synthetic super-hard tool materials, *Soviet Engineering Research*, Vol. 4, No.7, pp50-51.
- Park Y W**, 1994, A model and empirical validation of plastic deformation in a machined surface, *PhD Thesis*, The Pennsylvania State University.
- Peate S S and Gregory E N**, 1980, Weld surfacing in perspective, *Weld surfacing and hardfacing*, Published by Welding Institute, pp1-2.
- Popok N N and Khejfets M L**, On favourable conditions of contacting at cutting of hard-work materials and coatings, *Trenie I Iznos*, Vol. 14, No.3, 1993, p552-562.
- Poulachon G and Moisan A**, 1998, A contribution to the study of the cutting mechanisms during high speed machining of hardened steel, *Annals of the CIRP*, Vol. 47, No. 1, pp73-77.
- Pullum O J and Lewis M H**, 1990, Microstructural analysis of a cubic boron nitride ceramic, *Materials Letters*, Vol.9, No.2-3, pp83-86.
- Quigley O, Monaghan J and O'Reilly P**, 1994, Factors affecting the machinability of an Al/Si metal -matrix composite, *J. Mater. Process. Technol.*, Vol.43, pp21-36.
- Richard N, and Aspinwall D K**, 1989, Use of ceramic tools for machining nickel based alloys, *J. Mach. Tools Manufact.*, Vol.29, No. 4, pp575-588.
- Roebuck B**, 1995, *Technologies and Markets for Cutting Tool Materials*, National Physical Laboratory.
- Sadat A B**, 1987, Surface characteristics of machined Inconel-718 Nickel-base superalloy using natural and controlled contact length tools, *J. Mach. Tools Manufact.*, Vol.27, No.3, pp333-342.
- Sadik M I and Lindström B**, 1993, The role of tool-chip contact length in metal cutting, *Journal of Materials Processing Technology*, Vol.37, pp613-627.
- Schey J A**, 1987, *Introduction to manufacturing processes*, McGRAW-HILL, International Edition.
- Seco Tools (U.K.) Ltd.**, 1996, Technical Guide for PCBN - Polycrystalline Cubic Boron Nitride.
- Shaw M C and Vyas A**, 1998, The mechanism of chip formation when hard turning steel, *Annals of the CIRP*, Vol.47, No.1, pp77-82.

**Shaw M C**, 1984, *Metal Cutting Principles*, Oxford University Press, Oxford.

**Shintani K, Ueki M and Fujimura Y**, 1989, Optimum tool geometry of CBN tool for continuous turning of carburized steel, *J. of Mach. Tools Manufact.*, Vol.29, No. 3, pp403-413.

**Shintani K, Ueki M and Fujimura Y**, 1989, Optimum tool geometry of CBN tool for interrupted turning of carburized steel, *J. of Mach. Tools Manufact.*, Vol.29, No. 3, pp. 413-423.

**Silveri P**, 1985, Pump producer goes for Amborite, *Industrial Diamond Review*, no.6, pp287-288.

**Stephenson D A**, 1991, An inverse method for investigating deformation zone temperatures in metal cutting, *Journal of Engineering For Industry-Transactions of The ASME*, Vol. 113, No.2, pp129-136.

**Stephenson D A, Agapiou J S**, 1996, *Metal Cutting Theory and Practice*, Marcel Dekker, Inc., New York.

**Takatsu S, Shimoda H, and Otani K**, 1983, Effects of CBN content on the cutting performance of polycrystalline CBN tools, *International Journal of Refractory and Hard Metals*, Vol. 2 No.4, pp175-178

**Taylor F W**, 1907, On the art of cutting metals, *Transactions of the ASME*, Vol. 28.

**TC Limited**, International Thermocouple Reference tables for Ni-Cr/Ni-Al, Uxbridge, UK.

**Tieu A K, Fang X D and Zhang D**, 1998, FE analysis of cutting tool temperature field with adhering layer formation, *Wear*, Vol.214, pp252-258.

**Tonshoff H K et al**, 1979, Micro-cinematograph Investigations of Cutting Process, *Colloquium on Cutting of Metals*, St. Etienne, France.

**Tonshoff H K, Bussmann W and Stanske C**, 1986, Requirements on tools and machines when machining hard materials, in: S.A. Davies (Ed.), *Proc. 25th MTDR Conf.*, 17-18 Sept., Manchester, Macmillan, London, pp. 349-357.

**Trent, E. M.**, 1991, *Metal cutting*, ( Third edition), Butterworths, London

**Vorm T**, 1976, Development of a quick-stop device and an analysis of the "frozen-chip" technique, *Int. J. Mach. Tool. Des. Res.*, Vol.16, pp241-250.

**Wager J G and Brown R H**, 1980, A new quick-stop device for milling and grinding, *Annals of the CIRP*, vol.29, No.1, pp15-18.

- Walmsley J C and Lang A R**, 1987, A transmission electron microscope study of a cubic boron nitride-based compact material with AlN and AlB<sub>2</sub> binder phases, *Journal of Materials Science*, vol.22, pp4093-4102.
- Wang Y**, 1995, Theoretical and experimental study of the cutting mechanics of graphite fiber reinforced preimpregnated composite and the effect of tool geometry on cutting quality and fiber deflection, *MASC Thesis*, Concordia University, Canada.
- Wang Z Y, Rajurkar K P and Murugappan M**, 1996, Cryogenic PCBN turning of ceramic (Si<sub>3</sub>N<sub>4</sub>), *Wear*, Vol.195, pp1-6.
- Weinert K**, 1994, Relation between process energy and tool wear when turning hardfacing alloys, *Annals of the CIRP*, Vol 43, pp97-101.
- Wentorf R H, DeVries R C and Bundy F P**, 1980, Sintered Superhard Materials, *Science*, (May) Vol.208, pp873-880.
- Williams J E, Smart E F and Milner D R**, 1970, *Metallurgis*, 81.
- Wright P K and Bagchi A**, 1981, Wear mechanisms that dominate tool-life in machining, *J. Applied Metal Working*, Vol.1, No.4, pp15-23.
- Xiao H**, 1990, Wear behaviour and wear mechanism of ceramic tools in machining hardened alloy steel, *Wear*, Vol.139, pp439-451.
- Yeo S H, Lui W W and Phung V**, 1992, A quick-stop device for orthogonal machining, *Journal of Materials Processing Technology*, Vol. 29, pp41-46.
- Younis M A**, 1992, Mechanical and thermal stress in clamped, brazed, and bonded carbide tools, *Journal of Engineering for Industry*, November, Vol. 114, pp377-385.
- Zone C L, Wen C P, and Ship P L**, 1995, Study of orthogonal cutting with tool flank wear and sticking behaviour on the chip-tool interface, *Journal of Materials Processing Technology*, Vol. 52, No. 2-4, pp524-538.
- Zorev N N**, 1963, *International Production Engineering Research Conference*, Pittsburgh.